# BIOPROSPECTING AND BIOTECHNOLOGY OF EXTREMOPHILES

EDITED BY: Milko A. Jorquera, Steffen P. Graether and Fumito Maruyama
PUBLISHED IN: Frontiers in Bioengineering and Biotechnology

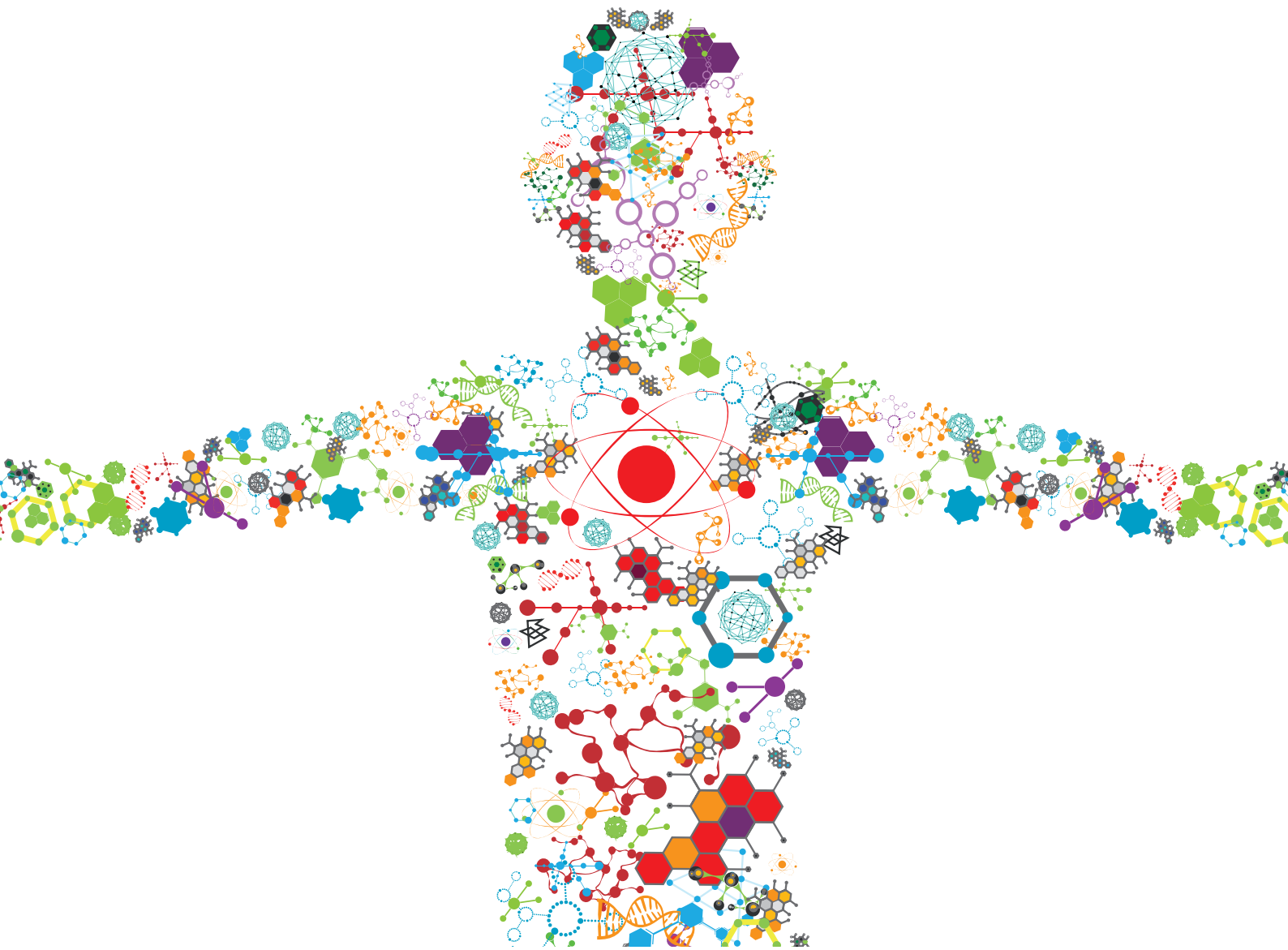

frontiers Research Topics

# frontiers



ISSN 1664-8714
ISBN 978-2-88963-130-8
DOI 10.3389/978-2-88963-130-8

## About Frontiers

Frontiers is more than just an open-access publisher of scholarly articles: it is a pioneering approach to the world of academia, radically improving the way scholarly research is managed. The grand vision of Frontiers is a world where all people have an equal opportunity to seek, share and generate knowledge. Frontiers provides immediate and permanent online open access to all its publications, but this alone is not enough to realize our grand goals.

## Frontiers Journal Series

The Frontiers Journal Series is a multi-tier and interdisciplinary set of open-access, online journals, promising a paradigm shift from the current review, selection and dissemination processes in academic publishing. All Frontiers journals are driven by researchers for researchers; therefore, they constitute a service to the scholarly community. At the same time, the Frontiers Journal Series operates on a revolutionary invention, the tiered publishing system, initially addressing specific communities of scholars, and gradually climbing up to broader public understanding, thus serving the interests of the lay society, too.

## Dedication to Quality

Each Frontiers article is a landmark of the highest quality, thanks to genuinely collaborative interactions between authors and review editors, who include some of the world's best academicians. Research must be certified by peers before entering a stream of knowledge that may eventually reach the public - and shape society; therefore, Frontiers only applies the most rigorous and unbiased reviews.
Frontiers revolutionizes research publishing by freely delivering the most outstanding research, evaluated with no bias from both the academic and social point of view. By applying the most advanced information technologies, Frontiers is catapulting scholarly publishing into a new generation.

## What are Frontiers Research Topics?

Frontiers Research Topics are very popular trademarks of the Frontiers Journals Series: they are collections of at least ten articles, all centered on a particular subject. With their unique mix of varied contributions from Original Research to Review Articles, Frontiers Research Topics unify the most influential researchers, the latest key findings and historical advances in a hot research area! Find out more on how to host your own Frontiers Research Topic or contribute to one as an author by contacting the Frontiers Editorial Office: researchtopics@frontiersin.org

# BIOPROSPECTING AND BIOTECHNOLOGY OF EXTREMOPHILES

Topic Editors:
**Milko A. Jorquera,** Universidad de La Frontera, Chile
**Steffen P. Graether,** University of Guelph, Canada
**Fumito Maruyama,** Hiroshima University, Japan

**Citation:** Jorquera, M. A., Graether, S. P., Maruyama, F., eds. (2019). Bioprospecting and Biotechnology of Extremophiles. Lausanne: Frontiers Media. doi: 10.3389/978-2-88963-130-8

# Table of Contents

frontiers in Bioengineering and Biotechnology

EDITORIAL
published: 23 August 2019
doi: 10.3389/fbioe.2019.00204

# Editorial: Bioprospecting and Biotechnology of Extremophiles

*Milko A. Jorquera*[1,2]*, *Steffen P. Graether*[3] *and Fumito Maruyama*[1,4]

[1] *Laboratorio de Ecología Microbiana Aplicada, Departamento de Ciencias Químicas y Recursos Naturales, Universidad de La Frontera, Temuco, Chile,* [2] *Network for Extreme Environment Research, Scientific and Technological Bioresource Nucleus, Universidad de La Frontera, Temuco, Chile,* [3] *Department of Molecular and Cellular Biology, University of Guelph, Guelph, ON, Canada,* [4] *Office of Industry-Academia-Government and Community Collaboration, Hiroshima University, Hiroshima, Japan*

**Keywords: airborne, andean highland, bacteria, fish, hydrothermal vent, hot spring, microorganisms, plants**

## Editorial on the Research Topic

## Bioprospecting and Biotechnology of Extremophiles

Extreme environments are defined as those environments that contains conditions that are difficult to survive for most life forms. They include natural environments (hyper-arid deserts and rocks, oceanic deeps, salt lakes, volcanoes, high mountains, and upper atmosphere, etc.), as well as artificial ones (operating rooms, aircrafts, spaceships, etc.). Because most of the earth's surface (>80%) is covered by extreme environments, it is not surprising that a wide diversity of organisms (e.g., animals, plants, insects, fungi, and bacteria) are able to colonize, survive, and proliferate in these extreme environments. Those organisms living in extreme environments, also known as extremophiles, have evolved and developed a wide variety of strategies and mechanisms to live under harsh conditions, such as exceptionally high or low values of temperature, pressure, oxygen, carbon dioxide, acidity, radiation, nutrient content, water content, salt content, sugars, etc. Thus, extremophiles have opened a new window into bioprospecting for the discovery and application of novel bioactive products.

In this sense, the classic example of extremophiles and their bioactive compounds is the DNA polymerase from thermophilic bacteria (e.g., *Thermus aquaticus*) from hydrothermal environments (Chien et al., 1976). Without a doubt, the advances in molecular biology and life sciences during the last three decades would not have been possible without these extremozymes. Another example is the cold-active enzymes from Artic or Antarctic extremophiles (animals, plants, and microorganisms), which are highly attractive for biotechnologists since they can be used in food processing to improve milk fermentation, to store frozen yogurt, and to improve ice-cream production (Cid et al., 2016). Therefore, extremozymes and bioactive compounds produced by extremophiles, and their potential application in biotechnology, have been recognized in various fields, such as medicine (e.g., antibiotics and antitumors), food technology (e.g., phytases and phosphatases), biofuel production (e.g., proteases and lipases), cosmetic industry (carotenoids), biomining and contaminated soil remediation (xenobiotic-degrading enzymes), agriculture (plant-growth inducers), and organic residue cycling (cellulose and lignocellulose) (Rampelotto, 2016; Dumorné et al., 2017).

This Research Topic highlights microbial communities inhabiting extreme environments or in extremophile microbiomes as an unexplored source of novel biological resources, with a huge potential for biotechnology and its industry. In this sense, ureolytic bacteria from desert salt lakes could be used as a new technology for bio-precipitation of ion crystals (e.g., calcium and magnesium), improving water use in mining. Similarly, the core microbiome of Arctic fish is a possible tool in aquatic biotechnology to assist in improving fish health and waste management practices in aquaculture. The bioprospecting of airborne microbial communities can give clues to their application in the degradation of toxic compounds and increased

OPEN ACCESS

***Edited and reviewed by:***
*Manfred Zinn,*
*HES-SO Valais-Wallis, Switzerland*

***Correspondence:**
*Milko A. Jorquera*
*milko.jorquera@ufrontera.cl*

***Specialty section:***
*This article was submitted to Bioprocess Engineering, a section of the journal Frontiers in Bioengineering and Biotechnology*

***Received:*** *16 July 2019*
***Accepted:*** *09 August 2019*
***Published:*** *23 August 2019*

***Citation:***
*Jorquera MA, Graether SP and Maruyama F (2019) Editorial: Bioprospecting and Biotechnology of Extremophiles. Front. Bioeng. Biotechnol. 7:204. doi: 10.3389/fbioe.2019.00204*

tolerance of heavy metal stress in plants. In a similar context, epoxide hydrolases found in the metagenomes from hot springs have also been proposed for use in the detoxication of xenobiotics, and as a defense against pathogen attack and stress response in plants.

In addition, climate change is affecting the distribution and abundance of flora and fauna in diverse regions around the globe, including extreme environments. The characterization of nitrous oxide (a recognized greenhouse gas) reducing bacteria in deep-sea hydrothermal vents is also noted in this Topic Research, emphasizing their capability to reduce gas emissions in the environment. With respect to climate change, microbial communities and plants from extreme environments are also being evaluated as biotechnological tools to improve the tolerance of cereal crops and trees from adverse climate events (such as droughts, flooding, frosts, hot, and cold waves, etc.), and can therefore prevent economical losses in agriculture. Plant-growth microorganisms from cold and hot deserts are possible alternatives to improve the salt tolerance of agriculturally relevant plants. Similarly, cold-stress related dehydrin genes can be a suitable tool in genetic engineering to improve cold tolerance in plants.

As noted in this Research Topic, advances in omics technologies have allowed for the investigation of extremophile properties and their bioactive compounds as has never been seen before, revealing their relevance in multiple disciplines in science, and in many aspects of bioprospecting and biotechnology, including medicine, bioenergy and biofuels, bioinformatics, biomaterials, biosafety and biosecurity, aquatic biotechnology, agriculture, environmental science, nanobiotechnology, industrial process, synthetic biology, DNA/protein engineering, and even more.

Lastly, we list here several international initiatives that could be useful for readers interested in extremophiles bioprospecting, such as: The Network for Extreme Environment Research (NEXER; http://www.nexerchile.cl/), The International Society for Extremophiles (https://www.extremophiles2018.org/), Swissaustral Chile Ltda. (http://www.swissaustral.ch/), Latin American Network of Extremophiles (https://redlae.science/), Spanish Network of Extremophiles Microorganisms (https://web.ua.es/en/rnme/spanish-network-of-extremophile-microorganisms.html), and the following related Research Topics in Frontiers:

(1) Microbial Life Under Stress: Biochemical, Genomic, Transcriptomic, Proteomic, Bioinformatics, Evolutionary Aspects and Biotechnological Applications of Poly-Extremophilic Bacteria (https://www.frontiersin.org/research-topics/7007/microbial-life-under-stress-biochemical-genomic-transcriptomic-proteomic-bioinformatics-evolutionary).
(2) Enzymes from Extreme Environments (https://www.frontiersin.org/research-topics/3054/enzymes-from-extreme-environments).
(3) Extremophilic Industrially Important Enzymes and Molecular Mechanisms (https://www.frontiersin.org/research-topics/3700/extremophilic-industrially-important-enzymes-and-molecular-mechanisms).
(4) Recent Advances in Acidophile Microbiology: Fundamentals and Applications (https://www.frontiersin.org/research-topics/5002/recent-advances-in-acidophile-microbiology-fundamentals-and-applications).
(5) Actinobacteria, a Source of Biocatalytic Tools (https://www.frontiersin.org/research-topics/5513/actinobacteria-a-source-of-biocatalytic-tools).

## AUTHOR CONTRIBUTIONS

MJ conceived of the idea for the Research Topic: Bioprospecting and Biotechnology of Extremophiles and served as editor. SG and FM served as co-editors for the Research Topic. MJ wrote the editorial, with editing help from SG and FM.

## REFERENCES

Chien, A., Edgar, D. B., and Trela, J. M. (1976). Deoxyribonucleic acid polymerase from the extreme thermophile *Thermus aquaticus*. *J. Bacteriol.* 127, 1550–1157.

Cid, F. P., Rilling, J. I., Graether, S. P., Bravo, L. A., Mora, M. L., and Jorquera, M. A. (2016). Properties and biotechnological applications of ice-binding proteins in bacteria. *FEMS Microbiol. Lett.* 363: fnw099. doi: 10.1093/femsle/fnw099

Dumorné, K., Córdova, D. C., Astorga-Eló, M., and Renganathan, P. (2017). Extremozymes: a potential source for industrial applications. *J. Microbiol. Biotechnol.* 27, 649–659. doi: 10.4014/jmb.1611.11006

Rampelotto, P. H. (2016). *Biotechnology of Extremophiles: Advances and Challenges*. Cham: Springer International Publishing. doi: 10.1007/978-3-319-13521-2

**Conflict of Interest Statement:** The authors declare that the research was conducted in the absence of any commercial or financial relationships that could be construed as a potential conflict of interest.

frontiers in Bioengineering and Biotechnology

ORIGINAL RESEARCH
published: 16 October 2018
doi: 10.3389/fbioe.2018.00144

# New Thermophilic α/β Class Epoxide Hydrolases Found in Metagenomes From Hot Environments

*Erica Elisa Ferrandi[1], Christopher Sayer[2], Simone Antonio De Rose[2], Elisa Guazzelli[1], Carlotta Marchesi[1], Vahid Saneei[2], Michail N. Isupov[2], Jennifer A. Littlechild[2]* and Daniela Monti[1]**

[1] Istituto di Chimica del Riconoscimento Molecolare, C.N.R., Milan, Italy, [2] The Henry Wellcome Building for Biocatalysis, Biosciences, College of Life and Environmental Sciences, University of Exeter, Exeter, United Kingdom

Two novel epoxide hydrolases (EHs), Sibe-EH and CH65-EH, were identified in the metagenomes of samples collected in hot springs in Russia and China, respectively. The two α/β hydrolase superfamily fold enzymes were cloned, over-expressed in *Escherichia coli,* purified and characterized. The new EHs were active toward a broad range of substrates, and in particular, Sibe-EH was excellent in the desymmetrization of *cis*-2,3-epoxybutane producing the (2*R*,3*R*)-diol product with *ee* exceeding 99%. Interestingly these enzymes also hydrolyse (4*R*)-limonene-1,2-epoxide with Sibe-EH being specific for the *trans* isomer. The Sibe-EH is a monomer in solution whereas the CH65-EH is a dimer. Both enzymes showed high melting temperatures with the CH65-EH being the highest at 85°C retaining 80% of its initial activity after 3 h thermal treatment at 70°C making it the most thermal tolerant wild type epoxide hydrolase described. The Sibe-EH and CH65-EH have been crystallized and their structures determined to high resolution, 1.6 and 1.4 Å, respectively. The CH65-EH enzyme forms a dimer via its cap domains with different relative orientation of the monomers compared to previously described EHs. The entrance to the active site cavity is located in a different position in CH65-EH and Sibe-EH in relation to other known bacterial and mammalian EHs.

**Keywords: epoxide hydrolase, metagenomics, industrial biocatalysis, stereoselectivity, protein structure**

OPEN ACCESS

***Edited by:***
*Steffen P. Graether, University of Guelph, Canada*

***Reviewed by:***
*Yasser Gaber, Beni-Suef University, Egypt*
*Ning Li, South China University of Technology, China*

****Correspondence:***
*Jennifer A. Littlechild*
*j.a.littlechild@exeter.ac.uk*
*Daniela Monti*
*daniela.monti@icrm.cnr.it*

***Specialty section:***
*This article was submitted to Process and Industrial Biotechnology, a section of the journal Frontiers in Bioengineering and Biotechnology*

***Received:*** *13 August 2018*
***Accepted:*** *21 September 2018*
***Published:*** *16 October 2018*

***Citation:***
*Ferrandi EE, Sayer C, De Rose SA, Guazzelli E, Marchesi C, Saneei V, Isupov MN, Littlechild JA and Monti D (2018) New Thermophilic α/β Class Epoxide Hydrolases Found in Metagenomes From Hot Environments. Front. Bioeng. Biotechnol. 6:144. doi: 10.3389/fbioe.2018.00144*

## INTRODUCTION

Epoxide hydrolases (EHs, EC 3.3.2.9) are enzymes that catalyze the *in vivo* hydrolysis of an epoxide ring to the corresponding vicinal diols. This activity was originally reported in mammalian cells more than 40 years ago (Jerina et al., 1968; Brooks et al., 1970). Since then, EHs have been found in a wide range of different organisms including bacteria and fungi (Arand et al., 1999; Kotik et al., 2007; Liu et al., 2007), plants and insects (Kiyosue et al., 1994; Stapleton et al., 1994; Guo et al., 1998; Linderman et al., 2000; Morisseau et al., 2000). The physiological roles of EHs have been widely studied. These enzymes have been shown to be involved in the detoxification of xenobiotics in mammals (Oesch, 1973; Morisseau and Hammock, 2005) and fungi (Sutherland, 1992), in the general defense system against pathogens and stress response in plants (Kiyosue et al., 1994; Guo et al., 1998) and in hormone biosynthesis in insects (Linderman et al., 2000).

The majority of EHs described to date belong to the α/β hydrolase superfamily, where the core domain with a particular direction and connectivity of β-strands is covered by a mainly

α-helical cap domain, with the active site located on the interface of the two domains (Widersten et al., 2010). An Asp-His-Asp/Glu catalytic triad located in the core domain is essential for the epoxide hydrolytic activity. The reaction proceeds via a two-steps catalytic mechanism involving the formation of a covalently bound enzyme-substrate intermediate. The first step of the reaction is the nucleophilic attack by the catalytic aspartate carboxylate group on one of the epoxide carbons of the substrate, resulting in the formation of an ester intermediate. The subsequent nucleophilic attack on the ester intermediate by an activated water molecule results in the formation of a diol product. Two conserved tyrosine residues in the cap domain point toward the catalytic triad and participate in the catalytic mechanism by binding the substrate and activating its protonation for catalysis (Nardini et al., 1999).

In recent years EHs have found industrial applications where they are used for the synthesis of optically pure chiral epoxides and 1,2-diols, both by the kinetic resolution of racemic epoxide mixtures, as well as through enantioconvergent processes or by the de-symmetrisation of *meso*-epoxides. The products are valuable building blocks for the synthesis of different pharmaceutical and agrochemical bioactive molecules (Bala and Chimni, 2010; Kotik et al., 2012; Wohlgemuth, 2015; Archelas et al., 2016). For example, EHs have been employed for the preparation of optically active phenylpropylene oxides which are useful building blocks for the synthesis of antibiotics and C-glycosides (Capriati et al., 2004), (*R*)-*para*-nitrostyrene oxide, which is a precursor of the β-blocker Nifenalol (Pedragosa-Moreau et al., 1997), and (*S*)-*para*-chloro styrene oxide, a precursor of a *N*-methyl-D-aspartate receptors (NMDA) receptor antagonist (Karboune et al., 2005).

The biocatalytic application of EHs in the synthesis of enantiopure epoxides and 1,2-diols represents a green and efficient alternative to traditional chemical methods which usually involve the use of potentially toxic heavy metal-based catalysts with only low to moderate turnover frequencies (Katsuki and Sharpless, 1980; Kolb and Sharpless, 1992; Kolb et al., 1994; Jacobsen, 2000). The EHs offer some inherent advantages, such as a usually high regio- and stereoselectivity on different substrates and the lack of expensive cofactor requirements (Bala and Chimni, 2010).

However, the need of integrating a biocatalytic synthetic step into existing industrial processes frequently requires the exploitation of thermostable enzymes that do not demand the reaction mixture to be cooled and reheated between the synthetic chemistry and biocatalytic steps, thereby making the whole process cheaper and less time and energy consuming. In addition, thermostable biocatalysts are usually more stable under the process conditions such as the presence of organic solvents which are used to solubilize the substrates. The thermostable biocatalyst can also be used at ambient temperatures with a lower specific activity but for extended reaction times. It can be reused for further reaction cycles and easily recovered if it is immobilized (Vieille et al., 2001; Littlechild, 2015; Zarafeta et al., 2016).

New innovative approaches such as the use of metagenomics for the discovery of new enzymes with improved process performance and broader substrate specificity are being used. This will help to meet the growing demand for more efficient and stable biocatalysts that are more suitable for industrial applications (Singh et al., 2009; Wilson and Piel, 2013; Ferrer et al., 2016).

The metagenomics approach has recently been used to identify some novel enzymes with industrially interesting features (Zhao et al., 2004; Kotik et al., 2009, 2010; Ferrandi et al., 2015b; Berini et al., 2017). For example, BD-EHs, isolated from environmental samples by Zhao and co-workers (Diversa Corporation), that are able to catalyze the desymmetrization of bulky internal epoxides such as *cis*-stilbene oxide and its derivatives (Zhao et al., 2004). Another enzyme, Kau2-EH has been isolated from a bacterial biomass, which was extracted from a bio-filter installed in a sewage disposal plant. This enzyme has shown broad substrate specificity and has been successfully used for the kinetic resolution of racemic α,β-di-substituted aromatic epoxides and for the desymmetrization of *cis*-stilbene oxide resulting in nearly enantiomerically pure diol and epoxide products (Kotik et al., 2010; Zhao et al., 2015). New genes coding for putative EHs have been recently identified in metagenomes collected in the Andean forest soil and mangrove forest soil (Montaña et al., 2012; Jiménez et al., 2015). In our previous work, we have identified two new epoxide hydrolases belonging to the small subfamily of the limonene epoxide hydrolases (LEH, E.C. 3.3.2.8) in the metagenomes of samples collected in hot terrestrial environments (Ferrandi et al., 2015b). These novel LEHs, which differ from the α/β hydrolase fold EHs, have a smaller size, different fold and different catalytic mechanism (Barbirato et al., 1998). They show high thermostability with a melting temperature in excess of 70°C (Ferrandi et al., 2015b) and have been successfully used for the resolution of (+)- and (–)-*cis*/*trans*-limonene oxides at the gram scale (Ferrandi et al., 2015a).

Soluble α/β EHs from a number of mammalian (Argiriadi et al., 1999; Pilger et al., 2015), plant (Mowbray et al., 2006), fungal (Reetz et al., 2009), insect (Zhou et al., 2014) and bacterial (Nardini et al., 1999; Biswal et al., 2008; Kong et al., 2014) sources have been structurally characterized and were found to bear strong resemblance to another family of the Asp nucleophile containing α/β hydrolase enzymes, the haloalkane dehalogenases (Franken et al., 1991; Novak et al., 2014). Many α/β EHs are monomers, however dimers (Reetz et al., 2009; Zhou et al., 2014; cyanobacterium *Nostoc* sp. EH, PDB 3QYJ) and tetramers (Nardini et al., 1999) were also observed. Structural features extending the classical α/β fold are present in fungal and insect EHs (Reetz et al., 2009; Zhou et al., 2014) and soluble dimeric mammalian EHs contain additional domains (Argiriadi et al., 1999; Pilger et al., 2015).

This paper presents the results obtained in the search of EHs of the α/β hydrolase fold class within the metagenomes of samples collected in hot terrestrial environments, which was part of the EU FP7 collaborative project HotZyme (www.hotzyme.com). A

**Abbreviations:** CH65-EH, epoxide hydrolase from the metagenomic DNA from the Chinese sample; *ee*, enantiomeric excess; EH, epoxide hydrolase; LEH, limonene-1,2-epoxide hydrolase; Sibe-EH, epoxide hydrolase from the metagenomic DNA from the Tomsk sample.

bio-informatics search has been carried out from metagenomic samples from a variety of hot springs. Two open reading frames (ORFs) showing good similarity with known EHs have been found in samples collected in Russia and China at 46° and 65°C respectively. The two proteins have been successfully over-expressed in *Escherichia coli* and have been characterized both biochemically and structurally. It has been possible to rationalize the differences observed in their substrate specificity using information obtained from the high resolution X-ray structures.

# MATERIALS AND METHODS

## Chemicals

Diols, racemic and enantiopure epoxides and rhamnose were purchased from Sigma-Aldrich (USA) or Alfa Aesar (Germany). Tryptone and yeast extract were from Sigma-Aldrich (USA). All other reagents were of analytical grade and commercially available.

## Analytical Methods

Gas-chromatographic (GC) analyses to determine enantiomeric excesses of epoxides, diols and conversions were performed on a AGILENT 6850 (Network GC System) gas chromatograph equipped with a chiral capillary column (MEGA DEX DAC-BETA, Italy), having 0.25 mm-diameter, 25 m length and 0.25 μm-thickness, and with a Flame Ionization Detector (FID). The stereochemical outcome of the transformations was expressed as enantiomeric excess (*e.e.*) of the major enantiomer or as enantiomeric ratio (*E*) (Chen et al., 1982).

Analytical conditions, derivatization procedures and retention times of compounds (**1**, **2**), and (**4**)-(**6**) were previously reported (Ferrandi et al., 2015b). For details, see also **Figure S5** (**Supplementary Materials**).

For GC analysis of compound (**3**), the column temperature was raised from 40° to 100°C at 5°C/min, then from 100° to 110°C at 1°C/min and finally from 110° to 200°C at 10°C/min at a 2 ml/min flow rate. Under these conditions retention times were: (**3**), 5.26′; (2*S*,3*S*)-diol, 16.0′; (2*R*,3*R*)-diol, 16.5′. The stereochemical configuration was determined using the commercially available standard (2*R*,3*R*)-diol.

The CD spectra were recorded on a Jasco J-1100 spectropolarimeter interfaced to a personal computer for data collection and manipulation and equipped with a thermostatically controlled cell holder. The spectropolarimeter was calibrated with a D-10-camphorsulfonic acid solution.

The far-UV CD analysis was carried out with purified protein samples dissolved in degassed water (0.15 mg/ml final concentration) in quartz cuvettes with 0.1 cm path length. Spectra were recorded in the range between 180 and 250 nm at 20° or 95°C.

For the determination of apparent melting temperature ($T_M$), unfolding transitions as a function of temperature were monitored by the CD signal at 193 nm or 220 nm varying the temperature as follows:

### Sibe-EH Sample

20°C up to 40°C at 5°C/min_ data pitch each 2°C, hold 30″
40°C up to 70°C at 2.5°C/min_data pitch each 0.5°C, hold 30″
70°C up to 95°C at 5°C/min pitch data each 2°C, hold 30″

### CH65-EH Sample

20°C up to 70°C at 5°C/min_ data pitch each 2°C, hold 30″
70°C up to 90°C at 2.5°C/min_data pitch each 0.5°C, hold 30″
90°C up to 95°C at 5°C/min pitch data each 2°C, hold 30″

## *In silico* Screening of Metagenomes Assemblies

The HotZyme assemblies available on the Galaxy based platform ANASTASIA (Automated Nucleotide Aminoacid Sequences Translational platform for Systemic Interpretation and Analysis) (Menzel et al., 2015) were analyzed by using the ORF finder "getorf" program (http://emboss.bioinformatics.nl/cgi-bin/emboss/getorf) and the resulting ORFs were aligned with the query sequences [GenBank CAA73331.1 (*Agrobacterium radiobacter*-EH), CAB59813.1 (*Aspergillus niger*-EH), ACO95125.1 (kau2-EH), 2CJP_A (*Solanum tuberosum*-EH)] using the program LAST (http://last.cbrc.jp/).

## Enzyme Cloning Into the pJet Vector

The genes coding for Sibe-EH and CH65-EH were amplified using the primers F1/R1 and F2/R2, respectively (see **Table S1**), and the DNA extracted from the corresponding environmental samples as a. template (Ferrandi et al., 2015b; Menzel et al., 2015). The PCR amplification was carried out on 50 μL reaction mixtures containing 100 ng of metagenomic DNA, primers (1 μM each), dNTPs (0.2 mM each), 4 U of XtraTaq Pol and 5 μL of the XtraTaq buffer (both from Genespin, Italy). The PCR conditions were as follows: 95°C for 3 min, followed by 40 cycles at 94°C for 30 s, 50–55°C (according to the primer annealing temperatures) for 30 s, 72°C for 1 min, and then 72°C for 10 min. The genes were cloned in the pJet vector using the CloneJET PCR Cloning Kit (Thermo Scientific, United States) and the resulting plasmids pJetSibe-EH and pJetCH65-EH were transformed into *E. coli* TOP 10 (Invitrogen, United States) using standard techniques (Sambrook and Russell, 2001). The two plasmids were purified by using the HiSpeed Plasmid Midi Kit from Qiagen (Germany) and the cloned PCR amplicons were sequenced on both strands by Bio-Fab Research (Italy) using the primers F8/R8 (**Table S1**).

## Enzyme Expression and Purification

Sibe-*eh* and CH65-*eh* genes were amplified using pJetSibe-EH and pJetCH65-EH as template, respectively. Primers F3/R3 and F4/R4 (**Table S1**) suitable for the cloning of EH genes in the pRham expression vector (*Expresso* Rhamnose Cloning and Protein Expression kit, Lucigen), were used for PCR gene amplifications under the PCR conditions described above. The PCR products were cloned in the pRham vector giving pRhamSibe-EH and pRhamCH65-EH plasmids respectively, and transformed in *E. coli* 10G. pRhamSibe-EH and pRhamCH65-EH were purified using the HiSpeed Plasmid Midi Kit from Qiagen (Germany) and subsequently transformed in *E. coli*

BL21 codon plus RIPL competent cells (Agilent Technologies, United States) according to manufacturer instructions.

The transformants obtained were grown in LB supplemented with 30 μg $mL^{-1}$ kanamycin ($LB_{kan30}$) medium (50 mL) overnight and then inoculated in 0.5 L LB $_{kan30}$ at 37°C and 220 rpm. When the $OD_{600}$ reached 0.3–0.6, gene expression was induced by the addition of 5 mL 20% rhamnose solution (w/v in water) and the culture was maintained at 30°C for 24 h. Then cells were harvested by centrifugation (5,000 rpm for 30 min), resuspended in 20 mL of wash buffer (20 mM potassium phosphate (KP) buffer, pH 7.0, 500 mM NaCl, 20 mM imidazole) and disrupted by sonication. In the case of CH65-EH, another expression trial was carried out lowering the culture incubation temperature to 17°C after induction of protein expression and the cells were harvested after 72 h.

Recombinant EHs were subsequently purified using a Nickel Sepharose 6 Fast Flow agarose resin (Ni-NTA) (GE-Healthcare, Italy) as follows. The cell extract, recovered by centrifugation (10,000 rpm for 30 min) after cell lysis, was incubated with the Ni-NTA resin for 1 h at 4°C with mild shaking and loaded onto a glass column (10 × 110 mm). The resin was then washed with 10 mL of wash buffer and His-tagged EHs were eluted using a 3 step gradient (10 mL washing buffer containing 100, 200, and 300 mM imidazole, respectively) and dialyzed against 20 mM KP buffer, pH 7.2, at 4°C. The protein content was measured using the Bio-Rad Protein Assay according to the Bradford method and the protein purity was verified by SDS-PAGE analysis (10% T, 2.6% C).

Due to unsatisfactory results obtained using the metagenome-derived CH65-*eh* gene, the codon-optimized CH65-*eh* gene was synthesized and cloned into the pUC57 vector obtaining pUC-CH65-EHopt by BaseClear (Leiden, The Netherlands). The CH65-*eh* codon optimized gene was then amplified using the primers F5/R5 (**Table S1**) and pUC-CH65-EHopt as a template for the suitable cloning into the pETite vector. Gene amplification was carried out under the PCR conditions described above and PCR products were cloned into the pETite vector and transformed into the *E. coli* Hi control 10 G using the *Expresso* T7 Cloning and Expression kit from Lucigen. The resulting plasmid pETiteCH65-EHopt was purified and transformed into *E. coli* BL21(DE3) containing the plasmid pG-Tf2 (Takara Bio Inc., Kyoto, Japan) that allows co-expression of the target protein with the chaperone proteins GroES and GroEL.

Transformants were grown overnight in 50 mL of LB medium supplemented with 30 μg $mL^{-1}$ kanamycin and 20 μg $mL^{-1}$ chloramphenicol ($LB_{kan30cam20}$) and then inoculated in 0.5 L $LB_{kan30cam20}$ medium containing 5 ng $\mu L^{-1}$ tetracycline for induction of chaperon proteins at 37°C. Subsequently, when the cell density reached $OD_{600}$ 0.4–0.6, the gene expression was induced by the addition of 1 mL solution of IPTG (1 M in water) and the culture was incubated at 30°C. The cells were harvested by centrifugation (5,000 rpm for 30 min) 24 h after induction, resuspended in 20 mL of wash buffer (see above), and lysed by sonication. The CH65-EH was purified as described above.

## Enzyme Characterization

Hydrolysis of epoxides (**1**)-(**6**) was performed with the purified Sibe-EH [0.25 mg for the hydrolysis of (**1**), (**2**), (**4**), 0.5 mg for the hydrolysis of (**3**), 0.05 mg for the hydrolysis of (**5**), 0.125 mg for the hydrolysis of (**6**)] or with the purified CH65-EH [0.5 mg for the hydrolysis of (**1**-**4**) and (**6**), 0.01 mg for the hydrolysis of (**5**)] in 1 mL 25 mM KP buffer, pH 8.0, 10% (v/v) $CH_3CN$, containing 10 mM substrate, at 20°C (SibeEH) or 45°C (CH65-EH). At scheduled times, samples (50 μL) were extracted with an equal volume of a 0.025 mg/mL benzophenone solution in AcOEt in the presence of saturating NaCl and analyzed by chiral GC analyses. The substrates and products peak area were normalized to the internal standard benzophenone and concentrations were calculated using calibration curves obtained with authentic substrate/product standards (2.5–20 mM). One unit of activity (U) is defined as the enzyme activity that hydrolyzes 1 μmol of substrate per min under the assay conditions described above.

The evaluation of the influence of temperature on Sibe-EH activity and CH65-EH were determined by assaying the hydrolysis of (**2**) at a temperature ranging from 20° to 90°C.

The thermal stability was evaluated by incubating purified Sibe-EH or CH65-EH samples at different temperatures (20–70°C) for 3 h, then assaying the residual activity using (**2**) as a substrate under the above described conditions.

## Crystallization and Structure Solution

Prior to crystallization both the purified Sibe-EH and CH65-EH were applied to a calibrated Superdex 200 HiLoad 16/60 size exclusion column (GE Healthcare) and were eluted with one column volume of a buffer of 25 mM Tris-HCl, pH 7.5, 0.1 M NaCl at 1.0 ml/min.

The Sibe-EH and CH65-EH were then concentrated to ∼15 mg/ml and ∼30 mg/ml respectively using a 10 kDa membrane Vivaspin (Vivaproducts) and microbatch crystallization trials were set up using an Oryx6 crystallization robot (Douglas Instruments) using the JCSG Screen+™, SG1™ Morpheus™ (Molecular Dimensions) protein crystallization screens. The droplet contained a 50:50 ratio of protein solution to screen and was covered with Al's oil (50:50 mix of silicon and paraffin oils) before being stored at 20°C.

Sibe-EH native crystals appeared within 1 week in the majority of the conditions of the Morpheus screen. The crystals were harvested straight from the crystallization droplet and plunged into liquid nitrogen. Preliminary data were collected to 2.4 Å resolution at 100 K on the Diamond beamline I03. Further crystals grown from 0.1 M Sodium HEPES, MOPS buffer pH 7.5, 12.5% v/v methyl pentanediol (MPD), 12.5% w/v PEG 1,000, 12.5 % w/v PEG 3350 diffracted to a higher resolution of 1.7 Å in the same space group on the Diamond beamline I04 and these data were used for final refinement.

The CH65-EH native crystals appeared within 1 week. The best crystals grew in 0.2 M magnesium formate dehydrate, 100 mM sodium HEPES pH 7.5 20% w/v PEG 3350 and were cryocooled in liquid nitrogen using a cryoprotectant consisting of 0.2 M magnesium formate dehydrate, 0.1 M sodium chloride, 0.1 M sodium HEPES pH 7.5, 16% w/v PEG 3350, 30% v/v PEG 400.

The Sibe-EH and CH65-EH crystals diffracted to 1.6 Å and 1.4 Å, respectively on the beamlines I03 and I04 at the Diamond Synchrotron light source (Didcot, United Kingdom) at 100 K in a stream of gaseous nitrogen using a Pilatus detector (Dectris). Data were processed and scaled using XDS (Kabsch, 2010) and AIMLESS (Evans and Murshudov, 2013) in the Xia2 pipeline (Winter et al., 2013). All further data and model manipulations were carried out using the CCP4 suite of programs (Winn et al., 2011). The Sibe-EH crystals belonged to the spacegroup $C222_1$ with unit cell parameters $a = 41.2$, $b = 84.2$, $c = 157.5$Å, $\alpha = \beta = \gamma = 90^\circ$ and the CH65-EH crystal belonged to the spacegroup C2 with unit cell parameters $a = 163.9$, $b = 46.2$, $c = 73.9$ Å, $\alpha = \gamma = 90^\circ$ $\beta = 106.9^\circ$.

The Sibe-EH structure was solved using the epoxide hydrolase from *Bacillus megaterium* (31% sequence identity; PDB: 4INZ; Kong et al., 2014) using Molrep (Vagin and Teplyakov, 2010) with its sequence-based model modification option (Lebedev et al., 2008). The rotation function gave a clear peak of 8.7 σ with a background of 4.9 σ or lower and a translation peak of 8.2 σ with a background of 3.5 σ. The resulting structure was subjected to refinement in REFMAC5 (Murshudov et al., 2011) and rebuilding in COOT (Emsley et al., 2010; **Table 2**). The structure of CH65-EH was solved by the molecular replacement pipeline MORDA (Lebedev and Vagin, 2015) with PDB 4INZ (35% sequence identity) being the best model.

## Molecular Modeling

For both Sibe-EH and CH65-EH structures, the chain A of each structure was used in the ligand docking experiments. The protein structures were initially prepared using the Protein Preparation Wizard (Sastry et al., 2013) in the Schrödinger Maestro release 2017-1 (Schrödinger). All rigid (rigid protein, flexible ligand) and flexible (flexible protein side chains, flexible ligand) dockings were carried out using AutoDock Vina version 1.1.2 (Trott and Olson, 2010). The receptors and ligands PDBQT files, required by the docking program, were generated using AutoDockTools (Morris et al., 2009). In rigid docking experiments, the two cavities around the Asp101, Tyr148, and Tyr209 for CH56-EH and Asp102, Tyr150, and Tyr209 for Sibe-EH were chosen as the binding sites of the ligands. In all rigid docking experiments, exhaustiveness of the global search was set to 100, maximum number of binding modes was set to 20, and the energy range was set to 10.

In flexible docking experiments, side chains of residues surrounding the potential substrate binding site of the two enzymes were set to be flexible. These include the residues Phe34, Asp101, Trp102, Tyr148, Tyr209, Ala243, Ile244, His270 for CH65-EH, and Asp102, Trp103, Tyr150, Tyr209, Asp249, Ala251, Leu252, His277 for Sibe-EH. The ligand binding sites for the AutoDock Vina docking experiments were chosen to be large enough to include all of the flexible residues and the two binding site cavities. In all rigid docking experiments, exhaustiveness of the global search was set to 8, maximum number of binding modes was set to 20, and the energy range was set to 10.

Docking results were visualized and analyzed using the ViewDock tool in UCSF Chimera (Pettersen et al., 2004) and in COOT (Emsley et al., 2010). The best ligand docking poses were chosen according to their binding affinities as reported by AutoDock Vina, and also according to their configurations in relation to the binding site residues.

The programs CAVER (Chovancova et al., 2012; Kozlikova et al., 2014; Pavelka et al., 2015) and UCSF Chimera were used for the analysis and visualization of the active sites tunnels and surfaces. For the calculation and visualization of tunnels and surfaces using CAVER and UCSF Chimera programs, probes with a radii of 1.1 and 1.4 Å were used. Additional ligand and transient state models were generated by JLIGAND (Lebedev et al., 2012).

# RESULTS AND DISCUSSION

## Discovery of New EH Homologs

When the metagenomic ORFs identified in the HotZyme project were aligned with the amino acid sequences of the well characterized α/β EHs from *Agr. radiobacter*, *B. megaterium*, *Asp. niger*, and *S. tuberosum*, as well as the metagenome derived enzyme Kau2-EH, two ORFs showed good similarity. These were found in the metagenomes of samples collected at 46° and 65°C in the West Siberian Plain of Russia (Tomsk sample) and in the Yunnan region of China (Ch2-EY65S sample), respectively, at around neutral pH. It is worth noting that the new EH α/β class homologs were identified in the same two environments, where we had previously isolated the LEHs which belong to a different structural family (Ferrandi et al., 2015b). These environments were characterized by moderate temperature and neutral pH. As in the case of the LEH search, no EH homologs were found in samples collected at higher temperatures, suggesting that under extreme conditions EHs are not required in hyperthermophilic organisms since the epoxides used as substrates for these enzymes would spontaneously hydrolyse. A detailed description of the Tomsk and Ch2-EY65S sampling sites has been previously reported (Ferrandi et al., 2015b; Menzel et al., 2015).

The ORF found in the Chinese metagenomic DNA sample (CH65-*eh*) consists of 879 nucleotides and encodes for a protein (CH65-EH) of 293 amino acids. According to the BLAST analysis, this protein shows the highest similarity to a α/β hydrolase from *Nitrosomonas marina* (GenBank WP_090634503.1) (50% identity and 99% query cover sequence at the deduced amino acid level) and presents 35% identity with the EH from *B. megaterium* (Zhao et al., 2011).

The ORF found in the Russian metagenome (Sibe-*eh*) is 891 nt long and encodes for a protein (Sibe-EH) of 297 amino acids that has 30% identity with the CH65-EH protein sequence. The closest relative of Sibe-EH is an α/β hydrolase from *Porphyrobacter* sp. LM 6 (GenBank WP_083234595.1) showing 92% identity and 100% query cover sequence at the deduced amino acid level. Such a high identity suggests that the organism that expresses Sibe-EH may be a bacterium that belongs to the genus *Porphyrobacter*. When compared to other functionally characterized bacterial EHs, the highest similarity shown by Sibe-EH was again with *B. megaterium*-EH (32% identity) (Zhao et al., 2011). A Pfam-A database analysis confirmed that the two new EH homologs belong to the α/β hydrolase superfamily. A sequence alignment with related EH homologs shows the expected conservation of

the amino acids of the catalytic triad (Asp-His-Asp), as well as of the two tyrosine residues involved in the epoxide ring opening, and of the EH conserved motif HGXP (the oxyanion hole) (**Figure 1**; Van Loo et al., 2006). In contrast the previously reported conserved motif GXSmXS/T (where X is usually an aromatic amino acid and Sm is a small amino acid such as Gly, Ala or Cys) was only partially conserved since the basic amino acid, arginine, R64, was present in Sibe-EH and an asparagine residue, N63, in CH65-EH at the Sm position. It is worth noting that an asparagine residue is also present at this position in *B. megaterium*-EH (Zhao et al., 2011). **Figure S1** shows a phylogenetic analysis for Sibe-EH and CH65-EH in relation to selected known EHs.

## Expression Trials and Purification of EHs

The genes CH65-*eh* and Sibe-*eh* were successfully cloned in the pRham expression vector in frame with the C-terminal His6x-tag sequence under the control of the L-rhamnose inducible promoter. A rare Codon Calculator (RaCC, http://people.mbi.ucla.edu/sumchan/caltor.html) analysis of CH65-*eh* and Sibe-*eh* (see **Doc S1**) revealed that both genes contained codons that are rarely recognized by tRNAs in *E. coli* which is a potential problem for good expression yields of heterologous proteins in this host. For this reason, *E. coli* BL21 codon plus RIPL, a strain containing two plasmids that encode for rare tRNAs that recognize the rare codons for Arg, Ile, Pro, and Leu, was chosen as host for the expression of CH65-*eh* and Sibe-*eh*.

The His-tagged Sibe-EH fusion protein was successfully over-expressed in soluble form in *E. coli* BL21 codon plus RIPL and purified from the cell extracts by $Ni^{2+}$-NTA affinity chromatography with an excellent recovery yield (288 mg $L^{-1}$) (see **Figure S2**).

On the contrary, very low levels of expression were observed for the His-tagged CH65-EH fusion protein using the same host. Moreover, this recombinant protein formed insoluble aggregates within the *E. coli* cells and almost no soluble protein was observed in the cell free extracts as shown by SDS-PAGE analysis. Lowering of the culture incubation temperature to 17°C after induction of protein expression did not prevent the formation of the inclusion bodies and little soluble protein was detected (data not shown).

To improve the recombinant production of CH65-EH in *E. coli*, a codon optimized CH65-*eh* synthetic gene (BaseClear) was cloned into the pETite (Lucigen) vector under the control of the strong IPTG inducible T7 promoter. Moreover, to tackle the previously observed solubility issues, the gene was expressed in *E. coli* BL21(DE3) containing the plasmid pG-Tf2 (Takara Bio Inc.) which allows the co-expression of the target protein with the chaperon proteins GroES and GroEL. This improved the expression and the solubility of the His-tagged CH65-EH (see **Figure S3**) resulting in a yield of 50 mg $L^{-1}$ of pure enzyme after purification by $Ni^{2+}$-NTA chromatography.

## Characterization of EHs

The substrate specificity of the novel EHs was carried out by evaluating the conversion of a set of structurally different epoxide substrates (**Figure 2**) after 24 h under standard reaction conditions (0.5 mg $mL^{-1}$ of purified EHs, 20°C). The Sibe-EH was active on all tested substrates resulting in conversions > 99% for substrates (**2**), (**5**), and (**6**), around 90% for substrates (**3**) and (**4**), and around 40% for substrate (**1**) (**Figure 3**). The CH65-EH showed a preference for substrates (**4**) and (**6**) (conversions >60%) and in particular for substrate (**5**) (conversion > 99%), while negligible activity was shown on substrates (**1**) and (**3**).

The overall thermostability of the two novel EH enzymes was investigated by far UV Circular Dichroism (CD) spectra at temperatures of 20° and 95°C to monitor any conformational changes of the enzyme secondary structures. This showed that at 95°C the far UV CD spectrum of Sibe-EH (see **Figure S4**) is significantly different from the spectrum recorded at 20°C. In contrast, the comparison of the far UV CD spectrum of CH65-EH at 95°C and at 20°C suggests only partial unfolding at 95°C. The higher thermostability of CH65-EH in relation to Sibe-EH was subsequently confirmed by determining the apparent $T_M$ of the two enzymes by the thermal shift CD analysis. The Sibe-EH showed the behavior of a moderately thermophilic enzyme with an apparent $T_M$ of 55°C, while CH65-EH showed higher thermal stability with an apparent $T_M$ of 85°C, which is, to our knowledge, the highest $T_M$ recorded for a wild-type EH to date.

When the thermostability of Sibe-EH and CH65-EH was further investigated by incubating the enzymes for 3 h at temperatures ranging from 20° to 90°C and then assaying the hydrolysis of compound (**2**) by the two heat-treated enzymes (**Figure 4A**) the results were in agreement with those obtained from CD and thermal shift analysis. The CH65-EH was significantly more thermostable than Sibe-EH, with no decrease of activity after incubation at temperatures of 60°C and retaining about 80% of the initial activity after thermal treatment at 70°C, while Sibe-EH was relatively stable at temperatures below 40°C and was able to retain 10% of initial activity after incubation at 60°C.

The temperature dependence of EH activity of both enzymes was evaluated by carrying out the hydrolysis of compound (**2**) at temperatures ranging from 20 to 90°C, pH 8.0. As shown in **Figure 4B**, Sibe-EH displayed an optimum temperature at 30°C and retained more than 40% of activity at 40°C, while CH65-EH showed the highest activity at temperatures around 50°C and retained more than 60% of activity at 70°C.

Subsequently, considering the different optimal temperatures, the specific activity and selectivity of the recombinant EHs was assessed at 30° and 45°C for Sibe-EH and CH65-EH, respectively, using chiral GC analyses of the hydrolysis reactions of the epoxide substrates (**1**)-(**6**) (**Figure 2**, **Table 1**).

When investigating the stereoselective hydrolysis of the *meso*-epoxides (**1**)-(**3**), both Sibe-EH and CH65-EH hydrolysed compound (**2**) with comparable velocity and stereoselectivity (**Table 1**). However, compounds (**1**) and (**3**) were hydrolysed only by Sibe-EH, which additionally showed an excellent stereoselectivity [>99% enantiomeric excess ($ee_p$)] for the synthesis of the (2*R*,3*R*)-diol from the achiral starting compound (**3**). Although highly enantioselective variants have been recently obtained by protein engineering (van Loo et al., 2009; Zheng and Reetz, 2010), to our knowledge this is the best result that has been obtained with a wild-type EH for the enantioselective hydrolysis of compound (**3**) to give the corresponding (2*R*,3*R*)-diol. The best

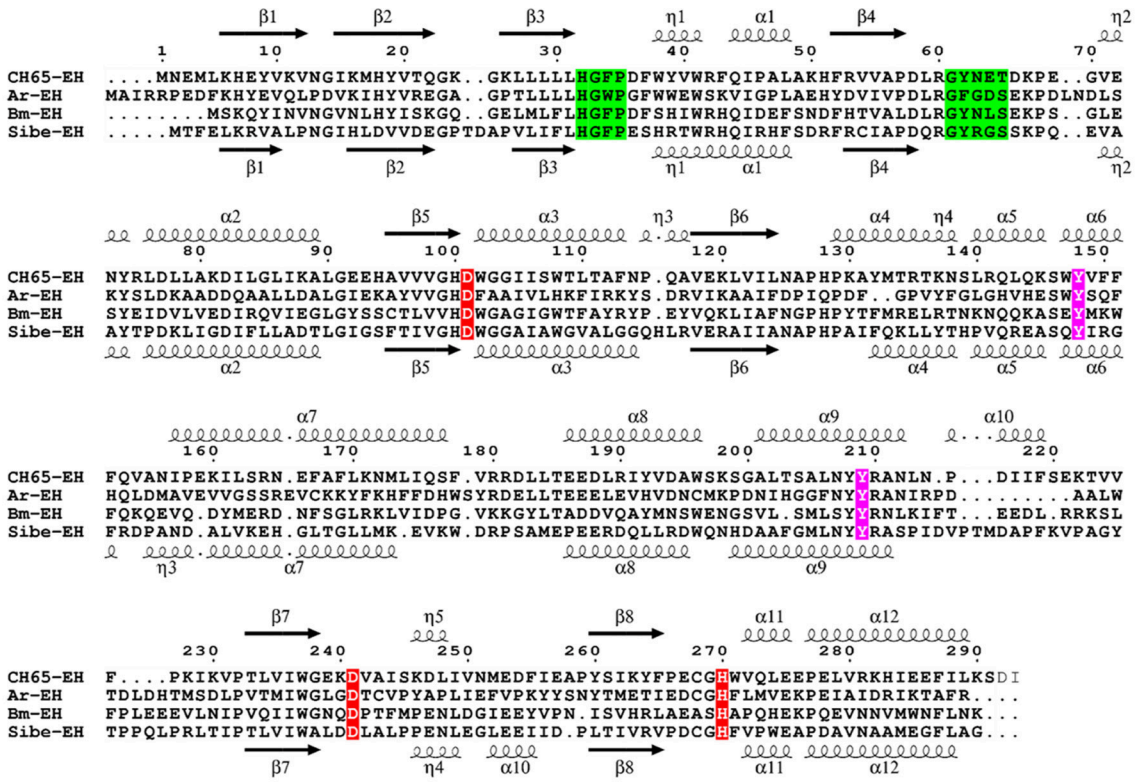


**FIGURE 1 |** Multiple sequence alignment of Sibe-EH and CH65-EH with *Agr. radiobacter* EH (*Ar*-EH) and *B. megaterium* EH (*Bm*-EH). Arrows indicate β-strands, and helical curves denote α-helices of the structure of CH65-EH above and Sibe-EH below. The three putative active site residues (D/H/D) are marked in red. Ring opening tyrosines are shown in purple. The conserved HGXP and GXSmXS/T motifs are highlighted in green. The figure was prepared with ESPript3 (Robert and Gouet, 2014).

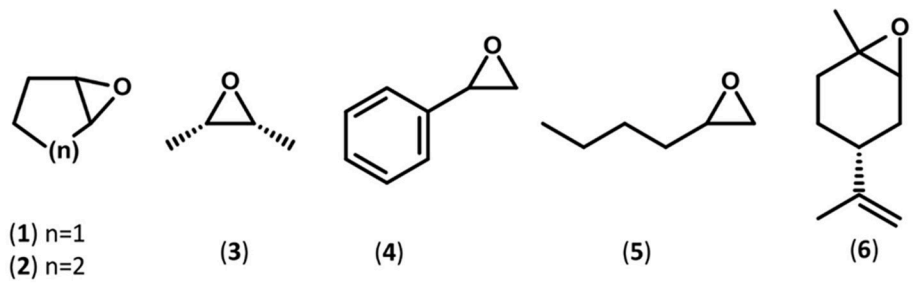


**FIGURE 2 |** Schematic representations of the substrates used in this study.

results that had been obtained previously were with whole cells of *Rhodotorula glutinis* CIMW 147 which achieved the formation of the (2*R*,3*R*)-diol with 90% $ee_p$ (Weijers, 1997).

The specific activity and enantioselectivity of the two enzymes were also compared in the kinetic resolution of compounds (**4**)-(**5**). As shown in **Table 1**, compound (**4**) was hydrolysed by both enzymes with similar velocity and no selectivity, while CH65-EH hydrolysed compound (**5**) four times faster than Sibe-EH, with both enzymes showing very low enantio-preference for the (*R*)- enantiomer. The preference showed by both enzymes for the hydrolysis of compound (**5**) compared to compound (**4**) [the specific activity for compound (**5**) is two orders of magnitude higher than the specific activity for compound (**4**)] could be due to the absence of the aromatic ring in substrate (**5**).

Finally, the two new EHs were also tested for the hydrolysis of the mixture of *cis* (1*R*,2*S*,4*R*) and *trans* (1*S*,2*R*,4*R*) isomers of (+)-limonene oxide [compound (**6**), i.e., the natural substrate of limonene EHs (LEHs)]. Surprisingly, although EHs belonging to the α/β superfamily and LEHs represent two completely distinct enzyme classes with different structures and catalytic mechanisms, both the new EHs were able to efficiently hydrolyse compound (**6**) forming (1*S*,2*S*,4*R*)-limonene-1,2-diol as the only

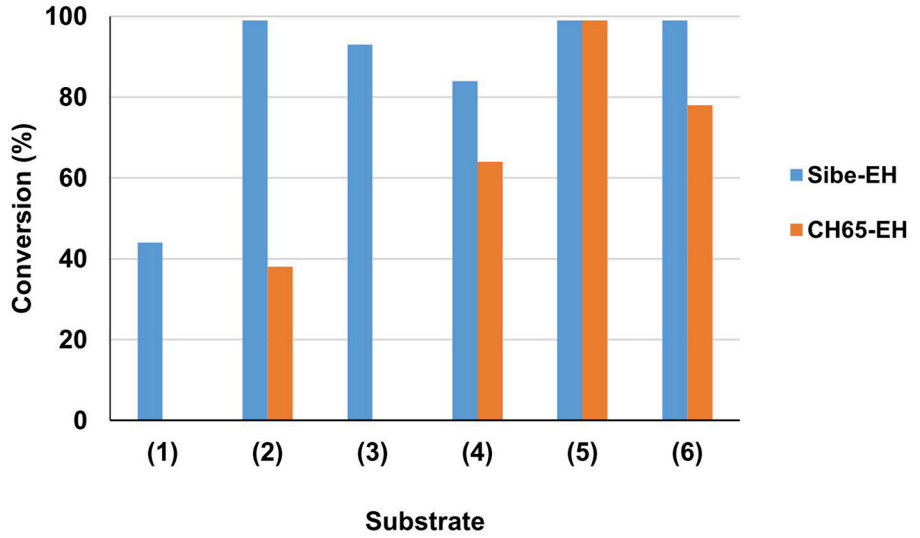


**FIGURE 3 |** Preliminary investigation of EHs substrate specificity. Reactions were carried out in 25 mM KP buffer, pH 8.0, 10% (*v/v*) $CH_3CN$ containing 0.5 mg of purified EH, 10 mM substrate (**1**–**6**) in 1 ml total volume, at 20°C. Substrate conversion was evaluated by GC analysis after 24 h.

product through the same enantio-convergent process previously described for LEHs (Van Loo et al., 2006). Moreover, Sibe-EH showed an almost exclusive preference for the *trans* isomer, which was hydrolysed in the first hour of the reaction leaving the *cis* isomer untouched and was even more efficient than the previously described Tomsk-LEH and CH65-LEH in the enantioselective hydrolysis of (**6**). In fact, the specific activity for the hydrolysis of the *trans* isomer (1,628 $U \cdot g^{-1}$, **Table 1**) was significantly higher than those shown by LEHs (Tomsk-LEH: 220 $U \cdot g^{-1}$; CH55-LEH: 400 $U \cdot g^{-1}$) (Ferrandi et al., 2015b).

This is the first time that the hydrolysis of compound (**6**) has been described to be catalyzed by epoxide hydrolases belonging to the α/β superfamily. In fact, to our best knowledge, hydrolysis of this compound has only been verified using either a LEH or whole cell biotransformations such as cultures of *R. glutinis* CIMW147 (Weijers, 1997) without investigating whether the EH responsible for the hydrolysis of (**6**) was a LEH or not.

## X Ray Structure Quality

The structures of both Sibe-EH and CH65-EH have been determined and refined to a high resolution of 1.6 and 1.4 Å, respectively (**Figure 5** shows the quality of the CH65-EH electron density and crystallographic values are shown in **Table 2**). All residues of Sibe-EH plus one His residue belonging to the C-terminal His tag have been modeled into the electron density. Residues 1–2 and 231–233 of Sibe-EH have been modeled with alternative conformations of the main chain. The amino acids Pro36 and Pro266 are in the *cis*- conformation in the Sibe-EH structure. Residues Arg64, His117 and the catalytic Asp102 of Sibe-EH are in a generously allowed conformation regions of the Ramachandran plot as defined by PROCHECK (Laskowski et al., 1993). Residues 2–293 were modeled in monomer A and 2–291 in monomer B out of the total 293 in the CH65-EH sequence with the C-termini having different conformations in monomers A and B beyond residue Ile288. The amino acid residues 253–255 and 157–258 in monomer A and 12–14 in monomer B of CH65-EH were modeled with alternative conformations of the main chain. The Pro35 is in the *cis*- conformation in both monomers of CH65-EH. The residues Asn63 and Asn156 are Ramachandran plot outliers in both monomers of CH65-EH with Phe37 and the catalytic Asp101 of both monomers in the generously allowed regions of the Ramachandran plot.

## EH Structure

The overall monomer structures of both Sibe-EH and CH65-EH are similar to the structures of other α/β-hydrolases (the monomer of Sibe-EH is shown in **Figure 6**), consisting of a catalytic α/β domain built around an eight stranded β-sheet with connectivity 1,2,-1x,2x,1x,1x,1x and direction +-+ + + + ++ (Richardson, 1981) and an α-helical cap domain that forms a cap over the active site. The key active site residues are highly conserved with previously known epoxide hydrolase enzymes of the α/β hydrolase fold family such as the *B. megaterium* EH (Kong et al., 2014) which shares 35% amino acid sequence identity with both EHs.

Sibe-EH is monomeric in the crystal structure and in solution which is similar to many other bacterial EHs and plant, such as potato, EHs (Mowbray et al., 2006). CH65-EH forms a dimer in solution according to its elution profile on the size exclusion chromatography column and in the crystal structure, as suggested by PISA (Krissinel and Henrick, 2007). Within the formation of the dimer of CH65-EH (shown in **Figure 7**) 1,090 $Å^2$ or 9% of the available surface area of the monomers is buried. The dimer interface is formed by the cap domains of the two monomers as shown in **Figure 7**. The interactions on the dimer interface are mainly hydrophobic (**Figure 8**) although several H-bonds are also formed upon dimer formation.

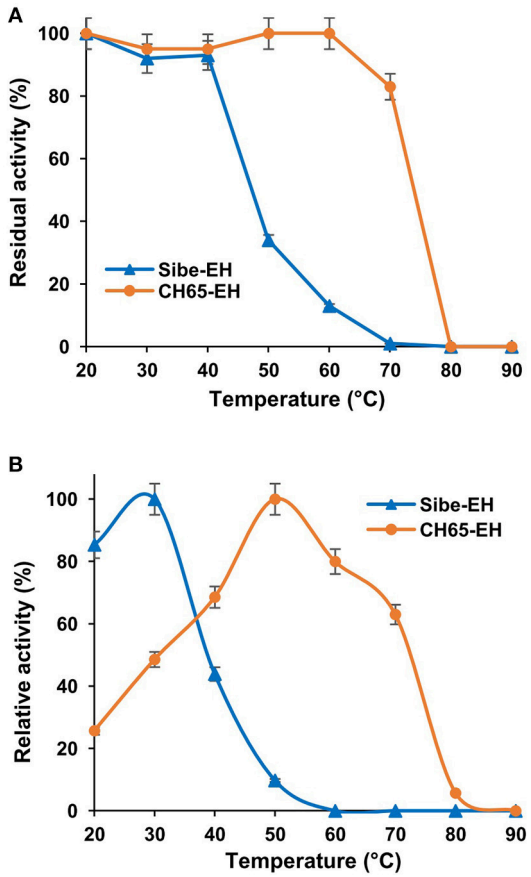


**FIGURE 4 | (A)** The effects of temperature on stability of the Sibe-EH (blue triangles) and CH65-EH (orange circles) **(B)** The effects of temperature on enzymatic activity of the Sibe-EH (blue triangles) and CH65-EH (orange circles).

**TABLE 1 |** Substrate scope and selectivity of Sibe-EH and CH65-EH.

| Substrate | Sibe-EH[a] | | CH65-EH[a] | |
|---|---|---|---|---|
| | Specific activity ($U \cdot g^{-1}$) | Selectivity[b] | Specific activity ($U \cdot g^{-1}$) | Selectivity[b] |
| (**1**) | 12 | $ee_p$ (%) = 66 (*1R,2R*) | n.d.[c] | – |
| (**2**) | 80 | $ee_p$ (%) = 80 (*1R,2R*) | 68 | $ee_p$ (%) = 85 (*1R,2R*) |
| (**3**) | 107 | $ee_p$ (%) ≥ 99% (*2R,3R*) | n.d.[c] | – |
| (**4**) | 71 | *E* = 1 | 87 | *E* = 1 |
| (**5**) | 1730 | *E* = 5 (*R*) | 6,359 | *E* = 2 (*R*) |
| (**6**)[d] | 1628<br>n.d.[c] | (*trans*)<br>(*cis*) | 95<br>34 | (*trans*)<br>(*cis*) |

[a] *Reactions catalyzed by Sibe-EH were performed at 30°C, while reactions catalyzed by CH65-EH were performed at 45°C.*
[b] *selectivity is indicated as enantiomeric excesses of the products ($ee_p$) in the case of meso-epoxides (**1**–**3**), and E values in the case of the racemic substrates (**4**–**5**).*
[c] *n.d., not detected.*
[d] *substrate (**6**) is a commercially available mixture of cis and trans isomers of (4R)-limonene-1,2-epoxide.*

Known multi-domain mammalian murine and human EHs (Argiriadi et al., 1999; Pilger et al., 2015) form a dimer where both domains are involved in adjacent monomer interactions. The main contact is via the formation of an inter-subunit β-sheet involving strands β1 of the EH domains of both monomers. Interestingly, this inter-subunit β-sheet is preserved in the crystal structure of a truncated single domain human EH (Thalji et al., 2013) which is reported to be a monomer. The *Agr. radiobacter* EH is reported to be a monomer, although in its crystal structure four monomers form a tetramer with point group symmetry 222 and around 10% of the accessible surface area is buried upon tetramer formation, suggesting the possibility of a stable tetramer in solution. None of the monomer contacts within the *Agr. radiobacter* EH structure are similar to the interactions within the CH65-EH dimer. The *Nostoc* sp. EH (pdb 3QYJ), *Asp. niger* EH (Reetz et al., 2009) and insect EH from the silkworm *Bombyx mori* (Zhou et al., 2014) all form dimers via interactions of the cap domain, similar to those in CH65-EH, however the relative orientation of the monomers differs between these different EH dimers.

The nucleophile Asp102 in Sibe-EH (Asp101 in CH65-EH), is complemented by His277 and Asp249 (His270 and Asp241) to form a catalytic triad. The oxyanion hole is formed by the main chain nitrogen's of Phe35 and Trp103 (Phe34 and Trp102 in CH65-EH). Phe35 is followed by a *cis*-Pro residue conserved in other known EHs. The epoxide oxygen is co-ordinated by the side chain hydroxyls of Tyr150 and Tyr209 (Tyr148 and Tyr209 in CHE65-EH) where the tyrosine residues are located on the two adjacent helices of the cap domain.

Since the catalytic triad residues and most other residues implicated in the EH catalysis are conserved between eukaryotic and bacterial EHs it appears that the overall shape of the catalytic funnel and the precise positioning of the catalytic residues are important to explain the differences in substrate specificity.

All EH enzymes have a deep and hydrophobic active site cavity on the interface of the two domains (Kong et al., 2014). The volumes of the active site cavities were calculated using the program CASTp (Tian et al., 2018) with a probe radius of 1.4 Å. These are 239 $Å^3$ in CH65-EH and 215 $Å^3$ in Sibe-EH. Although the active site cavities of CH65-EH and Sibe-EH appear to have the same regions as described for other EHs (**Figure S6**), their funnel entrance to the active site cavity is located in a different position in relation to other known bacterial and mammalian EHs. The *B. megaterium* EH has a large open active site entrance to allow easy access of the substrate to the catalytic residues, compared to the human EH and *Agrobacterium* EH which have smaller active site funnel entrances at the same location. In the case of CH65-EH and Sibe-EH the entrance to the active site cavity as seen in *B. megaterium* EH is totally obstructed by the adjacent monomer in the CH65-EH dimer and by a very different conformation in Sibe-EH in the region of residues 159–180. Instead, there is a separate small active site entrance funnel on the other side of protein monomer (**Figure 9**). The position of

**TABLE 2 |** Summary of data processing and refinement statistics.

| | Sibe-EH | CH65-EH |
|---|---|---|
| Diffraction source | I04, I03, Diamond | I04, I03, Diamond |
| Wavelength (Å) | 0.9795 | 0.9795 |
| Space group | $C222_1$ | C2 |
| *a*, *b*, *c* (Å) | 41.20, 84.18, 157.45 | 163.94, 46.22, 73.87 |
| α, β, γ (°) | 90.0, 90.0, 90.0 | 90.0, 106.9, 90.0 |
| Resolution range (Å) | 39.36–1.60 (1.64–1.60)[a] | 39.53–1.39 (1.41–1.39) |
| Number of unique reflections | 35.698 (2,070) | 104,819 (4,187) |
| Completeness (%) | 97.4 (78.3) | 98.2 (79.0) |
| Average redundancy | 6.0 (4.1) | 3.2 (2.5) |
| $<I/\sigma(I)>$ | 9.5 (1.3) | 15.6 (1.2) |
| $R_{sym}$ (%)[b] | 10.6 (101.5) | 3.5 (77.0) |
| $CC^c_{1/2}$ | 0.996 (0.516) | 99.9 (48.2) |
| Overall *B* factor from Wilson plot (Å$^2$)[c] | 26.9 | 24.9 |
| $R_{fact}$ (%) | 16.2 | 17.3 |
| $R_{free}$ (%) | 19.8 | 20.4 |
| Refined protein atoms | 2,635 | 5,401 |
| Refined solvent atoms | 386 | 645 |
| Average B factor (Å$^2$) | | |
| Protein | 19.8 | 23.5 |
| Solvent | 37.1 | 35.5 |
| R.m.s.d. bond lengths (Å) | 0.011 | 0.013 |
| R.m.s.d. bond angles (°) | 1.42 | 1.64 |
| Ramachandran plot analysis, residues in (%)[e] | | |
| Most favored regions | 89.8 | 91.2 |
| Additional allowed regions | 8.9 | 7.3 |
| Generously allowed regions | 1.2 | 0.8 |
| Disallowed regions | 0 | 0.8 |

[a] *Values for the highest resolution shell are given in parentheses.*
[b] $R_{sym} = \Sigma_h \Sigma_i |I_{h,i} - <I_h>| / \Sigma_h \Sigma_i I_{h,i}$.
[c] $CC_{1/2}$ *is defined in Karplus and Diederichs (2012).*
[d] *Wilson B-factor was estimated by SFCHECK (Vaguine et al., 1999).*
[e] *Ramachandran plot analysis was performed by PROCHECK (Laskowski et al., 1993).*

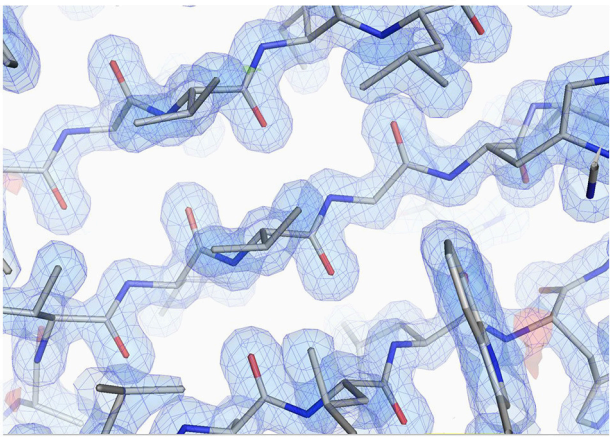

**FIGURE 5 |** The quality of the electron density from the CH65-EH in the β-sheet region. The 2Fo-Fc map is shown in blue at a level of 1.3 σ. The Fo-Fc map is shown at 3.0 σ level (green) and −3.0 σ level (red). Figure was prepared using PyMOL (DeLano, 2002).

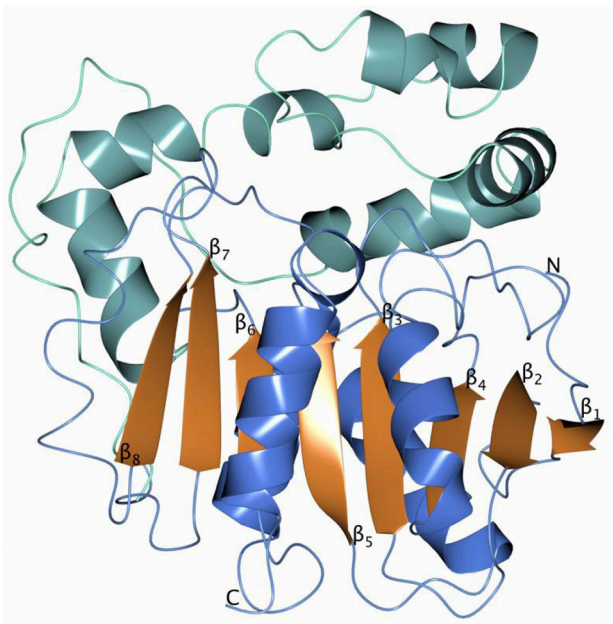


**FIGURE 6 |** A cartoon diagram of the monomer Sibe-EH with the helices of the catalytic domain shown in blue and the helices of the cap domain in sea blue.

this funnel is approximately the same in CH65-EH and Sibe-EH, although it appears significantly more occluded in the CH65-EH enzyme. There is no access to the active site cavity in this region of the protein in the *B. megaterium* EH or the human EH.

## Structural Basis for EH Thermostability

The CH65-EH was shown to be significantly more thermostable than Sibe-EH, with no decrease of activity after incubation at temperatures of 60°C and retaining about 80% of the initial activity after thermal treatment at 70°C, while Sibe-EH was relatively stable at temperatures below 40°C and was able to retain 10% of initial activity after incubation at 60°C. This was also confirmed by CD analysis as described earlier. When analyzing the structures of the enzymes the higher thermostability of CH65-EH appears to result from a significant amount of hydrophobic interactions on the dimer interface (**Figure 8**) and a higher proportion of secondary structure in this enzyme (56.8%) as calculated by PROMOTIF (Hutchinson and Thornton, 1996). Whereas, the Sibe-EH has a lower proportion of secondary structure (53.3%) and is only a monomer. In comparison, the structure of a previously studied human EH hydrolase domain (PDB 4C4X) has a lower proportion of secondary structure of 49%. There are many general structural features that have been identified which are thought to contribute to protein thermostability which varies amongst different organisms (Littlechild et al., 2007; Littlechild, 2015). Examples of these features include using hydrophobic interactions at

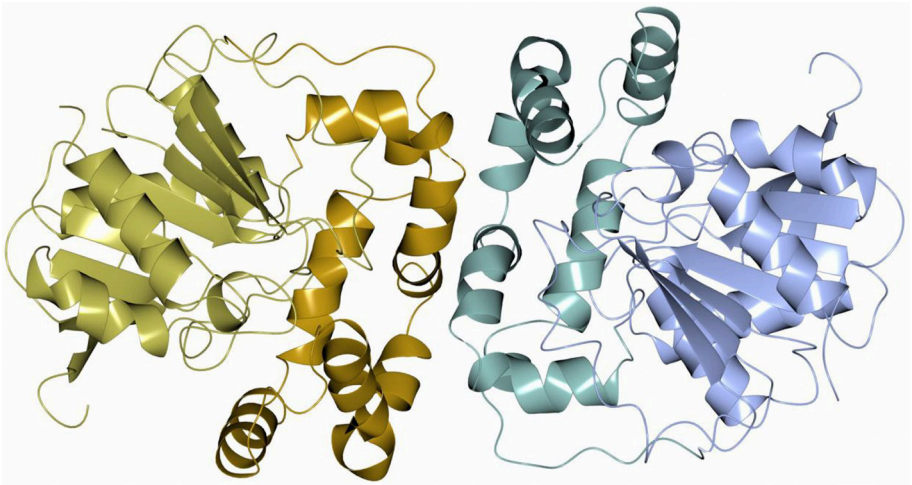

**FIGURE 7 |** A cartoon diagram of the dimer of CH65-EH viewed along the molecular dyad. The cap domains that form the interaction within the dimer are shown in different colors.

oligomeric interfaces which are often observed in thermostable proteins with temperature optima up to approximately 75°C such as the *Sulfolobus solfataricus* serine transaminase (Sayer et al., 2012) and *Thermococcus litoralis* pyrrolidone carboxyl peptidase (Singleton et al., 1999).

## Structural Basis for EH Substrate Specificity and Stereospecificity

The substrate range of the enzyme is determined by two structural components. The compound is an unlikely substrate if it cannot reach the catalytic site due to substrate channel limitations. Provided the compounds are able to get into the active site the activity depends on the potential substrate positioning in relation to the catalytic residues. This positioning is defined by the residues lining the active site cavity.

The modeling studies that have been carried out as part of this study have shown that compounds (**1**)-(**6**) can easily reach the active site cavity of the Sibe-EH and CH65-EH regardless of the different position and size of the active site funnel in these enzymes. This suggests that the enzyme reactivity towards these epoxides is defined by the precise substrate positioning in the active site. None of the substrates could be docked in the catalytic position (epoxide oxygen coordinated by hydroxyls of the catalytic tyrosines and the scissile epoxide bond co-linear with the line of attack of the catalytic aspartate oxygen) even when docking calculations were performed using both flexible side chains and flexible substrates. The results of the modeling suggest that the space between catalytic aspartate and the tyrosine residues is too restrictive to allow the epoxides (**1**)-(**6**) to bind since the movement of the side chains of these residues is limited. The tyrosine residues are held in position by neighboring hydrophobic residues and the side chain of the catalytic aspartic acid by interaction with the oxyanion hole. However, since the catalytic triad residues and catalytic tyrosine residues come together from different domains a relatively small domain movement (in the range of 0.7–1.2 Å) would allow the epoxide to move into the position required for catalysis. The tyrosines 148 and 209 (CH65-EH numbering) are located on two different intersecting helices which would move as a rigid body during domain movement.

The importance of the active site cavity residues for the EH reaction has been demonstrated by van Loo et al. (2009), where a change in substrate preference and stereospecificity of *Agr. radiobacter* EH was achieved by mutation of a single residue (Phe108, which follows the catalytic Asp107).

The first stage of the EH catalytic reaction is an attack by the OD1 of the active site Asp on one of the substrate epoxide carbons. The line of attack should be co-linear with the direction of the epoxide CO bond. The substrate epoxide oxygen binds to the side chain hydroxyls of Tyr150 and Tyr209 in Sibe-EH, and its likely position is marked by a conserved water molecule interacting with these residues. The orientation and position of the catalytic Asp side chain is fixed due to its binding in the oxyanion hole. When the structures of Sibe-EH and CH65-EH are superimposed the positions of OD1 of catalytic Asp102 (Asp101) and OH of Tyr209 (Tyr209) match quite well (within 0.5 Å), however the positions of OH of Tyr150 of Sibe-EH and Tyr148 of CH65-EH differ by 1.1Å which displaces the epoxide oxygen site by 0.8 Å.

The ligand models were positioned in the active sites of the two EHs as follows. The epoxide carbon under attack [e.g., (*S*)- or (*R*)- carbon in compound (**3**)] was aligned between OD1 of the catalytic aspartate and the epoxide oxygen. This oxygen was positioned at the location of the conserved water coordinated by the two active site tyrosine residues with the cap domain shifted (opened) by about 1.0 Å by rotation around line connecting residues 128 and 224 (CH65-EH numbering; **Figure 10**). The substrates were then rotated around the epoxide bond subject to attack in order to find a position where they make hydrophobic contact with the active site cavity wall and have no steric clashes. Interestingly, when ligands (**1**) and (**3**) were thus positioned and rotated in CH65-EH they appear not to make good hydrophobic

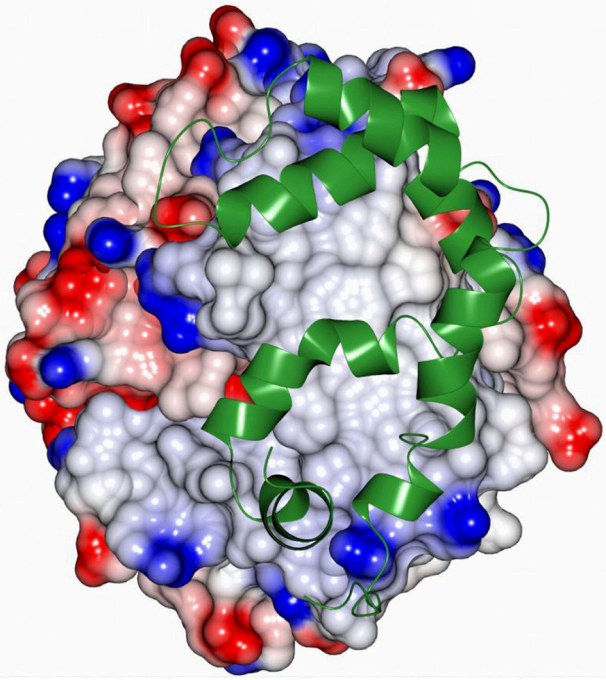

**FIGURE 8 |** The hydrophobic interactions at the dimer interface of CH65-EH.The electrostatic surface potential of one monomer of CH65-EH that has been rotated by 90° around the vertical axis from that presented in **Figure 7** is shown alongside a ribbon representation of the cap domain of the adjacent monomer (green). The areas of positive charge are shown in blue, with the areas of negative charge in red and the hydrophobic surfaces are represented in light gray.

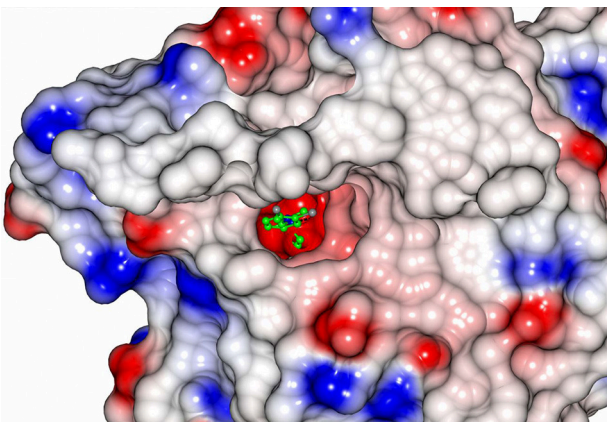

**FIGURE 9 |** An electrostatic surface potential representation showing the entrance to the active site cavity of Sibe-EH (colors as explained in legend of **Figure 8**). A ligand 3-(3,4-dichlorophenyl)-1,1-dimethyl-urea that was bound to human EH (pdb code 4C4X; Pilger et al., 2015) is shown as a ball-and stick model. The position of the ligand was obtained by superimposition of the human structure onto the structure of Sibe-EH.

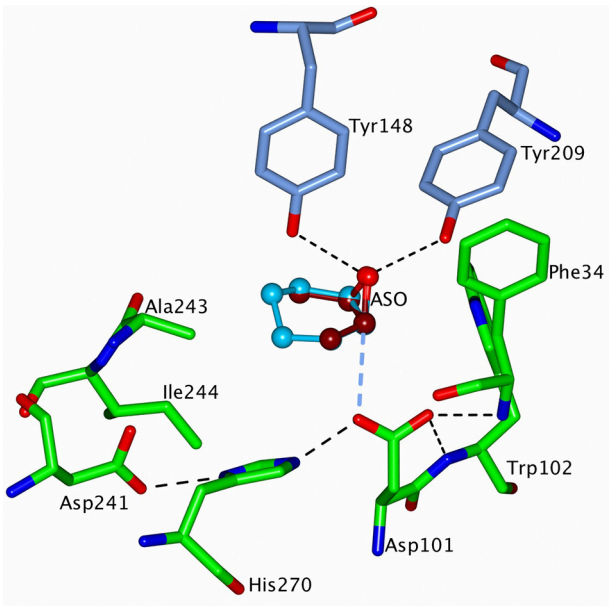


**FIGURE 10 |** A representation of the modeled structure of CH65-EH with the putative substrates, *cis*-2,3-epoxybutane (ASO) **(3)** and cyclohexene oxide **(2)** positioned into the active site of the enzyme. ASO is shown in dark red carbons and the cyclohexene oxide in sky blue carbons**.** The cap domain of CH65-EH has been rotated around the line connecting the Cα atoms of residues 128 and 224 to reach a 1.2 Å displacement of OH atoms of Tyr148 and Tyr209 away from the catalytic domain. The active site residues are shown as cylinders with carbon atoms of the cap domain residues in blue and of the catalytic domain residues in green. H-bonds within the catalytic triad, in the oxyanion hole and between the epoxide oxygen and OH atoms of the two tyrosine residues, are shown as dashed black lines. The larger cyclohexene oxide is able to interact with the hydrophobic side chains of residues Ala243 and Ile244 which would lead to turnover of this substrate whereas the smaller ASO is not a substrate. **Figures 6–10** were prepared using ccp4 mg (McNicholas et al., 2011).

contacts in any orientation. This could explain the absence of activity of CH65-EH toward these two small epoxides, since they cannot stay in the reaction position for long enough to allow catalysis to occur. However, bulkier/longer (**2**), (**4**), and (**5**) substrates make limited contacts with residues in the active site cavity, such as with residue Ile244, and are consequently turned over. The rotation of compounds (**1**) and (**3**) into the active site of Sibe-EH around a somewhat different axis allowed at least one favorable orientation to be found where the ligand interacts with Asp251 and Leu252. For both (**1**) and (**3**) this interaction exists when the (*S*)-carbon is attacked. This suggests that a hydrophobic interaction between the protein and the substrate slows down the substrate displacement and favors the reaction. The high *ee* observed for the *meso*-epoxide (**3**) in the Sibe-EH reaction can be explained by the formation of favorable protein-ligand hydrophobic interactions when the ligand is attacked at the (*S*)-carbon to release the (*R, R*) product. These interactions do not occur when the attack is at the (*R*)-carbon.

## CONCLUSIONS

Two novel EH enzymes of the α/β fold class have been identified from metagenomic samples from diverse locations in Russia

and China. These two new thermostable EHs have been cloned and over-expressed in *E. coli* and have been characterized both biochemically and structurally. Both enzymes are thermostable with the CH65-EH enzyme retaining activity at 70°C.

The EHs were active toward a broad range of substrates including racemic (4*R*)-limonene-1,2-epoxide which is associated with a different class of epoxide hydrolases (LEHs) which have a different structure and mechanism and have been named by their ability to use the limonene epoxide as a substrate.

The Sibe-EH is a monomer whereas the CH65-EH enzyme forms a dimer by the interaction of its two cap domains as described for other dimeric EHs. However, the monomer orientation that makes up the dimer of CH65-EH is different from related enzymes. The funnel that forms the entrance to the active site cavity is located in a different position in CH65-EH and Sibe-EH in relation to other known bacterial and mammalian EHs.

The results obtained from this study also pose interesting questions about the evolution of the EH enzymes and their varied substrate specificities which has an important impact for their potential use as commercial biocatalysts. The high thermal stability of the CH65-EH enzyme which ranks as the most thermostable natural EH enzyme described to date, makes it an important addition to the industrial bio-catalytic "tool box."

The detailed structural analysis of these two novel EH enzymes has allowed a greater understanding of their stability and substrate specificity. It has also demonstrated the importance of the positioning of the substrate within the active site of the enzymes to allow the catalytic turnover.

The discovery of new novel enzymes using metagenomic DNA to access the biodiversity offered by "Nature" during the HotZyme project has been clearly demonstrated within this study. This approach allows access to the large resource of enzymes encoded within the DNA of micro-organisms which are currently not able to be cultured in the laboratory.

## ACCESSION NUMBERS

Nucleotide sequence data are available in the GenBank databases under the accession numbers KX505385 for Sibe-EH and KX505386 for CH65-EH. The atomic coordinates and structure factors of the crystal structures have been deposited in the Protein Data Bank with the codes 5NG7 for Sibe-EH and 5NFQ for CH65-EH.

## AUTHOR CONTRIBUTIONS

EF performed the discovery, cloning and expression of the novel enzymes, while CS, SD, EG, and CM performed the protein purification. CS and SD carried out the crystallization and structure determination studies with MI carrying out data collection and analysis and structural refinement. VS carried out the molecular modeling studies with MI to rationalize the substrate specificity. EG and CM performed the biochemical characterization of functional properties and the substrate specificity studies. JL and DM coordinated the work and wrote the manuscript with input from all authors.

## ACKNOWLEDGMENTS

This work has been carried out in the framework of the HotZyme Project (http://hotzyme.com, grant agreement no. 265933) financed by the European Union 7th Framework Programme FP7/2007–2013, that aimed to use a metagenomics approach to identify new thermostable hydrolases which have improved performances and/or novel functionalities for different industrial processes from diverse hot environments. In particular, we thank Prof. Xu Peng (University of Copenhagen) and Prof. Elizaveta Bonch-Osmolovskaya (Winogradsky Institute of Microbiology of the Russian Academy of Sciences) for providing us with the metagenome samples. DM would like to thank the SusChemLombardia: prodotti e processi sostenibili per l'industria lombarda project, Accordo Quadro Regione Lombardia-CNR, 16/07/2012 (protocol no. 18096/RCC) for additional support. JL and DM would also like to acknowledge the COST Action Systems Biocatalysis CM-1303 for supporting the visit of the student EG to Exeter to carry out the initial crystallization of CH65-EH. MI would like to thank the BBSRC-funded ERA-IB grant BB/L002035/1 and the University of Exeter for support. The authors would like to thank the Diamond Synchrotron Light Source for access to beamline I03, I04-1 and I04 (proposal Nos. MX8889 and MX11945) and beamline scientists for assistance.

## SUPPLEMENTARY MATERIAL

The Supplementary Material for this article can be found online at: https://www.frontiersin.org/articles/10.3389/fbioe.2018.00144/full#supplementary-material

## REFERENCES

Arand, M., Hemmer, H., Dürk, H., Baratti, J., Archelas, A., Furstoss, R., et al. (1999). Cloning and molecular characterization of a soluble epoxide hydrolase from *Aspergillus niger* that is related to mammalian microsomal epoxide hydrolase. *Biochem. J.* 344, 273–280. doi: 10.1042/bj3440273

Archelas, A., Iacazio, G., and Kotik, M. (2016). "Epoxide Hydrolases and their Application in Organic Synthesis," in *Green Biocatalysis*, ed. R. N. Patel (Hoboken, NJ: John Wiley & Sons, Inc.), 179–229.

Argiriadi, M. A., Morisseau, C., Hammock, B. D., and Christianson, D. W. (1999). Detoxification of environmental mutagens and carcinogens: structure, mechanism, and evolution of liver epoxide hydrolase. *Proc. Natl. Acad. Sci. U.S.A.* 96, 10637–10642. doi: 10.1073/pnas.96.19.10637

Bala, N., and Chimni, S. S. (2010). Recent developments in the asymmetric hydrolytic ring opening of epoxides catalysed by microbial epoxide hydrolase. *Tetrahedron Asymmetry* 21, 2879–2898. doi: 10.1016/j.tetasy.2010.11.013

Barbirato, F., Verdoes, J. C., de Bont, J. A. M., and van der Werf, M. J. (1998). The *Rhodococcus erythropolis* DCL14 limonene-1,2-epoxide hydrolase gene encodes an enzyme belonging to a novel class of epoxide hydrolases. *FEBS Lett.* 438, 293–296. doi: 10.1016/S0014-5793(98)01322-2

Berini, F., Casciello, C., Marcone, G. L., and Marinelli, F. (2017). Metagenomics: novel enzymes from non-culturable microbes. *FEMS Microbiol. Lett.* 364, 1–19. doi: 10.1093/femsle/fnx211

Biswal, B. K., Morisseau, C., Garen, G., Cherney, M. M., Garen, C., Niu, C., et al. (2008). The molecular structure of epoxide hydrolase B from *Mycobacterium tuberculosis* and its complex with a urea-based inhibitor. *J. Mol. Biol.* 381, 897–912. doi: 10.1016/j.jmb.2008.06.030

Brooks, G. T., Harrison, A., and Lewis, S. E. (1970). Cyclodiene epoxide ring hydration by microsomes from mammalian liver and houseflies. *Biochem. Pharmacol.* 19, 255–273. doi: 10.1016/0006-2952(70)90346-1

Capriati, V., Florio, S., Luisi, R., and Nuzzo, I. (2004). Stereospecific synthesis of optically active phenylpropylene oxides. *J. Org. Chem.* 69, 3330–3335. doi: 10.1021/jo035858w

Chen, C. S., Fujimoto, Y., Girdaukas, G., and Sih, C. J. (1982). Quantitative analyses of biochemical kinetic resolutions of enantiomers. *J. Am. Chem. Soc.* 104, 7294–7299. doi: 10.1021/ja00389a064

Chovancova, E., Pavelka, A., Benes, P., Strnad, O., Brezovsky, J., Kozlikova, B., et al. (2012). CAVER 3.0: a tool for the analysis of transport pathways in dynamic protein structures. *PLoS Comput. Biol.* 8, 23–30. doi: 10.1371/journal.pcbi.1002708

DeLano, W. L. (2002). *The PyMOL Molecular Graphics System, Version 1.8* New York, NY: Schrödinger, LLC.

Emsley, P., Lohkamp, B., Scott, W. G., and Cowtan, K. (2010). Features and development of Coot. *Acta Crystallogr. Sect. D Biol. Crystallogr.* 66, 486–501. doi: 10.1107/S0907444910007493

Evans, P. R., and Murshudov, G. N. (2013). How good are my data and what is the resolution? *Acta Crystallogr. Sect. D Biol. Crystallogr.* 69, 1204–1214. doi: 10.1107/S0907444913000061

Ferrandi, E. E., Marchesi, C., Annovazzi, C., Riva, S., Monti, D., and Wohlgemuth, R. (2015a). Efficient epoxide hydrolase catalyzed resolutions of (+)- and (−)- cis / trans -limonene oxides. *ChemCatChem* 7, 3171–3178. doi: 10.1002/cctc.201500608

Ferrandi, E. E., Sayer, C., Isupov, M. N., Annovazzi, C., Marchesi, C., Iacobone, G., et al. (2015b). Discovery and characterization of thermophilic limonene-1,2-epoxide hydrolases from hot spring metagenomic libraries. *FEBS J.* 282, 2879–2894. doi: 10.1111/febs.13328

Ferrer, M., Martínez-Martínez, M., Bargiela, R., Streit, W. R., Golyshina, O. V., and Golyshin, P. N. (2016). Estimating the success of enzyme bioprospecting through metagenomics: current status and future trends. *Microb. Biotechnol.* 9, 22–34. doi: 10.1111/1751-7915.12309

Franken, S. M., Rozeboom, H. J., Kalk, K. H., and Dijkstra, B. W. (1991). Crystal structure of haloalkane dehalogenase: an enzyme to detoxify halogenated alkanes. *EMBO J.* 10, 1297–1302. doi: 10.1002/j.1460-2075.1991.tb07647.x

Guo, A., Durner, J., and Klessig, D. F. (1998). Characterization of a tobacco epoxide hydrolase gene induced during the resistance response to TMV. *Plant J.* 15, 647–656. doi: 10.1046/j.1365-313x.1998.00241.x

Hutchinson, E. G., and Thornton, J. M. (1996). PROMOTIF–a program to identify and analyze structural motifs in proteins. *Protein Sci.* 5, 212–220. doi: 10.1002/pro.5560050204

Jacobsen, E. N. (2000). Asymmetric catalysis of epoxide ring-opening reactions. *Acc. Chem. Res.* 33, 421–431. doi: 10.1021/ar960061v

Jerina, D., Guroff, G., and Daly, J. (1968). Enzymic and nonenzymic hydroxylation and chlorination of p-deuteroanisole. *Arch. Biochem. Biophys.* 124, 612–615. doi: 10.1016/0003-9861(68)90374-3

Jiménez, D. J., Dini-Andreote, F., Ottoni, J. R., de Oliveira, V. M., van Elsas, J. D., and Andreote, F. D. (2015). Compositional profile of α/β-hydrolase fold proteins in mangrove soil metagenomes: prevalence of epoxide hydrolases and haloalkane dehalogenases in oil-contaminated sites. *Microb. Biotechnol.* 8, 604–613. doi: 10.1111/1751-7915.12157

Kabsch, W. (2010). XDS. *Acta Crystallogr. Sect. D Biol. Crystallogr.* 66, 125–132. doi: 10.1107/S0907444909047337

Karboune, S., Archelas, A., Furstoss, R., and Baratti, J. (2005). Immobilization of epoxide hydrolase from *Aspergillus niger* onto DEAE-cellulose: enzymatic properties and application for the enantioselective resolution of a racemic epoxide. *J. Mol. Catal. B Enzym.* 32, 175–183. doi: 10.1016/j.molcatb.2004.11.001

Karplus, P. A., and Diederichs, K. (2012). Linking crystallographic model and data quality. M&M, supporting info. *Science* 336, 1030–1033. doi: 10.1126/science.1218231

Katsuki, T., and Sharpless, K. B. (1980). The first practical method for asymmetric epoxidation. *J. Am. Chem. Soc.* 102, 5974–5976. doi: 10.1021/ja00538a077

Kiyosue, T., Beetham, J. K., Pinot, F., Hammock, B. D., Yamaguchi-Shinozaki, K., and Shinozaki, K. (1994). Characterization of an *Arabidopsis* cDNA for a soluble epoxide hydrolase gene that is inducible by auxin and water stress. *Plant J.* 6, 259–269. doi: 10.1046/j.1365-313X.1994.6020259.x

Kolb, H. C., and Sharpless, K. B. (1992). A simplified procedure for the stereospecific transformation of 1,2-diols into epoxides. *Tetrahedron* 48, 10515–10530. doi: 10.1016/S0040-4020(01)88349-6

Kolb, H. C., Vannieuwenhze, M. S., and Sharpless, K. B. (1994). Catalytic asymmetric dihydroxylation. *Chem. Rev.* 94, 2483–2547. doi: 10.1021/cr00032a009

Kong, X.-D., Yuan, S., Li, L., Chen, S., Xu, J.-H., and Zhou, J. (2014). Engineering of an epoxide hydrolase for efficient bioresolution of bulky pharmaco substrates. *Proc. Natl. Acad. Sci. U.S.A.* 111, 15717–15722. doi: 10.1073/pnas.1404915111

Kotik, M., Archelas, A., and Wohlgemuth, R. (2012). Epoxide hydrolases and their application in organic synthesis. *Curr. Org. Chem.* 16, 451–482. doi: 10.2174/138527212799499840

Kotik, M., Štěpánek, V., Grulich, M., Kyslík, P., and Archelas, A. (2010). Access to enantiopure aromatic epoxides and diols using epoxide hydrolases derived from total biofilter DNA. *J. Mol. Catal. B Enzym.* 65, 41–48. doi: 10.1016/j.molcatb.2010.01.016

Kotik, M., Štěpánek, V., Kyslík, P., and Marešová, H. (2007). Cloning of an epoxide hydrolase-encoding gene from *Aspergillus niger* M200, overexpression in *E. coli.* and modification of activity and enantioselectivity of the enzyme by protein engineering. *J. Biotechnol.* 132, 8–15. doi: 10.1016/j.jbiotec.2007.08.014

Kotik, M., Štěpánek, V., Marešová, H., Kyslík, P., and Archelas, A. (2009). Environmental DNA as a source of a novel epoxide hydrolase reacting with aliphatic terminal epoxides. *J. Mol. Catal,. B Enzym.* 56, 288–293. doi: 10.1016/j.molcatb.2008.05.018

Kozlikova, B., Sebestova, E., Sustr, V., Brezovsky, J., Strnad, O., Daniel, L., et al. (2014). CAVER Analyst 1.0: graphic tool for interactive visualization and analysis of tunnels and channels in protein structures. *Bioinformatics* 30, 2684–2685. doi: 10.1093/bioinformatics/btu364

Krissinel, E., and Henrick, K. (2007). Inference of macromolecular assemblies from crystalline state. *J. Mol. Biol.* 372, 774–797. doi: 10.1016/j.jmb.2007.05.022

Laskowski, R. A., MacArthur, M. W., Moss, D. S., and Thornton, J. M. (1993). PROCHECK: a program to check the stereochemical quality of protein structures. *J. Appl. Crystallogr.* 26, 283–291. doi: 10.1107/S0021889892009944

Lebedev, A., and Vagin, A. (2015). MoRDa, an automatic molecular replacement pipeline. *Acta Crystallogr. Sect. A Found. Adv.* 71:s19. doi: 10.1107/S2053273315099672

Lebedev, A. A., Vagin, A. A., and Murshudov, G. N. (2008). Model preparation in MOLREP and examples of model improvement using X-ray data. *Acta Crystallogr. Sect. D Biol. Crystallogr.* 64, 33–39. doi: 10.1107/S0907444907049839

Lebedev, A. A., Young, P., Isupov, M. N., Moroz, O. V., Vagin, A. A., and Murshudov, G. N. (2012). JLigand: a graphical tool for the CCP4 template-restraint library. *Acta Crystallogr. Sect. D Biol. Crystallogr.* 68, 431–440. doi: 10.1107/S090744491200251X

Linderman, R. J., Roe, R. M., Harris, S. V., and Thompson, D. M. (2000). Inhibition of insect juvenile hormone epoxide hydrolase: asymmetric synthesis and assay of glycidol-ester and epoxy-ester inhibitors of *Trichoplusia ni* epoxide hydrolase. *Insect Biochem. Molecul. Biol.* 767–774. doi: 10.1016/S0965-1748(00)00048-5

Littlechild, J. A. (2015). Enzymes from extreme environments and their industrial applications. *Front. Bioeng. Biotechnol.* 3:161. doi: 10.3389/fbioe.2015.00161

Littlechild, J. A., Guy, J., Connelly, S., Mallett, L., Waddell, S., Rye, C. A., et al. (2007). Natural methods of protein stabilization: thermostable biocatalysts. *Biochem. Soc. Trans.* 35, 1558–1563. doi: 10.1042/BST0351558

Liu, Z., Li, Y., Ping, L., Xu, Y., Cui, F., Xue, Y., et al. (2007). Isolation and identification of a novel *Rhodococcus* sp. ML-0004 producing epoxide hydrolase and optimization of enzyme production. *Process Biochem.* 42, 889–894. doi: 10.1016/j.procbio.2007.01.009

McNicholas, S., Potterton, E., Wilson, K. S., and Noble, M. E. M. (2011). Presenting your structures: the CCP4mg molecular-graphics software. *Acta Crystallogr. Sect. D Biol. Crystallogr.* 67, 386–394. doi: 10.1107/S0907444911007281

Menzel, P., Gudbergsdóttir, S. R., Rike, A. G., Lin, L., Zhang, Q., Contursi, P., et al. (2015). Comparative metagenomics of eight geographically remote terrestrial hot springs. *Microb. Ecol.* 70, 411–424. doi: 10.1007/s00248-015-0576-9

Montaña, J. S., Jiménez, D. J., Hernández, M., Ángel, T., and Baena, S. (2012). Taxonomic and functional assignment of cloned sequences from high Andean forest soil metagenome. *Antonie van Leeuwenhoek* 101, 205–215. doi: 10.1007/s10482-011-9624-8

Morisseau, C., Beetham, J. K., Pinot, F., Debernard, S., Newman, J. W., and Hammock, B. D. (2000). Cress and potato soluble epoxide hydrolases: purification, biochemical characterization, and comparison to mammalian enzymes. *Arch. Biochem. Biophys.* 378, 321–332. doi: 10.1006/abbi.2000.1810

Morisseau, C., and Hammock, B. D. (2005). Epoxide hydrolases: mechanisms, inhibitor designs, and biological roles. *Annu. Rev. Pharmacol. Toxicol.* 45, 311–333. doi: 10.1146/annurev.pharmtox.45.120403.095920

Morris, G. M., Huey, R., Lindstrom, W., Sanner, M. F., Belew, R. K., Goodsell, D. S., et al. (2009). AutoDock4 and AutoDockTools4: automated docking with selective receptor flexibility. *J. Comput. Chem.* 30, 2785–2791. doi: 10.1002/jcc.21256

Mowbray, S. L., Elfström, L. T., Ahlgren, K. M., Andersson, C. E., and Widersten, M. (2006). X-ray structure of potato epoxide hydrolase sheds light on substrate specificity in plant enzymes. *Protein Sci.* 15, 1628–1637. doi: 10.1110/ps.051792106

Murshudov, G. N., Skubák, P., Lebedev, A. A., Pannu, N. S., Steiner, R. A., Nicholls, R. A., et al. (2011). REFMAC5 for the refinement of macromolecular crystal structures. *Acta Crystallogr. Sect. D Biol. Crystallogr.* 67, 355–367. doi: 10.1107/S0907444911001314

Nardini, M., Ridder, I. S., Rozeboom, H. J., Kalk, K. H., Rink, R., Janssen, D. B., et al. (1999). The x-ray structure of epoxide hydrolase from *Agrobacterium radiobacter* AD1. An enzyme to detoxify harmful epoxides. *J. Biol. Chem.* 274, 14579–14586. doi: 10.1074/jbc.274.21.14579

Novak, H. R., Sayer, C., Isupov, M. N., Gotz, D., Spragg, A. M., and Littlechild, J. A. (2014). Biochemical and structural characterisation of a haloalkane dehalogenase from a marine *Rhodobacteraceae*. *FEBS Lett.* 588, 1616–1622. doi: 10.1016/j.febslet.2014.02.056

Oesch, F. (1973). Mammalian epoxide hydrases: inducible enzymes catalysing the inactivation of carcinogenic and cytotoxic metabolites derived from aromatic and olefinic compounds. *Xenobiotica* 3, 305–340. doi: 10.3109/00498257309151525

Pavelka, A., Sebestova, E., Kozlikova, B., Brezovsky, J., Sochor, J., and Damborsky, J. (2015). CAVER: algorithms for analyzing dynamics of tunnels in macromolecules. *IEEE/ACM Trans. Comput. Biol. Bioinforma* 13, 505–517. doi: 10.1109/TCBB.2015.2459680

Pedragosa-Moreau, S., Morisseau, C., Baratti, J., Zylber, J., Archelas, A., and Furstoss, R. (1997). Microbiological transformations 37. An enantioconvergent synthesis of the β-blocker (R)-Nifenalol® using a combined chemoenzymatic approach. *Tetrahedron* 53, 9707–9714. doi: 10.1016/S0040-4020(97)00639-X

Pettersen, E. F., Goddard, T. D., Huang, C. C., Couch, G. S., Greenblatt, D. M., Meng, E. C., et al. (2004). UCSF Chimera–a visualization system for exploratory research and analysis. *J. Comput. Chem.* 25, 1605–1612. doi: 10.1002/jcc.20084

Pilger, J., Mazur, A., Monecke, P., Schreuder, H., Elshorst, B., Bartoschek, S., et al. (2015). A combination of spin diffusion methods for the determination of protein-ligand complex structural ensembles. *Angew. Chemie - Int. Ed.* 54, 6511–6515. doi: 10.1002/anie.201500671

Reetz, M. T., Bocola, M., Wang, L. W., Sanchis, J., Cronin, A., Arand, M., et al. (2009). Directed evolution of an enantioselective epoxide hydrolase: uncovering the source of enantioselectivity at each evolutionary stage. *J. Am. Chem. Soc.* 131, 7334–7343. doi: 10.1021/ja809673d

Richardson, J. S. (1981). The anatomy and taxonomy of protein structure. *Adv. Protein Chem.* 34, 167–339. doi: 10.1016/S0065-3233(08)60520-3

Robert, X., and Gouet, P. (2014). Deciphering key features in protein structures with the new ENDscript server. *Nucleic Acids Res.* 42, W320–W324. doi: 10.1093/nar/gku316

Sambrook, J., and Russell, D. W. (2001). *Molecular Cloning: A Laboratory Manual*. New York, NY: Cold Spring Harbor Laboratory Press.

Sastry, M. G., Adzhigirey, M., Day, T., Annabhimoju, R., and Sherman, W. (2013). Protein and ligand preparation: parameters, protocols, and influence on virtual screening enrichments. *J. Comput. Aided Mol. Des.* 27, 221–234. doi: 10.1007/s10822-013-9644-8

Sayer, C., Bommer, M., Isupov, M., Ward, J., and Littlechild, J. (2012). Crystal structure and substrate specificity of the thermophilic serine:pyruvate aminotransferase from *Sulfolobus solfataricus*. *Acta Crystallogr. Sect. D Biol. Crystallogr.* 68, 763–772. doi: 10.1107/S0907444912011274

Schrödinger (2017). *Schrödinger Release−1: Maestro*. New York, NY: Schrödinger, LLC.

Singh, J., Behal, A., Singla, N., Joshi, A., Birbian, N., Singh, S., et al. (2009). Metagenomics: concept, methodology, ecological inference and recent advances. *Biotechnol. J.* 4, 480–494. doi: 10.1002/biot.200800201

Singleton, M. R., Isupov, M. N., and Littlechild, J. A. (1999). Crystallization and preliminary X-ray diffraction studies of pyrrolidone carboxyl peptidase from the hyperthermophilic archaeon *Thermococcus litoralis*. *Acta Crystallogr. Sect. D Biol. Crystallogr.* 55, 702–703. doi: 10.1107/S0907444998016035

Stapleton, A., Beetham, J. K., Pinot, F., Garbarino, J. E., Rockhold, D. R., Friedman, M., et al. (1994). Cloning and expression of soluble epoxide hydrolase from potato. *Plant J.* 6, 251–258. doi: 10.1046/j.1365-313X.1994.6020251.x

Sutherland, J. B. (1992). Detoxification of polycyclic aromatic hydrocarbons by fungi. *J. Ind. Microbiol.* 9, 53–61. doi: 10.1007/BF01576368

Thalji, R. K., McAtee, J. J., Belyanskaya, S., Brandt, M., Brown, G. D., Costell, M. H., et al. (2013). Discovery of 1-(1,3,5-triazin-2-yl)piperidine-4-carboxamides as inhibitors of soluble epoxide hydrolase. *Bioorganic Med. Chem. Lett.* 23, 3584–3588. doi: 10.1016/j.bmcl.2013.04.019

Tian, W., Chen, C., Lei, X., Zhao, J., and Liang, J. (2018). CASTp 3.0: computed atlas of surface topography of proteins. *Nucleic Acids Res.* 46, W363–W367. doi: 10.1093/nar/gky473

Trott, O., and Olson, A. J. (2010). AutoDock Vina: improving the speed and accuracy of docking with a new scoring function, efficient optimization and multithreading. *J. Comput. Chem.* 31, 455–461. doi: 10.1002%2Fjcc.21334

Vagin, A., and Teplyakov, A. (2010). Molecular replacement with MOLREP. *Acta Crystallogr. D Biol. Crystallogr.* 66, 22–25. doi: 10.1107/S0907444909042589

Vaguine, A. A., Richelle, J., and Wodak, S. J. (1999). SFCHECK: a unified set of procedures for evaluating the quality of macromolecular structure-factor data and their agreement with the atomic model. *Acta Crystallogr. D Biol. Crystallogr.* 55, 191–205. doi: 10.1107/S0907444998006684

Van Loo, B., Kingma, J., Arand, M., Wubbolts, M. G., and Janssen, D. B. (2006). Diversity and biocatalytic potential of epoxide hydrolases identified by genome analysis. *Appl. Environ. Microbiol.* 72, 2905–2917. doi: 10.1128/AEM.72.4.2905-2917.2006

van Loo, B., Kingma, J., Heyman, G., Wittenaar, A., Lutje Spelberg, J. H., Sonke, T., et al. (2009). Improved enantioselective conversion of styrene epoxides and meso-epoxides through epoxide hydrolases with a mutated nucleophile-flanking residue. *Enzyme Microb. Technol.* 44, 145–153. doi: 10.1016/j.enzmictec.2008.09.016

Vieille, C., Zeikus, G. J., and Vieille, C. (2001). Hyperthermophilic enzymes: sources, uses, and molecular mechanisms for thermostability. *Microbiol. Mol. Biol. Rev.* 65, 1–43. doi: 10.1128/MMBR.65.1.1-43.2001

Weijers, C. A. G. M. (1997). Enantioselective hydrolysis of aryl, alicyclic and aliphatic epoxides by *Rhodotorula glutinis*. *Tetrahedron Asymmetry* 8, 639–647. doi: 10.1016/S0957-4166(97)00012-8

Widersten, M., Gurell, A., and Lindberg, D. (2010). Structure-function relationships of epoxide hydrolases and their potential use in biocatalysis. *Biochim. Biophys. Acta - Gen. Subj.* 1800, 316–326. doi: 10.1016/j.bbagen.2009.11.014

Wilson, M. C., and Piel, J. (2013). Metagenomic approaches for exploiting uncultivated bacteria as a resource for novel biosynthetic enzymology. *Chem. Biol.* 20, 636–647. doi: 10.1016/j.chembiol.2013.04.011

Winn, M. D., Ballard, C. C., Cowtan, K. D., Dodson, E. J., Emsley, P., Evans, P. R., et al. (2011). Overview of the CCP4 suite and current developments. *Acta Crystallogr. Sect. D Biol. Crystallogr.* 67, 235–242. doi: 10.1107/S0907444910045749

Winter, G., Lobley, C. M. C., and Prince, S. M. (2013). Decision making in xia2. *Acta Crystallogr. Sect. D Biol. Crystallogr.* 69, 1260–1273. doi: 10.1107/S0907444913015308

Wohlgemuth, R. (2015). "Epoxide hydrolysis," in *Biocatalysis in Organic Synthesis*, eds K. Faber, W.-D. Fessner, and N. J. Turner (Stuttgart: Georg Thieme Verlag KG), 529–555.

Zarafeta, D., Kissas, D., Sayer, C., Gudbergsdottir, S. R., Ladoukakis, E., Isupov, M. N., et al. (2016). Discovery and characterization of a thermostable and highly halotolerant GH5 cellulase from an icelandic hot spring isolate. *PLoS ONE* 11:e0146454. doi: 10.1371/journal.pone.0146454

Zhao, J., Chu, Y. Y., Li, A. T., Ju, X., Kong, X. D., Pan, J., et al. (2011). An unusual (R)-selective epoxide hydrolase with high activity for facile preparation of enantiopure glycidyl ethers. *Adv. Synth. Catal.* 353, 1510–1518. doi: 10.1002/adsc.201100031

Zhao, L., Han, B., Huang, Z., Miller, M., Huang, H., Malashock, D. S., et al. (2004). Epoxide hydrolase-catalyzed enantioselective synthesis of chiral 1,2-diols via desymmetrization of meso-epoxides. *J. Am. Chem. Soc.* 126, 11156–11157. doi: 10.1021/ja0466210

Zhao, W., Kotik, M., Iacazio, G., and Archelas, A. (2015). Enantioselective bio-hydrolysis of various racemic and meso aromatic epoxides using the recombinant epoxide hydrolase Kau2. *Adv. Synth. Catal.* 357, 1895–1908. doi: 10.1002/adsc.201401164

Zheng, H., and Reetz, M. T. (2010). Manipulating the stereoselectivity of limonene epoxide hydrolase by directed evolution based on iterative saturation mutagenesis. *J. Am. Chem. Soc.* 132, 15744–15751. doi: 10.1021/ja1067542

Zhou, K., Jia, N., Hu, C., Jiang, Y., Jie-Pin, Y., Chen, Y., et al. (2014). Crystal structure of juvenile hormone epoxide hydrolase from the silkworm *Bombyx mori*. *Proteins* 82, 3224–3229. doi: 10.1002/prot.24676

**Conflict of Interest Statement:** The authors declare that the research was conducted in the absence of any commercial or financial relationships that could be construed as a potential conflict of interest.

frontiers in Bioengineering and Biotechnology

ORIGINAL RESEARCH
published: 28 November 2018
doi: 10.3389/fbioe.2018.00184

# Enrichment and Genomic Characterization of a $N_2O$-Reducing Chemolithoautotroph From a Deep-Sea Hydrothermal Vent

*Sayaka Mino*[1]*, *Naoki Yoneyama*[1], *Satoshi Nakagawa*[2,3], *Ken Takai*[3] and *Tomoo Sawabe*[1]

[1] Laboratory of Microbiology, Faculty of Fisheries Sciences, Hokkaido University, Hakodate, Japan, [2] Laboratory of Marine Environmental Microbiology, Division of Applied Biosciences, Graduate School of Agriculture, Kyoto University, Kyoto, Japan, [3] Department of Subsurface Geobiology Analysis and Research (D-SUGAR), Japan Agency for Marine-Earth Science and Technology (JAMSTEC), Yokosuka, Japan

Nitrous oxide ($N_2O$) is a greenhouse gas and also leads to stratospheric ozone depletion. In natural environments, only a single $N_2O$ sink process is the microbial reduction of $N_2O$ to $N_2$, which is mediated by nitrous oxide reductase (NosZ) encoded by *nosZ* gene. The *nosZ* phylogeny has two distinct clades, clade I and formerly overlooked clade II. In deep-sea hydrothermal environments, several members of the class *Campylobacteria* are shown to harbor clade II *nosZ* gene and perform the complete denitrification of nitrate to $N_2$; however, little is known about their ability to grow on exogenous $N_2O$ as the sole electron acceptor. Here, we obtained an enrichment culture from a deep-sea hydrothermal vent in the Southern Mariana Trough, which showed a respiratory $N_2O$ reduction with $H_2$ as an electron donor. The single amplicon sequence variant (ASV) presenting 90% similarity to *Hydrogenimonas* species within the class *Campylobacteria* was predominant throughout the cultivation period. Metagenomic analyses using a combination of short-read and long-read sequence data succeeded in reconstructing a complete genome of the dominant ASV, which encoded clade II *nosZ* gene. This study represents the first cultivation analysis that shows the occurrence of $N_2O$-respiring microorganisms in a deep-sea hydrothermal vent and provides the opportunity to assess their capability to reduce $N_2O$ emission from the environments.

**Keywords: $N_2O$-reducing bacterium, deep-sea hydrothermal field, *Campylobacteria*, *Epsilonproteobacteria*, *nosZ*, nitrous oxide**

OPEN ACCESS

***Edited by:***
*Milko Alberto Jorquera, Universidad de La Frontera, Chile*

***Reviewed by:***
*Zongze Shao, Third Institute of Oceanography, China*
*Nikolai Ravin, Research Center of Biotechnology of the Russian Academy of Sciences, Russia*

***Correspondence:**
*Sayaka Mino*
*sayaka.mino@fish.hokudai.ac.jp*

***Specialty section:***
*This article was submitted to Process and Industrial Biotechnology, a section of the journal Frontiers in Bioengineering and Biotechnology*

***Received:*** *16 August 2018*
***Accepted:*** *13 November 2018*
***Published:*** *28 November 2018*

***Citation:***
*Mino S, Yoneyama N, Nakagawa S, Takai K and Sawabe T (2018) Enrichment and Genomic Characterization of a $N_2O$-Reducing Chemolithoautotroph From a Deep-Sea Hydrothermal Vent. Front. Bioeng. Biotechnol. 6:184. doi: 10.3389/fbioe.2018.00184*

## INTRODUCTION

Nitrous oxide ($N_2O$) is a stable greenhouse gas and a major stratospheric ozone layer-depleting substance of the 21th century (Ravishankara et al., 2009). Its 100-years global warming potential is around 300 times higher than $CO_2$ (IPPC., 2007). Since atmospheric $N_2O$ concentration has steadily increased at a rate of 0.2–0.3% per year and this increase is thought be due to anthropogenic emissions (IPCC., 2006), mitigation of $N_2O$ release is an international challenge in the context of controlling global nitrogen cycle.

Nitrous oxide ($N_2O$) can be reduced at the final step of the microbial denitrification pathway, which consists of the sequential reduction of $NO_3^-$ to $NO_2^-$, NO, $N_2O$, and $N_2$. $N_2O$

reductase (NosZ), encoded by *nosZ* gene, is the only known enzyme that converts $N_2O$ to $N_2$ gas. NosZ is phylogenetically classified into two clades; clade I (typical NosZ) and clade II (atypical NosZ). Newly described clade II NosZ (Sanford et al., 2012; Jones et al., 2013) is often identified within non-denitrifying $N_2O$-reducing microorganisms that lack other denitrification genes or perform dissimilatory nitrate reduction to ammonium. The abundance of microorganisms possessing the clade II NosZ outnumbers that of microorganisms possessing the clade I NosZ in the diverse environments (Jones et al., 2013, 2014), and clade II organisms have been reported with the higher affinity to $N_2O$ than clade I organisms (Yoon et al., 2016), suggesting that microorganisms possessing the clade II NosZ play a crucial role in attenuating $N_2O$ emission in the various natural environments.

Deep-sea hydrothermal vent fields are representative environments where the ecosystem is fueled by chemosynthetic microorganisms that are taxonomically and metabolically diverse (Takai and Nakamura, 2011; Waite et al., 2017; Mino and Nakagawa, 2018). Members of the class *Campylobacteria* are known as one of the predominant bacterial groups there (Muto et al., 2017). Nitrate is a primary electron acceptor for chemosynthetic *Campylobacteria* (Sievert and Vetriani, 2012), and several campylobacterial isolates mediate complete denitrification of $NO_3^-$ to $N_2$ (Nakagawa et al., 2005; Takai et al., 2006), indicating their ability to reduce $N_2O$ to $N_2$. Clade II *nosZ* gene has been detected in the genomes of several *Campylobacteria* isolated from deep-sea hydrothermal environments (Inagaki et al., 2003, 2004; Nakagawa et al., 2005; Giovannelli et al., 2016). In addition to metabolic and genetic characteristics of the isolates, multiple omics analyses have provided the insights into the *in situ* $N_2O$-reducing metabolic potential of *Campylobacteria* (Fortunato and Huber, 2016; Pjevac et al., 2018). The reduction of exogeneous $N_2O$, however, has never been characterized for *Campylobacteria* living in deep-sea hydrothermal vents. Here, we, for the first time, report on the direct $N_2O$ reduction of deep-sea vent chemolithoautotrophs and on its ability of $N_2O$ consumption.

# MATERIALS AND METHODS

## Sample Collection and Enrichment of $N_2O$-Reducing Microorganisms

The chimney structure was taken with R/V Yokosuka and DSV Shinkai 6500 from the Baltan chimney at the Urashima site (12°55.3014'N, 143°38.8946'E) in the South Mariana Trough in 2010 during the JAMSTEC cruise YK10-10. After retrieval on board, the sample was anaerobically processed as described previously (Mino et al., 2013). Samples were stored at 4°C until use. Serial dilution cultures were performed using HNN medium. HNN medium contained 0.1% (w/v) $NaHCO_3$ per liter of modified MJ synthetic seawater (Sako et al., 1996). Modified MJ synthetic seawater is composed of 25 g NaCl, 4.2 g $MgCl_2$ $6H_2O$, 3.4 g $MgSO_4$ $7H_2O$, 0.5g KCl, 0.25 g $NH_4Cl$, 0.14 g $K_2HPO_4$, 0.7 g $CaCl_2$ $2H_2O$, and 10 ml trace mineral solution per liter of distilled water. To prepare HNN medium, concentrated solution of $NaHCO_3$ was added before gas purging of 100% $N_2O$. The tubes were then tightly sealed with butyl rubber stopper, autoclaved, and pressurized the headspace to 300 kPa with 80% $H_2$ + 20% $CO_2$. $H_2$ is a sole energy source of the medium. The enrichment was performed with HNN medium under 33°C. The $N_2$ production under $N_2O$-reducing condition was confirmed using a Shimazu GC-2014 gas chromatograph (Shimadzu, Kyoto, Japan).

## Cultivation Experiments for the Community Analysis

The microbial community was precultured in HNN medium for 24 h at 38°C. Then, 2 mL of preculture was inoculated to 50 mL glass vials each containing 20 mL medium (33% $N_2O$ + 54% $H_2$ + 13% $CO_2$, 300 kPa). 5 vials were cultivated at once at 38°C, with mixing using a magnetic stirrer (MS-51M; AS ONE, Osaka, Japan) at 850 rpm. The concentration of headspace $N_2O$ of each cultivation vial at each time point ($t$ = 0, 12, 18, 24, 36, 42, and 48 h) was measured using a gas chromatograph (GC-2014; Shimadzu, Kyoto, Japan) with the SHINCARBON ST 50/80 (2 m × 3 mmϕ) column (Shinwa Chemical Industries, Kyoto, Japan). The cultivation was continued until decrease of $N_2O$ concentration reaches a plateau. At each time point ($t$ = 12, 18, 24, 36, and 48 h), one of the replicate vials was used and 20 mL of culture medium was transferred into 50 ml plastic centrifugation tubes. After centrifugation at 10,000 × g for 20 min, the supernatant was removed and cell pellet was stored at −30°C until DNA extraction. Cultivation experiment was carried out in triplicate.

## DNA Extraction

DNA extraction from the pelleted cell culture samples were performed with NucleoSpin Soil DNA kit (Macherey-Nagel, Düren, Germany) according to the protocol provided by the manufacturer. The DNA samples were stored at −30°C until sequencing analysis. A total of 15 DNA samples was used for 16S rRNA gene-based microbial community analysis. Four DNA samples from two time points ($t$ = 12 and 36 h, $n$ = 2) were also used for metagenomic analysis.

## Illumina 16S rRNA Gene Region Amplification and Sequencing

Each amplicon library was constructed by amplifying V1-V2 paired-end libraries using 27Fmod (5′-AGRGTTTGATYM TGGCTCAG-3′) and 338R (5′-TGCTGCCTCCCGTAGGAG T-3') according to Nextera library preparation methods. Equal amounts of each PCR amplicons were pooled, followed by amplification and 2 × 300 bp paired-end sequencing on the MiSeq platform according to the manufacturer's instructions.

## Data Analysis of 16S rRNA Gene Amplicons

A total of 519,290 raw reads across 15 samples, with an average 34,619 reads per sample, was further processed by QIIME 2 software package (version 2018.4). Quality control was performed using DADA2 (Callahan et al., 2016) by removing chimeras and residual PhiX reads, and low-quality regions of sequences. Forward and reverse reads were, respectively,

truncated to 230 and 209 bp for DADA2 analysis based on the average quality scores determined. After quality filtering, the dataset contained 421,406 reads, with an average of 28,093 sequences per samples. Dereplication was then performed by DADA2, which combines identical reads into amplicon sequence variants (ASVs), which is analog to the traditional Operational Taxonomic Unit (OTU). Representative sequences were classified into taxonomic groups using the SILVA 132 database. Mitochondrial and chloroplast sequences were then removed from the feature table, and bacterial and archaeal sequences were used further analysis. We used BLASTN search against the online nucleotide collection (nr/nt) database on NCBI to find the closest GenBank neighbor for these representative sequences.

## Metagenome Analyses by Illumina and Nanopore Sequencing

For two replicates from two time points ($t$ = 12 and 36 h), paired-end libraries for metagenome sequencing were generated using Nextera library preparation methods. Genome sequencing was then performed on an Illumina MiSeq platform (2 × 300 bp paired-end). Read data from Illumina sequencing were trimmed with Platanus_trim (Kajitani et al., 2014).

Nanopore sequencing was conducted with a DNA sample from a time point 36 h ($n$ = 1). Sequencing library preparation was carried out using the Rapid Barcoding Sequence kit (SQK-RBK001) (Oxford Nanopore Technologies, Oxford, UK) according to the standard protocol provided by the manufacturer. The constructed library was loaded into the FlowCell (FLO-MIN106) on a MinION device and performed 24 h sequencing run with MinKNOW1.7.14 software. The fast5 read file was basecalled with ONT Albacore command line tool (v2.0.2). The adapter sequences were trimmed from the fastq read file using Porechop v0.2.1 (https://github.com/rrwick/Porechop).

## Construction of Metagenome Assembled Genome (MAG)

For assembly, Canu version 1.6 (Koren et al., 2017) was run using Nanopore reads with following options: genome size 2.1 Mb, and correctedErrorRate = 0.120. The Illumina short reads were mapped to the Canu's assembly by BWA version 0.7.12 (Li, 2013). Pilon version 1.22 (Walker et al., 2014) was run on the alignments to polish the assembly sequences. Circlator version 1.5.1 (Hunt et al., 2015) program was used for circularizing the genome assembly. Two contigs were again polished by Pilon using Illumina reads. Metagenome assembled genome (MAG) sequences were assessed using CheckM v1.0.8 (Parks et al., 2015) for the completion estimate, and then larger MAG was annotated with the Rapid Annotation using Subsystem Technology (RAST) server v2.0 (Aziz et al., 2008). rRNA genes were predicted using RNAmmer (Lagesen et al., 2007). 16S rRNA gene sequences of the MAG were compared to a representative sequence of a dominant ASV obtained by 16S rRNA amplicon analysis. MAG was functionally annotated using KEGG database with the BlastKOALA pipeline (Kanehisa et al., 2016) and KO numbers were mapped using KEGG mapper to compare the metabolic pathway with a closely related species.

## Taxonomic Analysis of MAG

Taxonomic placement of the MAG was assessed based on both 16S rRNA and genomic approaches. 16S rRNA gene sequence of the MAG was aligned to closely related species using SILVA Incremental Aligner v1.2.11 (Pruesse et al., 2012). A phylogenetic tree was constructed by Maximum Likelihood (ML) method using MEGA 7.0.26 package (Kumar et al., 2016) with GTR+I+G substitution model. Phylogenomic tree construction was performed using PhyloPhlAn (Segata et al., 2013), which extracts up to 400 conserved proteins coded in the genomes of closely related species and generates multiple alignments of each protein. Multiple alignments of each universal protein were then concatenated into a single amino acid sequence. The optimal model for phylogenomic analysis was determined by Modelgenerator (Keane et al., 2006), and then ML tree was constructed using RAxML version 8.2.11 (Stamatakis, 2014) with BLOSUM62+G+F model. Average nucleotide identity (ANI), average amino acid identity (AAI) and *in-silico* DNA-DNA hybridization (DDH) values were calculated by ANI calculator (http://enve-omics.ce.gatech.edu/ani/index), AAI calculator (http://enve-omics.ce.gatech.edu/aai/) and Genome-to-Genome Distance Calculator (GGDC 2.1) (Meier-Kolthoff et al., 2013), respectively.

## Comparison of *nos* Clusters and *nosZ* Gene Sequences Within Related *Campylobacteria*

The genomes of chemosynthetic *Campylobacteria* were used to reconstruct the *nos* gene clusters. Sequences of functionally characterized NosZ protein and its accessory genes from *Wolinella succinogenes* were used to search the genes adjacent to inferred *nosZ* on *Hydrogenimonas* sp. MAG. Multiple amino acid sequence alignment was generated from representatives of clade I and clade II *nosZ* sequences using MUSCLE version 3.8.31 (Edgar, 2004). ML tree based on *nosZ* amino acid sequences was constructed by MEGA with WAG+G model based upon 500 bootstrapped replicates. Trees were visualized using FigTree v1.4.2 (http://tree.bio.ed.ac.uk/software/figtree/).

## Growth Characteristics

In attempt to evaluate the nitrate-respiring ability of the enrichment, each of the potential electron donors, such as $H_2$, elemental sulfur (1%, w/v), or thiosulfate (0.1%, w/v) was tested with nitrate (0.1%, w/v) as an electron acceptor under 40°C. The ability to use $H_2$ was examined with 80% $H_2$ + 20% $CO_2$ (300 kPa) in the headspace. For testing growth on elemental sulfur and thiosulfate as an electron donor, 80% $N_2$ + 20 % $CO_2$ was used as the gas phase (300 kPa).

## RESULTS AND DISCUSSION

### $N_2O$ Consumption and Community Structure of the Enrichment Culture

Approximately 90% of initial headspace $N_2O$ was consumed after 42 h of cultivation (**Figure 1**). The maximum rate of $N_2O$ consumption was 3.3 μmol $h^{-1}$ per ml of culture, higher than other clade I and II reducers (Sanford et al., 2012; Yoon et al., 2016), though a higher initial $N_2O$ concentration in this study was provided than in the previous studies. The aqueous-phase $N_2O$ concentration was calculated from the Ostwald coefficient (0.4190) at 1 atm partial pressure and 40°C (Wilhelm et al., 1977). 2.75 mmol of vessel $N_2O$ in 20 ml of medium corresponded to an initial aqueous-phase $N_2O$ concentration 56.5 mM. This concentration is more than million-fold higher than the $N_2O$ level observed in deep-sea hydrothermal environments, where $N_2O$ is mainly supplied by microbial nitrification and denitrification processes (Lilley et al., 1982; Kawagucci et al., 2010).

To identify the $N_2O$-reducing organisms in the enrichment culture, we analyzed the time-series community structure during the cultivation under the HNN medium. Dereplicate 421,406 Illumina reads resulted in 11 bacterial ASVs. The genus *Hydrogenimonas* consisting of a single ASV was the most predominant bacterial group through the cultivation period and its relative abundance was above 98% (**Figure 1** and **Figure S1**). In order to further identify this dominant ASV, a representative sequence was extracted from the sequence data and analyzed by BLAST search. The best match represented *Hydrogenimonas thermophila* EP1-55-1%$^T$ (=JCM 11971$^T$ = ATCC BAA-737$^T$) with 90% identity, suggesting the host organism of the ASV would be a new species of *Hydrogenimonas* or even a new genus of the class *Campylobacteria*. Strain EP1-55-1%, isolated from a deep-sea hydrothermal vent field in the Indian Ocean, is able to utilize nitrate as an electron acceptor and shows the optimum growth at 55°C (Takai et al., 2004). These characteristics are different from the $N_2O$-reducing enrichment culture in this study, which shows an optimum growth at 40°C and no growth under nitrate-respiring condition. The genus *Thalassospira* consisting of a single ASV accounted for about 0.7% of reads at 12 h, and its abundance gradually decreased to 0.1% at 36 h of cultivation. The representative sequence of the ASV assigned to *Thalassospira* showed 100% similarity to *T. xianhensis* P-4$^T$ (=CGMCC 1.6849$^T$ = JCM 14850$^T$) isolated from an oil-polluted saline soil (Zhao et al., 2010). *T. xianhensis* engages denitrification, possibly having $N_2O$-reducing ability, but it cannot grow under autotrophic condition. Along with the increase of relative abundance of *Hydrogenimonas*, headspace $N_2O$ decreased and reached 0.05 mmol/vessel at 48 h, showing that members belonging to *Hydrogenimonas* significantly contribute to $N_2O$ consumption of the enrichment culture.

### Reconstruction of the Genome, Taxonomy, and Denitrification Pathway of a Novel $N_2O$-Reducing Campylobacterium Strain BAL40

In order to understand the genomic characteristics of most dominant ASV species, we employed the MAG reconstruction

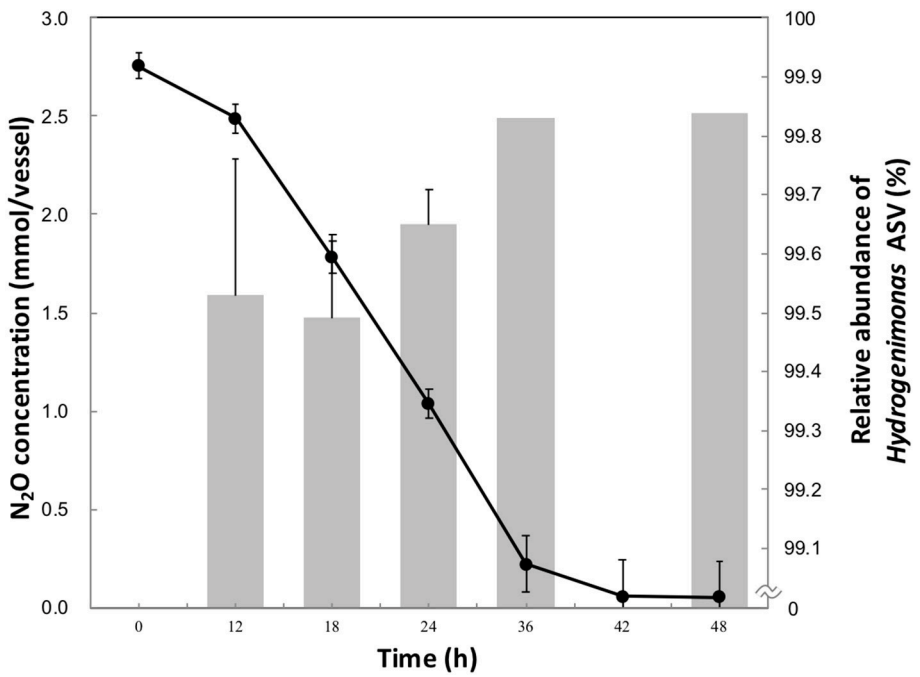


**FIGURE 1 |** $N_2O$ consumption (•) and relative abundance of *Hydrogenimonas* ASV in the enrichment culture (bar chart) during the 48 h-cultivation. The data points and error bars represent the means and standard errors, respectively.

strategy, because cells formed pellicle-like structures that was unable to be purified to a single pure strain by the dilution-to-extinction technique. High-quality 14,951,908 reads (4.6 Gb) and 236,546 reads (1.1 Gb) of metagenomic data were obtained by Illumina and Nanopore sequencing, respectively, and assembled into two contigs. After circularization, a larger contig resulted in a complete circular, which is 2,193,435 bp in length with an average G + C content of 50.2% and >99% genome completeness (**Figure S2**). In total, 2,185 coding sequence (CDS) regions and 54 RNAs were annotated. Three copies of 16S rRNA gene were annotated by RNAmmer, and its V1-V2 regions were identical with each other and with the represent sequence of the dominant ASV. With full length of 16S rRNA gene sequences as a query in BLAST search, the highest similarity was estimated with *H. thermophila* EP1-55-1%$^T$ (94%). The size of the other contig is 49,484 bp with 0% completeness level estimated by CheckM.

Both 16S rRNA gene-based and genome-based phylogenetic trees revealed that the MAG was most closely related to *H. thermophila* (**Figures 2**,**3**). *In-silico* DDH and ANI values between the strain BAL40 MAG and *H. thermophila* genome sequences were 17.4% and 74.4%, respectively, well below species cutoff (Richter and Rosselló-Móra, 2009). AAI value with *H. thermophila* was 71.4%, which is higher than the genus criterion level (Konstantinidis and Tiedje, 2005; Konstantinidis et al., 2017). Taken together, the strain BAL40 MAG described here represents a novel species within the genus *Hydrogenimonas*.

Reconstruction of denitrification pathway using KEGG database revealed that the MAG possessed whole set of denitrification genes (*nap*, *nir*, *nor,* and *nos*) (**Figure S3**), suggesting the ability to utilize nitrate as an electron acceptor. However, the enrichment culture did not show any growth under the nitrate-respiring condition in this study. This discrepancy between genetic and physiological characteristics implies the existence of heretofore overlooked $N_2O$-reducing microorganisms, which are genetically denitrifiers *sensu stricto* but are physiologically non-denitrifiers. However, the influence of *in situ* physicochemical conditions on their denitrification metabolisms could not be examined here. Considering our results, we speculate that together diverse microbial species drive different steps to the full denitrification pathway of nitrate to $N_2$ in deep-sea hydrothermal environments. It should be noted that because most environmental studies investigating abundance, diversity and function of denitrifiers have been performed based solely on the PCR-based marker gene analysis (Braker and Tiedje, 2003; Henry et al., 2006; Smith et al., 2007; Sanford et al., 2012; Jones et al., 2013), it is virtually impossible to identify which organism is actually responsible for specific steps of the denitrification process. Further culture-dependent studies could demonstrate the actual function of both denitrifying and non-denitrifying microorganisms. In addition, cultivation under $N_2O$-respiring condition might decrease the number of yet-to-be cultured microorganisms and unveil the $N_2O$ mitigation potential hidden in deep-sea hydrothermal environments.

## Reconstruction of the *nos* Gene Cluster and Comparison of *nosZ* Sequences in *Campylobacteria*

We reconstructed *nos* gene clusters from the genomes of MAG and related *Campylobacteria* including *Wolinella succinogenes*, which has been used as a campylobacterial model organism (**Figure 3**). Similar to *W. succinogenes*, *Hydrogenimonas* sp. MAG possessed a clade II *nos* gene cluster that contains *nosZ, -B, -D, -G, -H, -C1, -C2, -H, -Y, -L* genes, and the presence and

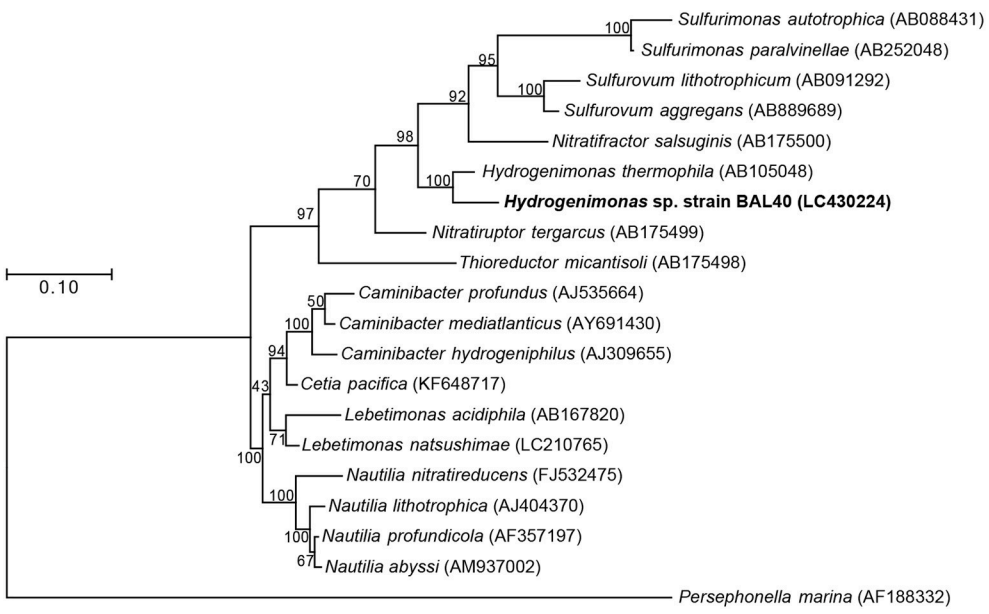


**FIGURE 2 |** ML Phylogenetic tree based on 1,196 nucleotide position of 16S rRNA gene sequences. Bootstrap values based on 500 resampling replicates are shown as percentages at branch nodes.

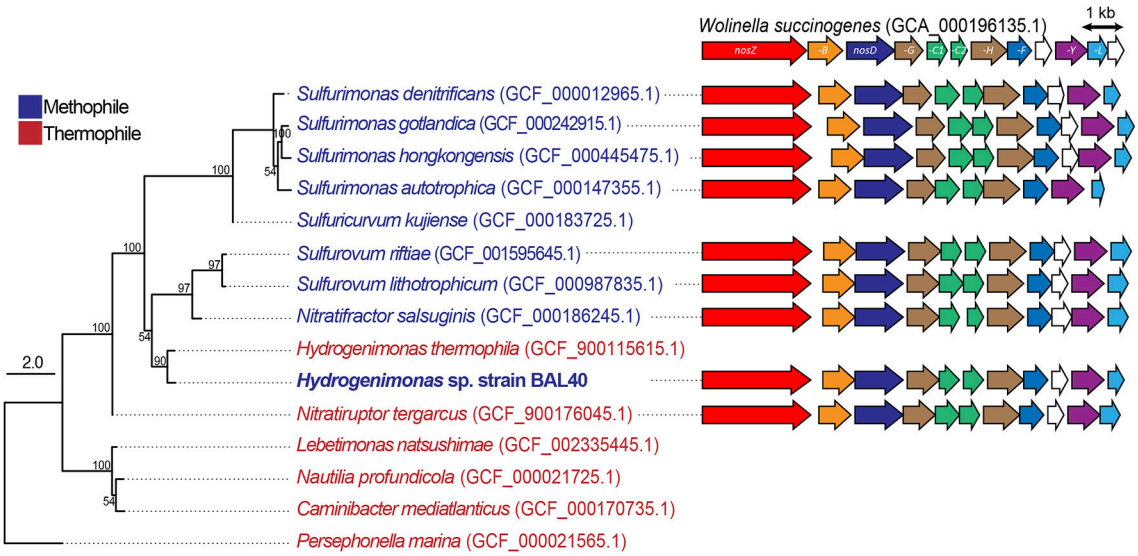


**FIGURE 3 |** ML tree based on genome sequences and schematic comparison of the *nos* gene clusters in different *Campylobacteria*. Bootstrap values based on 500 resampling replicates are shown as percentages at branch nodes. Clade II *nosZ* and its accessory genes (BDFGHLY) are labeled and colored according to homology across the different species.

organization of these genes were well-conserved in the related *Campylobacteria* members, as previously described (Torres et al., 2016). A phylogenetic tree based on amino acid sequences of *nosZ* gene indicated that the sequence of *Hydrogenimonas* sp. MAG is closely related to *Nitratifractor salsuginis* E9I37-1$^T$, which is known as a nitrate-reducing mesophile (Nakagawa et al., 2005) (**Figure S4**). Multiple alignment of NosZ amino acid sequences that contained both clade I and clade II sequences showed that NosZ of *Campylobacteria* including *Hydrogenimonas* sp. MAG conserved ligands of two cooper sites; $Cu_A$ electron transfer center and $Cu_Z$ catalytic center (Zumft and Kroneck, 2007) (**Figure S5**). It is therefore deduced that $N_2O$-respiring metabolism supports more diverse *Campylobacteria* in deep-sea hydrothermal environments.

## $N_2O$ Emission and Sink in Deep-Sea Hydrothermal Environments

A variety of microorganisms contributing to the denitrification process have been reported in a wide range of environments such as sediments, paddy soils, hydrothermal vents, and geothermal streams (Shao et al., 2010; Masuda et al., 2017; Kato et al., 2018). $N_2O$ emissions by denitrification are the net result of the balance between its production and reduction to $N_2$. In deep-sea hydrothermal environments, diverse microorganisms including *Campylobacteria* involved in denitrification processes (Bourbonnais et al., 2012; Bowles et al., 2012; Fortunato and Huber, 2016; Pjevac et al., 2018). The occurrence of microorganisms with the high ability to reduce exogenous $N_2O$ could explain the previous physicochemical results that *in situ* $N_2O$ level is quite low (Lilley et al., 1982; Kawagucci et al., 2010), and its flux to the deep waters is negligible (Bange and Andreae, 1999). Our findings imply the capacity of deep-sea hydrothermal environments to act as a sink for $N_2O$ is greater than its capacity to emit $N_2O$.

## CONCLUSION

We conducted, to the best of our knowledge, the first culture-dependent study of deep-sea hydrothermal vent $N_2O$-reducing microorganisms. Evaluation of $N_2O$ consumption ability and genome reconstruction from metagenomic data demonstrated that the notable $N_2O$ consumption rate of the novel member within genus *Hydrogenimonas*. Our findings will open door for new ideas to implement biotechnological applications of NosZ from thermophiles, such as nitrogen removal from wastewater. Future studies, such as comparative cultivation analysis of $N_2O$-reducing *Campylobacteria*, transcriptional analysis of *nos* genes, and measurement of $N_2O$ consumption kinetics, may provide the insights into the mechanisms allowing to their high $N_2O$ consumption ability.

## DATA AVAILABILITY

This project has been deposited at DDBJ/EMBL/GenBank under the BioProject PRJDB7296. Sequences for MAG and 16S rRNA gene of *Hydrogenimonas* sp. strain BAL40 are available with DDBJ/EMBL/GenBank AP019005 and LC430224, respectively.

## AUTHOR CONTRIBUTIONS

SM, SN, and TS designed research. SM, NY performed the experiments and analyzed the data. SN and KT contributed the sample collection. SM and TS contributed reagents, materials,

and analysis tools. SM wrote the paper with inputs from SN, KT, and TS.

## ACKNOWLEDGMENTS

We thank the captain and crew of *R/V Yokosuka* and *DSV Shinkai 6500* operation team on cruise JAMSTEC YK10-10. We are also grateful to Ms. Mami Tanaka (Hokkaido University, Hakodate, Japan) for invaluable help with Nanopore sequencing, and to Prof. Masahira Hattori and Dr. Wataru Suda (the University of Tokyo, Kashiwa, Japan) for assistance with sequencing of metagenome by Illumina. We would like to thank Muneyuki Fukushi (Hokkaido University, Hakodate, Japan) for kindly assistance with cultivation experiments. This work was partially supported by the JSPS KAKENHI (No. 12J03037 and No. 15H05991).

## SUPPLEMENTARY MATERIAL

The Supplementary Material for this article can be found online at: https://www.frontiersin.org/articles/10.3389/fbioe.2018.00184/full#supplementary-material

## REFERENCES

Aziz, R. K., Bartels, D., Best, A. A., DeJongh, M., Disz, T., Edwards, R. A., et al. (2008). The RAST server: rapid annotations using subsystems technology. *BMC Genomics* 9:75. doi: 10.1186/1471-2164-9-75

Bange, H. W., and Andreae, M. O. (1999). Nitrous oxide in the deep waters of the world's oceans. *Glob. Biogeochem. Cycles* 13, 1127–1135. doi: 10.1029/1999GB900082

Bourbonnais, A., Juniper, S. K., Butterfield, D. A., Devol, A. H., Kuypers, M. M. M., Lavik, G., et al. (2012). Activity and abundance of denitrifying bacteria in the subsurface biosphere of diffuse hydrothermal vents of the Juan de Fuca Ridge. *Biogeosciences* 9, 4661–4678. doi: 10.5194/bg-9-4661-2012

Bowles, M. W., Nigro, L. M., Teske, A. P., and Joye, S. B. (2012). Denitrification and environmental factors influencing nitrate removal in Guaymas Basin hydrothermally altered sediments. *Front. Microbiol.* 3:377. doi: 10.3389/fmicb.2012.00377

Braker, G., and Tiedje, J. M. (2003). Nitric oxide reductase (*norB*) genes from pure cultures and environmental samples. *Appl. Environ. Microbiol.* 69, 3476–3483. doi: 10.1128/AEM.69.6.3476-3483.2003

Callahan, B. J., McMurdie, P. J., Rosen, M. J., Han, A. W., Johnson, A. J., and Holmes, S. P. (2016). DADA2: high-resolution sample inference from amplicon data. *Nat. Methods* 13, 581–583. doi: 10.1038/nmeth.3869

Edgar, R. C. (2004). MUSCLE: multiple sequence alignment with high accuracy and high throughput. *Nucleic Acids Res.* 32, 1792–1797. doi: 10.1093/nar/gkh340

Fortunato, C. S., and Huber, J. A. (2016). Coupled RNA-SIP and metatranscriptomics of active chemolithoautotrophic communities at a deep-sea hydrothermal vent. *ISME J.* 10, 1925–1938. doi: 10.1038/ismej.2015.258

Giovannelli, D., Chung, M., Staley, J., Starovoytov, V., Le Bris, N., and Vetriani, C. (2016). Sulfurovum riftiae sp. *nov.,* a mesophilic, thiosulfate-oxidizing, nitrate-reducing chemolithoautotrophic epsilonproteobacterium isolated from the tube of the deep-sea hydrothermal vent polychaete *Riftia pachyptila*. *Int. J. Syst. Evol. Microbiol.* 66, 2697–2701. doi: 10.1099/ijsem.0.001106

Henry, S., Bru, D., Stres, B., Hallet, S., and Philippot, L. (2006). Quantitative detection of the *nosZ* gene, encoding nitrous oxide reductase, and comparison of the abundances of 16S rRNA, *narG*, *nirK*, and *nosZ* genes in soils. *Appl. Environ. Microbiol.* 72, 5181–5189. doi: 10.1128/AEM.00231-06

Hunt, M., Silva, N. D., Otto, T. D., Parkhill, J., Keane, J. A., and Harris, S. R. (2015). Circlator: automated circularization of genome assemblies using long sequencing reads. *Genome Biol.* 16:294. doi: 10.1186/s13059-015-0849-0

Inagaki, F., Takai, K., Kobayashi, H., Nealson, K. H., and Horikoshi, K. (2003). Sulfurimonas autotrophica gen. *nov., sp. nov.,* a novel sulfur-oxidizing ε-proteobacterium isolated from hydrothermal sediments in the Mid-Okinawa Trough. *Int. J. Syst. Evol. Microbiol.* 53, 1801–1805. doi: 10.1099/ijs.0.02682-0

Inagaki, F., Takai, K., Nealson, K. H., and Horikoshi, K. (2004). *Sulfurovum* lithotrophicum gen. *nov., sp. nov.,* a novel sulfur-oxidizing chemolithoautotroph within the ε-Proteobacteria isolated from Okinawa Trough hydrothermal sediments. *Int. J. Syst. Evol. Microbiol.* 54, 1477–1482. doi: 10.1099/ijs.0.03042-0

IPCC. (2006). *IPCC Guidelines for National Greenhouse Gas Inventories. Vol. 4.* Hayama: IGES.

IPPC. (2007). *Climate Change 2007: Mitigation of Climate Change; Contribution of Working Group III to the the 4th Assessment Report of the Intergovernmental Panel on Climate Change*, Cambridge University Press, Cambridge.

Jones, C. M., Graf, D. R., Bru, D., Philippot, L., and Hallin, S. (2013). The unaccounted yet abundant nitrous oxide-reducing microbial community: a potential nitrous oxide sink. *ISME J.* 7, 417–426. doi: 10.1038/ismej.2012.125

Jones, C. M., Spor, A., Brennan, F. P., Breuil, M.-C., Bru, D., Lemanceau, P., et al. (2014). Recently identified microbial guild mediates soil $N_2O$ sink capacity. *Nat. Clim. Chang.* 4, 801–805. doi: 10.1038/nclimate2301

Kajitani, R., Toshimoto, K., Noguchi, H., Toyoda, A., Ogura, Y., Okuno, M., et al. (2014). Efficient *de novo* assembly of highly heterozygous genomes from whole-genome shotgun short reads. *Genome Res.* 24, 1384–1395. doi: 10.1101/gr.170720.113

Kanehisa, M., Sato, Y., and Morishima, K. (2016). BlastKOALA and GhostKOALA: KEGG tools for functional characterization of genome and metagenome sequences. *J. Mol. Biol.* 428, 726–731. doi: 10.1016/j.jmb.2015.11.006

Kato, S., Sakai, S., Hirai, M., Tasumi, E., and Nishizawa, M., Suzuki, et al. (2018). Long-term cultivation and metagenomics reveal ecophysiology of previously uncultivated thermophiles involved in biogeochemical nitrogen cycle. *Microbes Environ.* 33, 107–110. doi: 10.1264/jsme2.ME17165

Kawagucci, S., Shirai, K., Lan, T. F., Takahata, N., Tsunogai, U., Sano, Y., et al. (2010). Gas geochemical characteristics of hydrothermal plumes at the HAKUREI and JADE vent sites, the Izena Cauldron, Okinawa Trough. *Geochem. J.* 44, 507–518. doi: 10.2343/geochemj.1.0100

Keane, T. M., Creevey, C. J., Pentony, M. M., Naughton, T. J., and Mclnerney, J. O. (2006). Assessment of methods for amino acid matrix selection and their use on empirical data shows that *ad hoc* assumptions for choice of matrix are not justified. *BMC Evol. Biol.* 6:29. doi: 10.1186/1471-2148-6-29

Konstantinidis, K. T., Rosselló-Móra, R., and Amann, R. (2017). Uncultivated microbes in need of their own taxonomy. *ISME J.* 11, 2399–2406. doi: 10.1038/ismej.2017.113

Konstantinidis, K. T., and Tiedje, J. M. (2005). Towards a genome-based taxonomy for prokaryotes. *J. Bacteriol.* 187, 6258–6264. doi: 10.1128/JB.187.18.6258-6264.2005

Koren, S., Walenz, B. P., Berlin, K., Miller, J. R., Bergman, N. H., and Phillippy, A. M. (2017). Canu: scalable and accurate long-read assembly via adaptive k-mer weighting and repeat separation. *Genome Res.* 27, 722–736. doi: 10.1101/gr.215087.116

Kumar, S., Stecher, G., and Tamura, K. (2016). MEGA7: molecular evolutionary genetics analysis version 7.0 for bigger datasets. *Mol. Biol. Evol.* 33, 1870–1874. doi: 10.1093/molbev/msw054

Lagesen, K., Hallin, P., Rødland, E. A., Staerfeldt, H. H., Rognes, T., and Ussery, D. W. (2007). RNAmmer: consistent and rapid annotation of ribosomal RNA genes. *Nucleic. Acids. Res.* 35, 3100–3108. doi: 10.1093/nar/gkm160

Li, H. (2013). Aligning sequence reads, clone sequences and assembly contigs with BWA-MEM. *arXiv*. arXiv:1303.3997. Available online at: http://arxiv.org/abs/1303.3997

Lilley, M. D., de Angelis, M. A., and Gordon, L. I. (1982). $CH_4$, $H_2$, CO and $N_2O$ in submarine hydrothermal vent waters. *Nature* 300, 48–50. doi: 10.1038/300048a0

Masuda, Y., Itoh, H., Shiratori, Y., Isobe, K., Otsuka, S., and Senoo, K. (2017). Predominant but previously-overlooked prokaryotic drivers of reductive nitrogen transformation in paddy soils, revealed by metatranscriptomics. *Microbes Environ.* 32, 180–183. doi: 10.1264/jsme2.ME16179

Meier-Kolthoff, J. P., Auch, A. F., Klenk, H. P., and Göker, M. (2013). Genome sequence-based species delimitation with confidence intervals and improved distance functions. *BMC Bioinformatics* 14:60. doi: 10.1186/1471-2105-14-60

Mino, S., Makita, H., Toki, T., Miyazaki, J., Kato, S., Watanabe, H., et al. (2013). Biogeography of *Persephonella* in deep-sea hydrothermal vents of the Western Pacific. *Front. Microbiol.* 4:107. doi: 10.3389/fmicb.2013.00107

Mino, S., and Nakagawa, S. (2018). "Deep-sea ven extrimophiles: cultivation, physiological characteristics, and ecological significance," in *Extremophiles: From biology to biotechnology*, eds R. V. Durvasula and D. V. S. Rao (New York, NY: CRC Press), 165–183.

Muto, H., Takaki, Y., Hirai, M., Mino, S., Sawayama, S., Takai, K., et al. (2017). A simple and efficient RNA extraction method from deep-sea hydrothermal vent chimney structures. *Microbes Environ.* 32, 330–335. doi: 10.1264/jsme2.ME17048

Nakagawa, S., Takai, K., Inagaki, F., Horikoshi, K., and Sako, Y. (2005). Nitratiruptor tergarcus gen. *nov., sp. nov.* and Nitratifractor salsuginis gen. *nov., sp. nov.,* nitrate-reducing chemolithoautotrophs of the ε-Proteobacteria isolated from a deep-sea hydrothermal system in the Mid-Okinawa Trough. *Int. J. Syst. Evol. Microbiol.* 55, 925–933. doi: 10.1099/ijs.0.63480-0

Parks, D. H., Imelfort, M., Skennerton, C. T., Hugenholtz, P., and Tyson, G. W. (2015), CheckM: assessing the quality of microbial genomes recovered from isolates, single cells, and metagenomes. *Genome Res.* 25, 1043–1055. doi: 10.1101/gr.186072.114

Pjevac, P., Meier, D. V., Markert, S., Hentschker, C., Schweder, T., Becher, D., et al. (2018). Metaproteogenomic profiling of microbial communities colonizing actively venting hydrothermal chimneys. *Front. Microbiol.* 9:680. doi: 10.3389/fmicb.2018.00680

Pruesse, E., Peplies, J., and Glöckner, F. O. (2012). SINA: accurate high-throughput multiple sequence alignment of ribosomal RNA genes. *Bioinformatics* 28, 1823–1829. doi: 10.1093/bioinformatics/bts252

Ravishankara, A. R., Daniel, J. S., and Portmann, R. W. (2009). Nitrous oxide ($N_2O$): the dominant ozone-depleting substance emitted in the 21st century. *Science* 326, 123–125. doi: 10.1126/science.1176985

Richter, M., and Rosselló-Móra, R. (2009). Shifting the genomic gold standard for the prokaryotic species definition. *Proc. Natl. Acad. Sci. USA.* 106, 19126–19131. doi: 10.1073/pnas.0906412106

Sako, Y., Takai, K., Ishida, Y., Uchida, A., and Katayama, Y. (1996). *Rhodothermus obamensis* sp. *nov.,* a modern lineage of extremely thermophilic marine bacteria. *Int. J. Syst. Bacteriol.* 46, 1099–1104. doi: 10.1099/00207713-46-4-1099

Sanford, R. A., Wagner, D. D., Wu, Q., Chee-Sanford, J. C., Thomas, S. H., Cruz-García, C., et al. (2012). Unexpected nondenitrifier nitrous oxide reductase gene diversity and abundance in soils. *Proc. Natl. Acad. Sci. USA.* 109, 19709–19714. doi: 10.1073/pnas.1211238109

Segata, N., Börnigen, D., Morgan, X. C., and Huttenhower, C. (2013). PhyloPhlAn is a new method for improved phylogenetic and taxonomic placement of microbes. *Nat. Commun.* 4:2304. doi: 10.1038/ncomms3304

Shao, M. F., Zhang, T., and Fang, H. H. (2010). Sulfur-driven autotrophic denitrification: diversity, biochemistry, and engineering applications. *Appl. Microbiol. Biotechnol.* 88, 1027–1042. doi: 10.1007/s00253-010-2847-1

Sievert, S. M., and Vetriani, C. (2012). Chemoautotrophy at deep-sea vents: past, present, and future. *Oceanography* 25, 218–233. doi: 10.5670/oceanog.2012.21

Smith, C. J., Nedwell, D. B., Dong, L. F., and Osborn, A. M. (2007). Diversity and abundance of nitrate reductase genes (*narG* and *napA*), nitrite reductase genes (*nirS* and *nrfA*), and their transcripts in estuarine sediments. *Appl. Environ. Microbiol.* 73, 3612–3622. doi: 10.1128/AEM.02894-06

Stamatakis, A. (2014). RAxML version 8: a tool for phylogenetic analysis and post-analysis of large phylogenies. *Bioinformatics.* 30, 1312–1313. doi: 10.1093/bioinformatics/btu033

Takai, K., and Nakamura, K. (2011). Archaeal diversity and community development in deep-sea hydrothermal vents. *Curr. Opin. Microbiol.* 14, 282–291. doi: 10.1016/j.mib.2011.04.013

Takai, K., Nealson, K. H., and Horikoshi, K. (2004). Hydrogenimonas thermophila gen. *nov., sp. nov.,* a novel thermophilic, hydrogen-oxidizing chemolithoautotroph within the ε-Proteobacteria, isolated from a black smoker in a Central Indian Ridge hydrothermal field. *Int. J. Syst. Evol. Microbiol.* 54, 25–32. doi: 10.1099/ijs.0.02787-0

Takai, K., Suzuki, M., Nakagawa, S., Miyazaki, M., Suzuki, Y., Inagaki, F., et al. (2006). *Sulfurimonas paralvinellae* sp. *nov.,* a novel mesophilic, hydrogen- and sulfur-oxidizing chemolithoautotroph within the *Epsilonproteobacteria* isolated from a deep-sea hydrothermal vent polychaete nest, reclassification of Thiomicrospira denitrificans as *Sulfurimonas* denitrificans comb. *nov.* and emended description of the genus *Sulfurimonas. Int. J. Syst. Evol. Microbiol.* 56, 1725–1733. doi: 10.1099/ijs.0.64255-0

Torres, M. J., Simon, J., Rowley, G., Bedmar, E. J., Richardson, D. J., Gates, A. J., et al. (2016). Nitrous oxide metabolism in nitrate-reducing bacteria: physiology and regulatory mechanisms. *Adv. Microb. Physiol.* 68, 353–432. doi: 10.1016/bs.ampbs.2016.02.007

Waite, D. W., Vanwonterghem, I., Rinke, C., Parks, D. H., Zhang, Y., Takai, K., et al. (2017). Comparative genomic analysis of the class *Epsilonproteobacteria* and proposed reclassification to Epsilonbacteraeota (phyl. *nov.). Front. Microbiol.* 8:682. doi: 10.3389/fmicb.2017.00682

Walker, B. J., Abeel, T., Shea, T., Priest, M., Abouelliel, A., Sakthikumar, S., et al. (2014). Pilon: an integrated tool for comprehensive microbial variant detection and genome assembly improvement. *PLoS ONE* 9:e112963. doi: 10.1371/journal.pone.0112963

Wilhelm, E., Battino, R., and Wilcock, R. J. (1977). Low-pressure solubility of gases in liquid water. *Chem. Rev.* 77, 219–262. doi: 10.1021/cr60306a003

Yoon, S., Nissen, S., Park, D., Sanford, R. A., and Löffler, F. E. (2016). Nitrous oxide reduction kinetics distinguish bacteria harboring clade I NosZ from those harboring clade II NosZ. *Appl. Environ. Microbiol.* 82, 3793–3800. doi: 10.1128/AEM.00409-16

Zhao, B., Wang, H., Li, R., and Mao, X. (2010). Thalassospira xianhensis sp. *nov.,* a polycyclic aromatic hydrocarbon-degrading marine bacterium. *Int. J. Syst. Evol. Microbiol.* 60, 1125–1129. doi: 10.1099/ijs.0.013201-0

Zumft, W. G., and Kroneck, P. M. (2007). Respiratory transformation of nitrous oxide ($N_2O$) to dinitrogen by Bacteria and Archaea. *Adv. Microb. Physiol.* 52, 107–227. doi: 10.1016/S0065-2911(06)52003-X

**Conflict of Interest Statement:** The authors declare that the research was conducted in the absence of any commercial or financial relationships that could be construed as a potential conflict of interest.

frontiers in Bioengineering and Biotechnology

ORIGINAL RESEARCH
published: 20 December 2018
doi: 10.3389/fbioe.2018.00202

# The Relationship Between Microbial Community Structures and Environmental Parameters Revealed by Metagenomic Analysis of Hot Spring Water in the Kirishima Area, Japan

*Eri Nishiyama[1,2]*, Koichi Higashi[3], Hiroshi Mori[3], Konomi Suda[4], Hitomi Nakamura[5], Soichi Omori[6], Shigenori Maruyama[7], Yuichi Hongoh[8] and Ken Kurokawa[3]*

*[1] Biotechnological Research Support Division, FASMAC Co. Ltd, Kanagawa, Japan, [2] Department of Biological Information, Tokyo Institute of Technology, Tokyo, Japan, [3] Center for Information Biology, National Institute of Genetics, Shizuoka, Japan, [4] Institute for Geo-Resources and Environment, National Institute of Advanced Industrial Science and Technology, Ibaraki, Japan, [5] Department of Solid Earth Geochemistry, Japan Agency for Marine-Earth Science and Technology, Yokosuka, Japan, [6] Faculty of Liberal Arts, The Open University of Japan, Chiba, Japan, [7] Department of Earth and Planetary Sciences, Tokyo Institute of Technology, Tokyo, Japan, [8] School of Life Science and Technology, Tokyo Institute of Technology, Tokyo, Japan*

OPEN ACCESS

**Edited by:**
*Milko Alberto Jorquera, Universidad de La Frontera, Chile*

**Reviewed by:**
*Pabulo Henrique Rampelotto, Universidade Federal do Rio Grande do Sul (UFRGS), Brazil*
*M. Sudhakara Reddy, Thapar University, India*

***Correspondence:**
*Eri Nishiyama*
*enishiyama@fasmac.co.jp*

**Specialty section:**
*This article was submitted to Process and Industrial Biotechnology, a section of the journal Frontiers in Bioengineering and Biotechnology*

**Received:** *16 August 2018*
**Accepted:** *10 December 2018*
**Published:** *20 December 2018*

**Citation:**
*Nishiyama E, Higashi K, Mori H, Suda K, Nakamura H, Omori S, Maruyama S, Hongoh Y and Kurokawa K (2018) The Relationship Between Microbial Community Structures and Environmental Parameters Revealed by Metagenomic Analysis of Hot Spring Water in the Kirishima Area, Japan. Front. Bioeng. Biotechnol. 6:202. doi: 10.3389/fbioe.2018.00202*

Diverse microorganisms specifically inhabit extreme environments, such as hot springs and deep-sea hydrothermal vents. To test the hypothesis that the microbial community structure is predictable based on environmental factors characteristic of such extreme environments, we conducted correlation analyses of microbial taxa/functions and environmental factors using metagenomic and 61 types of physicochemical data of water samples from nine hot springs in the Kirishima area (Kyusyu, Japan), where hot springs with diverse chemical properties are distributed in a relatively narrow area. Our metagenomic analysis revealed that the samples can be classified into two major types dominated by either phylum Crenarchaeota or phylum Aquificae. The correlation analysis showed that Crenarchaeota dominated in nutrient-rich environments with high concentrations of ions and total carbons, whereas Aquificae dominated in nutrient-poor environments with low ion concentrations. These environmental factors were also important explanatory variables in the generalized linear models constructed to predict the abundances of Crenarchaeota or Aquificae. Functional enrichment analysis of genes also revealed that the separation of the two major types is primarily attributable to genes involved in autotrophic carbon fixation, sulfate metabolism and nitrate reduction. Our results suggested that Aquificae and Crenarchaeota play a vital role in the Kirishima hot spring water ecosystem through their metabolic pathways adapted to each environment. Our findings provide a basis to predict microbial community structures in hot springs from environmental parameters, and also provide clues for the exploration of biological resources in extreme environments.

**Keywords: extreme environments, environmental parameters, microorganisms, metagenome, hot springs**

## INTRODUCTION

The increasingly widespread use of next-generation sequencing (NGS) has led to more information on the taxonomic composition of microorganisms from various environmental samples being obtained (Sun et al., 2014; Castelino et al., 2017). In particular, many hitherto unexamined microbial communities have been discovered in extreme environments, such as hot springs and deep-sea hydrothermal vents, and it has been reported that many of these microbes specifically live in extreme environments (Song et al., 2013; Tiago and Veríssimo, 2013; Chan et al., 2015; Zhang et al., 2016). It is assumed that microorganisms living in extreme environments have evolved various metabolic energy systems adapted to specific environmental factors derived from the local chemical milieu. Several studies of extreme environments, such as chimney 4143-1 in the Mothra hydrothermal vent field (Xie et al., 2011) and Yellowstone National Park (YNP) in the USA (Inskeep et al., 2010, 2013a; Jay et al., 2016) have reported specific microbial communities and their gene repertoires along with the environmental data. Recent studies have also revealed that specific environmental factors (e.g., temperature and sulfide concentrations) are related to microbial composition in the Philippines (Huang et al., 2013), the Tibetan Plateau in northwestern China (Wang et al., 2013), and in the Tengchong in southwest China (Hou et al., 2013). Research into microorganisms and environmental data from the YNP metagenome project reported that pH is one of important factors in forming the microbial community type in a hot spring environment (Inskeep et al., 2013b). There are limited studies discussing the kind of environmental factors that affect these community structures and their gene repertoires, as well as methods of predicting microbial taxon abundances from environmental factors.

Investigation of microorganisms living in extreme environments also plays a vital role in exploring biological resources. Various useful enzymes and bioactive compounds have been discovered from microbes derived from extreme environments, and have been applied to multiple fields, such as medicine and food production (Littlechild, 2015; Mahajan and Balachandran, 2017). If we can predict what kind of microbes live in an extreme environment from the environmental factors, this will lead to a more efficient search for useful biological resources. To establish a method for predicting the microbial community structure from environmental factors, it is essential to compare the community structures among multiple sampling points showing the diverse properties of environmental factors. An environment suitable for such comparative analysis is in the Kirishima area of Japan.

Many hot springs occur in the area where the volcanic front crosses the Kyushu region of Japan. The Kirishima area is located in the Kyushu region and has hot springs with various chemical properties distributed in a relatively narrow area (**Figure 1** and **Supplementary Figure 1**; **Supplementary Table 1**). The Kirishima area is mainly composed of andesite, and hot spring water from two origins is found there (Gokou et al., 1995): (1) geothermal fluid gushing from the surface of the earth through a fault at a depth of 2 km; and (2) high-temperature fluid originating from surface water and circulating at a depth of about 1 km. The hot spring water in the Kirishima area has various chemical properties, depending on the mixing ratio of the two types of water. For example, water with a low mixing ratio of volcanic gas and produced by heating and circulating surface water mainly at depth, has a pH close to neutral. Hot spring water produced by mixing high-temperature volcanic gas and surface water near the surface of the earth becomes acidic.

Thus, the wide variety of hot springs in the Kirishima area—and their relatively easy accessibility—allows many environmental parameters to be measured and to provide useful information. Samples from the area are suitable for investigating the relationships between the microbial community composition and environmental factors of the hot springs. Although one example of the microbial communities in the Kirishima area has been reported, the study targeted only the archaeal communities in acidic regions (Satoh et al., 2013).

We focused on the Kirishima area as a general model of a microbial ecosystem in a hot spring environment and performed metagenomic analysis in this environment, along with measurement of environmental data (metadata) of each water sample from a hot spring. We also constructed regression models which predicted the abundance of dominant phyla living in the Kirishima hot springs, using these metadata. Based on the verification of the model parameters and the results of the gene enrichment analysis of metagenomic data, we examined the relationship between environmental parameters and the metabolic features of each water sample.

## MATERIALS AND METHODS

### Sample Collection and DNA Preparation

The nine sampling sites were located in the Kirishima area in the central part of Kagoshima prefecture in Kyushu, Japan. All water samples from the hot springs were collected on two occasions: February 2012 and March 2015. To extract DNA for metagenomic sequencing, 1 L of each sample was filtered through a 0.2-μm pore size polycarbonate membrane. DNA was extracted from the materials on the filter membranes, using the Rapid Water DNA Isolation kit (QIAGEN) with bead homogenization on a Micro Smash MS-100R (TOMY) at 3,500 rpm for 20 s at 4°C.

### Physicochemical Analysis and Microbial Cell Counts

For the 2012 and 2015 samples, water temperature, pH, dissolved oxygen, electrical conductivity and salinity were measured onsite using a portable water-quality meter (P30 series, DKK-TOA Corporation). Water for chemical analysis was collected in 1 L polyethylene bottles and stored at 4°C. Both the metal and ion concentrations of water samples were measured after filtration (GF/F; pore size = 0.7 μm; Whatman). To determine the metals and major cations, 10 mL of water was acidified with $HNO_3$ (pH < 2) and then analyzed by inductively coupled plasma-atomic emission spectroscopy (ICP-AES) (ICPS8100, Shimadzu). To determine the major anions, another 10 mL of water was subsampled and analyzed by ion chromatography (Dionex Qic analyzer) equipped with an IonPAC AS11-HC column (Dionex). Some ions and turbidity from the 2015 samples were

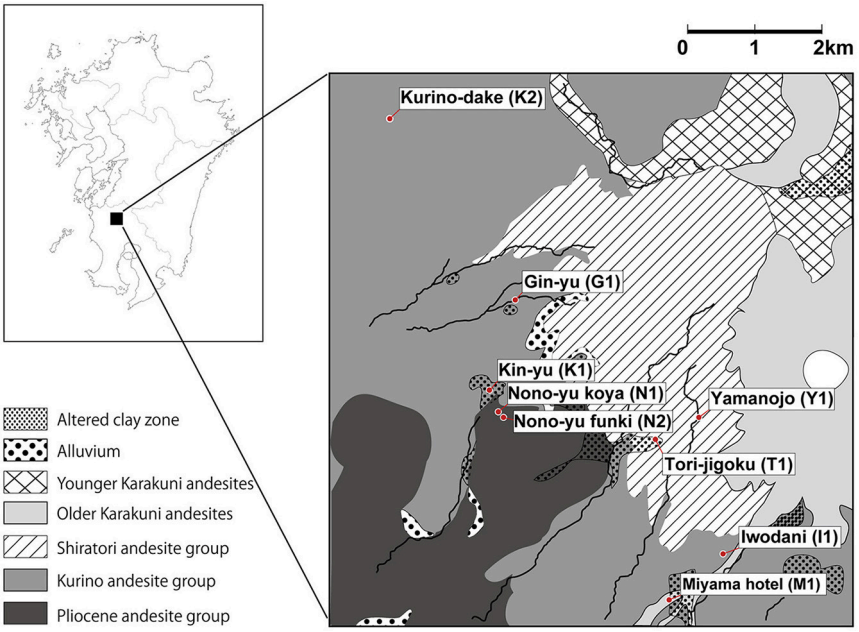


**FIGURE 1 |** Geological map of the Kirishima area showing locations of the sampling sites for metagenomic analysis.

measured using a water-quality meter (DPM-MT, KYORITSU CHEMICAL-CHECK). The concentrations of total carbon, total organic carbon (TOC), dissolved organic carbon and particulate organic carbon in the water samples were measured with a TOC-VCSH analyzer (Shimadzu). The concentrations of total nitrogen (TN), total organic nitrogen (TON), dissolved organic nitrogen and particulate organic nitrogen were measured with a U1800 spectrophotometer (Hitachi).

For microbial cell counts, 20 mL of water from a hot spring was filtered using a 0.2-μm pore size black polycarbonate membrane, and cells were stained with ethidium bromide and counted under a Nikon Eclipse 80i fluorescence microscope equipped with a Nikon Digital Sight DS-5Mc using the fluorescence filter GFP-L (excitation filter 510–560 nm, dichromatic mirror 575 nm, barrier filter 515 nm).

## Metagenomic Sequencing

To obtain sufficient DNA for metagenomic sequencing, the DNA samples prepared in 2012 were processed using the Nextera DNA Sample Prep kit (Illumina) for library construction with the following modifications of the manufacturer's instructions: addition of two polymerase chain reaction (PCR) cycles and alkaline denaturation after evaporation. Metagenomic sequencing of the libraries from the 2012 samples was performed using the Illumina GAIIx and MiSeq platforms (all in paired-end mode).

## Quality Filtering and Assembly of Illumina Sequence Reads

We discarded Illumina sequence reads that: (1) contained ambiguous nucleotides; (2) were mapped to the PhiX genome sequence by using Bowtie 2 version 2.1.0 with default parameters (Langmead and Salzberg, 2012); and (3) were identified as duplicates by comparing the first 30 nucleotides of reads. We then removed the adapter sequences in the reads using the cutadapt version 1.2.1 (Martin, 2011) and also removed low-quality 3′-end regions with a Phred-like quality score <17. We also discarded reads with <50 nucleotides, with an average Phred-like quality score <25, or with no paired reads. After the quality filtering of sequence reads from all samples, we assembled the reads using the Platanus assembler version 1.2.1 (Kajitani et al., 2014).

## Identification and Taxonomic Assignment of 16S rRNA Gene Sequences

The 16S rRNA genes from metagenomic sequences were identified by examining metagenomic sequence reads by BLASTN searches against the SILVA non-redundant (nr) small-subunit rRNA gene sequence database (SILVA NR SSU rRNA DB) version 115 (Quast et al., 2013) with an E-value of $<1e^{-8}$, identity >85% and alignment length >50 bp. The resulting sequences were taxonomically assigned at the phylum level or lower taxonomic ranks, and the abundance of assigned reads was calculated.

## Gene Prediction, Functional Annotation and Coverage Calculation

Protein-coding sequences (CDSs) in the scaffolds were predicted using MetaGeneMark (Zhu et al., 2010). Functional annotation of the predicted CDSs was performed by a BLASTP (version 2.2.26) search against the Kyoto Encyclopedia of Genes and Genomes (KEGG) protein database (Kanehisa et al., 2014) (March 2014) with an *E*-value of <0.01, identity >40% and score >70. The classification and abundance calculation of genes based on the KEGG Orthology was carried out

by dividing the number of reads assigned to each KEGG ortholog (KO) by the median length of amino acid sequences in the corresponding KO in the KEGG protein database. To obtain more information on functions we performed a BLASTP search using all the predicted CDSs as queries against the GenBank nr database (May 2014) with an *E*-value of $<0.01$.

## Analysis of Gene Enrichment in the Metagenome

From the KEGG protein database we chose prokaryotic genomes, one per genus, as a virtual reference microbiome (**Supplementary Table 2**). Enrichment scores were calculated by dividing the relative abundance of each KO in the Kirishima metagenomes by the average relative abundance of the corresponding KO in the virtual reference metagenome. To identify genes that were characteristically enriched in the Kirishima metagenomes, we selected genes with higher enrichment scores compared with average scores of the 35 universal single-copy genes (USCGs) and *gyrB* (Kato et al., 2015).

## Statistical Analysis

Principal component analysis (PCA) was performed using the function in the scikit-learn library (Pedregosa et al., 2011). For PCA using the relative abundance information of phylum- or genus-level taxonomic composition of the nine samples, the values of each feature (relative abundance of each taxon) were not scaled and used for the transformation as it was. For PCA using the KEGG module abundance data, KO abundance data and the measured values of 59 types of environmental parameters (two environmental parameters for which the measurement values were below detection limits in all samples were excluded), the values of each feature were first standardized as Z-scores and used for the transformation. To investigate the relationship between the coordinates of samples on the PCA plot and environmental parameters, the correlations between the principal component scores of samples and the measured values of each environmental parameter were calculated by the Pearson correlation coefficients using the SciPy library (Jones et al., 2001).

To detect the quantitative relationship between environmental parameters and microbial community structures, we constructed statistical models to predict the relative abundance of either Aquificae or Crenarchaeota from the measured values of environmental parameters. We performed principal component regression, which combines PCA with regression analysis, to avoid the multicollinearity problem caused by using a large number of explanatory variables. (1) The table of Z-score-converted environmental parameters was transformed to the table of principal component scores by performing PCA. By selecting only a subset of the obtained principal components, a small number of uncorrelated explanatory variables could be used for the regression model. Because the cumulative contribution rate of the first four principal components was more than 80%, these four principal components were used for regression analysis. (2) We constructed generalized linear models with a logit link and the binomial family, using all combinations (15 patterns) of these four principal components as explanatory variables, and compared the performance of these models by using Akaike's Information Criterion (AIC) (Aho et al., 2014) (**Supplementary Table 3**). The estimation of generalized linear models was done using the Statsmodels Python modules (Seabold and Perktold, 2010). (3) The models with minimum AIC values were selected, and we examined the environmental parameters affecting the relative abundances of phyla by inspecting the factor loadings obtained by the initial PCA.

# RESULTS AND DISCUSSION

## Physicochemical and Biological Properties of the Kirishima Hot Spring Samples

**Supplementary Table 4** presents the physicochemical and biological characteristics of the nine water samples from hot springs in the Kirishima area in 2012 and 2015 (**Supplementary Table 1**). We measured the water-quality data of 5 physical properties (e.g., total bacterial counts, turbidity, pH), 11 chemical properties (e.g., total carbon, TN), 10 anion species and 35 cation species, totaling 61 types (**Supplementary Table 4**).

Samples of G1, T1, K2, N2, and I1 from a hot spring with high water turbidity showed low pH; high concentrations of sulfate, Cu and Zn ions; and relatively high TOC and TN, in comparison to transparent and medium pH samples, such as K1, Y1, N1, and M1 (**Supplementary Table 4** and **Supplementary Figure 1**). The total cell counts were as low as $1.21 \times 10^4$-$4.03 \times 10^6$ cells $mL^{-1}$, as reported in YNP (Meyer-Dombard et al., 2005). In summary, the temperatures of the samples were similarly high (84.0–96.8°C) except sample N1 (68°C), but they showed diverse chemical properties within this narrow area; thus these samples were suitable for use in analyzing the relationship between microbial community structures and environmental parameters.

## Metagenomic Sequencing and Taxonomic Composition of the Kirishima Hot Spring Microbiomes

Because it was difficult to extract sufficient DNA from the Kirishima hot spring water samples with low cell density, we used a PCR-based method to prepare sequence libraries for the nine hot spring samples. Metagenomic sequences were obtained using the Illumina platforms, and standard quality filtering yielded 1,965,768–54,065,035 read pairs for each of the nine samples. We then assembled the reads to construct contigs and scaffolds (**Supplementary Table 5**). The total number of scaffolds >500 bp in length was 4,019–92,715, and the largest scaffold size was 493,449 bp in the K1 sample (**Supplementary Table 5**).

The phylum- and lower-level taxonomic composition for each sample was examined by identifying 16S rRNA genes from the standard quality filtered metagenomic reads (**Figure 2**). In the nine hot spring samples, 10 prokaryotic phyla accounted for

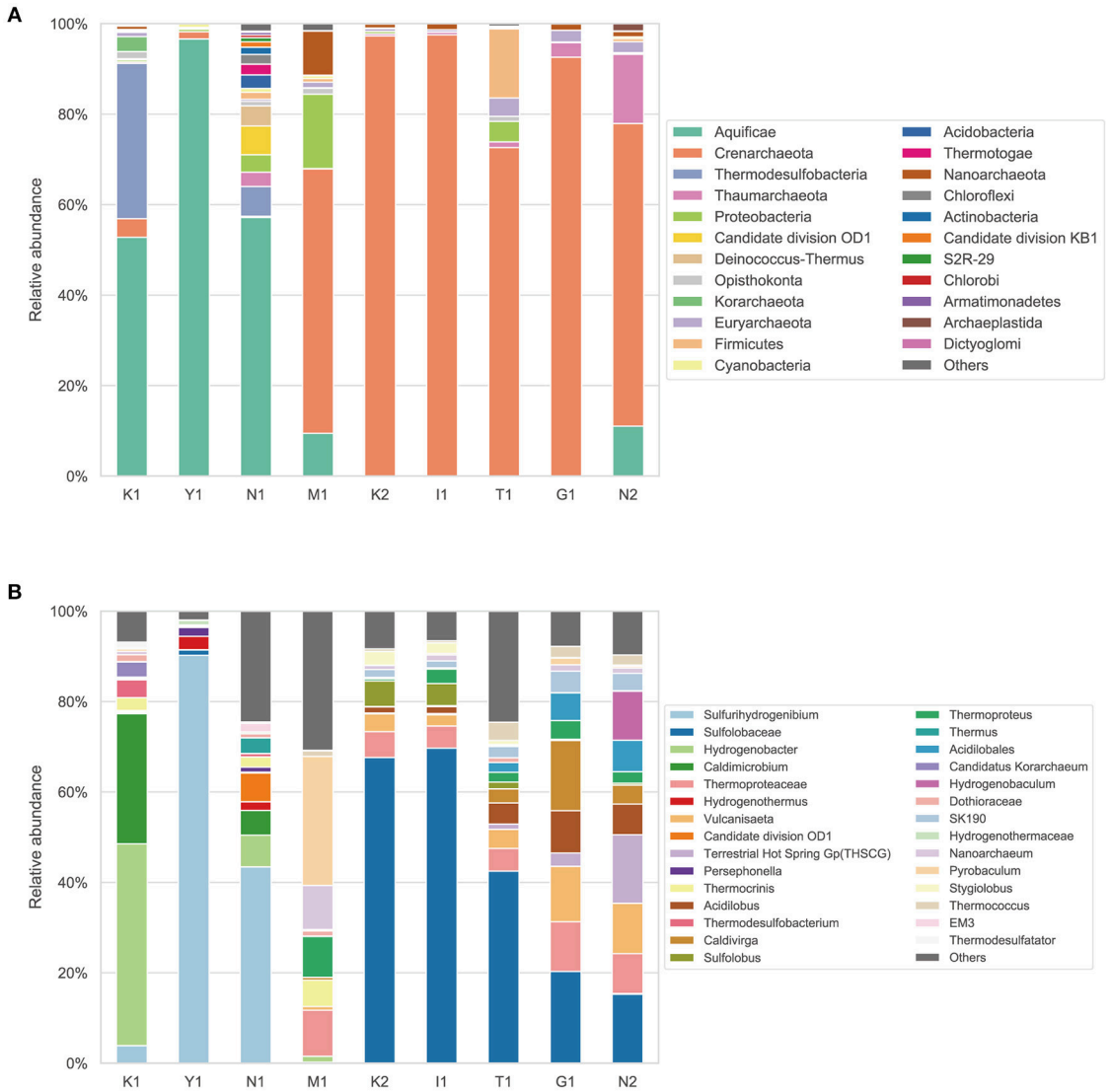


**FIGURE 2 |** Taxonomic composition and relative abundance of microbiota in water from Kirishima hot springs based on 16S rRNA genes identified from the metagenomic reads. **(A)** Taxonomic composition of the microbiota at phylum level. **(B)** Detailed taxonomic composition (i.e., genus, family or order) of the microbiota.

>80% of total taxonomically assigned reads, and either Aquificae or Crenarchaeota predominated. The Aquificae accounted for 52.7–96.6% of the taxonomically assigned reads in samples K1, Y1, and N1. The Crenarchaeota accounted for 52.5–96.6% in samples M1, K2, I1, T1, G1, and N2 (**Figure 2A**). The genus *Sulfurihydrogenibium* of the Aquificae dominated in Y1 and N1, and the family Sulfolobaceae of the Crenarchaeota dominated in K2, I1, T1, G1, and N2 (**Figure 2B**). This result was consistent with the previous report that archaea belonging to the order Sulfolobales were detected in samples (Pond-A and Pond-B) with higher dissolved element concentration in the Kirishima hot springs (Satoh et al., 2013). One isolate of the Sulfolobaceae from an acidic hot spring, *Sulfodiicoccus acidiphilus*, showed adaptation to low pH and high temperature (Sakai and Kurosawa, 2017).

The phylum Thermodesulfobacteria was also dominant in sample K1 (34.2% of the taxonomically assigned reads) and accounted for 6.5% in N1. The phyla candidate division OD1 ("Parcubacteria") and "Deinococcus-Thermus" were the third and fourth most dominant in sample N1, although other diverse phyla were also detected. The phylum Cyanobacteria was detected in seven of the nine samples, albeit with <1% relative abundance. The phylum Euryarchaeota was found in all samples with a low abundance (0.02–4.1%). These results showed confined phylogenetic diversity of the microbiomes in the water from the Kirishima hot springs with the predominance of either Crenarchaeota or Aquificae.

To compare the taxonomic compositions among these microbiomes, we performed PCA using the relative abundance data of the phylum- and lower-level taxonomic composition

(**Figure 3**). PCA showed that the first two principal components (PC1 and PC2) accounted for more than 95% of the variation in taxonomic composition among samples, and samples clustered into two major groups [(K1, Y1, and N1) vs. (M1, K2, I1, T1, G1, and N2)], each dominated by either Aquificae or Crenarchaeota, respectively. PCA of the lower taxonomic composition showed similar results, except for the position of sample K1, which was closer to M1 than to N1 and Y1 (**Figure 3B**). Next, to identify the environmental factors affecting the formation of these two major groups, we calculated the correlations between the principal component scores of all samples and the measured environmental data of each. In **Figure 3**, the positions indicated by the arrows represent the correlation coefficients between the measured values of environmental factors and the PC1 and PC2 scores. Most cations and TN show negative correlations with the PC1 scores and are densely plotted on the left-hand side of the plot, where samples dominated by Crenarchaeota (M1, K2, I1, T1, G1, and N2) are located. However, few environmental factors were positively correlated with the PC1 scores, so there are few arrows on the right-hand side of the plot where samples dominated by Aquificae (K1, Y1, and N1) are located. Sulfuric acid ($SO_4$ in **Figures 3A,B**) showed a strong negative correlation with PC1 and appeared to contribute to the variation in community structures, consistent with a previous report (Huang et al., 2013). These results suggested that the differences in community structures reflect the differences in environmental parameters among samples.

## Construction of a Model for Estimating Microbial Abundance From Environmental Parameters

We constructed multiple regression models to predict the relative abundance of the two dominant taxa, either Aquificae or Crenarchaeota, using 59 types of environmental data as explanatory variables. When two or more explanatory variables are highly correlated, the regression coefficient estimate becomes unstable (this is known as the multicollinearity problem). To overcome it, we performed principal component regression (see Statistical Analysis in Materials and Methods). We selected a model using PC1 and PC3 as explanatory variables for the prediction model of Aquificae abundance, based on the minimum AIC value (the "best" model) (**Supplementary Table 3** and **Supplementary Figure 2A**). For the prediction model of Crenarchaeota abundance, a model using PC1, PC3, and PC4 as explanatory variables exhibited the minimum AIC value (**Supplementary Table 3** and **Supplementary Figure 2B**). In the prediction model for Aquificae, the regression coefficients were positive for PC1 and negative for PC3, which were affected positively and negatively, respectively, by the abundance of Aquificae. The regression coefficients of the prediction model of Crenarchaeota were negative for PC1, and positive for PC3 and PC4 (**Supplementary Table 3**). These principal components were interpreted by examining the factor loadings of the PCA for environmental parameters (**Supplementary Figure 3**). The PC1 score increased as pH increased, and the PC1 score decreased as the concentrations of many cation species increased (**Supplementary Figure 3A**). The PC3 score increased as the TON or TOC increased (**Supplementary Figure 3C**), and the PC4 score increased as the sulfuric acid concentration increased (**Supplementary Figure 3D**). These results indicated that Aquificae dominated in a low-nutrient environment with high pH, low cation concentration and low TON and TOC; while Crenarchaeota dominated in a nutritious environment with high sulfuric acid concentration and with high TON and TOC. Thus, the quantitative prediction by our models supported the association between the environmental factors and community structures visualized in **Figure 3**.

## Enrichment Analysis of Functional Genes

To investigate the comprehensive ecological features of the microbiome in the Kirishima area, we performed a KEGG-based functional annotation of predicted CDSs in the metagenome scaffolds. We assigned 70% of all CDSs on the scaffolds to either functional categories of KEGG (**Supplementary Table 3**). We examined differences in gene function among samples by PCA based on the abundance of the KEGG module and KO (**Figure 4**). The overall distribution of samples in PCA (**Figure 4**) was very similar to the results based on the taxonomic composition shown in **Figure 3**. The nutrient-rich water samples from hot springs with high ion concentrations and high TN were well-separated from the other three samples (K1, Y1, and N1). Because the major differences among samples in **Figure 4** were probably attributable to the differences in functions between Aquificae and Crenarchaeota, we examined functional genes contributing to the differences in metabolic function among the samples. To characterize the metabolic functions of these two groups, we compared the KO abundance in the water from Kirishima hot spring metagenomes to the average KO abundance of representative prokaryotic genomes **Supplementary Tables 2**, **6**; see Analysis of Gene Enrichment in the Metagenome in Materials and Methods), and identified highly enriched KOs in the Kirishima samples (**Supplementary Table 6**). **Supplementary Table 7** shows key genes of major metabolic pathways and their enrichment scores in the Kirishima samples. Many of these enriched genes are related to autotrophic carbon fixation; that is, the 3-hydroxypropionate/4-hydroxybutyrate (3HP/4HB) cycle, the dicarboxylate/4-hydroxybutyrate (DC/4HB) cycle, the reverse tricarboxylic acid (rTCA) cycle and the reductive acetyl-CoA pathway. Genes related to sulfate and nitrogen metabolisms were also enriched, as described later. The genes assigned to K01535_$H^+$-transporting ATPase were enriched in samples K2, I1, T1, G1, and N2; this is probably an important enzyme in acidic environments to maintain intracellular pH (Vanderheyden et al., 1996). The genes encoding enzymes for regulating heavy metal concentrations in cells, including K07787_cusA, silA_Cu(I)/Ag(I) efflux system membrane protein and K02006_cbiO_cobalt/nickel transport system ATP-binding protein, were enriched only in K1 and N1. The gene encoding the heat-stable and bifunctional enzyme fructose 1,6-bisphosphate aldolase/phosphatase for gluconeogenesis (K01622) (Takami et al., 2012) was abundant in all samples, except in sample Y1

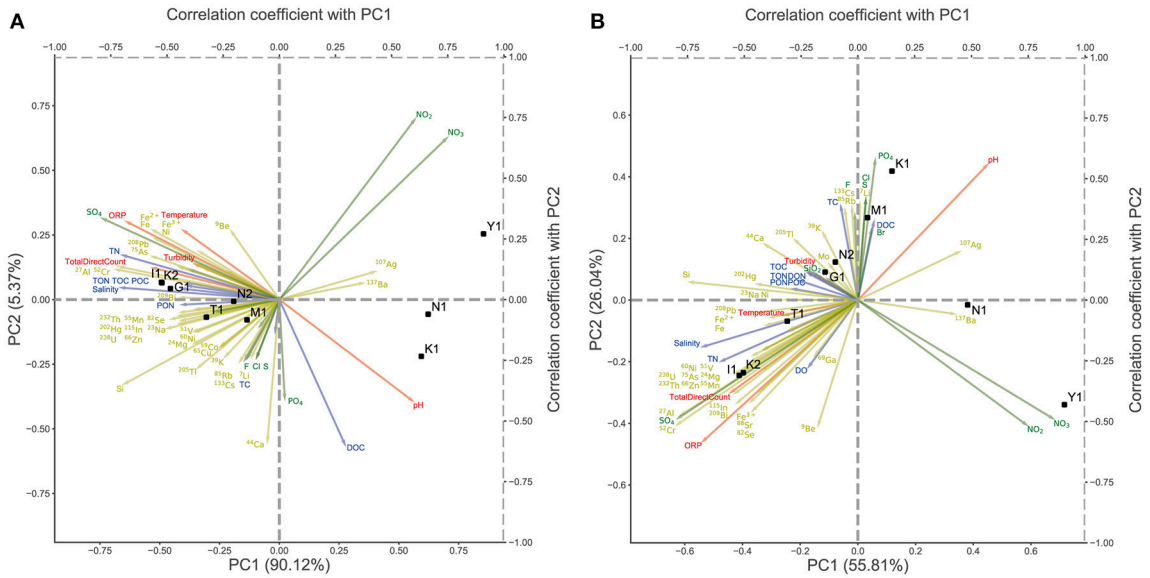


**FIGURE 3 |** Principal component analysis (PCA) of the relative abundance of each sample across nine sites. The arrows represent the correlation coefficient between the principal component scores and each environmental parameter. The yellow arrows represent cations, the green arrows represent anions, the blue arrows represent water quality and the red arrows represent physical properties. **(A)** PCA of the relative abundance at phylum level. **(B)** PCA of the relative abundance at detailed taxonomic level.

(**Supplementary Tables 6,7**). The gene (K01906_bioW) involved in the biosynthesis of biotin required the gluconeogenesis and autotrophic pathways was also enriched in K1, Y1 and N1 (**Supplementary Table 7**).

Various autotrophic carbon-fixing pathways, which produce organic matter from $CO_2$, have been reported in extreme environments (Hügler and Sievert, 2011). Genes (K15230_aclA, K15231_aclB) encoding ATP-citrate lyase, a key enzyme involved in determining the direction and citric acid cleavage of the rTCA cycle (Aoshima et al., 2004), were enriched in three samples (K1, Y1, and N1) but were not detected in other samples (**Supplementary Table 7**). The genes encoding enzymes for an alternative citrate cleavage pathway in the rTCA cycle (K15232_ccsA, K15233_ccsB, and K15234_ccl) were also found abundantly in K1, N1, and M1 but not detected in Y1 (**Supplementary Table 7**). These results suggest that the rTCA cycle is the primary pathway in the samples with relatively high transparency, low ion concentrations and low nutrition. The genes involved in this pathway are also enriched in a deep-sea chimney microbiome and considered to be an important $CO_2$ fixation pathway in the environment (Nakagawa and Takai, 2008; Xie et al., 2011).

The genes (K14465_succinate semialdehyde reductase, K14534_abfD) required for both the DC/4-HB and 3-HP/4-HB cycles (Scherf and Buckel, 1993) and the genes encoding K14467_4-hydroxybutyryl-CoA synthetase and K14466_4-hydroxybutyryl-CoA synthetase, which are characteristic of the DC/4-HB (Hawkins et al., 2013) and 3-HP/4-HB cycles, respectively, were enriched in samples that were highly turbid and had high nutrition (M1, K2, I1, T1, G1, and N2). Our data support a previous report based on transcriptomic analysis of microbiota in terrestrial hot springs of Tengchong, China (Li et al., 2010), which suggested that both cycles play important roles in nutrition-rich environments (**Supplementary Table 7**). Because genes (K14468_mcr, K14469 acrylyl-CoA reductase) responsible for the 3-Hydroxypropionate (3HP) bi-cycle (Zarzycki et al., 2009) were not found, the 3HP bi-cycle may not be necessary in the Kirishima hot spring water ecosystem.

Key genes coding the acetyl-CoA decarboxylase/synthase complex are required for the reductive acetyl-CoA pathway, each of which is classified into "bacteria type" and "archaea type" (Takami et al., 2012). The bacteria-type genes (e.g., K00198_cooS, acsA, K14138_acsB) for the ACDS complex were highly abundant in samples N1 and K1, while the archaea-type genes (e.g., K00192_cdhA and K00194_cdhD) were low in abundance. As reported in studies of deep-sea hydrothermal vents (Xie et al., 2011; Takami et al., 2012), the anaerobic ACDS complex might be used by anaerobic microorganisms to couple CO oxidation to sulfate reduction, or to reduce $CO_2$ to acetate in the Kirishima hot spring water ecosystem. With respect to other carbon-fixation pathways, the gene encoding ribulose bisphosphate carboxylase/oxygenase (RuBisCO) (K01601_rbcL and K01602_rbcS), the key enzyme of the Calvin cycle, was found only rarely in the samples. This suggests that this cycle is not a major metabolic pathway in the Kirishima hot spring water ecosystem.

Because water from hot springs generally contains sulfur compounds, sulfate metabolism is important for energy conservation in these extreme environments (Xie et al., 2011). The genes (K17222_soxA1, K17223_soxX, K17224_soxB1, K17226_soxY, and K17227_soxZ) coding the sulfur-oxidizing multienzyme system (sox), related to oxidation of thiosulfate (Friedrich et al., 2005), were frequently detected in samples with low nutrition (e.g., K1 and N1) (**Supplementary Table 7**),

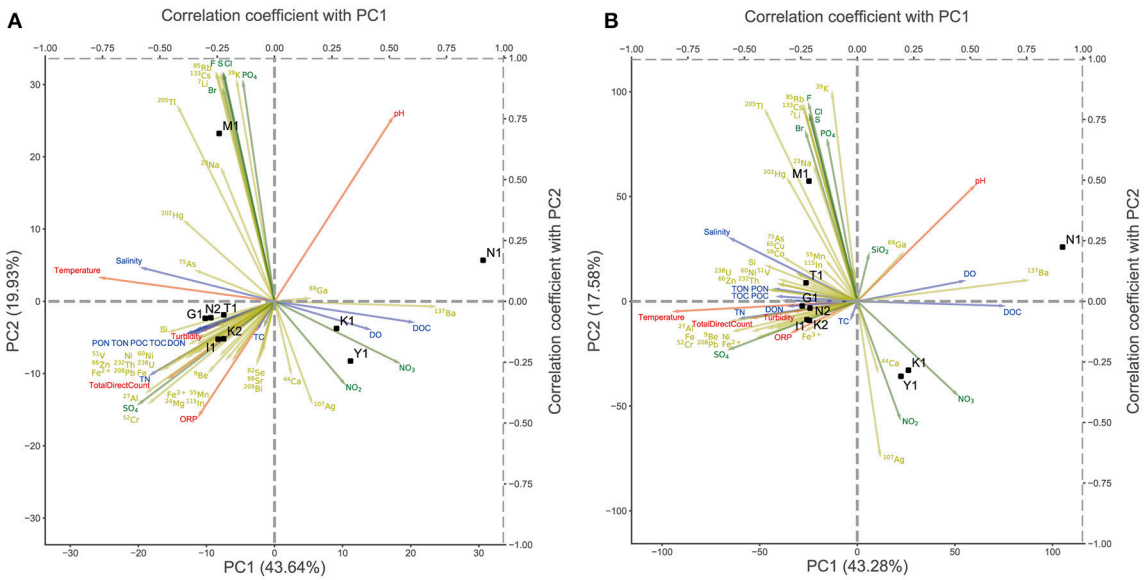


**FIGURE 4 |** Principal component analysis (PCA) of the abundance of gene categories for each sample across nine sites. The arrows represent the correlation coefficient between the principal component scores and each environmental parameter. The yellow arrows represent cations, the green arrows represent anions, the blue arrows represent water quality and the red arrows represent physical properties. **(A)** PCA of the KEGG module abundance. **(B)** PCA of the KEGG Orthology abundance.

in agreement with previous metagenomic analyses of YNP hot springs and deep-sea hydrothermal vents (Inskeep et al., 2010; Xie et al., 2011). Also, with respect to other sulfuric acid pathways, K16952_sor, which is involved in thiosulfate oxidation via the elemental sulfur metabolism (Friedrich et al., 2005), was abundant in the Y1, K2, I1, T1, G1, and N2 samples, but not in K1 and M1. One of the genes (K17218_sqr) encoding sulfide-quinone oxidoreductase (SQR) involved in sulfur oxidation by reducing sulfide (Gregersen et al., 2011) was detected at a high abundance in all samples (**Supplementary Table 7**). These data suggested the existence of these sulfur-reducing and oxidizing abilities via SOX and SQR systems in the Kirishima hot spring water ecosystem.

Dissimilatory sulfate reduction and oxidation can be involved in both energy conservation and sulfite metabolism via the adenylyl sulfate (APS) pathway with ATP production (Friedrich et al., 2005). In the Kirishima metagenomes, a set of genes (K11180_dsrA, K11181_dsrB, K00394_aprA, K00395_aprB) involved in this pathway was highly abundant in all samples, except in Y1 (**Supplementary Table 7**). High concentrations of sulfate ions were observed in several samples (K2, I1, T1, G1, and N2). A set of genes (K16933_doxB, K16936_doxA, K16934_doxC, and K16935_doxE) involved in oxidation of thiosulfate via tetrathionic acid was found in most Crenarchaeota (Müller et al., 2004) and was highly represented in K2, I1, T1, G1, and N2 (but not in Y1), depending on the high sulfate ion properties of the sample sites. As seen in *Sulfolobus* in a previous study (Quehenberger et al., 2017), some facultative autotrophs (e.g., *Sulfolobus* dominating sample N2) that can oxidize reduced sulfur compounds via various sulfur oxidation pathways may exist in the Kirishima environments.

Hydrogen metabolism is considered to be one of the most important processes in hydrogen-containing alkaline environments, such as serpentinite-hosted ecosystems (Brazelton et al., 2012). In the Kirishima metagenomes, however, the abundances of genes responsible for hydrogen metabolism (K05587_hoxF_bidirectional [NiFe] hydrogenase, K05588_hoxU_bidirectional [NiFe] hydrogenase, K18008_hydA2_[NiFe] hydrogenase) was low or not detected. Hydrogen metabolism cannot be crucial for the Kirishima ecosystem because hydrogen was below the detection limit in all samples (data not shown).

The importance of denitrification, nitrogen fixation and nitrification constituting the nitrogen cycle has been suggested by studies of deep-sea hydrothermal environments (Tamegai et al., 2007). In the Kirishima samples with high transparency and low nutrition, genes involved in denitrification were much more abundant than those for nitrogen fixation and nitrification (**Supplementary Table 7**). The gene (K02567_napA) associated with nitrate reduction (denitrification and dissimilatory nitrate reduction) was frequently found in samples N1 and K1 (**Supplementary Table 7**). Likewise, gene (K00367_narB) for assimilatory nitrate (nitrite) reduction (Morozkina and Zvyagilskaya, 2007) was found in high proportions in M1, N1, and K1. In general, the oxidation of sulfur compounds can be coupled to the reduction of electron acceptors including oxygen and nitrate (Brunet and Garcia-Gil, 1996). These data imply that nitrate reduction, such as denitrification coupled to sulfur oxidation is likely to be an important energy-generating pathway fueling the microbial communities in the Kirishima hot spring water ecosystem.

However, the gene encoding nitrogenase reductase (K02588_nifH) for nitrogen fixation and the gene related to nitrate oxidation (K00368_nirK) were rarely found in any samples. These results indicate that nitrification is not a major metabolic pathway in the Kirishima hot spring water ecosystem.

The reliability of the gene enrichment analysis was also supported by the result of the correlation analysis between coordinates of samples on the PCA plot and measured values of environmental factors (**Figure 4**), in which the arrow of the nitrate ions directed to the position of sample K1.

In this study, based on the metagenomic and geochemical data, we clarified that the microbial ecosystem of the Kirishima hot spring water was dominated by either Crenarchaeota or Aquificae. These two types of microbial community structures, and the gradient of relative abundance between them, were strongly affected by their habitat-specific environmental factors, as suggested by both the PCA and regression analyses. The key environmental factors (such as sulfate and nitrate ions) identified by these analyses were consistent in the enrichment analysis of gene functions, especially for the sulfur and nitrogen metabolisms and autotrophic carbon fixation. These factors are probably crucial for the formation of specific community structural patterns. Compared with ocean or soil environments, many environmental factors impose severe restrictions on survival in extreme environments, so it is likely that specific community structures tend to be formed as a result of adaptation, according to the metabolic features of each microorganism.

Because the hot springs in the Kirishima area show diverse chemical properties and represent a wide variety of hot spring environments, our finding in the Kirishima ecosystem (i.e., the relationship between microorganisms and environmental parameters) may be applied to many other hot spring environments. To test the generality of our findings, we also investigated microbial and environmental data in the same way for a hot spring in Hachijo-jima, an island 850 km from Kyushu. Water from the Hachijo-jima hot spring is both low in nutrition and transparent (**Supplementary Table 4**) and, compared with the Kirishima samples, its microbial community was seen to belong to a group dominated by Aquificae (**Supplementary Figure 4**). This result suggests that the relationship we found between the environmental parameters and the microbial community structures could be a general pattern applicable to hot spring environments other than those in the Kirishima area. Our study shows that investigation of the chemical properties of hot springs makes it possible to predict, to some extent, the taxonomic composition and metabolic characteristics of the microorganisms living in the extreme environment. These data will provide clues to assist the more efficient exploration of biological resources, such as useful enzymes and bioactive compounds and lead to potential biotechnology applications.

Enrichment analysis among samples in the Kirishima area revealed that genes encoding autotrophic carbon fixation, such as the 3HP/4HB cycle, the DC/4HB cycle and the reductive acetyl-CoA pathway, were detected at a high abundance in the nutrition-rich samples. On the other hand, genes encoding the rTCA cycle were detected in high proportions only in the samples with low nutrition. The reason for the variations in these functions is presumed to be the difference between the dominant taxa; Crenarchaeota may use the 3HP/4HB or DC/4HB cycle, and Aquificae may use the rTCA cycle, considering information on cultured strains (Hügler and Sievert, 2011). In addition, genes related to various sulfate metabolic pathways were enriched in all samples. Previous metagenomic studies of the YNP hot springs and hydrothermal vent chimney 4143-1 also revealed a high abundance of genes involved in sulfur metabolism (Inskeep et al., 2010; Xie et al., 2011). Sulfate utilization is the main mechanism of energy acquisition, and may be crucial for the survival of sulfate-oxidizing and reducing facultative autotrophs in Kirishima and other hot springs. The presence of the key genes of carbon fixation and sulfur oxidation pathways detected in the metagenomes of water from the Kirishima hot springs implies that both obligate and facultative autotrophs are present, and contribute to biomass production in the Kirishima hot spring water ecosystem.

The unique environmental features of the Kirishima area provide us an opportunity to investigate diverse hot spring ecosystems in proximal locations. Further studies of microbial ecosystems in various extreme environments (including the Kirishima area), using detailed environmental data, will provide valuable information that will assist in the prediction of microbial ecosystems from environmental data, and the exploration of biological resources in extreme environments.

## DATA AVAILABILITY

Metagenomic sequence reads have been deposited in the DNA Databank of Japan (DDBJ) with BioProject ID PRJDB7293.

## AUTHOR CONTRIBUTIONS

EN, KS, SO, SM, YH, and KK designed the research. EN, KS, HN, SM, YH, and KK collected the samples. EN, KS, HN, and SO performed biological and chemical experiments. EN, KH, and HM performed *in silico* analysis. EN, KH, HM, YH, and KK wrote the manuscript.

## FUNDING

This study was supported by a Grant-in-Aid for Hadean Bioscience (No. 26106001) and in part by the Global Centre of Excellence Program from the Ministry of Education, Culture, Sports, Science and Technology of Japan.

## ACKNOWLEDGMENTS

We thank Seiya Morita (Nittetsu Mining Co. Ltd) and Akihiko Koba (Nittetsu Mining Consultants Co. Ltd) for providing water samples from Kirishima hot springs and helping with sampling in the field study. We thank Elaine Monaghan, BSc(Econ), from Edanz Group (www.edanzediting.com/ac) for editing a draft of this manuscript.

## SUPPLEMENTARY MATERIAL

The Supplementary Material for this article can be found online at: https://www.frontiersin.org/articles/10.3389/fbioe.2018.00202/full#supplementary-material

## REFERENCES


Aho, K., Derryberry, D., and Peterson, T. (2014). Model selection for ecologists: the worldview of AIC and BIC. *Ecology* 95, 631–636. doi: 10.1890/13-1452.1

Aoshima, M., Ishii, M., and Igarashi, Y. (2004). A novel enzyme, citryl-CoA lyase, catalysing the second step of the citrate cleavage reaction in Hydrogenobacter thermophilus TK-6. *Mol. Microbiol.* 52, 763–770. doi: 10.1111/j.1365-2958.2004.04010.x

Brazelton, W. J., Nelson, B., and Schrenk, M. O. (2012). Metagenomic evidence for h(2) oxidation and h(2) production by serpentinite-hosted subsurface microbial communities. *Front. Microbiol.* 2:268. doi: 10.3389/fmicb.2011.00268

Brunet, R. C., and Garcia-Gil, L. J. (1996). Sulfide-induced dissimilatory nitrate reduction anaerobic freshwater sediments. *FEMS Microbiol. Ecol.* 21, 131–138. doi: 10.1111/j.1574-6941.1996.tb00340.x

Castelino, M., Eyre, S., Moat, J., Fox, G., Martin, P., Ho, P., et al. (2017). Optimisation of methods for bacterial skin microbiome investigation: primer selection and comparison of the 454 versus MiSeq platform. *BMC Microbiol.* 17:23. doi: 10.1186/s12866-017-0927-4

Chan, C. S., Chan, K. G., Tay, Y. L., Chua, Y. H., and Goh, K. M. (2015). Diversity of thermophiles in a Malaysian hot spring determined using 16S rRNA and shotgun metagenome sequencing. *Front. Microbiol.* 6:177. doi: 10.3389/fmicb.2015.00177

Friedrich, C. G., Bardischewsky, F., Rother, D., Quentmeier, A., and Fischer, J. (2005). Prokaryotic sulfur oxidation. *Curr. Opin. Microbiol.* 8, 253–259. doi: 10.1016/j.mib.2005.04.005

Gokou, K., Kodama, M., and Nobumoto, R. (1995). Geothermal exploration and development of the Ogiri field in the Kirishima geothermal area. *Resour. Geol.* 45, 377–390.

Gregersen, L. H., Bryant, D. A., and Frigaard, N. U. (2011). Mechanisms and evolution of oxidative sulfur metabolism in green sulfur bacteria. *Front. Microbiol.* 2:116. doi: 10.3389/fmicb.2011.00116

Hawkins, A. S., Han, Y., Bennett, R. K., Adams, M. W., and Kelly, R. M. (2013). Role of 4-hydroxybutyrate-CoA synthetase in the $CO_2$ fixation cycle in thermoacidophilic archaea. *J. Biol. Chem.* 288, 4012–4022. doi: 10.1074/jbc.M112.413195

Hou, W., Wang, S., Dong, H., Jiang, H., Briggs, B. R., Peacock, J. P., et al. (2013). A comprehensive census of microbial diversity in hot springs of Tengchong, Yunnan Province China using 16S rRNA gene pyrosequencing. *PLoS ONE* 8:e53350. doi: 10.1371/journal.pone.0053350

Huang, Q., Jiang, H., Briggs, B. R., Wang, S., Hou, W., Li, G., et al. (2013). Archaeal and bacterial diversity in acidic to circumneutral hot springs in the Philippines. *FEMS Microbiol. Ecol.* 85, 452–464. doi: 10.1111/1574-6941.12134

Hügler, M., and Sievert, S. M. (2011). Beyond the Calvin cycle: autotrophic carbon fixation in the ocean. *Ann. Rev. Mar. Sci.* 3, 261–289. doi: 10.1146/annurev-marine-120709-142712

Inskeep, W. P., Jay, Z. J., Herrgard, M. J., Kozubal, M. A., Rusch, D. B., Tringe, S. G., et al. (2013a). Phylogenetic and functional analysis of metagenome sequence from high-temperature archaeal habitats demonstrate linkages between metabolic potential and geochemistry. *Front. Microbiol.* 4:95. doi: 10.3389/fmicb.2013.00095

Inskeep, W. P., Jay, Z. J., Tringe, S. G., Herrgård, M. J., Rusch, D. B., et al. (2013b). The YNP metagenome project: environmental parameters responsible for microbial distribution in the yellowstone geothermal ecosystem. *Front. Microbiol.* 4:67. doi: 10.3389/fmicb.2013.00067

Inskeep, W. P., Rusch, D. B., Jay, Z. J., Herrgard, M. J., Kozubal, M. A., Richardson, T. H., et al. (2010). Metagenomes from high-temperature chemotrophic systems reveal geochemical controls on microbial community structure and function. *PLoS ONE* 5:e9773. doi: 10.1371/journal.pone.0009773

Jay, Z. J., Beam, J. P., Kozubal, M. A., Jennings, R. D., Rusch, D. B., and Inskeep, W. P. (2016). The distribution, diversity and function of predominant Thermoproteales in high-temperature environments of Yellowstone National Park. *Environ. Microbiol.* 18, 4755–4769. doi: 10.1111/1462-2920.13366

Jones, E., Oliphant, T., and Peterson, P. (2001). *SciPy: Open Source Scientific Tools for Python*. Available online at: http://www.scipy.org/ (accessed).

Kajitani, R., Toshimoto, K., Noguchi, H., Toyoda, A., Ogura, Y., Okuno, M., et al. (2014). Efficient de novo assembly of highly heterozygous genomes from whole-genome shotgun short reads. *Genome Res.* 24, 1384–1395. doi: 10.1101/gr.170720.113

Kanehisa, M., Goto, S., Sato, Y., Kawashima, M., Furumichi, M., and Tanabe, M. (2014). Data, information, knowledge and principle: back to metabolism in KEGG. *Nucleic Acids Res.* 42, D199–205. doi: 10.1093/nar/gkt1076

Kato, H., Mori, H., Maruyama, F., Toyoda, A., Oshima, K., Endo, R., et al. (2015). Time-series metagenomic analysis reveals robustness of soil microbiome against chemical disturbance. *DNA Res.* 22, 413–424. doi: 10.1093/dnares/dsv023

Langmead, B., and Salzberg, S. L. (2012). Fast gapped-read alignment with Bowtie 2. *Nat. Methods* 9, 357–359. doi: 10.1038/nmeth.1923

Li, W., Song, Z., Chen, J., Jiang, H., Zhou, E., Wang, F., et al. (2010). "Diversity and ecological functions of crenarchaeota in terrestrial hot springs of Tengchong, China," in *American Geophysical Union, Fall Meeting 2010* (San Francisco, CA).

Littlechild, J. A. (2015). Enzymes from extreme environments and their industrial applications. *Front. Bioeng. Biotechnol.* 3:161. doi: 10.3389/fbioe.2015.00161

Mahajan, G. B., and Balachandran, L. (2017). Sources of antibiotics: hot springs. *Biochem. Pharmacol.* 134, 35–41. doi: 10.1016/j.bcp.2016.11.021

Martin, M. (2011). Cutadapt removes adapter sequences from high-throughput sequencing reads. *EMBnet J.* 17, 10–12. doi: 10.14806/ej.17.1.200

Meyer-Dombard, D. R., Shock, E. L., and Amend, J. P. (2005). Archaeal and bacterial communities in geochemically diverse hot springs of Yellowstone National Park, USA. *Geobiology* 3, 211–227. doi: 10.1111/j.1472-4669.2005.00052.x

Morozkina, E. V., and Zvyagilskaya, R. A. (2007). Nitrate reductases: structure, functions, and effect of stress factors. *Biochem Mosc.* 72, 1151–1160. doi: 10.1134/S0006297907100124

Müller, F. H., Bandeiras, T. M., Urich, T., Teixeira, M., Gomes, C. M., and Kletzin, A. (2004). Coupling of the pathway of sulphur oxidation to dioxygen reduction: characterization of a novel membrane-bound thiosulphate:quinone oxidoreductase. *Mol. Microbiol.* 53, 1147–1160. doi: 10.1111/j.1365-2958.2004.04193.x

Nakagawa, S., and Takai, K. (2008). Deep-sea vent chemoautotrophs: diversity, biochemistry and ecological significance. *FEMS Microbiol. Ecol.* 65, 1–14. doi: 10.1111/j.1574-6941.2008.00502.x

Pedregosa, F., Varoquaux, G., Gramfort, A., Michel, V., Thirion, B., Grisel, O., et al. (2011). Scikit-learn: Machine Learning in Python. *JMLR* 12, 2825–2830.

Quast, C., Pruesse, E., Yilmaz, P., Gerken, J., Schweer, T., Yarza, P., et al. (2013). The SILVA ribosomal RNA gene database project: improved data processing and web-based tools. *Nucleic Acids Res.* 41, D590–D596. doi: 10.1093/nar/gks1219

Quehenberger, J., Shen, L., Albers, S. V., Siebers, B., and Spadiut, O. (2017). Sulfolobus–a potential key organism in future biotechnology. *Front. Microbiol.* 8:2474. doi: 10.3389/fmicb.2017.02474

Sakai, H. D., and Kurosawa, N. (2017). *Sulfodiicoccus acidiphilus* gen. nov., sp. nov., a sulfur-inhibited thermoacidophilic archaeon belonging to the order Sulfolobales isolated from a terrestrial acidic hot spring. *Int. J. Syst. Evol. Microbiol.* 67, 1880–1886. doi: 10.1099/ijsem.0.001881

Satoh, T., Watanabe, K., Yamamoto, H., Yamamoto, S., and Kurosawa, N. (2013). Archaeal community structures in the solfataric acidic hot springs with different temperatures and elemental compositions. *Archaea* 2013, 1–11. doi: 10.1155/2013/723871

Scherf, U., and Buckel, W. (1993). Purification and properties of an iron-sulfur and FAD-containing 4-hydroxybutyryl-CoA dehydratase/vinylacetyl-CoA delta 3-delta 2-isomerase from Clostridium aminobutyricum. *Eur. J. Biochem.* 215, 421–429. doi: 10.1111/j.1432-1033.1993.tb18049.x

Seabold, S., and Perktold, J. (2010). "Statsmodels: econometric and statistical modeling with python," in *Proceedings of the 9th Python in Science Conference* (Austin, TX).

Song, Z. Q., Wang, F. P., Zhi, X. Y., Chen, J. Q., Zhou, E. M., Liang, F., et al. (2013). Bacterial and archaeal diversities in Yunnan and Tibetan hot springs, China. *Environ. Microbiol.* 15, 1160–1175. doi: 10.1111/1462-2920.12025

Sun, J., Zhang, Q., Zhou, J., and Wei, Q. (2014). Illumina amplicon sequencing of 16S rRNA tag reveals bacterial community development in the rhizosphere of apple nurseries at a replant disease site and a new planting site. *PLoS ONE* 9:e111744. doi: 10.1371/journal.pone.0111744

Takami, H., Noguchi, H., Takaki, Y., Uchiyama, I., Toyoda, A., Nishi, S., et al. (2012). A deeply branching thermophilic bacterium with an ancient acetyl-CoA pathway dominates a subsurface ecosystem. *PLoS ONE* 7:e30559. doi: 10.1371/journal.pone.0030559

Tamegai, H., Aoki, R., Arakawa, S., and Kato, C. (2007). Molecular analysis of the nitrogen cycle in deep-sea microorganisms from the Nankai Trough: genes for nitrification and denitrification from deep-sea environmental DNA. *Extremophiles* 11, 269–275. doi: 10.1007/s00792-006-0035-0

Tiago, I., and Veríssimo, A. (2013). Microbial and functional diversity of a subterrestrial high pH groundwater associated to serpentinization. *Environ. Microbiol.* 15, 1687–1706. doi: 10.1111/1462-2920.12034

Vanderheyden, N., Benaim, G., and Docampo, R. (1996). The role of a H(+)-ATPase in the regulation of cytoplasmic pH in Trypanosoma cruzi epimastigotes. *Biochem. J.* 318 (Pt 1), 103–109. doi: 10.1042/bj3191007v

Wang, S., Hou, W., Dong, H., Jiang, H., Huang, L., Wu, G., et al. (2013). Control of temperature on microbial community structure in hot springs of the Tibetan Plateau. *PLoS ONE* 8:e62901. doi: 10.1371/journal.pone.0062901

Xie, W., Wang, F., Guo, L., Chen, Z., Sievert, S. M., Meng, J., et al. (2011). Comparative metagenomics of microbial communities inhabiting deep-sea hydrothermal vent chimneys with contrasting chemistries. *ISME J.* 5, 414–426. doi: 10.1038/ismej.2010.144

Zarzycki, J., Brecht, V., Müller, M., and Fuchs, G. (2009). Identifying the missing steps of the autotrophic 3-hydroxypropionate $CO_2$ fixation cycle in *Chloroflexus aurantiacus*. *Proc. Natl. Acad. Sci. U.S.A.* 106, 21317–21322. doi: 10.1073/pnas.0908356106

Zhang, L., Kang, M., Xu, J., Xu, J., Shuai, Y., Zhou, X., et al. (2016). Bacterial and archaeal communities in the deep-sea sediments of inactive hydrothermal vents in the Southwest India Ridge. *Sci. Rep.* 6:25982. doi: 10.1038/srep 25982

Zhu, W., Lomsadze, A., and Borodovsky, M. (2010). Ab initio gene identification in metagenomic sequences. *Nucleic Acids Res.* 38:e132. doi: 10.1093/nar/gkq275

**Conflict of Interest Statement:** EN was employed by FASMAC Co., Ltd.

The remaining authors declare that the research was conducted in the absence of any commercial or financial relationships that could be construed as a potential conflict of interest.

frontiers in Bioengineering and Biotechnology

ORIGINAL RESEARCH
published: 18 January 2019
doi: 10.3389/fbioe.2018.00209

# Bioprospecting of Ureolytic Bacteria From Laguna Salada for Biomineralization Applications

*Dayana Arias*[1,2], *Luis A. Cisternas*[1,3], *Carol Miranda*[2] *and Mariella Rivas*[2,3]*

[1] Departamento de Ingeniería Química y Procesos de Minerales, Universidad de Antofagasta, Antofagasta, Chile, [2] Laboratorio de Biotecnología Algal y Sustentabilidad (BIOAL), Departamento de Biotecnología, Facultad de Ciencias del Mar y Recursos Biológicos, Universidad de Antofagasta, Antofagasta, Chile, [3] Centro de Investigación Científico Tecnológico Para la Minería, Antofagasta, Chile

The processes of biomineralization, mediated by ureolytic bacteria, possess a wide range of technological applications, such as the formation of biocements and remediation of water and soil environments. For this reason, the bioprospecting of new ureolytic bacteria is interesting for its application to these technologies, particularly for water treatment. This study demonstrates the isolation, selection, and identification of halotolerant ureolytic bacteria from Laguna Salada (inland from Atacama Desert) and the evaluation of their ability to precipitate calcium carbonate crystals in freshwater in the presence of calcium ions, as well as the ability to induce the precipitation of crystals from different ions present in seawater. Twenty-four halotolerant ureolytic bacteria whose molecular identification gives between 99 and 100% identity with species of the genus *Bacillus, Porphyrobacter, Pseudomonas*, *Salinivibrio,* and *Halomonas* were isolated. When cultivated in freshwater, urea, and calcium chloride, all species are able to biomineralize calcium carbonate in different concentrations. In seawater, the strains that biomineralize the highest concentration of calcium carbonate correspond to *Bacillus subtilis* and *Halomonas* sp. SEM–EDX and XRD analyses determined that both bacteria induce the formation of 9–33% halite (NaCl), 31–66% monohydrocalcite ($CaCO_3 \times H_2O$), and 24–27% struvite ($MgNH_4PO_4 \times 6H_2O$). Additionally, *B.subtilis* induces the formation of 7% anhydrite ($CaSO_4$). In seawater, *B.subtilis* and *Halomonas* sp. were able to precipitate both calcium (96–97%) and magnesium (63–67%) ions over 14 days of testing. Ion removal assays with *B.subtilis* immobilized in beads indicate a direct relationship between the urea concentration and a greater removal of ions with similar rates to free cells. These results demonstrate that the biomineralization mediated by bacterial urea hydrolysis is feasible in both freshwater and seawater, and we propose its application as a new technology in improving water quality for industrial uses.

**Keywords: biomineralization, ureolytic bacteria, struvite, monohydrocalcite, bioprospecting, urease**

## HIGHLIGHTS

- It is proposed to use ureolytic bacteria for the selective removal of calcium and magnesium from seawater.
- *Bacillus subtilis* produces the highest concentration of monohydrocalcite, close to 7,802 mg/L.
- In biomineralization tests, *B.subtilis* and *Halomonas* sp. removes 97 and 96% of the calcium ion in 5 days and 67 and 63% of magnesium in 14 days, respectively.
- The XRD analysis determined that the crystals formed by *B.subtilis* strain LN8B correspond to 33% monohydrocalcite, 33% halite, 27% struvite, and 7% anhydrite.

OPEN ACCESS

***Edited by:***
*Milko Alberto Jorquera, Universidad de La Frontera, Chile*

***Reviewed by:***
*M. Sudhakara Reddy, Thapar University, India*
*Mimi Cho Yung, Lawrence Livermore National Security, United States*

***Correspondence:**
*Mariella Rivas*
*mariella.rivas@uantof.cl*

***Specialty section:***
*This article was submitted to Bioprocess Engineering, a section of the journal Frontiers in Bioengineering and Biotechnology*

***Received:*** *24 August 2018*
***Accepted:*** *18 December 2018*
***Published:*** *18 January 2019*

***Citation:***
*Arias D, Cisternas LA, Miranda C and Rivas M (2019) Bioprospecting of Ureolytic Bacteria From Laguna Salada for Biomineralization Applications. Front. Bioeng. Biotechnol. 6:209. doi: 10.3389/fbioe.2018.00209*

## INTRODUCTION

Biomineralization refers to the process in which living organisms form minerals (Dove et al., 2004; Achal et al., 2015). There are several types of biominerals, such as organic crystals, oxides, hydroxides, sulfates, sulfides, chlorides, phosphates, and carbonates (Barabesi et al., 2007; Achal et al., 2009; Silva-Castro et al., 2015). Each biomineral has specific properties, like an unique size, crystal structure, and isotopic composition of trace elements (Perry et al., 2007; Cartwright et al., 2012). From all the biominerals known so far, carbonate precipitation, specifically of calcium carbonates, has become greatly important due to its wide range of technological applications, such as the formation of biocements, remediation of water and soil environments, and uptake of carbon dioxide (Hammes et al., 2003; Dhami et al., 2013; Phillips et al., 2013; Achal et al., 2015).

Microorganisms possessing specific metabolisms, including denitrifying, iron-reducing, sulfate-reducing, and ureolytic bacteria, play key roles during carbonate biomineralization (DeJong et al., 2010; Dhami et al., 2013). Particularly, ureolytic bacteria create an increase in ambient pH, favoring the formation of supersaturated conditions necessary for carbonate precipitation (Whiffin et al., 2007; DeJong et al., 2010). Ureolytic bacteria use the action of urease (urea amidohydrolase; EC 3.5.1.5), which catalyzes urea hydrolysis to produce ammonium and carbamate. The carbamate spontaneously decomposes to produce an ammonium and carbonic acid molecule. Both ammonium molecules and the carbonic acid in aqueous solution, in equilibrium with their deprotonated and protonated forms, generate an increase in the pH of the solution, which induces ion precipitation (Al-Thawadi, 2011; Cheng and Cord-Ruwisch, 2013; Anbu et al., 2016).

An attractive application of biomineralization mediated by ureolytic bacteria is the pretreatment of water (Arias et al., 2017a). Industrial wastewaters, hard water, and groundwater have excessive levels of contaminants, such as heavy metals, radionuclides, phosphates, and salts. On the other hand, seawater is characterized by a high $SO_4/HCO_3$ molar ratio, generally between 11 and 15 (El-Manharawy and Hafez, 2003), with an abundance of calcium sulfate (>90% wt/wt) over other species, such as $CaCO_3$, $MgSO_4$, $MgCO_3$, $MgSiO_3$, $SiO_2$, and $CaPO_4$ (Millero et al., 2008). Specifically, calcium and magnesium ions, in the presence of $SO_4^{2-}$, play an important role in calcium carbonate scaling (Waly et al., 2012; Li et al., 2015). Furthermore, the $Cl^-$ ion can react with the $Fe^{2+}$ ions that are present to create $FeCl_2$. This reacts with dissolved oxygen, generating $Fe_2O_3$ and $FeCl_3$, which are strong oxidizing agents of pipes and other equipment (Liang et al., 2013).

The advantages of using this type of microorganism is their ability to efficiently immobilize toxic metals, radionuclides, or ions by precipitation or coprecipitation with $CaCO_3$, dependent on metal valence status and redox potential (Kumari et al., 2016).

Numerous studies have been carried out using *Sporosarcina pasteurii* in processes of biomineralization and coprecipitation of $CaCO_3$ because it is non-pathogenic and has high urease activity (Whiffin et al., 2007; Achal et al., 2009; Al-Thawadi, 2011). However, studies on alternative species for the hydrolysis of urea are scarce, especially of ecologically relevant species capable of surviving a given remediation site. For these reasons, the search for biotechnologically relevant microbes capable of removing the previously described minerals/elements is of great interest. Here, the bioprospecting of halotolerant ureolytic bacteria from Laguna Salada, the evaluation of the bacterial capacity to precipitate calcium carbonate crystals in freshwater in the presence of calcium ions, and the ability to induce the precipitation of crystals from the different ions present in seawater are evaluated.

This evaluation is our first approximation for using biomineralization processes to pretreat freshwater and seawater to improve the quality for industrial processes, such as pretreatment for reverse osmosis desalination and mineral processing.

**Abbreviations:** SEM–EDX, scanning electron microscopy with energy dispersive X-ray; XRD, X-ray diffraction.

## MATERIALS AND METHODS

### Study Area

The sampling site is located in the water system from Peine village on the south edge of the Atacama Salar, which is formed by three superficially connected lagoons: Salada, Saladita, and Interna. Samples of water and sediments from sites LS1, LS2, and LS3 were collected in June 2014 from Laguna Salada, located at 2,300 meters above sea level (m.a.s.l.) at latitude 23°S and at longitude 68°W in the Chilean Altiplano. The geographical location, altitude, and physicochemical parameters of the points sampled in this site are shown in **Table 1**.

### Bioprospecting of Ureolytic Bacteria

Environmental samples were taken in sterile plastic tubes and stored at −20°C for further analysis. Five grams of samples were enriched in 50 mL of the following four culture media: TN medium (Tryptone Soya Broth (TSB, DIFCO TM) dissolved in freshwater and supplemented with 35 g/L NaCl), TM medium (TSB dissolved in seawater), LN culture medium (LB (MoBio Lab., Inc.) dissolved in freshwater and supplemented with 35 g/L NaCl), and LM medium (LB dissolved in seawater). For the isolation of cultured halophilic bacteria, the described culture media were prepared on plates with 15 g/L agar (Oxoid); 10 μL of each enriched sample was added and incubated at 30°C until growth was observed. The colony forming units (CFU) were selected according to their morphology and sub-cultured to identify the presence of urease activity.

In order to determine the presence of urease activity, the bacterial isolates were cultured in tubes with Christensen's Urea Agar, modified with 20 g/L NaCl (Atlas, 2010; Arias et al., 2017b). The bacterial isolates were seeded on the agar surface and incubated at 37°C until a coloration change from yellow to pink was observed. Trials were performed in triplicate. *Proteus mirabilis* was used as a positive control and *Escherichia coli* JM109 as a negative control.

### Identification of Microbial Strains

Genomic DNA was extracted using the Power Soil kit (Mobio Cat. No. 1288-100), according to the manufacturer's instructions.

**TABLE 1 |** Physicochemical parameters of sampling sites at Laguna Salada.

| Sites | Latitude S | Longitude W | Altitude (m.a.s.l.) | Water temperature °C | pH | $O_2$ (mg/L) | NaCl (mg/L) | Ca (mg/L) | Mg (mg/L) |
|---|---|---|---|---|---|---|---|---|---|
| LS1 | 23° 39′ 5′ | 68° 10′ 0″ | 2293 | 14.70 | 7.56 | 5.44 | 274,000 | 2760 | 4880 |
| LS2 | 23° 39′12′ | 68° 8′ 24″ | 2282 | 25.00 | 7.98 | 6.41 | 274,000 | 3240 | 800 |
| LS3 | 23° 39′12′ | 68° 8′ 19″ | 2293 | 13.20 | 8.13 | 16.52 | 93,000 | 2320 | 1600 |

PCR amplification of the rRNA gene was performed using universal primers 27F (5′-AGAGTTTGATCMTGGCTCAG-3′) and 1492R (5′TACGGYTACCTTGTTACGACTT-3′) (Frank et al., 2008). The samples were sequenced at Macrogen Inc. (South Korea). The sequences were edited using FinchTV software version 1.4 (www.geospiza.com). The sequences were then assembled using ChromasPro version 1.6 (2012) and analyzed using the BLASTN database (www.ncbi.nlm.nih.gov) using the non-redundant GenBank nucleotide collection. The identified bacterial strain sequences were then deposited in GenBank (KX185693, KX185689, KX185695, KX185692, KX185696, KX185685, KX185686, KX185691, KX185687, KX185688, KX185690, KX185684, KX018264, KX018260, KX018261, KX018262, KX018263, KX018265, KX018266, KX018267, KX018268, KX018269, KX018270, KX185694, and KX018271).

## Analysis of Nucleotide Sequence and Access Numbers

Evolutionary analyses were conducted in MEGA7.0 using Maximum Likelihood with a bootstrap of 1,000. The model used was General Time Reversible, while the branch swap filter analysis setting used was weak. The tree is drawn to scale, with branch lengths measured in the number of substitutions per site. The nucleotide sequences from this study are available in GenBank (http://www.ncbi.nlm.nih.gov) under access numbers indicated in brackets at the tree in **Figure 1**.

## Analysis of Biomineralization Capacity in Water

The strains were grown first in LN medium, with 20 g/L of $CaCl_2 \times 2H_2O$, and later in LM medium, both with 20 g/L urea. The assays were called the freshwater and seawater biomineralization test, respectively. All assays were performed in triplicate and incubated for 7 days at 30°C and 120 rpm. The pH of the assays was measured daily. At the end of day 7, the concentrations of total carbonates, bicarbonates, calcium, and soluble magnesium were quantified. The medium without bacteria acted as the negative control. The precipitates obtained were washed three times with distilled water and dried for 24 h at 60°C for SEM–EDX and XRD analyses.

## Biomass Immobilization in Polyvinyl Alcohol-Alginate Beads

Concentrated cells of *B.subtilis* strain LN8B were mixed with a 12 and 2% of polyvinyl alcohol solution (Sigma-Aldrich, MW 89,000–98,000, 99% hydrolyzed) and alginic acid (Sigma-Aldrich), respectively, to a final concentration of $4.5 \times 10^9$ cells/ml. The mixture was dripped via a peristaltic pump into a sterile solution of 4% $CaCl_2 \times H_2O$ (Merck) and 4% $H_3BO_3$ (Merck) for 2 h to form immobilized cell spheres of 0.4 cm diameter. After 2 h, the beads were washed 3 times with sterile distilled water and stored at 4°C until use.

## Experiments of $Ca^{2+}$ and $Mg^{2+}$ Biomineralization From Seawater (SW) With Immobilized Biomass

The removal studies with immobilized biomass of *B.subtilis* strain LN8B were performed in 250 mL Erlenmeyer flasks at an incubation temperature of 30°C and constant shaking at 120 rpm for 2 weeks. The concentrations of urea evaluated were 5, 10, 20, and 30 g/L, and the ratio of SW:spheres were of 1:1.

## Chemical Analysis

Calcium and magnesium ions were analyzed by atomic absorption spectrophotometry (220FS, Varian), with direct suction. Total carbonates and bicarbonates were measured through acid–base titration (Jagadeesha Kumar et al., 2013).

## Ammonium Quantification

As a measure of urease activity, the concentration of ammonium produced from urea hydrolysis was quantified according to the phenol-hypochlorite method (Achal et al., 2009).

## SEM–EDX Analyses

Crystal morphology visualization was done using a scanning electron microscope (JEOL model JSM 6360LV) coupled to an X-ray detector (Oxford Inca). The samples were prepared on a carbon tape and covered with gold via sputtering (Denton Desk II). The secondary electron current used was between 10 and 20 kV. The magnification was between 250× and 5,000×. The working distance used was 10 nm, with a spot size between 40 and 55.

## XRD Analyses

The XRD analyses were obtained using a diffractometer (Siemens D5000) with a graphite secondary monochromator and CuKα radiation. Data were collected for a 1.0 s integration time in 0.02° 2θ steps at 40 kV and 30 mA. Scanning was from 3° to 70° 2θ. The components of the sample were identified by comparing them with standards established by the International Center for Diffraction Data.

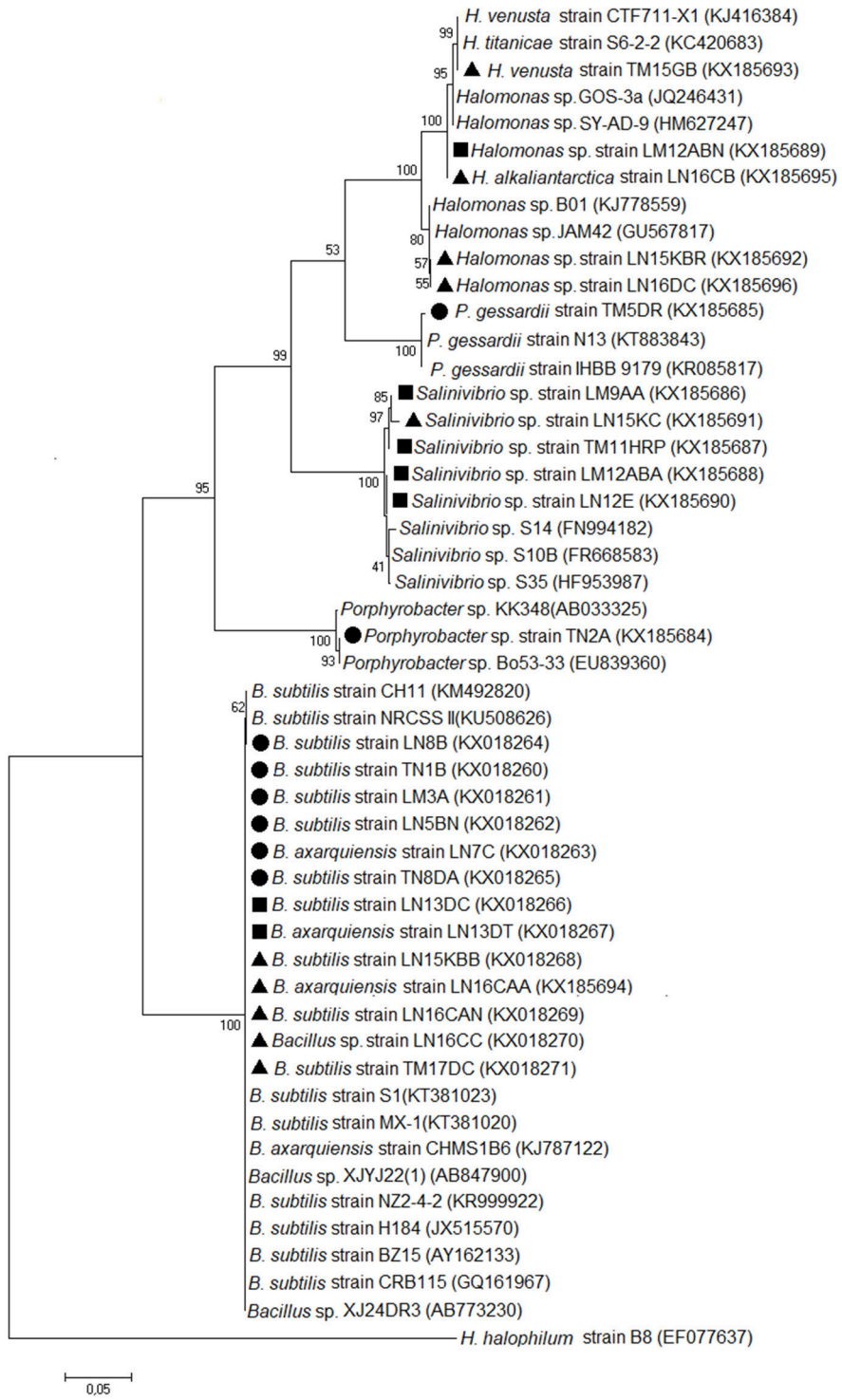


**FIGURE 1 |** Molecular phylogenetic analysis by Maximum Likelihood method. The evolutionary history was inferred by using the Maximum Likelihood method based on the General Time Reversible model (Nei and Sudhir, 2000). The tree with the highest log likelihood (−6,288, 2,707) is shown. The percentage of trees in which the associated taxa clustered together is shown next to the branches. Initial tree(s) for the heuristic search were obtained automatically by applying Neighbor-Joining and BioNJ algorithms to a matrix of pairwise distances estimated using the Maximum Composite Likelihood (MCL) approach and by selecting the topology with a superior log likelihood value. The tree is drawn to scale, with branch lengths measured in the number of substitutions per site. The analysis involved 50 nucleotide sequences. Codon positions included were 1st + 2nd + 3rd + Noncoding. All positions containing gaps and missing data were eliminated. There were a total of 1,268 positions in the final dataset. Evolutionary analyses were conducted in MEGA7 (Kumar et al., 2016). The circle corresponds to LS1. The square corresponds to LS2. The triangle corresponds to LS3.

## Statistical Analysis

Unless otherwise indicated, the presented data are the means of three independent experiments. The standard deviations of each set of experiments are represented in the corresponding figure (as bars). The comparisons of the mean $CaCO_3$ production between isolated bacteria were conducted to identify statistical significance. This was done using Minitab software version 17.0 (www.minitab.com) through unidirectional ANOVA and Dunnett tests or Student's *t*-test and Tukey test a posteriori. In all cases, comparisons for which $p < 0.05$ were considered significant.

# RESULTS

## Bioprospecting of Ureolytic Bacteria

The enrichment of each sample in 4 different media generated a total of 72 enrichment cultures, resulting in 104 colony forming units (CFU) with different appearances, colorations, and morphologies. Twenty-four bacterial isolates demonstrated the ability to hydrolyze urea in the Christensen's Urea Agar assay (23.07% of total isolates). All isolates with ureolytic activity were phylogenetically identified based on their 16S rRNA sequences by BLASTN. 98–100% identity was obtained with species of the *Bacillus*, *Salinivibrio*, *Halomonas*, *Pseudomonas*, and *Porphyrobacter* genera (**Table 2**).

From the isolates with urease activity, 50% are of the *Bacillus* species, 20.83% are of the *Salinivibrio* species, and 20% are of the *Halomonas* species. The TN2A isolate, making up 4.17% of the isolates, is closely related to the *Porphyrobacter* species, and the TM5DR strain, making up another 4.17%, is *Pseudomonas gessardii*. These last two had 99% identity. A phylogenetic tree was generated based on the 16S rRNA. The relatedness of the sequences is shown in **Figure 1**.

## Analysis of Biomineralization Capacity in Water

The freshwater biomineralization test was performed with all the isolates, evaluating the total produced carbonates and the pH evolution at the end of the seventh day (**Figure 2**). All identified strains were capable of forming calcium carbonate crystals. Quantification of the produced carbonates and pH was grouped by bacterial genus. Results showed that the highest concentration in the *Bacillus* genus was produced by *Bacillus subtilis* strain LN8B (7,802 ± 0.025 mg/L; pH of 9.07 ± 0.03). This was followed, in descending order, by *B.subtilis* strain LN13DC (7,547 ± 0.025 mg/L; pH of 8.25 ± 0.03), *Bacillus* sp. strain LN16CC (7,153 ± 0.087 mg/L; pH of 8.33 ± 0.08), and *B.subtilis* TN1B (6,834 ± 0.049 mg/L; pH of 9.00 ± 0.04). In the other genera, highlights include *Halomonas* sp. strain

**TABLE 2 |** Phylogenetic identification of halotolerant ureolytic bacterial strains isolated from Laguna Salada.

| Bacterial strain | Closest species in BLASTN[a] | E value | Coverage (%) | Identity (%) | Homolog GenBank accession no. |
|---|---|---|---|---|---|
| TN1B | *Bacillus subtilis* S1 | 0.0 | 100 | 100 | KT381023 |
| TN2A | *Porphyrobacter* sp. | 0.0 | 100 | 99 | EU839360 |
| TN8DA | *Bacillus subtilis* NZ2-4-2 | 0.0 | 100 | 100 | KR999922 |
| TM5DR | *Pseudomonas gessardii* N13 | 0.0 | 100 | 99 | KT883843 |
| TM11HRP | *Salinivibrio* sp. S10B | 0.0 | 100 | 98 | FR668583 |
| TM15GB | *Halomonas venusta* CTF711-X1 | 0.0 | 100 | 99 | KJ416384 |
| TM17DC | *Bacillus subtilis* NZ2-4-2 | 0.0 | 100 | 100 | KR999922 |
| LM3A | *Bacillus subtilis* S1 | 0.0 | 100 | 100 | KT381023 |
| LM9AA | *Salinivibrio* sp. S10B | 0.0 | 100 | 99 | FR668583 |
| LM12ABA | *Salinivibrio* sp. S10B | 0.0 | 100 | 99 | FR668583 |
| LM12ABN | *Halomonas* sp. GOS-3a | 0.0 | 100 | 99 | JQ246431 |
| LN5BN | *Bacillus subtilis* S1 | 0.0 | 100 | 100 | KT381023 |
| LN7C | *Bacillus axarquiensis* CHMS1B6 | 0.0 | 100 | 99 | KJ787122 |
| LN8B | *Bacillus subtilis* CH11 16S | 0.0 | 100 | 99 | KM492820 |
| LN12E | *Salinivibrio* sp. S10B | 0.0 | 100 | 99 | FR668583 |
| LN13DC | *Bacillus subtilis* H184 16S | 0.0 | 100 | 100 | JX515570 |
| LN15KBB | *Bacillus subtilis* S1 | 0.0 | 100 | 99 | KT381023 |
| LN15KBR | *Halomonas* sp. JAM42 | 0.0 | 99 | 99 | GU567817 |
| LN15KC | *Salinivibrio* sp. S10B | 0.0 | 100 | 99 | FR668583 |
| LN16CAA | *Bacillus axarquiensis* CHMS1B6 | 0.0 | 100 | 99 | KJ787122 |
| LN16CAN | *Bacillus subtilis* CRB115 | 0.0 | 100 | 99 | GQ161967 |
| LN16CB | *Halomonas alkaliantarctica* CRSS | 0.0 | 100 | 99 | NR114902 |
| LN16CC | *Bacillus* sp. XJ24DR3 | 0.0 | 100 | 99 | AB773230 |
| LN16DC | *Halomonas* sp. JAM42 | 0.0 | 100 | 99 | GU567817 |

[a] *Sequence homology was determined with BLASTN.*

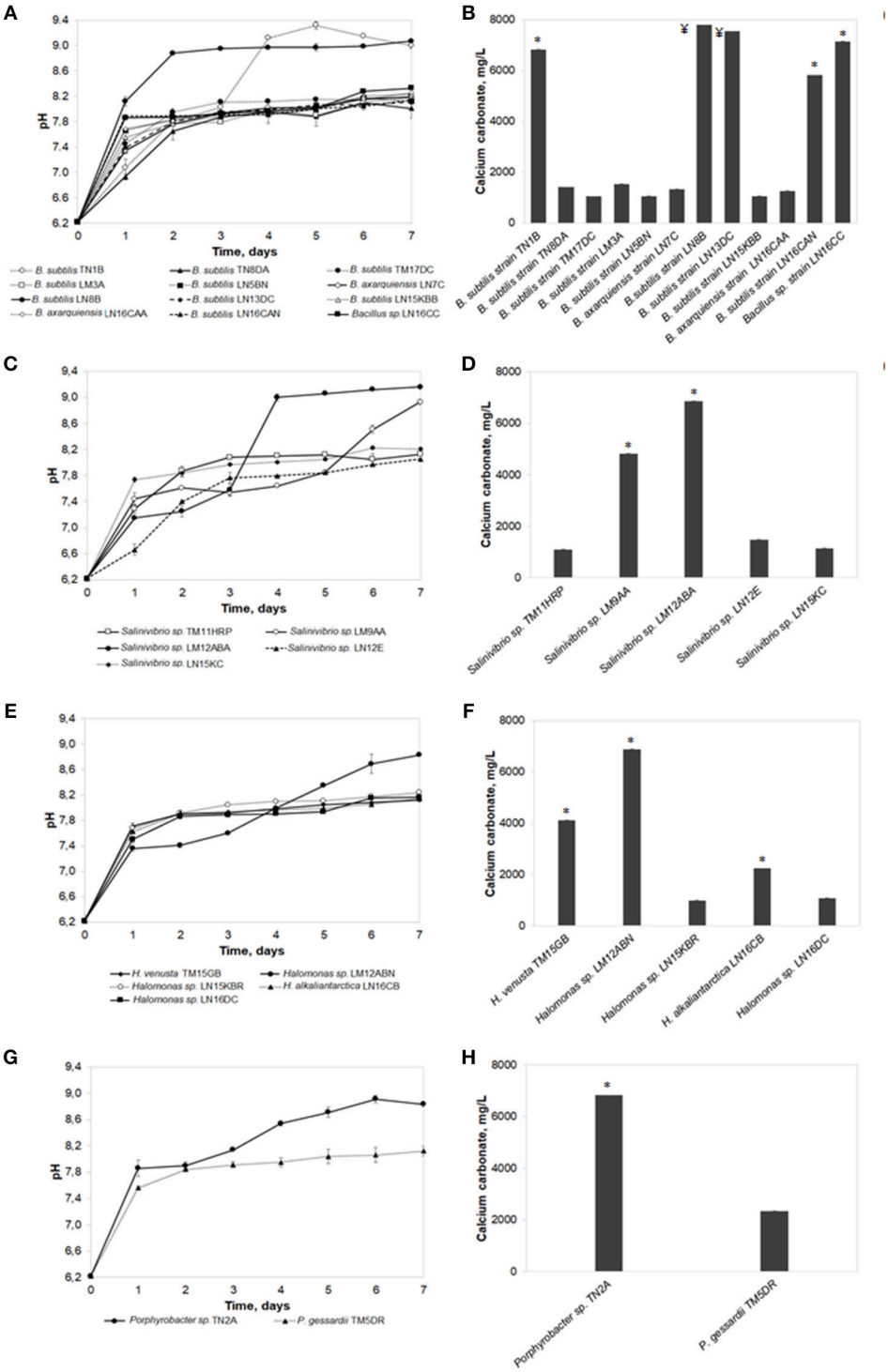


**FIGURE 2 |** The freshwater biomineralization test. pH evolution and calcium carbonate precipitation of bacterial strains belonging to *Bacillus* genus **(A,B)**, *Salinivibrio* genus **(C,D)**, *Halomonas* genus **(E,F)**, and others genera **(G,H)**. Error bars show the standard deviations for three replications per sample. Asterisks indicate significant differences ($p < 0.05$) among the values. ¥ indicates no significant differences among the values but there being differences with respect to all the other isolates.

LM12ABN (6,881 ± 0.076 mg/L; pH of 8.83 ± 0.07), *Salinivibrio* sp. strain LM12ABA (6,871 ± 0.048 mg/L; pH of 9.16 ± 0.04), *B.subtilis* strain, and *Porphyrobacter* sp. strain TN2A (6,830 ± 0.019 mg/L; pH of 8.84 ± 0.03). No biomineralization signals or precipitate formations were observed in the controls without bacteria.

Regarding the pH evolution on the seventh day of the bioassay, in most cultures, a direct relationship was observed between higher concentrations of total precipitated carbonate and higher final pH levels reached by *B.subtilis* strain LN8B. The pH of the negative control remained constant throughout the test at 6.34 ± 0.01.

The strains that precipitated the highest concentration of calcium carbonate (>6 g/L) were selected to perform the seawater biomineralization test (**Figure 3**). Of the strains evaluated in these conditions, *Salinivibrio* sp. strain LM12ABA grew to the highest cell density (**Figure 3A**) ($2 \times 10^{10}$ cells/mL). The pH of the medium increased over time for all strains, with *B. subtilis* LN8B (**Figure 3B**), *Porphyrobacter* sp. strain TN2A, and *Halomonas* sp. strain LM12ABN showing the highest pH change relative to the control (pH of 7.35 ± 0.10). When evaluating ammonium production as an indirect measure of urease activity, the same trend was observed in these three strains (**Figure 3C**).

The quantification of total calcium, magnesium, carbonates, and bicarbonates of the seven strains, compared to the control, in the seawater biomineralization test are shown in **Figure 3D**. The greatest ion biomineralization compared to the control was from calcium (concentration of $Ca^{2+}$ in the control was 403.33 ± 2.31 mg/L). *B.subtilis* strain TN1B, *Porphyrobacter* sp. strain TN2A, *Salinivibrio* sp. strain LM12ABA, *B.subtilis* strain LN13DC, and *Bacillus* sp. strain LN16CC biomineralize $Ca^{2+}$, decreasing its concentration, on average, by 27.92% after 7 days of bioassay. *B.subtilis* strain LN8B showed decreases of 98%, and *Halomonas* sp. strain LM12ABN showed decreases of 92.77%. Magnesium biomineralization—evidenced by decreases in the concentration of $Mg^{2+}$ in solution in the presence of *B.subtilis* strain TN1B, *Porphyrobacter* sp. strain TN2A, *Salinivibrio* sp. strain LM12ABA, *B.subtilis* strain LN13DC, and *Bacillus* sp. strain LN16CC—was only reduced 2.75% compared to the control (concentration of $Mg^{2+}$ in control was 1300.67±2.31 mg/L). In contrast, the *B.subtilis* strain LN8B diminished $Mg^{2+}$ concentrations by 49.32% compared to the control, reaching a final concentration of 659.2 ± 37.5 mg/L, while *Halomonas* sp. strain LM12ABN decreased $Mg^{2+}$ concentrations by 7.86%. Concentrations of total carbonates and bicarbonates at the

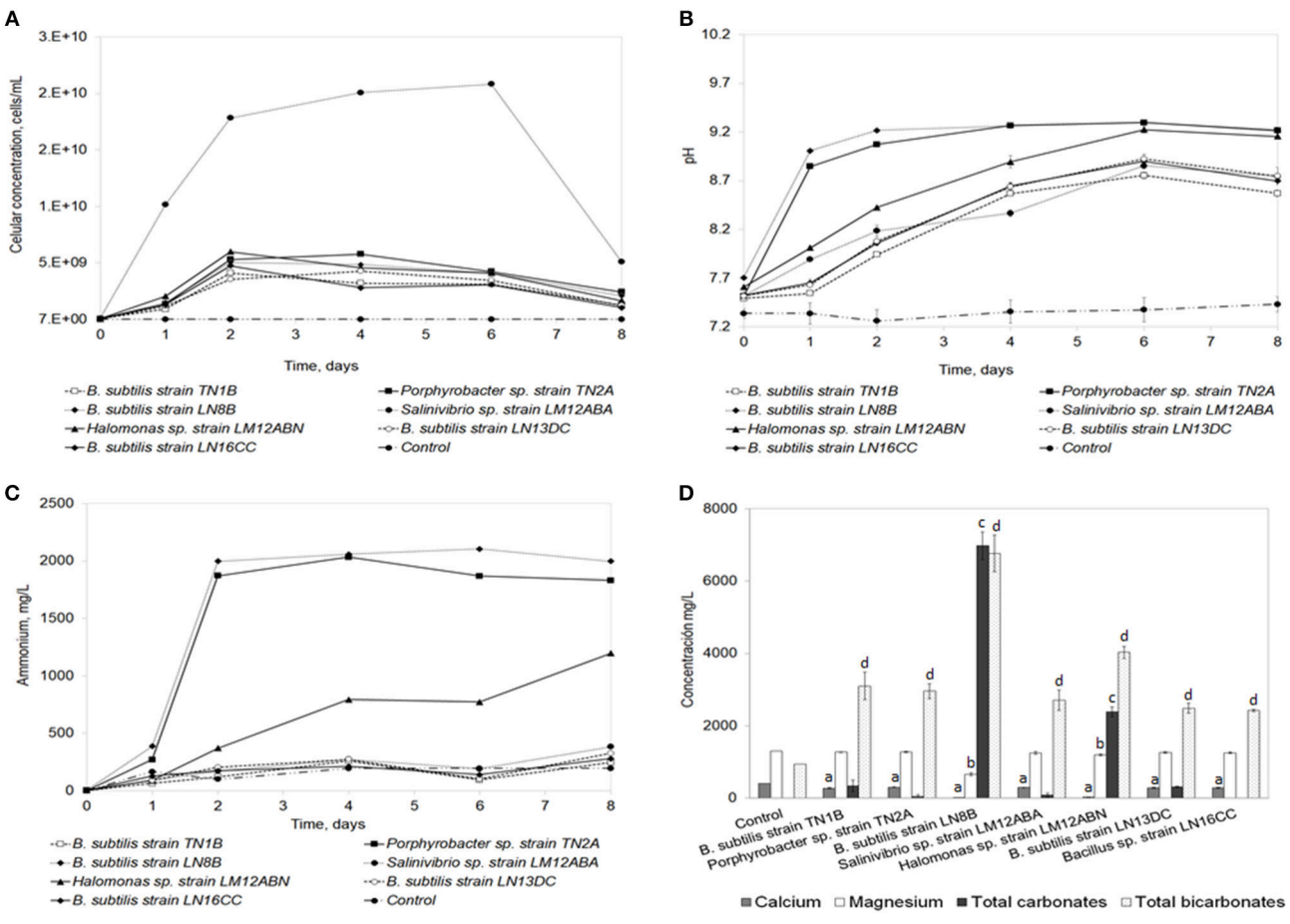


**FIGURE 3 |** Seawater biomineralization test. Analysis of the ammonium production **(A)**, pH evolution **(B)**, cellular density **(C)**, and ion quantification **(D)**. Error bars show the standard deviations for three replications per sample. "a" indicates significant differences with respect to control for calcium. "b" indicates significant differences with respect to the control for magnesium. "c" indicates significant differences with respect to the control for total carbonates. "d" indicates significant differences with respect to the control for total bicarbonates.

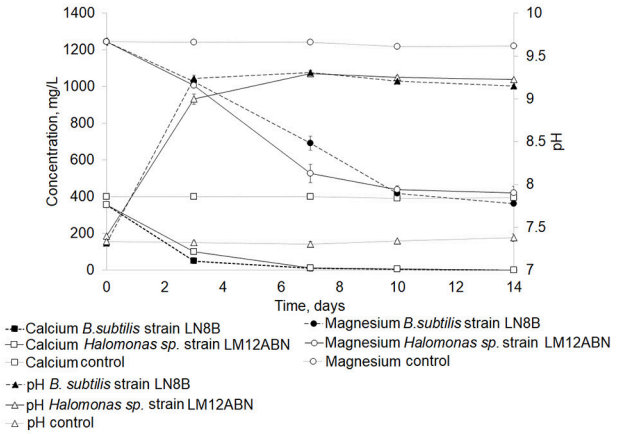


**FIGURE 4 |** Evolution of the biomineralization of calcium and magnesium ions in seawater by *B. subtilis* strain LN8B and *Halomonas sp.* strain LM12ABN at day 14 of the cultures. Error bars show the standard deviations for three replications per sample.

end of the bioassay generated by *B.subtilis* strain LN8B were 9773.1 ± 386.7 mg/L and 6767.2 ± 512.7 mg/L, respectively. In comparison, *Halomonas* sp. strain LM12ABN produced 2387.22 ± 130.69 and 4030.12 ± 164.37, respectively (**Figure 3D**).

Since *B.subtilis* strain LN8B and *Halomonas* sp. strain LM12ABN were the strains capable of biomineralizing the greatest amount of calcium and magnesium ions and producing the highest concentrations of total carbonates and bicarbonates. These strains were subjected to a new seawater biomineralization test for 14 days to determine the evolution of ion biomineralization. On the fifth day of the bioassay, *B.subtilis* strain LN8B, and *Halomonas* sp. strain LM12ABN biomineralized 97 and 96% of the calcium, respectively (**Figure 4**). Concerning the biomineralization of magnesium, by the third day of the bioassay, 67 and 63% of $Mg^{2+}$ was biomineralized by *B.subtilis* strain LN8B and *Halomonas* sp. strain LM12ABN, respectively. For both bacteria, a significant increase in pH also happened on the third day of the bioassay, rising from 7.5 to 9.3 (**Figure 4**).

## SEM–EDX and XRD Analysis

The scanning electron micrographs of the precipitates produced by some of the strains in the freshwater biomineralization assays are shown in **Figure 5**.

The precipitates biomineralized by *B.subtilis* strain LN8B and *Halomonas* sp. strain LM12ABN in the seawater biomineralization test at the end of the bioassay are shown in **Figures 6A,C**, respectively. EDX analyses indicated the presence of C, $Ca^{2+}$, $Na^{+}$, $Cl^{-}$, and $Mg^{+}$ (data not shown). These results were corroborated by XRD (**Figures 6B**, **7D**), indicating that *B.subtilis* strain LN8B is capable of inducing the precipitation of 33.08% halite (NaCl), 31.35% monohydrocalcite ($CaCO_3 \times H_2O$), 27.73% struvite ($MgNH_4PO_4 \times 6H_2O$), and 7.84% anhydrite ($CaSO_4$) (**Figure 6B**). The composition of the biominerals generated by *Halomonas* sp. strain LM12ABN was 9.40% halite, 66.03% monohydrocalcite, and 24.57% struvite (**Figure 6D**).

## $Ca^{2+}$ and $Mg^{2+}$ Removal Capacity From SW at Different Urea Concentrations With Immobilized Biomass of *B. Subtilis* Strain LN8B

**Figure 7** shows the first approximation of the influence of urea concentration on the removal of $Ca^{2+}$ and $Mg^{2+}$ from SW with immobilized biomass in a PVA-Al matrix of *B. sutilis* strain LN8B. It is observed that the urea concentration has no great influence on the pH increase in SW (**Figure 7A**). The increase in pH as the urea concentration increases does not exceed 9.3 because of the equilibrium of the ammonium buffer. However, under the conditions tested, there is a direct relationship between urea concentration, ammonium production, and removal of the ions of interest (**Figures 7B–D**). It is also evidenced, as with free cells, that there is a tendency to precipitate $Ca^{2+}$ ions first, then $Mg^{2+}$ ions. This trend is also marked because the latter ion has a higher concentration in SW. Finally, the removal of $Ca^{2+}$ with the immobilized cells reached 100 and 94% for urea concentrations of 20 and 30 g/L, respectively, at 8 days of testing. Removal of $Mg^{2+}$ reaches 53 and 62% for the same concentrations of urea at 15 days of testing. These values are similar to those observed with free cells and can be optimized, for example, by increasing the cell concentration in the PVA-Al beads.

# DISCUSSION

## Bacterial Biodiversity With Urease Activity From Laguna Salada

The biomineralization process through bacterial urea hydrolysis is one of the studied mechanisms that has a great potential to produce various biomaterials at high concentrations in short periods of time (Bachmeier et al., 2002; Al-Thawadi, 2011). Particularly, urease activity is widely distributed in organisms present in the water and soil (Burbank et al., 2012). Lloyd and Sheaffe (1973) estimated that only 17–30% of aerophilic, microaerophilic, and anaerobic microorganisms are capable of hydrolyzing urea. However, various studies have identified ureolythic bacteria in different environments, including *Acinobacter* sp. (Sanchez-Moral et al., 2003), *Deleyahlophila* (Rivadeneyra et al., 1996), *E. coli* (Bachmeier et al., 2002), and *Myxococcus xanthus* (Holt et al., 1993; González-Muñoz et al., 2000). In our study we demonstrate the selection of halotolerant bacteria with ureolytic activity from Laguna Salada in the Atacama Desert. Specifically, 24 bacterial isolates demonstrated the ability to hydrolyze urea in the Christensen's Urea Agar assay (23.07% of total isolates). All isolates with ureolytic activity were phylogenetically identified based on their 16S rRNA sequences by BLASTN. 98–100% identity was obtained with species from the *Bacillus*, *Salinivibrio*, *Halomonas*, *Pseudomonas*, and *Porphyrobacter* genera (**Table 2**).

*Bacillus* bacteria are widely distributed in natural environments and have been widely described for their ability to precipitate calcium carbonate (Castanier et al., 2000;

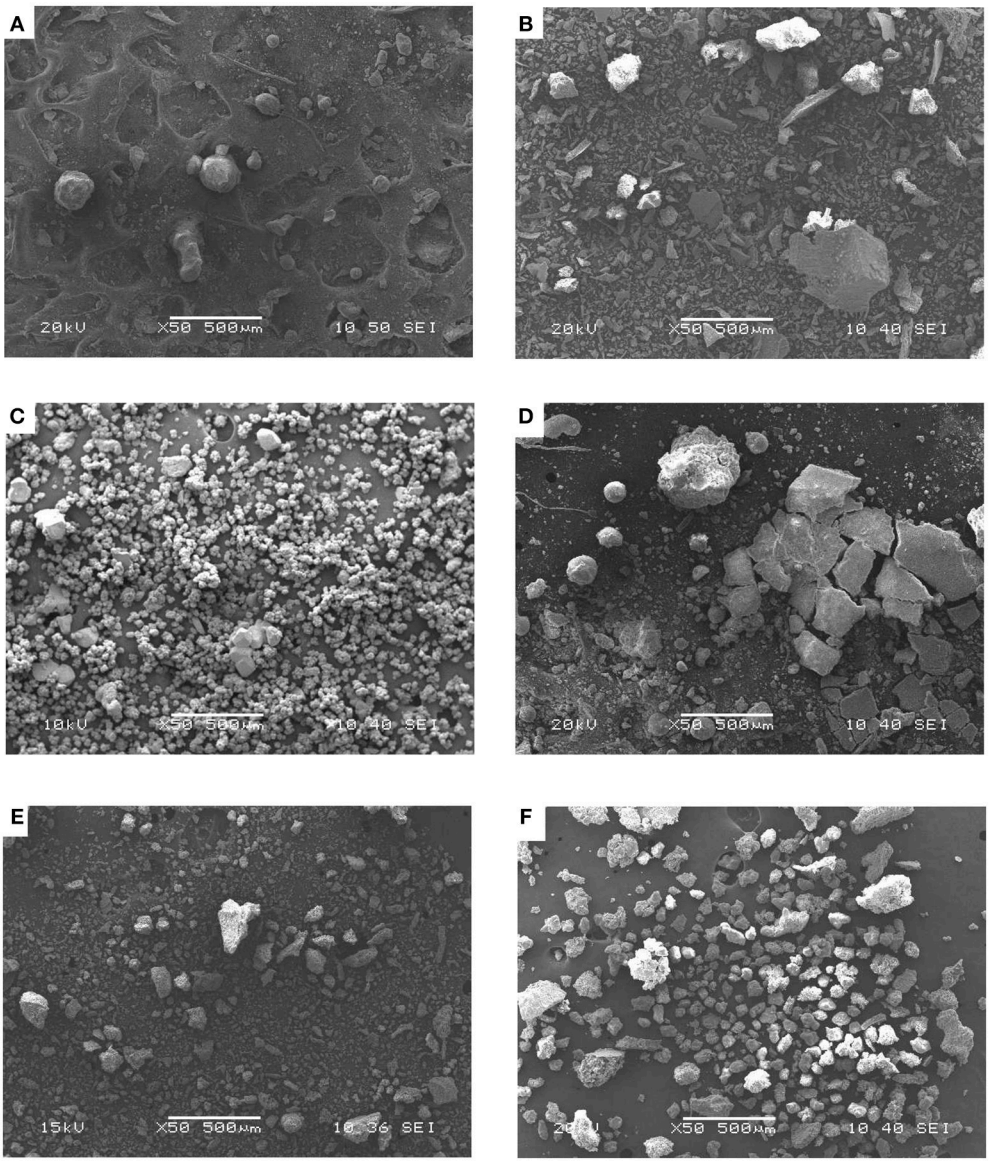


**FIGURE 5 |** Scanning electron micrograph of crystals precipitated in freshwater by *B.subtilis* strain LM3A **(A)**, *B. axarquiensis* strain LN7C **(B)**, *B.subtilis* strain LN8B **(C)**, *Salinivibrio sp.* strain LM9AA **(D)**, *Halomonas sp.* strain LM12ABN **(E)**, and *P. gessardii* strain TM5DR **(F)**.

Hammes et al., 2003), which coincides with 50% of the isolates in this study. Its easy cultivation and ability to absorb heavy metals and biomineralize calcite have made this genus one of the most promising for biomineralization as a biotechnological tool for the construction industry and bioremediation (Phillips et al., 2013; Zhu and Dittrich, 2016). It was also possible to determine that there are different strains of the same bacterial species, which have distinctly evident characteristics.

Knorre and Krumbein (2000) described bacteria isolated from freshwater, marine, and hypersaline environments as being capable of precipitating carbonates. However, there are differences in the mineralogy of precipitates that depends on the species of halophilic bacteria involved (Ferrer et al., 1988; Rivadeneyra et al., 2006). Halophilic bacteria, such as *Halomonas* and *Salinivibrio*, have been reported to precipitate calcium, magnesium carbonates, and phosphates by bypassing the inhibitory effect of high $Mg^{2+}$ ion concentrations in bacteria-mediate precipitation of $CO_3^{2+}$ (Raz et al., 2000; Rivadeneyra et al., 2006). In addition, one of advantages of using halophilic bacteria is their low potential for pathogenicity (Stabnikov et al., 2013).

## Biomineralization Applications in Seawater

In recent years, freshwater consumption has reached critical levels in Northern Chile, as they have around the world. Industrial use places great pressure on this resource, especially

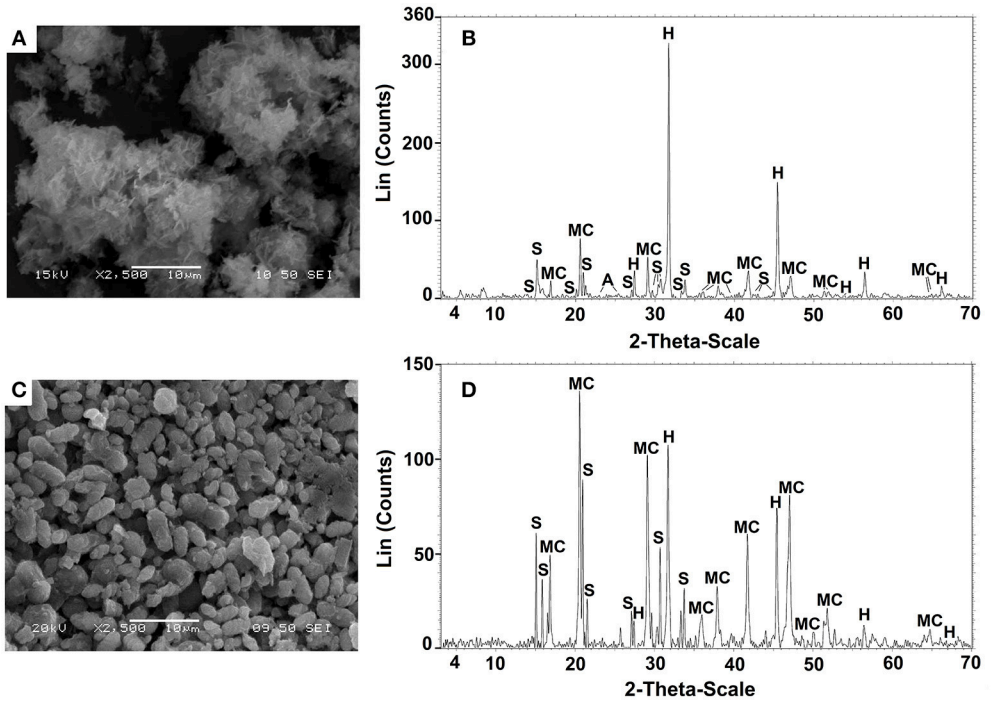


**FIGURE 6 |** SEM and XRD analysis of the precipitates produced by *B.subtilis* strain LN8B **(A,B)** and *Halomonas* sp. strain LM12AB **(C,D)**. Struvite, monohydrocalcite, and halite were represented by (S), (M), and (H), respectively.

in arid areas where there is a shortage of freshwater resources. Desalinated and non-desalinated seawater hold a real alternative for sustained industrial development in these regions. However, its use has disadvantages, mostly due to problems with chemical composition and high concentrations of calcium and magnesium ions, which have a negative effect on reverse osmosis plants and other industries, such as copper and molybdenum mining.

All bacteria with urease activity described in this study can precipitate calcium crystals from ions present in seawater in different percentages and times. In biomineralization tests in seawater, *Bacillus subtilis* and *Halomonas* sp. were able to biomineralize both calcium (96–97%) and magnesium (63–67%) ions over 14 days of testing. SEM–EDX and XRD analyses determined that both bacteria induce the formation of 9–33% halite (NaCl), 31–66% monohydrocalcite ($CaCO_3 \times H_2O$), and 24–27% struvite ($MgNH_4PO_4 \times 6H_2O$). Additionally, *B.subtilis* induces the formation of 7% anhydrite ($CaSO_4$).

These results suggest that bacterial ureolytic metabolism in culture media produces the necessary conditions to induce heterogeneous calcium carbonate crystallization (Whiffin et al., 2007; Stabnikov et al., 2013). Le Corre et al. (2009) and Pastor et al. (2008) described how calcium interferes with struvite formation, inhibiting the reaction by blocking active struvite growth sites and competing for orthophosphate to form calcium phosphate. Given that the highest percentage of calcium is removed from the solution in the first 3 days of culture (84%), this would permit the subsequent precipitation of magnesium through struvite formation. Struvite precipitation depends on different other factors, such as pH, the $Mg^{2+}$:$NH_4^+$:$PO_4^{3-}$ molar ratio, concentrations of potentially interfering ions, and ionic strength (Desmidt et al., 2013). The ability to form struvite is not widely described in nature (Laiz et al., 2009). Rivadeneyra et al. (1983, 1992b) have described struvite precipitation by *Pseudomonas*, *Flavobacterium*, *Arthrobacter* (Rivadeneyra et al., 1983, 1992a,b), and *Chromohalobacter* species (Rivadeneyra et al., 2006). Also, Sánchez-Román et al. (2007) found that moderately halophilic gamma-proteobacteria, including *Halomonas* spp., *Salinivibrio costicola*, *Marinomonas communis*, and *Marinobacter hydrocarbonoclasticus*, precipitate struvite.

Additionally, several authors have found that an increase in pH, as a result of the metabolic activity of the bacteria, provides the necessary ions for the formation of minerals, e.g., $NH_4^+$ and $PO_4^{3-}$ for struvite or $CO_3^{2-}$ for carbonates (Sánchez-Román et al., 2007; Silva-Castro et al., 2013). This clearly demonstrates that bacteria do not act simply as a nucleation site for biomineralization but, rather, act as active mediators in the process (Sánchez-Román et al., 2007; Silva-Castro et al., 2013).

According to the results determined in the biomineralization tests, the biomineralization of *B.subtilis* strain LN8B and *Halomonas* sp. grown in the seawater biomineralization test have a tendency to form calcium crystals. This is followed by the biomineralization of magnesium crystals. This could be because the $Ca^{2+}$ ion is adsorbed more frequently than the $Mg^{2+}$ ion on the negatively charged cellular envelope of the bacteria, which has a greater power for ionic selectivity

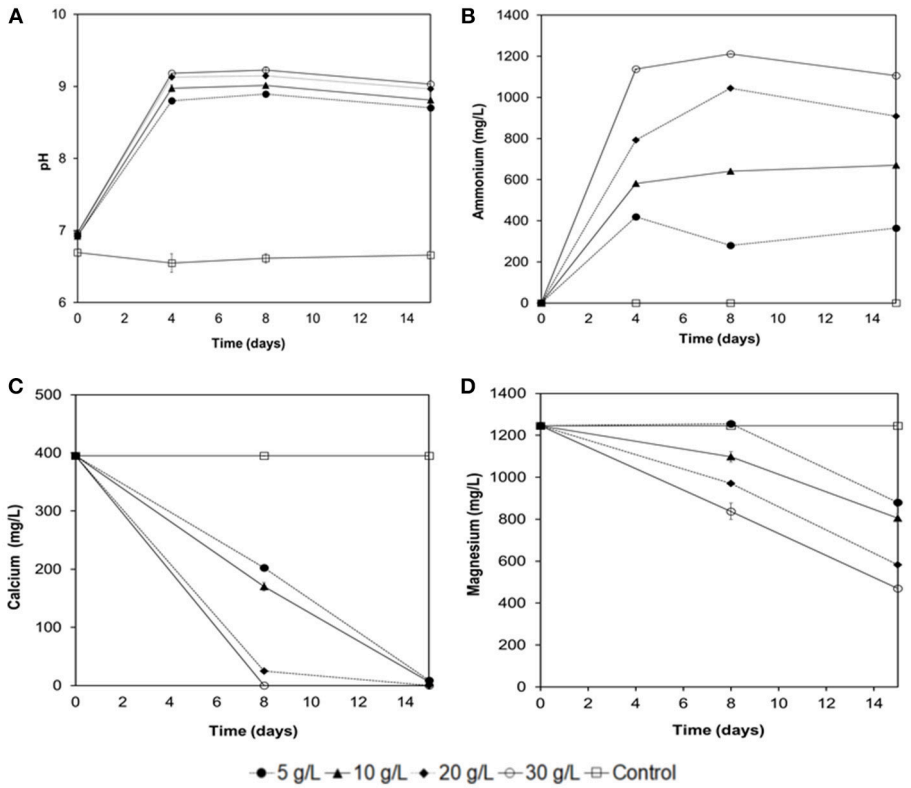


**FIGURE 7 |** Experiments of $Ca^{2+}$ and $Mg^{2+}$ removal from seawater with immobilized biomass of *B.subtilis* strain LN8B at different concentrations of urea. Evolution of the pH **(A)**, ammonium **(B)**, calcium **(C)**, and magnesium **(D)** ions at the 15th day of the assay. Error bars show the standard deviations for three replications per sample.

(Rivadeneyra et al., 1998; Silva-Castro et al., 2013). Liquid media and high salt concentrations seem to favor the formation of monohydrocalcite. In this context, our results are consistent with those described by Rivadeneyra et al. (2004), who found that, in the cultures of *Halobacillus trueperi*, monohydrocalcite is precipitated only in liquid media with high salt concentrations. Our results are different from those previously described by Rivadeneyra et al. (1991), which indicated that the presence of magnesium ions may prevent the precipitation of calcium carbonate crystals. This is because the inhibitory effect of magnesium mostly affects non-halotolerant, rather than halotolerant, bacteria (Rivadeneyra et al., 2006; Delgado et al., 2008).

The use of free bacterial cells for the removal of $Ca^{2+}$ and $Mg^{2+}$ from SW may not be fully feasible due to the need for a further separation of the biomass suspended from SW or due to low cell viability when faced with mechanical changes (Khoo and Ting, 2001). However, one of the main advantages of immobilized enzymes or microorganisms is that they can be used in continuous flow reactors because of their importance in industrial applications (Moynihan et al., 1989). The results obtained with *B.subtilis* LN8B immobilized in spheres of PV-Al, including urea and without LB, demonstrated the removal of 100% of $Ca^{2+}$ at 8 days of testing and the removal of 62% of $Mg^{2+}$ at 15 days. These values are similar to those observed in the free cell assays (**Figures 4**, **7**). Unlike in our study, it had only been known that the partially purified *S. pasteurii* (previously *Bacillus pasteurii*) urease was immobilized in polyurethane (PU) foam to compare the efficacy of calcite precipitation between the free and immobilized enzymes. The immobilized urease showed higher Km and lower $V_{max}$ values, which were reflected by slower overall calcite precipitation (Bachmeier et al., 2002). According to Bachmeier et al. (2002), the increase in pH is due to the presence of ammonium ions in the medium. This, in turn, is a consequence of the hydrolysis of urea accelerating the biomineralization rate of calcite, even with the immobilized enzyme. The biomineralization assays with *B.subtilis* LN8B immobilized in PV-Al spheres show that the interaction between ions and the surface of the bacteria would not be essential for the formation of calcite, in our case. However, it was not feasible to evaluate the distribution of the bacteria in the spheres, which does not allow for ruling out a feasible interaction. On the other hand, PV-Al is a water-soluble polymer that acts as a colloid mainly used for the active release of detergents and agrichemicals. This allows the interaction between the bacteria and the surrounding medium.

## CONCLUSIONS

Calcium biomineralization has only been tested through urea hydrolysis in freshwater and biomineralization in seawater from the ions present. These tests only allow us to improve water quality with respect to these ions, but biomineralization has not been tested in other types of water with other types of ions or contaminants, such as heavy metals or radionuclides.

Through the exploration of the bacterial capacity to precipitate calcium and magnesium ions from SW, it has been demonstrated that *B.subtilis* strain LN8B and *Halomonas* sp. strain LN12ABN have the biomineralization capability to precipitate these ions. The bacterial metabolism of both bacteria induces the formation of calcium biominerals (such as monohydrocalcite and anhydrite) and magnesium biominerals (such as struvite) from the ions present in SW. Additionally, *Halomonas* sp. LN12ABN formed 9% halite and *B.subtilis* formed 33%.

Despite the success in the search for bacteria able to precipitate calcium and magnesium from SW, the components needed to optimize the precipitation of these ions, the design of a bioreactor to pretreat the SW, and the means of immobilizing bacteria in a matrix that increases their survival and efficiency in ion removal are currently still under study. However, the positive results of these preliminary experiments certainly justify further development of the process.

Finally, this study reinforces the application of biomineralization mediated by bacteria as a biotechnological tool to improve the quality of SW for industrial processes and, alternatively, as reverse osmosis pretreatment.

## AUTHOR CONTRIBUTIONS

DA performed all the experiments and the analysis of the results. CM performed all the statistical analyzes and contributed to the writing of the manuscript. DA also participated in writing this article. LAC participated in writing this article. MR participated in the design of the trials, analysis of results, and in writing this article.

## ACKNOWLEDGMENTS

This publication was supported by Anillo–Grant no. ACM 170005 (CONICYT), CICITEM Project no. R15A10002, and the Regional Government of Antofagasta. DA thanks CONICYT for Ph.D. Scholarship CONICYT-PCHA/2013/21130712. LAC thanks to CONICYT, Grant Fondecyt 1180826, for their support. The authors thank the Dirección de Gestión de la Investigación of the Universidad de Antofagasta.

## REFERENCES

Achal, V., Mukherjee, A., Basu, P. C., and Reddy, M. S. (2009). Strain improvement of *Sporosarcina pasteurii* for enhanced urease and calcite production. *J. Ind. Microbiol. Biotechnol.* 36, 981–988. doi: 10.1007/s10295-009-0578-z

Achal, V., Mukherjee, A., Kumari, D., and Zhang, Q. (2015). Biomineralization for sustainable construction—A review of processes and applications. *Earth Sci. Rev.* 148, 1–17. doi: 10.1016/j.earscirev.2015.05.008

Al-Thawadi, S. M. (2011). Ureolytic bacteria and calcium carbonate formation as a mechanism of strength enhancement of sand. *J. Adv. Sci. Eng. Res.* 1, 98–114.

Anbu, P., Kang, C.-H., Shin, Y.-J., and So, J.-S. (2016). Formations of calcium carbonate minerals by bacteria and its multiple applications. *Springerplus* 5:250. doi: 10.1186/s40064-016-1869-2

Arias, D., Cisternas, L. A., and Rivas, M. (2017a). Biomineralization mediated by ureolytic bacteria applied to water treatment: a review. *Crystals* 7:345. doi: 10.3390/cryst7110345

Arias, D., Cisternas, L. A., and Rivas, M. (2017b). Biomineralization of calcium and magnesium crystals from seawater by halotolerant bacteria isolated from Atacama Salar (Chile). *Desalination* 405, 1–9. doi: 10.1016/j.desal.2016.11.027

Atlas, R. M. (2010). *Handbook of Microbiological Media, 4th Edn*. Boca Raton, FL: CRC Press. doi: 10.1201/EBK1439804063

Bachmeier, K. L., Williams, A. E., Warmington, J. R., and Bang, S. S. (2002). Urease activity in microbiologically-induced calcite precipitation. *J. Biotechnol.* 93, 171–181. doi: 10.1016/S0168-1656(01)00393-5

Barabesi, C., Galizzi, A., Mastromei, G., Rossi, M., Tamburini, E., and Perito, B. (2007). *Bacillus subtilis* gene cluster involved in calcium carbonate biomineralization. *J. Bacteriol.* 189, 228–235. doi: 10.1128/JB.01450-06

Burbank, M. B., Weaver, T. J., Williams, B. C., and Crawford, R. L. (2012). Urease activity of ureolytic bacteria isolated from six soils in which calcite was precipitated by indigenous bacteria. *Geomicrobiol. J.* 29, 389–395. doi: 10.1080/01490451.2011.575913

Cartwright, J. H. E., Checa, A. G., Gale, J. D., Gebauer, D., and Sainz-Díaz, C. I. (2012). Calcium carbonate polyamorphism and its role in biomineralization: how many amorphous calcium carbonates are there? *Angew. Chem. Int. Ed.* 51, 11960–11970. doi: 10.1002/anie.201203125

Castanier, S., Métayer-Levrel, G. L., and Perthuisot, J. P. (2000). Bacterial roles in the precipitation of carbonate minerals. *Microb. Sediments* 32–39. doi: 10.1007/978-3-662-04036-2_5

Cheng, L., and Cord-Ruwisch, R. (2013). Selective enrichment and production of highly urease active bacteria by non-sterile (open) chemostat culture. *J. Ind. Microbiol. Biotechnol.* 40, 1095–1104. doi: 10.1007/s10295-013-1310-6

DeJong, J. T., Mortensen, B. M., Martinez, B. C., and Nelson, D. C. (2010). Bio-mediated soil improvement. *Ecol. Eng.* 36, 197–210. doi: 10.1016/j.ecoleng.2008.12.029

Delgado, G., Delgado, R., Párraga, J., Rivadeneyra, M. A., and Aranda, V. (2008). Precipitation of carbonates and phosphates by bacteria in extract solutions from a semi-arid saline soil. Influence of $Ca^{2+}$ and $Mg^{2+}$ concentrations and $Mg^{2+}/Ca^{2+}$ molar ratio in biomineralization. *Geomicrobiol. J.* 25, 1–13. doi: 10.1080/01490450701828974

Desmidt, E., Ghyselbrecht, K., Monballiu, A., Rabaey, K., Verstraete, W., and Meesschaert, B. D. (2013). Factors influencing urease driven struvite precipitation. *Separation and Purification Technology,* 110, 150–157. doi: 10.1016/j.seppur.2013.03.010

Dhami, N. K., Reddy, M. S., and Mukherjee, A. (2013). Biomineralization of calcium carbonates and their engineered applications: a review. *Front. Microbiol.* 4, 314. doi: 10.3389/fmicb.2013.00314

Dove, P. M., De Yoreo, J. J., and Weiner, S. (eds.). (2004). *Biomineralization*. Washington, DC: Mineralogical Society of America and the Geochemical Society; Reviews in Mineralogy and Geochemistry, 381.

El-Manharawy, S., and Hafez, A. (2003). Study of seawater alkalization as a promising RO pretreatment method. *Desalination* 153, 109–120. doi: 10.1016/S0011-9164(02)01110-4

Ferrer, M. R., Quevedo-Sarmiento, J., Rivadeneyra, M. A., Bejar, V., Delgado, R. and Ramos-Cormenzana, A. (1988). Calcium carbonate precipitation by two groups of moderately halophilic microorganisms at different temperatures and salt concentrations. *Curr. Microbiol.* 17, 221–227. doi: 10.1007/BF01589456

Frank, J. A., Reich, C. I., Sharma, S., Weisbaum, J. S., Wilson, B. A., and Olsen, G. J. (2008). Critical evaluation of two primers commonly used for amplification of bacterial 16S rRNA genes. *Appl. Environ. Microbiol.* 74, 2461–2470. doi: 10.1128/AEM.02272-07

González-Muñoz, M. T., Ben-Chekroun, K., Ben-Aboud, A., Arias, J. M., and Rodríguez-Gallego, M. (2000). Bacterially induced Mg-calcite formation: role of $Mg^{2+}$ in development of crystal morphology. *J. Sediment. Res.* 70, 559–564. doi: 10.1306/2DC40928-0E47-11D7-8643000102C1865D

Hammes, F., Seka, A., Van Hege, K., Van De Wiele, T., Vanderdeelen, J., Siciliano, S. D., et al. (2003). Calcium removal from industrial wastewater by bio-catalytic $CaCO_3$ precipitation. *J. Chem. Technol. Biotechnol.* 78, 670–677. doi: 10.1002/jctb.840

Holt, J. G., Kried, N. R., Senath, P. H. A., Staley, J. T., and Williams, S. T. (eds.). (1993). *Bergey's Manual of Determinative Bacteriology*. Philadelphia. PA: Lippincott, Williams and Wikins.

Jagadeesha Kumar, B. G., Prabhakara, R., and Pushpa, H. (2013). Effect of bacterial calcite precipitation on compressive strength of mortar cubes. *Int. J. Eng. Adv. Technol.* 2, 486–491.

Khoo, K. M., and Ting, Y. P. (2001). Biosorption of gold by immobilized fungal biomass. *Biochem. Eng. J.* 8, 51–59. doi: 10.1016/S1369-703X(00)00134-0

Knorre, H., and Krumbein, W. E. (2000). "Bacterial calcification," in *Microbial Sediments*, eds R. Riding and S. Awaramik (Berlin: Springer), 25–31.

Kumar, S., Stecher, G., and Tamura, K. (2016). MEGA7: molecular evolutionary genetics analysis version 7.0 for bigger datasets. *Mol. Biol. Evol.* 33, 1870–1874. doi: 10.1093/molbev/msw054

Kumari, D., Qian, X. Y., Pan, X., Achal, V., Li, Q., and Gadd, G. M. (2016). Microbially-induced carbonate precipitation for immobilization of toxic metals. *Adv. Appl. Microbiol.* 94, 79–108. doi: 10.1016/bs.aambs.2015.12.002

Laiz, L., Miller, A. Z., Jurado, V., Akatova, E., Sánchez-Moral, S., Gonzalez, J. M., et al. (2009). Isolation of five Rubrobacter strains from biodeteriorated monuments. *Naturwissenschaften* 96, 71–79. doi: 10.1007/s00114-008-0452-2

Le Corre, K. S., Valsami-Jones, E., Hobbs, P., and Parsons, S. A. (2009). Phosphorus recovery from wastewater by struvite crystallization: A Review. *Crit. Rev. Environ. Sci. Technol.* 39, 433–477. doi: 10.1080/10643380701640573

Li, Z., Valladares Linares, R., Bucs, S., Aubry, C., Ghaffour, N., Vrouwenvelder, J. S., et al. (2015). Calcium carbonate scaling in seawater desalination by ammonia-carbon dioxide forward osmosis: mechanism and implications. *J. Memb. Sci.* 481, 36–43. doi: 10.1016/j.memsci.2014.12.055

Liang, J., Deng, A., Xie, R., Gomez, M., Hu, J., Zhang, J., et al. (2013). Impact of seawater reverse osmosis (SWRO) product remineralization on the corrosion rate of water distribution pipeline materials. *Desalination* 311, 54–61. doi: 10.1016/j.desal.2012.11.010

Lloyd, A. B., and Sheaffe, M. J. (1973). Urease activity in soils. *Plant Soil* 39, 71–80. doi: 10.1007/BF00018046

Millero, F. J., Feistel, R., Wright, D. G., and McDougall, T. J. (2008). The composition of standard seawater and the definition of the reference-composition salinity scale. *Deep. Res. Part I Oceanogr. Res. Pap.* 55, 50–72. doi: 10.1016/j.dsr.2007.10.001

Moynihan, H. J., Lee, C. K., Clark, W., and Wang, N. H. (1989). Urea hydrolysis by immobilized urease in a fixed-bed reactor: analysis and kinetic parameter estimation. *Biotechnol. Bioeng.* 34, 951–963. doi: 10.1002/bit.260340710

Nei, M., and Sudhir, K. (2000). *Molecular Evolution and Phylogenetics*. Oxford: Oxford University Press.

Pastor, L., Mangin, D., Barat, R., and Seco, A. (2008). A Pilot-scale study of struvite precipitation in a stirred tank reactor: conditions influencing the process. *Bioresour. Techno.* 99, 6285–6291. doi: 10.1016/j.biortech.2007.12.003

Perry, R. S., Mcloughlin, N., Lynne, B. Y., Sephton, M. A., Oliver, J. D., Perry, C. C., et al. (2007). Defining biominerals and organominerals: direct and indirect indicators of life. *Sediment. Geol.* 201, 157–179. doi: 10.1016/j.sedgeo.2007.05.014

Phillips, A. J., Gerlach, R., Lauchnor, E., Mitchell, A. C., Cunningham, A. B., and Spangler, L. (2013). Engineered applications of ureolytic biomineralization: a review. *Biofouling* 29, 715–733. doi: 10.1080/08927014.2013.796550

Raz, S., Weiner, S., and Addadi, L. (2000). Formation of high-magnesian calcites vía an amorphous precursor phase: possible biological implications. *Advanced Materials*. 12, 38–42. doi: 10.1002/(SICI)1521-4095(200001)12:1<38::AID-ADMA38>3.0.CO;2-1

Rivadeneyra, M. A., Delgado, G., Ramos-Cormenzana, A., and Delgado, R. (1998). Biomineralization of carbonates by *Halomonas eurihalina* in solid and liquid media with different salinities: crystal formation sequence. *Res. Microbiol.* 149, 277–287. doi: 10.1016/S0923-2508(98)80303-3

Rivadeneyra, M. A., Delgado, R., Quesada, E., and Ramos-Cormenzana, A. (1991). Precipitation of calcium carbonate by *Deleya halophila* in media containing NaCl as sole salt. *Curr. Microbiol.* 22, 185–190. doi: 10.1007/BF02092132

Rivadeneyra, M. A., Martín-Algarra, A., Sánchez-Navas, A., and Martín-Ramos, D. (2006). Carbonate and phosphate precipitation by *Chromohalobacter marismortui*. *Geomicrobiol. J.* 23, 89–101. doi: 10.1080/01490450500533882

Rivadeneyra, M. A., Párraga, J., Delgado, R., Ramos-Cormenzana, A., and Delgado, G. (2004). Biomineralization of carbonates by *Halobacillus trueperi* in solid and liquid media with different salinities. *FEMS Microbiol. Ecol.* 48, 39–46. doi: 10.1016/j.femsec.2003.12.008

Rivadeneyra, M. A., Pérez-García, I., and Ramos-Cormenzana, A. (1992a). Influence of ammonium ion on bacterial struvite production. *Geomicrobiol. J.* 10, 125–137. doi: 10.1080/01490459209377912

Rivadeneyra, M. A., Pérez-García, I., and Ramos-Cormenzana, A. (1992b). Struvite precipitation by soil and fresh water bacteria. *Curr. Microbiol.* 24, 343–347. doi: 10.1007/BF01571105

Rivadeneyra, M. A., Ramos-Cormenzana, A., Delgado, G., and Delgado, R. (1996). Process of carbonate precipitation by *Deleya halophila*. *Curr. Microbiol.* 32, 308–313. doi: 10.1007/s002849900055

Rivadeneyra, M. A., Ramos-Cormenzana, A., and García Cervigón, A. (1983). Bacterial formation of struvite. *Geomicrobiol. J.* 3,151–163. doi: 10.1080/01490458309377792

Sanchez-Moral, S., Canaveras, J. C., Laiz, L., Saiz-Jimenez, C., Bedoya, J., and Luque, L. (2003). Biomediated precipitation of calcium carbonate metastable phases in hypogean environments: a short review. *Geomicrobiol. J.* 20, 491–500. doi: 10.1080/713851131

Sánchez-Román, M., Rivadeneyra, M. A., Vasconcelos, C., and McKenzie, J. A. (2007). Biomineralization of carbonate and phosphate by moderately halophilic bacteria. *FEMS Microbiol. Ecol.* 61, 273–284. doi: 10.1111/j.1574-6941.2007.00336.x

Silva-Castro, G. A., Uad, I., Gonzalez-Martínez, A., Rivadeneyra, A., Gonzalez-Lopez, J., and Rivadeneyra, M. A. (2015). Bioprecipitation of calcium carbonate crystals by bacteria isolated from saline environments grown in culture media amended with seawater and real brine. *Biomed. Res. Int.* 2015, 1–12. doi: 10.1155/2015/816102

Silva-Castro, G. A., Uad, I., Rivadeneyra, A., Vilchez, J. I., Martin-Ramos, D., González-López, J., et al. (2013). Carbonate precipitation of bacterial strains isolated from sediments and seawater: formation mechanisms. *Geomicrobiol. J.* 30, 840–850. doi: 10.1080/01490451.2013.777492

Stabnikov, V., Jian, C., Ivanov, V., and Li, Y. (2013). Halotolerant, alkaliphilic urease-producing bacteria from different climate zones and their application for biocementation of sand. *World J. Microbiol. Biotechnol.* 29, 1453–1460. doi: 10.1007/s11274-013-1309-1

Waly, T., Kennedy, M. D., Witkamp, G. J., Amy, G., and Schippers, J. C. (2012). The role of inorganic ions in the calcium carbonate scaling of seawater reverse osmosis systems. *Desalination* 284, 279–287. doi: 10.1016/j.desal.2011.09.012

Whiffin, V. S., van Paassen, L. A., and Harkes, M. P. (2007). Microbial carbonate precipitation as a soil improvement technique. *Geomicrobiol. J.* 24, 417–423. doi: 10.1080/01490450701436505

Zhu, T., and Dittrich, M. (2016). Carbonate precipitation through microbial activities in natural environment, and their potential in biotechnology: a review. *Front. Bioeng. Biotechnol.* 4, 1–21. doi: 10.3389/fbioe.2016.00004

**Conflict of Interest Statement:** The authors declare that the research was conducted in the absence of any commercial or financial relationships that could be construed as a potential conflict of interest.

frontiers in Bioengineering and Biotechnology

ORIGINAL RESEARCH
published: 05 February 2019
doi: 10.3389/fbioe.2019.00010

# Soil Bacterial Communities From the Chilean Andean Highlands: Taxonomic Composition and Culturability

*Felipe Maza*[1,2], *Jonathan Maldonado*[1,2], *Javiera Vásquez-Dean*[1], *Dinka Mandakovic*[1,2], *Alexis Gaete*[1,2], *Verónica Cambiazo*[1,2] *and Mauricio González*[1,2]*

[1] Laboratorio de Bioinformática y Expresión Génica, Instituto de Nutrición y Tecnología de los Alimentos, Universidad de Chile, Santiago, Chile, [2] Center for Genome Regulation, Santiago, Chile

OPEN ACCESS

**Edited by:**
Milko Alberto Jorquera, Universidad de La Frontera, Chile

**Reviewed by:**
Daniel Moya, Universidad de Castilla La Mancha, Spain
Pabulo Henrique Rampelotto, Universidade Federal do Rio Grande do Sul (UFRGS), Brazil

***Correspondence:**
Mauricio González
mgonzale@inta.uchile.cl

**Specialty section:**
This article was submitted to Bioprocess Engineering, a section of the journal Frontiers in Bioengineering and Biotechnology

**Received:** 15 October 2018
**Accepted:** 16 January 2019
**Published:** 05 February 2019

**Citation:**
Maza F, Maldonado J, Vásquez-Dean J, Mandakovic D, Gaete A, Cambiazo V and González M (2019) Soil Bacterial Communities From the Chilean Andean Highlands: Taxonomic Composition and Culturability. Front. Bioeng. Biotechnol. 7:10. doi: 10.3389/fbioe.2019.00010

The Atacama Desert is a highly complex, extreme ecosystem which harbors microorganisms remarkable for their biotechnological potential. Here, a soil bacterial prospection was carried out in the high Altiplano region of the Atacama Desert (>3,800 m above sea level; m a.s.l.), where direct anthropogenic interference is minimal. We studied: (1) soil bacterial community composition using high-throughput sequencing of the 16S rRNA gene and (2) bacterial culturability, by using a soil extract medium (SEM) under a factorial design of three factors: temperature (15 and 30°C), nutrient content (high and low nutrient disposal) and oxygen availability (presence and absence). A total of 4,775 OTUs were identified and a total of 101 isolates were selected for 16S rRNA sequencing, 82 of them corresponded to unique or non-redundant sequences. To expand our view of the Altiplano landscape and to obtain a better representation of its microbiome, we complemented our Operational Taxonomic Units (OTUs) and isolate collection with data from other previous data from our group and obtained a merged set of OTUs and isolates that we used to perform our study. Taxonomic comparisons between culturable microbiota and metabarcoding data showed an overrepresentation of the phylum Firmicutes (44% of isolates vs. 2% of OTUs) and an underrepresentation of Proteobacteria (8% of isolates vs. 36% of OTUs). Within the Next Generation Sequencing (NGS) results, 33% of the OTUs were unknown up to genus, revealing an important proportion of putative new species in this environment. Biochemical characterization and analysis extracted from the literature indicated that an important number of our isolates had biotechnological potential. Also, by comparing our results with similar studies on other deserts, the Altiplano highland was most similar to a cold arid desert. In summary, our study contributes to expand the knowledge of soil bacterial communities in the Atacama Desert and complements the pipeline to isolate selective bacteria that could represent new potential biotechnological resources.

**Keywords: atacama desert, altiplano highland, bacterial community, bacterial isolation, NGS, PGP**

## INTRODUCTION

Soils are an extraordinarily diverse microbiome (Torsvik and Øvreås, 2002; Philippot et al., 2013). Microorganisms harbored in these environments have crucial roles in plant growth promotion and nutrient cycling (Fierer, 2017). Among, the Atacama Desert is often considered one of the harshest soil environments, displaying a spectrum of variables make it an extreme environment (Costello et al., 2009). It is the most arid desert on Earth (Gómez-Silva et al., 2008), it exhibits severe day-night temperature fluctuations (McKay et al., 2003; Azua-Bustos et al., 2012), and the highest UV radiations ever measured on Earth (Piacentini et al., 2003; Cordero et al., 2014), these environmental conditions are exacerbated in the highlands from the Altiplano region of the Atacama Desert.

The Andean Altiplano is a volcanic-sedimentary plateau located between 28 and 24°S with an average altitude of 4,000 m a.s.l. This environment is the second highest Altiplano region on Earth and is characterized by low mean annual temperature (<10°C) and precipitation (<170 mm), making it a cold arid environment within the Atacama Desert (Díaz et al., 2016).

Extremophile microorganisms that exist in environmental conditions like the Atacama arid highlands have unique metabolic capacities and/or physical structures which allow them to survive in these oligotrophic conditions (Tse and Ma, 2016). It is intriguing to understand how these microorganisms use various substrates and metabolic pathways to endure and how this undiscovered chemical diversity could be used for biotechnological applications (Bull and Asenjo, 2013).

Microbial communities in the soils of the Atacama Desert have been well-studied, because this region is considered the dry edge for life (Azua-Bustos et al., 2012; Azua-Bustos and González-Silva, 2014) and for its similarities with the soils of Mars (Navarro-González et al., 2003). The annual output of research publications on Atacama microbiology increased 10-fold during the last decade, reflecting an increasing interest in both fundamental and applied topics (Bull et al., 2016, 2018). However, most of the analyses have been performed with the use of molecular-genetic methods, and the study of isolates has mainly centered on members of the taxonomically distinct *Streptomyces* clade isolated from the Atacama Desert (Okoro et al., 2009; Rateb et al., 2011; Schulz et al., 2011; Goodfellow et al., 2017). Also, the studies mentioned have been mainly performed in soils from the lower parts of the Desert. Little is known about the diversity of bacterial communities associated with the Andean highlands (Lugo et al., 2008; Ferrero et al., 2010; Jorquera et al., 2016; Menoyo et al., 2017), which is precisely what we aim to uncover. We hypothesize that bacterial communities harbored in the highlands from the Atacama Desert display new candidates with biotechnological potential. To achieve our aim, we performed a soil bacteria prospection of three sites in the Atacama Desert highland and then tested the isolates for plant growth proportion properties (PGP) to evaluate the biotechnological potential harbored in this extreme environment.

The sampling sites of this study were between 3,800 and 4,500 m a.s.l., in the Altiplano highlands, nested below the Lascar Volcano. Lascar is the most active volcano of the northern Chilean Andes, with frequent small to medium eruptions and sporadic explosive events accompanied by ash rain extending over wide areas in Chile (Risacher et al., 1999; Tassi et al., 2009). Despite its extreme conditions, a diverse group of bacteria have been found to reside in the Lejía Lake, located at the base of Lascar Volcano (Demergasso et al., 2010; Mandakovic et al., 2018a). Thus, Altiplano highlands, especially close to the permanent influence of chemical components generated by volcano activity, constitute a relevant model to investigate how organisms adapt to live under particular extreme conditions.

As a first approach, we carried out a soil bacterial prospection using NGS technology to examine the bacterial community present in the Altiplano highland (>3,500 m a.s.l.) in the central region of the Atacama Desert. Once bacterial metabarcoding data was acquired, we evaluated bacterial culturability, using a soil extract medium (SEM) (Mandakovic et al., 2018a) under a factorial design of three factors: contrasting temperatures (15 and 30°C), nutrient contents (high and low nutrient disposal) and oxygen availability (presence and absence).

In the course of this study we uncovered part of the microbial biodiversity using these two different approaches. The combination of cultivation techniques coupled with high throughput sequencing allowed us to describe the microbial landscape of the high altitude areas of the Atacama Desert, and also to recover a part of the culturable fraction of the microorganisms inhabiting this natural extreme habitat.

Taxonomic comparisons between culturable microbiota and metabarcoding data showed overrepresentation and underrepresentation of different taxa that could grow in culture, revealing several candidates that may provide support for the biotechnological applications of soil bacteria species living in a stressful environment that is highly challenging for life.

## MATERIALS AND METHODS

### Site Description, Sample Collection and Processing

The sampling sites were located in highlands of Altiplano region of the Atacama Desert (between 23°30′0.0″S 67°41′24.0″W and 23°19′42.8″S 67°47′56.0″W), located between 3,870 and 4,480 m a.s.l. Soil samples were obtained from two sampling sites: upper highland (4,480 m a.s.l.) and lower highland (3,870 m a.s.l.). Upper and lower highlands correspond to the TLT01 and TLT08 sites, respectively, of the Talabre-Lejía Transect (TLT; Díaz et al., 2016). Samples were taken in April, 2014, and again on April, 2017. Mineral soil samples (∼200 g each) were randomly obtained in sterility between 5 and 10 cm deep in the soil and were used for the metabarcoding analysis, preparation of Soil Extract Medium (SEM), bacterial isolation and for physicochemical analyses. This depth was chosen as it has minimum effect of superficial phenomena like wind and rain with the highest microbial diversity (Eilers et al., 2012). Samples were kept at 4°C for isolate culture and −20°C for metabarcoding, and transported to the laboratory, where they were kept at the same temperature and processed a few days after sampling.

## Local Environmental Measurements and Soil Physicochemical Analyses

Soil physicochemical characteristics, pH and electrical conductivity were retrieved from Mandakovic et al. (2018a,b). Furthermore, environmental mean annual temperature (MAT) and mean annual precipitation (MAP) of each site were taken from Díaz et al. (2016). Solar radiation was measured using the *in situ* insolation sensor S-LIB-M003 (**Table 1**).

## Soil DNA Extractions and Sequencing

Soil DNA was extracted according to Mandakovic et al. (2018a) with some modifications. Total DNA from soils was extracted from 10 g of each sample using the NucleoSpin® Food kit (Macherey-Nagel), following the manufacturer's instructions, and the CTAB extraction buffer published by Zhou et al. (1996). Microbial 16S rRNA genes were amplified according to Mandakovic et al. (2018b) without modifications. DNA libraries were constructed following the TruSeq DNA sample preparation (Illumina, USA) protocol. Sequencing was performed by MrDNA Next Generation Sequencing Service Provider (Shallowater, Texas, USA) on an Illumina MiSeq platform in an overlapping 2 × 300 bp configuration, to obtain a minimum throughput of 40,000 sequences (reads) per sample.

## Metabarcoding and Isolate Complementary Data

In order to obtain a broader representation of the highland microbial community, the data obtained in this study was complemented with metabarcoding data and isolate collection from Mandakovic et al. (2018a,b). Metabarcoding data from TLT8 and Lejía Lake shore were taken from Mandakovic et al. (2018a,b) respectively, and merged with the data of TLT1 obtained in this study. To represent the Lejía Lake shore soil among the isolates collection, we included the bacterial isolates recovered by Mandakovic et al. (2018a) in this study as well.

## Processing of Illumina Sequence Data

Microbial 16S rRNA raw amplicon sequences were processed and analyzed following previously described protocols (Dowd et al., 2008; Handl et al., 2011). Briefly, sequences were joined (overlapping pairs) and depleted of barcodes. Then, sequences < 150 bp or with ambiguous base calls were removed. Sequences were filtered using the USEARCH clustering algorithm at 4% sequence divergence to remove chimeras and clusters consisting of only one sequence (i.e., singletons) (Edgar, 2010; Edgar et al., 2011). Finally, sequences were quality filtered with Mothur v.1.22.2 (Schloss et al., 2009) with the minimal quality average set to 30.

## Accession Numbers

All 16S rRNA gene sequence data used in this study are deposited in the Sequence Read Archive (SRA) of the National Center for Biotechnology Information (NCBI) under the BioProject accession number PRJNA489888.

## Sequence Analysis and Taxonomic Identification Using the Silva Database

Following Mandakovic et al. (2018b), sequences were analyzed with the software Quantitative Insights Into Microbial Ecology (QIIME v1.8.0; Caporaso et al., 2010). We used QIIME script "pick_closed_reference_otus.py" to extract all 16S rRNA reads from the amplicon data that matched Silva r16S database (Quast et al., 2012) (release 132) at 97% similarity or 3% divergence, with the taxonomy of the resulting Operational Taxonomic Units (OTUs) assigned directly from the closest reference sequence match. The OTU picking process was done with USearch v6.1.544 (Edgar, 2010; Edgar et al., 2011) using QIIME default parameter values (-s 0.97 –z True –max_accepts 1 –max_rejects 8 –word_length 8 –minlen 64 –usearch61_sort_method abundance). OTUs unassigned or assigned to mitochondria and chloroplasts were removed.

## Alpha Diversity Analysis

We calculated alpha OTU diversity by randomly sub-sampling (without replacement) each soil sample using the alpha_rarefaction.py script in QIIME. The Chao1, Shannon, Faith's phylogenetic diversity (PD) and Evenness indices were calculated, along with the observed number of OTUs. Rarefaction curves for each of these metrics were obtained by serial subsampling in increments of 4,199 sequences and 10 iterations per increment, to a standardized 42,000 sequences per sample.

## Factorial Culture Design

For culture experiments, Soil Extract Medium (SEM) was used and prepared according to Mandakovic et al. (2018a). Briefly, SEM was prepared by mixing agar with the water soluble portion of the soil from the sampling sites, supplemented with Fungizone (2.5 μg/ml). This medium was either: (1) supplemented with Lysogeny Broth (LB-SEM; 10 g/l Bacto Tryptone (BD), 5 g/l Yeast Extract (BD), 10 g/l NaCl); or (2) supplemented with Diluted Lysogeny Broth (10% LB-SEM; 1 g/l Bacto Tryptone (BD), 0.5 g/l Yeast Extract (BD), 1 g/l NaCl). The pH of these media was adjusted to pH 7. Each medium was incubated in a combination of 2 conditions: temperature (15 or 30°C) and oxygen availability (aerobic or anaerobic conditions). This factorial design of three factors returned the eight conditions used in this study, and offered a wider range of conditions that the highland environment displayed, to isolate a higher diversity of soil bacteria.

## Isolation and Identification of Unique Bacteria

Collected samples were passed through a sterile 2 mm sieve for homogenization. To obtain soil bacterial isolates from the Altiplano region of the Atacama Desert, 1.5 g of sieved-homogenized soil was solubilized in 2 mL sterile PBS for 2 h. Tubes were then centrifuged for 5 min at 500 rpm and 100 μl of supernatant were plated in triplicate and cultured for 2 weeks in the combination of conditions previously described. A total of 101 morphologically different colonies were isolated. Bacterial DNA from these isolates was extracted and purified

**TABLE 1 |** Average climatic and soil characteristics of the sites included in this study.

| Sampling location | Latitude °S | Longitude °W | Elevation (m) | pH | MAP | MAT | Electric conductivity (mS/cm) | %C | %N |
|---|---|---|---|---|---|---|---|---|---|
| LLS* | −23.83 | −68.15 | 4,314 | 8.5 | 161.9** | 8.5 | ND | $2.43 \times 10^{-3}$ | $3.98 \times 10^{-4}$ |
| TLT1† | −23.50305 | −67.72371 | 4,480 | 5.23 | 161.9 | 4.2 | 0.06 | 0.16 | 0.01 |
| TLT8† | −23.32856 | −67.79890 | 3,870 | 5.77 | 75.1 | 6.9 | 0.04 | 0.32 | 0.02 |

*Lejía Lake Soil (Mandakovic et al., 2018a); **MAP from LLS was extrapolated from TLT1 given the proximity of the sites; †TLT, Talabre-Lejía Transect (Díaz et al., 2016); ND, No Data.*

using the DNeasy Blood & Tissue Kit for DNA (Qiagen). The 16S rRNA genes were amplified by PCR using the primers 27F (5′-AGA GTT TGA TCA TGG CTC AG-3′) and 1492R (5′-CGG TTA CCT TGT TAC GAC TT-3′) according to Mandakovic et al. (2018a). PCR products were visualized in 2% (w/v) agarose gel electrophoresis in Tris-acetate-EDTA (TAE) buffer (1X) and stained with ethidium bromide. PCR products were purified and sequenced by Macrogen (Macrogen Corp., Maryland, USA). Forward and reverse sequences were assembled in a single contig using the Contig Assembly Program in the Bioedit software. The phylogenetic classification of these sequences was determined using the RDP database tools (Cole et al., 2014). Sequence identity was then determined comparing the 16S sequence of all the isolates obtained using the TaxonDC software (Tarlachkov and Starodumova, 2017). Those exhibiting higher than 99% sequence similarity and also identical morphological features were collapsed to one.

## 16S rRNA Phylogenetic Analysis

For phylogenetic analyses of the unique 16S rRNA sequences recovered, reference species sequences and outgroups were obtained from the Silva database. Sequences were aligned using the MAFFT v7.313 software using the default (FFT-NS-2) algorithm and subsequently trimmed and realigned using the G-INS-I algorithm. Phylogenetic trees were constructed using MEGA7 software with the following settings: Maximum likelihood tree, Tamura-Nei model, with 1,000 bootstrap replications. The trees were visualized and annotated using the FigTree Software[1].

## Determination of Biotechnological Applications

Bacterial isolates were taxonomically matched to known species using the RDP database (**Supplementary Table 1**). They were studied in depth in order to describe their biotechnological potentials by literature search using the NCBI Pubmed database. The main keywords used were the "genus" and "species" assigned for each isolate, and the keyword "review" was added when more than 200 results were retrieved with the aforementioned keywords (e.g., "*Streptomyces vinaceus,*" "*Bacillus megaterium* review"). Articles were taken into account if they declared any kind of biotechnological potential information in their abstract. Functions described in published articles were classified as: "Biomedical potential," "Bioremediation," "PGP," "Agricultural potential," "Food industry potential," "Pharmaceutical Industry potential," among others.

## Identification of Plant Growth-Promoting (PGP)

To classify the isolates as plant growth-promoting (PGP), we evaluated 5 attributes (siderophore production, Indole Acetic Acid (IAA) production, nitrogen fixation, 1-Aminocyclopropane-1-Carboxylate (ACC) deaminase activity and phosphate solubilization), each with different selective culture media. Siderophore production was detected using the method described by Schwyn and Neilands (1987). Using chromeazurol agar (CAS), bacterial colonies that exhibited a yellow halo after proliferation were classified as positive for siderophore production. IAA production was assessed using a colorimetric method. Bacterial isolates were cultured in TSB media supplemented with 0.1% L-tryptophan as the precursor for IAA. Using Salkowski's reagent (Mohite, 2013), TSB media acquires color depending on the IAA concentration, which is then compared to a standard curve of Indole-3-acetic acid (Merck®) ranging from 5 to 180 μg/ml. Nitrogen fixation was determined using Nitrogen-Free Medium (NFM). Isolates were incubated for 7 days, and bacterial proliferation was evidence of atmospheric nitrogen fixation (Grobelak et al., 2015). ACC deaminase activity was measured by culturing bacteria with 3 mM of 1-Aminocyclopropane-1-carboxylic Acid (ACC; Merck®) as the sole source of nitrogen (Penrose and Glick, 2003). The phosphate-solubilizing ability was determined by the presence of a halo surrounding colonies in Pikovskayas Agar medium after 4 days of cultivation at 30°C (Ahmad et al., 2008).

# RESULTS

## Sampling Location and Soil Characterization

The highland sampling sites used in this study were Altiplano soils defined as the upper highland (TLT1: 4,480 and LLS: 4,314 m a.s.l.) and the lower highland (TLT8: 3,870 m a.s.l.). Physicochemical features of each site are displayed in **Table 1**. Average physicochemical features of the sampled soils were: electric conductivity (mS/cm) 0.8 ± 0.6, pH 6.2 ± 1.3, MAT was 5.5°C, MAP 118.5 mm, 0.16% C and 0.01% N. The solar radiation reported by the insolation sensor station at 4,090 m a.s.l. was 960 W/m$^2$. According to the MAP value, highlands from the Atacama Desert are classified as an arid environment, less arid than the

[1]FigTree Software Available online at: http://tree.bio.ed.ac.uk/software/figtree/

Atacama hyper-arid core at 2,500 m a.s.l. Considering the high altitude of the Lascar Volcano, this area is seasonally covered by snow, which contributes to decrease the MAT and increase MAP. Also, according to Díaz et al. (2016) the highest plant coverage (%) is reached at 4,000 m a.s.l. a feature that is probably driven by the higher MAP of this highland environment.

## Bacterial Community Composition and Diversity Analysis

To identify the complete bacterial community (microbiome) present in the soil, we used NGS technologies to sequence the 16S rRNA gene directly from the environment. A total of 417,671 good quality (clean) reads were obtained, of which 151,245 were classified in a 16S rRNA sequence (mapped reads). The total number of different OTUs recovered from soil microbiome were 9,961, with only 1,211 (12,2%) containing >80% of the relative abundance, showing a typical power law distribution pattern found in most soil microbial communities (Bailey et al., 2013). After applying a quality filter of 0.005% of the total read abundance, the number of OTUs was reduced to 4,775. The minimum taxonomic level assigned to each OTU was phylum; 53.3% were assigned to genus and 6.6% to species.

Soil bacterial community alpha diversity was calculated as indicated in material and methods. We obtained Shannon diversity values of 9.5 ± 0.0 in the upper highland, 10 ± 0.0 in the lower highland and 6.7 ± 0.0 for Lejía Lake shore. The estimated richness values (Chao1) were 7,324.7 ± 88.3 for the upper highland, 8,351.5 ± 149.5 for the lower highland and 3,212.4 ± 43.5 for Lejía Lake shore. The mean diversity (H') of the highland was 8.8 ± 0.0 and the mean richness (Chao1) was 6,296.2 ± 93.8. Soil bacterial diversity appeared to be responding positively to altitude, since we obtained higher diversity values in upper highland sampling sites. It appears that lake soil limits the diversity because it is located at the same altitude than the upper highland but harbors less diversity levels.

A total of 37 bacterial phyla were found in these soil samples, Proteobacteria (36.52%) being the most abundant (dominant), followed by Acidobacteria (20.82%), Actinobacteria (17.42%), and Bacteroidetes (5.93%). Of the 4,775 OTUs, 2,547 were identified to genus, representing 480 different genera (**Supplementary Figure 1**).

## Characterization of Culturable Bacteria

The community characterization allowed us to have a vision of the bacterial community inhabiting highlands from the Altiplano region of the Atacama Desert. Nevertheless, since bacterial physiological characterization is primarily achieved in culture, we applied culture-based approaches that simulated the natural conditions and permitted the identification of the complete set of bacteria recovered in culture. To accomplish this, we used several culture conditions, described in methods. These culture conditions were proposed to cover a wide range of bacterial growth conditions and isolate a high variety of microorganisms, and the use of SEM intended to generate a medium that could represent many qualities encountered in Altiplano soils by using the nutrients present in the water-soluble fraction obtained directly from the soil.

About 1,000 bacterial isolates were recovered from the initial culture, from which 101 were selected as morphologically unique. The 16S rRNA of these isolates was sequenced and their sequence similarity was evaluated using the TaxonDC software in order to collapse identical sequences. From the 101 isolates, a total of 82 were then selected as unique phylotypes by their 16S rRNA gene sequence and morphological features. Isolates recovered by Mandakovic et al. (2018a) ($n = 11$) were added to this pool of 82 isolates. Further analyses of phyla abundance were determined with the 93 bacterial isolates recovered in the Altiplano highland (**Supplementary Table 1**).

Culturing revealed four phyla present in the soil bacterial community (**Figure 1**). The most abundant was Firmicutes (46.2%), followed by Actinobacteria (43%), Proteobacteria (8.6%), and Bacteroidetes (2.2%). These four phyla comprised 14 genera: the most abundant were *Streptomyces*, *Bacillus,* and *Arthrobacter* (**Table 2**). Interestingly, we isolated one member of the genus *Variovorax*, which has only seven other species described in its group.

Contrary to what could be expected, not all 14 genera recovered by culture were identified by NGS. Though, only 4 genus were not recovered: *Carnobacterium*, *Chryseobacterium*, *Hymenobacter,* and *Rhodococcus*, they only represented 6 isolates. The culturable strategy recovered the same most dominant phyla found in the metabarcoding analysis (Proteobacteria, Actinobacteria, and Firmicutes). However, these phyla were represented in different proportions in the NGS results: the proportion of Actinobacteria was 2.5 times higher in culture and Firmicutes was 20 times higher than NGS. On the contrary, the culture dependent identification recovered four times less Proteobacteria than NGS. Moreover, no isolation of any Acidobacteria was accomplished.

## Putative Biotechnological Potential

Bacterial isolates taxonomically identified to putative species using the RDP database (**Supplementary Table 1**) were studied in depth to describe their biotechnological potential using the NCBI Pubmed database. The most abundant categories of biotechnological potential found were Biomedical, Bioremediation and PGP (**Table 3**). Most genera evaluated had at least one species linked to the three most abundant categories, e.g., *Bacillus*, *Microbacterium*, *Paenibacillus*, *Rhodococcus*, *Stenotrophomonas*, and *Streptomyces*. However, *Arthrobacter*, *Halomonas*, *Pseudomonas,* and *Variovorax*, have only been described as potential PGP or to be involved in bioremediation. The genus *Bacillus* has been linked mostly to PGP, while the genus *Streptomyces* has generally been described as well-known antibiotic producers. Proportionately, *Rhodococcus* and *Stenotrophomonas* were the genera with more biotechnological features described in journal articles (**Figure 2**). Therefore, isolates from these genera are more likely to have the most biotechnological features.

The isolates obtained in this study were identified in terms of their 16S rRNA sequence and a putative species affiliation was assigned to each isolate based on the RDP database's Sequence Match algorithm. For the 93 isolates, 43 potential species were assigned. The isolation source of the representative strain for

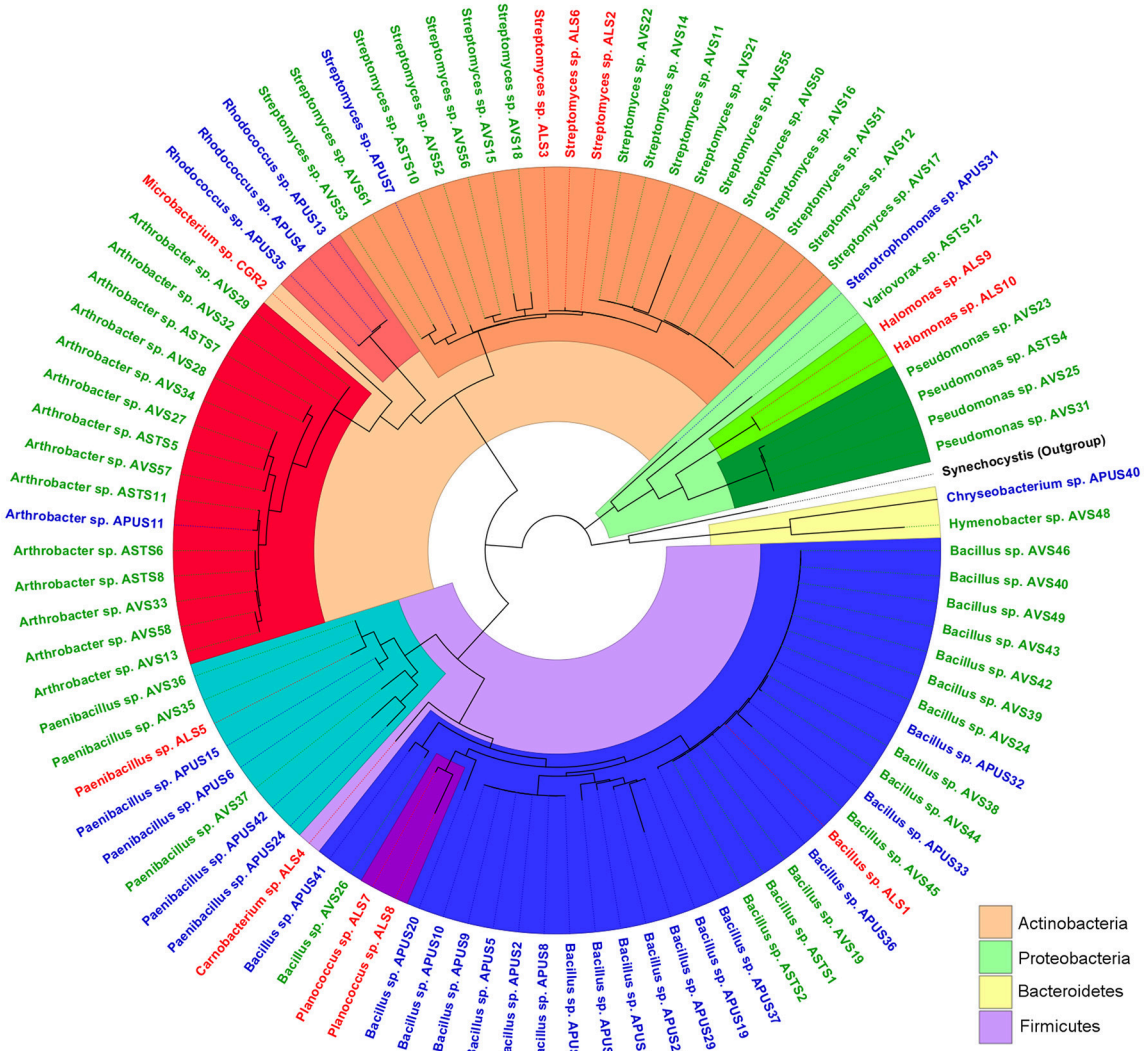


**FIGURE 1 |** Phylogenetic tree of the bacterial isolates recovered from the highlands of the Atacama Desert. Colors from the inner circle represent the phyla and genera of the bacterial isolates: Proteobacteria (green color range), Firmicutes (blue color range), Actinobacteria (orange color range), and Bacteroidetes (yellow); label color represents the isolation site: Lejía Lake (red), TLT1 (green), and TLT8 (blue). Synechocystis was used as outgroup and marked in black. The tree was constructed using the MEGA7 software and edited with the FigTree software.

each isolated species was determined using the Global Catalog of Microorganisms (gcm.wfcc.info). Out of the 43 potential species, 40 were obtained from soil, rhizosphere or plants. The other 3 species were isolated from scleromata (*Arthrobacter scleromae*), airborne (*Hymenobacter aerophilus*), and food (*Carnobacterium* sp.), indicating a potential new source of species isolation. However, the assigned species were not corroborated by DNA-DNA hybridization, GC content or fatty acid profile, meaning that we cannot reach a definitive species identity.

Nevertheless, most of the bacterial references were isolated from soil and had biotechnological potential capabilities reported in NCBI. An *in silico* exploration was carried out in NCBI, and the most common potential capabilities recovered were: Biomedical, Bioremediation, and Plant Growth Promotion (**Table 2**).

## Biochemical Characterization of Bacterial Isolates

We screened 12 of our isolates for PGP activities (**Supplementary Table 2**); 12 of them were positive to at least 1 of the conditions tested, making them potentially PGP bacteria. Among these 12 isolates, none of them showed all the essayed PGP activities, nine correspond to siderophore producers (*Planococcus* sp. ALS8, *Planococcus* sp. ALS7, *Streptomyces* sp. ALS6, *Microbacterium* sp. CGR2, *Bacillus* sp. ALS1, *Pseudomonas* sp. ASTS4, *Stenotrophomonas* sp. APUS31, *Paenibacillus* sp. APUS6, *Bacillus* sp. AVS49), two solubilized phosphate (*Microbacterium* sp. CGR2, *Bacillus* sp. ALS1), six were potential nitrogen fixers (*Bacillus* sp. APUS41, *Pseudomonas* sp. ASTS4, *Stenotrophomonas* sp. APUS31,

**TABLE 2 |** Isolates categorized by their genus assigned by 16S rRNA similarity index and isolated location.

| Genus | LLS* | TLT1† | TLT8† | Total |
|---|---|---|---|---|
| Arthrobacter | | 14 | 1 | 15 |
| Bacillus | 1 | 14 | 17 | 32 |
| Chryseobacterium | | | 1 | 1 |
| Hymenobacter | | 1 | | 1 |
| Paenibacillus | 1 | 3 | 4 | 8 |
| Pseudomonas | | 4 | | 4 |
| Rhodococcus | | | 3 | 3 |
| Stenotrophomonas | | | 1 | 1 |
| Streptomyces | 3 | 17 | 1 | 21 |
| Variovorax | | 1 | | 1 |
| Microbacterium | 1 | | | 1 |
| Carnobacterium | 1 | | | 1 |
| Planococcus | 2 | | | 2 |
| Halomonas | 2 | | | 2 |

*Lejía Lake Soil (Mandakovic et al., 2018a); †TLT, Talabre-Lejía Transect.*

**TABLE 3 |** Most prevalent biotechnological capabilities among the 93 isolates according to the literature.

| Genus | Biomedical | Plant growth promotion | Bioremediation |
|---|---|---|---|
| Arthrobacter | | 2 | |
| Bacillus | 3 | 8 | 6 |
| Halomonas | | | 1 |
| Microbacterium | 1 | 1 | 1 |
| Paenibacillus | 2 | 1 | 1 |
| Pseudomonas | | 1 | 1 |
| Rhodococcus | 2 | 1 | 1 |
| Stenotrophomonas | 1 | 1 | 1 |
| Streptomyces | 9 | 1 | 1 |
| Variovorax | | | 1 |

*Paenibacillus* sp. APUS6, *Bacillus* sp. AVS49, *Rhodococcus* sp. APUS4), four possessed ACC deaminase activity (*Streptomyces* sp. ALS6, *Bacillus* sp. APUS41, *Pseudomonas* sp. ASTS4, *Bacillus* sp. AVS49) and five were auxin producers (*Bacillus* sp. APUS41, *Pseudomonas* sp. ASTS4, *Paenibacillus* sp. APUS6, *Arthrobacter* sp. AVS27, *Bacillus* sp. AVS49). The strongest PGP potential was predicted in two isolates belonging to the genus *Pseudomonas* and *Bacillus*. PGP distribution across the different isolates revealed that the *Bacillus* sp. AVS49 and *Pseudomonas* sp. ASTS4 had the highest number of PGP potential activities, with four PGP potential traits, followed by and *Paenibacillus* sp. APUS6 with three different PGP potential traits.

## DISCUSSION

Current interest in terraforming Mars has led to a series of studies of the "Mars-like" Atacama Desert (Bull et al., 2018). Formerly presented as the "dry limit of microbial life" (Navarro-González et al., 2003), the desert soil was considered devoid of living organisms. Today, however, bacterial organisms from the Atacama Desert have gained interest from the scientific community for their ability to survive and thrive in this extreme environment, and the biotechnological potential they harbor (Connon et al., 2007; Escudero et al., 2007; Lester et al., 2007; Cabrol et al., 2009; Demergasso et al., 2010; Neilson et al., 2012; Crits-Christoph et al., 2013; Idris et al., 2017).

The environment studied displayed unique features within the Atacama Desert biotope. It is arid, but not hyper-arid, because of the high average MAP of all the sites studied, making it more diverse for microbial communities than other sites, like the hyper-arid core of the Atacama Desert (Neilson et al., 2017). Because of the higher MAP values it also displays the highest plant coverage in the altitude gradient of the Atacama Desert landscape (Díaz et al., 2016). Given the altitude, it displays lower MAT than the hyper-arid core, located at 2,500 m a.s.l (Crits-Christoph et al., 2013). These features make the studied landscape a cold arid highland with different environmental and biotic conditions than the rest of the Atacama Desert and, therefore, possibly harbor a different bacterial community.

Our first approach to describe the microbial communities of the Altiplano highlands was through NGS. From 7,829 OTUs obtained, 34.4% were assigned to a genus, but only 4.4% to species. Thus, 30% of the OTUs, identified to genus, did not match any species in the GreenGenes database. The fraction of OTUs identified to genus in this study was high compared to others. The low proportion of genera that could be identified to species could be proof of the novel genetic potential present in the Atacama Desert. Considering the large area of arid biotopes and its insufficient study, it is likely that a large part of unexplored microorganism biodiversity is still hidden in these soils.

There was discordance between the bacterial phyla found by NGS and culture. Thirty seven bacterial phyla were found by NGS, while the isolates belonged only to four phyla. Moreover, the phyla isolated did not reflect the most representative phyla found in NGS. The difference between phyla diversity of NGS and isolates has been previously reported, particularly in hot deserts. Chanal et al. (2006) studying the Tataouine Desert by 16S rRNA sequence, found an overrepresentation of Bacteroidetes and Firmicutes and an underrepresentation of Firmicutes and Actinobacteria compared to the isolates they found. Abdul-Majid et al. (2016), studying Sand Dunes from the Qatari Desert, reported the absence of Chloroflexi among isolates, while in NGS this phylum had 2% relative abundance. They suggested that special conditions would have been needed in order to isolate this metabolic specialist group. They also found an overrepresentation of Bacteroidetes and Proteobacteria with NGS, in contraposition to Actinobacteria, which were underrepresented in molecular identification as well as in our NGS. Dunbar et al. (1999), studying the isolates of the Southwestern Desert in the USA, did not find Acidobacteria among their isolates, while this phylum was the most predominant in their massive sequence analysis. This evidence indicates that there is a bias when isolating bacteria from arid soils. This may be due to the differential supply of nutritional requirements in the culture media and in the soil, the

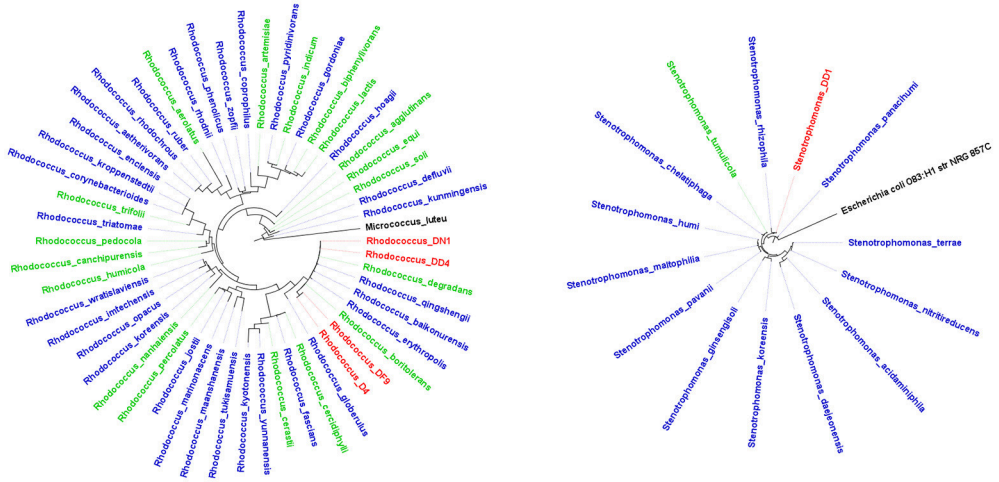


**FIGURE 2 |** Maximum-likelihood tree of some of the bacterial genera that exhibited the highest number of biotechnological features. **(A)** *Rhodococcus* and **(B)** *Stenotrophomonas*. Blue and green labels represent complete (available at NCBI) and incomplete (partial sequences available at NCBI) genomes, red labels represent isolates recovered in this study and black labels represent the outgroups.

removal of growth inhibitory components and/or the reduction of competitive interactions with members of the community, like competitive bacteria-bacteria interactions (Auld et al., 2013).

Different culture conditions also affected the bacterial diversity recovered. For example, in this study the *Arthrobacter* genus was mostly recovered under cold culture conditions, *Streptomyces* in hot culture conditions and the phylum Firmicutes was mostly recovered in media with low nutrient content. Other studies have focused on recovering rare taxa, e.g., optimizing media for isolating Acidobacteria, Actinobacteria, Proteobacteria, Verrucomicrobia, and the "Unculturable bacteria" (Janssen et al., 2002; Vartoukian et al., 2010; Campanharo et al., 2016). This information supports, in part, the discrepancy found between isolates and NGS.

As mentioned above, the Atacama Desert has been previously studied by several authors, but most studies have focused in the Yungay area, the hyper-arid core of the Atacama Desert (Connon et al., 2007; Lester et al., 2007; Navarro-Gonzalez et al., 2009; Neilson et al., 2012, 2017). Nevertheless, the Atacama Desert ranges from the Pacific Ocean to the highest areas of the Andes Mountain range, has several active volcanoes, arid to hyper-arid zones, etc.

The variety of these environmental conditions creates multiple niches for microorganism community development. Demergasso et al. (2010) studied physicochemical parameters and the microbial composition of water and sediment samples obtained from the saline Lejía Lake of the Atacama Desert. Remarkably, using NGS we were able to distinguish, in our merged set of OTUs all 6 bacterial phyla and 11 genera described by Demergasso and coworkers, together with 31 other mostly in low abundance. Similarly, Costello et al. (2009), studied the bacterial soil composition at Volcán Socompa (arid soil, 5,235 m a.s.l., pH 5.4), located 120 km to the South of Volcan Lascar and sharing similar environmental conditions. The predominant bacteria found belong to phyla Actinobacteria, Acidobacteria, Bacteroidetes, and Verrucomicrobia, with low abundance of Proteobacteria and Firmicutes. Except for the Proteobacteria, the other phyla show a similar pattern to the one found in our study. These bacterial community compositions reflect a pattern of microbial communities among Altiplano highland soils.

In the Yungay region, bacterial communities mostly exhibit a predominant abundance of Actinobacteria (between 70 and 94%), followed by Proteobacteria, Chloroflexi, Acidobacteria, and Firmicutes (Connon et al., 2007; Neilson et al., 2012; Crits-Christoph et al., 2013; Azua-Bustos et al., 2015). According to Maestre et al. (2015), Acidobacteria are inversely correlated with aridity, which explains higher abundance in our NGS OTUs than those reported in the hyper-arid core of the desert. Likewise, Neilson et al. (2017) state that Actinobacteria are mostly abundant in hyper-arid soils, which could explain the lower abundance of Actinobacteria found in the arid highlands. The bacterial community composition recovered in this study follows the trend portrayed in other studies of the Atacama Desert.

Fierer et al. (2012) stated that the microbial community profiles from desert environments were distinct from one another, but the differences observed between deserts were less than between desert and non-desert environments. Consequently, in order to compare the highlands of the Atacama Desert, we contrasted the diversity indexes (H' and Chao1) with other reports from arid environments. The most similar diversity index comes from Neilson et al. (2017), specifically in the highland sampling sites of the Atacama Desert. This result corroborates our methodology since the sampled environment was the same. Contrary to what could be expected, the second most similar diversity value, reported by McCann et al. (2016), comes from an Artic Desert in the Kongsfjorden region of Svalbard, Norway. Other articles about the Atacama Desert, including highlands (Demergasso et al., 2010) and hyper-arid

areas (Neilson et al., 2012; Crits-Christoph et al., 2013), were included in the comparison as well, but returned lower diversity indexes than the aforementioned. This unexpected result can be attributed to the comparable environmental physicochemical conditions described by McCann et al. (2016) and those described in this study, i.e., low MAT, near neutral pH, MAP around 100–200 mm per year, and presence of seasonal snowfall (**Supplementary Table 3**). These conditions make the highlands of the Atacama Desert more closely related to Arctic Deserts than other hot and cold deserts, corroborating its cold arid environmental conditions.

The high diversity values presented in this study compared to others from the Atacama Desert, could be explained by the methodology adopted by each group. More replicates and high-throughput strategies would increase the diversity indexes, making this study more similar to Neilson et al. (2017), than Demergasso et al. (2010). However, aridity has been described as inversely correlated with bacterial diversity (Maestre et al., 2015; Neilson et al., 2017). Considering the highlands of the Altiplano as an arid environment, it would be expected to be more closely related to other distant arid environments than to neighboring hyper-arid ones.

Comparing the bacterial community composition of the Atacama Desert to hot deserts, including southwestern USA deserts and Volcán Socompa (Costello et al., 2009; Fierer et al., 2012), and cold deserts, including Antarctic dry valleys and Polar deserts (**Supplementary Tables 4, 5**; Pointing et al., 2010; McCann et al., 2016), we observed higher similarities to the bacterial community recovered by McCann et al. (2016) in Kongsfjorden (Arctic circle). This observation can be attributed to the environmental similarities previously mentioned. These environmental drivers seem more relevant to microbial community composition than altitude or geographic location. The statement presented by Lourens Baas-Becking in 1934, "Everything is everywhere, but the environment selects" (O'Malley, 2008) might apply in this scenario, only in terms of phylum composition, but the genera and species are probably unique to each environment.

Some authors have reported different biotechnological capabilities found among isolates in the Atacama Desert. Within the phylum Actinobacteria, in the genus *Streptomyces*, some species are currently used in the pharmaceutical industry for their antibiotic, antitumoral and neurodegenerative protecting molecules (Okoro et al., 2009; Nachtigall et al., 2011; Rateb et al., 2011; Leirós et al., 2015; Idris et al., 2017). On the other hand, the genus *Acidithiobacillus*, has potential in the biomining industry, while the genera *Bacillus* and *Micrococcus* are good antibiotic producers (Azua-Bustos and González-Silva, 2014).

The biotechnological traits found *in silico* highlights the effect that these isolates could have in the agricultural industry, considering the amount of species that were associated with PGP capabilities and the number of isolates that were positive to the PGP experiments. However, given the dimension and different environmental conditions found along the Atacama Desert, these capabilities may arise mostly in the arid areas, considering the absence of plants in the hyper-arid sectors of this desert.

Studies about PGP have been developed in different environments, including other cold deserts. In the cold Leh Ladakh deserts (Yadav et al., 2015), most of the psychrotrophic bacterial isolates evaluated, exhibited positive results to PGP, including members of the Firmicutes, Proteobacteria, Actinobacteria, and Bacteroidetes phyla. Another study of PGP competences amongst isolates was carried out in the Sahara Desert (Cherif et al., 2015). Most of the isolates exhibited some degree of PGP capabilities, but the most relevant phylum was Firmicutes, specifically the *Bacillus* genus, a genus that has been reported to exhibit consistent and diverse PGP capacities (Cherif-Silini et al., 2016). The associations between culturable microorganisms from extreme environments and plant growth promoting potential supports our findings, in which all the isolates tested displayed PGP potential. This absolute proportion is higher than the ones found in other desert soil studies and is supported by the fact that there is higher plant coverage (%) around our sampling altitude (4,000 m a.s.l.; Díaz et al., 2016) than at other altitudes in the Atacama, accepting the hypothesis that the foundations for the adaptability to the harsh conditions of plant growth in arid lands are based on the co-evolution of the association between plant and microbes under harsh environmental conditions. The PGP potential of the strains used in this study requires further evaluation, but this precedent supports our pursuit to find bacterial isolates with new biotechnological attributes in this extreme environment.

The difference in PGP potential traits representation between siderophore release and auxin producers has been documented before by Marasco et al. (2012). They suggest that soil bacteria have higher nutrient supply capacities than endophytes which exhibit higher auxin production, suggesting an environmental-driven differentiation in PGP activities. This same report by Marasco et al. (2012) also reports higher PGP activities in non-cultivated soils than cultivated ones. Additionally, a study from Israel showed a significantly higher population of potentially PGP bacteria in the stressful sunny site than in the shadowed site (Timmusk et al., 2011), supporting our search in this arid—uncultivated environment.

For the first time in environmental microbiology research, we linked the Altiplano highlands from the Atacama Desert with cold arid soils from the Arctic desert. Based on their similarities in microbial community composition and physicochemical and environmental features, we added evidence to the hypothesis that environmental features determine the microbial community composition, rather than geography or altitude.

We sampled a substantial proportion of the strains (43 unique phylotypes according to the RDP database) in a highland soil microbial community and were able to detect a variety of taxonomic groups typical from arid soils, assessing their phylogenetic distribution and their culturability.

NGS had better depth and detection limit analyzing bacterial diversity, revealing the rare bacteria present in the community without the bias of disclosing only the most abundant microorganisms. We demonstrated that there is novel genetic potential in the soils sampled. Over 30% of the bacterial sequences of the total number of OTUs found in the community were phylogenetically unique.

These novel sequences may represent a previously unknown bacterial diversity that is endemic to this highly insular and harsh elevation ecosystem. This reinforces the need to recover isolates from extreme environments like the ones harbored in the Altiplano highlands microbiome of Chile.

Taxonomic comparisons between culturable microbiota and metabarcoding data showed overrepresentation and underrepresentation of different taxa that could grow in culture, revealing several candidates that may provide support for the biotechnological ability of soil bacterial species living in a stressful environment that is highly challenging for life.

## AUTHOR CONTRIBUTIONS

FM and JV-D wrote the manuscript. JM performed the bioinformatic analyses. FM performed the bacterial isolation. AG performed the PGP experiments. FM, JM, DM, MG, and VC designed and conceptualized the study.

## ACKNOWLEDGMENTS

This work was funded by FONDECYT N° 1151384, FONDECYT N° 1160802, FONDECYT N° 3170523, FONDAP N° 15090007, Center for Genome Regulation. JM was supported by CONICYT PhD fellowship N° 21120313. This research was partially supported by the supercomputing infrastructure of the NLHPC (ECM-02).

## SUPPLEMENTARY MATERIAL

The Supplementary Material for this article can be found online at: https://www.frontiersin.org/articles/10.3389/fbioe.2019.00010/full#supplementary-material

## REFERENCES

Abdul-Majid, S., Graw, M. F., Chatziefthimiou, A. D., Nguyen, H., Richer, R., Louge, M., et al. (2016). Microbial characterization of Qatari Barchans and Dunes. *PLoS ONE* 11, 1–22. doi: 10.1371/journal.pone.0161836

Ahmad, F., Ahmad, I., and Khan, M. S. (2008). Screening of free-living rhizospheric bacteria for their multiple plant growth promoting activities. *Microbiol. Res.* 163, 173–181. doi: 10.1016/j.micres.2006.04.001

Auld, R. R., Myre, M., Mykytczuk, N. C., Leduc, L. G., and Merritt, T. J. (2013). Characterization of the microbial acid mine drainage microbial community using culturing and direct sequencing techniques. *J. Microbiol. Methods* 93, 108–115. doi: 10.1016/j.mimet.2013.01.023

Azua-Bustos, A., Caro-Lara, L., and Vicuña, R. (2015). Discovery and microbial content of the driest site of the hyperarid Atacama Desert, Chile. *Environ. Microbiol. Rep.* 7, 388–394. doi: 10.1111/1758-2229.12261

Azua-Bustos, A., and González-Silva, C. (2014). Biotechnological applications derived from microorganisms of the atacama desert. *Biomed Res. Int.* 2014:909312. doi: 10.1155/2014/909312

Azua-Bustos, A., Urrejola, C., and Vicuña, R. (2012). Life at the dry edge: microorganisms of the Atacama Desert. *FEBS Lett.* 586, 2939–2945. doi: 10.1016/j.febslet.2012.07.025

Bailey, V. L., Fansler, S. J., Stegen, J. C., and McCue, L. A. (2013). Linking microbial community structure to β-glucosidic function in soil aggregates. *ISME J.* 7, 2044–2053. doi: 10.1038/ismej.2013.87

Bull, A. T., Andrews, B. A., Dorador, C., and Goodfellow, M. (2018). Introducing the Atacama Desert. *Antonie Van Leeuwenhoek* 111, 1269–1272. doi: 10.1007/s10482-018-1100-2

Bull, A. T., and Asenjo, J. A. (2013). Microbiology of hyper-arid environments: recent insights from the Atacama Desert, Chile. *Antonie van Leeuwenhoek, Int. J. Gen. Mol. Microbiol.* 103, 1173–1179. doi: 10.1007/s10482-013-9911-7

Bull, A. T., Asenjo, J. A., Goodfellow, M., and Gómez-Silva, B. (2016). The Atacama Desert: technical resources and the growing importance of novel microbial diversity. *Annu. Rev. Microbiol.* 70, 215–234. doi: 10.1146/annurev-micro-102215-095236

Cabrol, N. A., Grin, E. A., Chong, G., Minkley, E., Hock, A. N., Yu, Y., et al. (2009). The high-lakes project. *J. Geophys. Res. Biogeosci.* 114, 1–20. doi: 10.1029/2008JG000818

Campanharo, J. C., Kielak, A. M., Castellane, T. C. L., Kuramae, E. E., and Lemos, E. G., de M. (2016). Optimized medium culture for Acidobacteria subdivision 1 strains. *FEMS Microbiol. Lett.* 363, 1–7. doi: 10.1093/femsle/fnw245

Caporaso, J. G., Kuczynski, J., Stombaugh, J., Bittinger, K., Bushman, F. D., Costello, E. K., et al. (2010). correspondence QIIME allows analysis of high- throughput community sequencing data Intensity normalization improves color calling in SOLiD sequencing. *Nat. Publ. Gr.* 7, 335–336. doi: 10.1038/nmeth0510-335

Chanal, A., Chapon, V., Benzerara, K., Barakat, M., Christen, R., Achouak, W., et al. (2006). The desert of Tataouine: an extreme environment that hosts a wide diversity of microorganisms and radiotolerant bacteria. *Environ. Microbiol.* 8, 514–525. doi: 10.1111/j.1462-2920.2005.00921.x

Cherif, H., Marasco, R., Rolli, E., Ferjani, R., Fusi, M., Soussi, A., et al. (2015). Oasis desert farming selects environment-specific date palm root endophytic communities and cultivable bacteria that promote resistance to drought. *Environ. Microbiol. Rep.* 7, 668–678. doi: 10.1111/1758-2229.12304

Cherif-Silini, H., Silini, A., Yahiaoui, B., Ouzari, I., and Boudabous, A. (2016). Phylogenetic and plant-growth-promoting characteristics of *Bacillus* isolated from the wheat rhizosphere. *Ann. Microbiol.* 66, 1087–1097. doi: 10.1007/s13213-016-1194-6

Cole, J. R., Wang, Q., Fish, J. A., Chai, B., McGarrell, D. M., Sun, Y., et al. (2014). Ribosomal database project: data and tools for high throughput rRNA analysis. *Nucleic Acids Res.* 42, 633–642. doi: 10.1093/nar/gkt1244

Connon, S. A., Lester, E. D., Shafaat, H. S., Obenhuber, D. C., and Ponce, A. (2007). Bacterial diversity in hyperarid atacama desert soils. *J. Geophys. Res. Biogeosci.* 112, 1–9. doi: 10.1029/2006JG000311

Cordero, R. R., Seckmeyer, G., Damiani, A., Riechelmann, S., Rayas, J., Labbe, F., et al. (2014). The world's highest levels of surface UV. *Photochem. Photobiol. Sci.* 13, 70–81. doi: 10.1039/c3pp50221j

Costello, E. K., Halloy, S. R., Reed, S. C., Sowell, P., and Schmidt, S. K. (2009). Fumarole-supported islands of biodiversity within a hyperarid, high-elevation landscape on socompa volcano, puna de atacama, andes. *Appl. Environ. Microbiol.* 75, 735–747. doi: 10.1128/AEM.01469-08

Crits-Christoph, A., Robinson, C. K., Barnum, T., Fricke, W. F., Davila, A. F., Jedynak, B., et al. (2013). Colonization patterns of soil microbial communities in the Atacama Desert. *Microbiome* 1:28. doi: 10.1186/2049-2618-1-28

Demergasso, C., Dorador, C., Meneses, D., Blamey, J., Cabrol, N., Escudero, L., et al. (2010). Prokaryotic diversity pattern in high-altitude ecosystems of the Chilean Altiplano. *J. Geophys. Res. Biogeosci.* 115, 1–14. doi: 10.1029/2008JG000836

Díaz, F. P., Frugone, M., Gutiérrez, R. A., and Latorre, C. (2016). Nitrogen cycling in an extreme hyperarid environment inferred from δ15N analyses of plants, soils and herbivore diet. *Sci. Rep.* 6, 1–11. doi: 10.1038/srep22226

Dowd, S. E., Callaway, T. R., Wolcott, R. D., Sun, Y., McKeehan, T., Hagevoort, R. G., et al. (2008). Evaluation of the bacterial diversity in the feces of cattle using 16S rDNA bacterial tag-encoded FLX amplicon pyrosequencing (bTEFAP). *BMC Microbiol.* 8, 1–8. doi: 10.1186/1471-2180-8-125

Dunbar, J., Takala, S., Barns, S. M., Jody, A., Kuske, C. R., and Davis, J. A. (1999). Levels of bacterial community diversity in four arid soils compared by cultivation and 16S rRNA gene cloning levels of bacterial community diversity

in four arid soils compared by cultivation and 16S rRNA gene cloning. *Appl. Environ. Micobiol.* 65, 1662–1669.

Edgar, R. C. (2010). Search and clustering orders of magnitude faster than BLAST. *Bioinformatics* 26, 2460–2461. doi: 10.1093/bioinformatics/btq461

Edgar, R. C., Haas, B. J., Clemente, J. C., Quince, C., and Knight, R. (2011). UCHIME improves sensitivity and speed of chimera detection. *Bioinformatics* 27, 2194–2200. doi: 10.1093/bioinformatics/btr381

Eilers, K. G., Debenport, S., Anderson, S., and Fierer, N. (2012). Soil biology & biochemistry digging deeper to fi nd unique microbial communities : the strong effect of depth on the structure of bacterial and archaeal communities in soil. *Soil Biol. Biochem.* 50, 58–65. doi: 10.1016/j.soilbio.2012.03.011

Escudero, L., Chong, G., Demergasso, C., Farías, M. E., Cabrol, N. A., Grin, E., et al. (2007). "Investigating microbial diversity and UV radiation impact at the high-altitude lake Aguas Calientes, Chile," in *Proceedings SPIE 6694 Conference on Instruments, Methods, and Missions for Astrobiology* (San Diego, CA), 1–12.

Ferrero, M. A., Menoyo, E., Lugo, M. A., Negritto, M. A., Farías, M. E., Anton, A. M., et al. (2010). Molecular characterization and *in situ* detection of bacterial communities associated with rhizosphere soil of high altitude native Poaceae from the Andean Puna region. *J. Arid Environ.* 74, 1177–1185. doi: 10.1016/j.jaridenv.2010.04.008

Fierer, N. (2017). Embracing the unknown: disentangling the complexities of the soil microbiome. *Nat. Rev. Microbiol.* 15, 579–590. doi: 10.1038/nrmicro.2017.87

Fierer, N., Leff, J. W., Adams, B. J., Nielsen, U. N., Bates, S. T., Lauber, C. L., et al. (2012). Cross-biome metagenomic analyses of soil microbial communities and their functional attributes. *Proc. Natl. Acad. Sci.U.S.A.* 109, 21390–21395. doi: 10.1073/pnas.1215210110

Gómez-Silva, B., Rainey, F. A., Warren-Rhodes, K. A., McKay, C. P., and Navarro-González, R. (2008). "Atacama Desert Soil Microbiology," in *Soil Biology*, eds P. Dion and C. Shekhar-Nautiyal (Berlin; Heidelberg: Springer), 117–138.

Goodfellow, M., Busarakam, K., Idris, H., Labeda, D. P., Nouioui, I., Brown, R., et al. (2017). Streptomyces asenjonii sp. nov., isolated from hyper-arid Atacama Desert soils and emended description of Streptomyces viridosporus Pridham et al. 1958. *Antonie van Leeuwenhoek, Int. J. Gen. Mol. Microbiol.* 110, 1133–1148. doi: 10.1007/s10482-017-0886-7

Grobelak, A., Napora, A., and Kacprzak, M. (2015). Using plant growth-promoting rhizobacteria (PGPR) to improve plant growth. *Ecol. Eng.* 84, 22–28. doi: 10.1016/j.ecoleng.2015.07.019

Handl, S., Dowd, S. E., Garcia-Mazcorro, J. F., Steiner, J. M., and Suchodolski, J. S. (2011). Massive parallel 16S rRNA gene pyrosequencing reveals highly diverse fecal bacterial and fungal communities in healthy dogs and cats. *FEMS Microbiol. Ecol.* 76, 301–310. doi: 10.1111/j.1574-6941.2011.01058.x

Idris, H., Goodfellow, M., Sanderson, R., Asenjo, J. A., and Bull, A. T. (2017). Actinobacterial rare biospheres and dark matter revealed in habitats of the chilean atacama desert. *Sci. Rep.* 7, 1–11. doi: 10.1038/s41598-017-08937-4

Janssen, P. H., Yates, P. S., Grinton, B. E., Taylor, P. M., Sait, M., Janssen, P. H., et al. (2002). Improved culturability of soil bacteria and isolation in pure culture of novel members of the divisions acidobacteria, actinobacteria, proteobacteria, and verrucomicrobia improved culturability of soil bacteria and isolation in pure culture of novel Me. *Appl. Environ. Micobiol.* 68, 2391–2396. doi: 10.1128/AEM.68.5.2391

Jorquera, M. A., Maruyama, F., Ogram, A. V., Navarrete, O. U., Lagos, L. M., Inostroza, N. G., et al. (2016). Rhizobacterial community structures associated with native plants grown in chilean extreme environments. *Microb. Ecol.* 72, 633–646. doi: 10.1007/s00248-016-0813-x

Leirós, M., Alonso, E., Rateb, M. E., Ebel, R., Jaspars, M., Alfonso, A., et al. (2015). The Streptomyces metabolite anhydroexfoliamycin ameliorates hallmarks of Alzheimer's disease *in vitro* and *in vivo*. *Neuroscience* 305, 26–35. doi: 10.1016/j.neuroscience.2015.07.082

Lester, E. D., Satomi, M., and Ponce, A. (2007). Microflora of extreme arid Atacama Desert soils. *Soil Biol. Biochem.* 39, 704–708. doi: 10.1016/j.soilbio.2006.09.020

Lugo, M. A., Ferrero, M., Menoyo, E., Estévez, M. C., Siñeriz, F., and Anton, A. (2008). Arbuscular mycorrhizal fungi and rhizospheric bacteria diversity along an altitudinal gradient in south American Puna grassland. *Microb. Ecol.* 55, 705–713. doi: 10.1007/s00248-007-9313-3

Maestre, F. T., Delgado-Baquerizo, M., Jeffries, T. C., Eldridge, D. J., Ochoa, V., Gozalo, B., et al. (2015). Increasing aridity reduces soil microbial diversity and abundance in global drylands. *Proc. Natl. Acad. Sci. U.S.A.* 112:201516684. doi: 10.1073/pnas.1516684112

Mandakovic, D., Maldonado, J., Pulgar, R., Cabrera, P., Gaete, A., Urtuvia, V., et al. (2018a). Microbiome analysis and bacterial isolation from Lejía Lake soil in Atacama Desert. *Extremophiles* 22, 665–673. doi: 10.1007/s00792-018-1027-6

Mandakovic, D., Rojas, C., Maldonado, J., Latorre, M., Travisany, D., Delage, E., et al. (2018b). Structure and co-occurrence patterns in microbial communities under acute environmental stress reveal ecological factors fostering resilience. *Sci. Rep.* 8, 1–12. doi: 10.1038/s41598-018-23931-0

Marasco, R., Rolli, E., Ettoumi, B., Vigani, G., Mapelli, F., Borin, S., et al. (2012). A drought resistance-promoting microbiome is selected by root system under desert farming. *PLoS ONE* 7:e48479. doi: 10.1371/journal.pone.0048479

McCann, C. M., Wade, M. J., Gray, N. D., Roberts, J. A., Hubert, C. R., and Graham, D. W. (2016). Microbial communities in a high arctic polar desert landscape. *Front. Microbiol.* 7, 1–10. doi: 10.3389/fmicb.2016.00419

McKay, C. P., Friedmann, E. I., Gómez-Silva, B., Cáceres-Villanueva, L., Andersen, D. T., and Landheim, R. (2003). Temperature and moisture conditions for life in the extreme arid region of the atacama desert: Four Years of Observations Including the El Niño of 1997–1998. *Astrobiology* 3, 393–406. doi: 10.1089/153110703769016460

Menoyo, E., Lugo, M. A., Teste, F. P., and Ferrero, M. A. (2017). Grass dominance drives rhizospheric bacterial communities in a desertic shrub and grassy steppe highland. *Pedobiologia* 62, 36–40. doi: 10.1016/j.pedobi.2017.04.004

Mohite, B. (2013). Isolation and characterization of indole acetic acid (IAA) producing bacteria from rhizospheric soil and its effect on plant growth. *J. soil Sci. plant Nutr.* 13, 638–649. doi: 10.4067/S0718-95162013005000051

Nachtigall, J., Kulik, A., Helaly, S., Bull, A. T., Goodfellow, M., Asenjo, J. A., et al. (2011). Atacamycins A-C, 22-membered antitumor macrolactones produced by Streptomyces sp. C38. *J. Antibiot.* 64, 775–780. doi: 10.1038/ja.2011.96

Navarro-Gonzalez, R., Iniguez, E., de la Rosa, J., and McKay, C. P., (2009). Characterization of organics, microorganisms, desert soils, and mars-like soils by thermal volatilization coupled to mass spectrometry and their implications for the search for organics on mars by phoenix and future space missions. *Astrobiology* 9, 703–715. doi: 10.1089/ast.2008.0284

Navarro-González, R., Rainey, F. A., Molina, P., Bagaley, D. R., Hollen, B. J., de la Rosa, J., et al. (2003). Mars-like soils in the Atacama Desert, Chile, and the dry limit of microbial life. *Science* 302, 1018–1021. doi: 10.1126/science.1089143

Neilson, J. W., Califf, K., Cardona, C., Copeland, A., van Treuren, W., Josephson, K. L., et al. (2017). Significant Impacts of Increasing Aridity on the Arid Soil Microbiome. *mSystems* 2, e00195–e00116. doi: 10.1128/mSystems.00195-16

Neilson, J. W., Quade, J., Ortiz, M., Nelson, W. M., Legatzki, A., Tian, F., et al. (2012). Life at the hyperarid margin: novel bacterial diversity in arid soils of the Atacama Desert, Chile. *Extremophiles* 16, 553–566. doi: 10.1007/s00792-012-0454-z

Okoro, C. K., Brown, R., Jones, A. L., Andrews, B. A., Asenjo, J. A., Goodfellow, M., et al. (2009). Diversity of culturable actinomycetes in hyper-arid soils of the Atacama Desert, Chile. *Antonie van Leeuwenhoek, Int. J. Gen. Mol. Microbiol.* 95, 121–133. doi: 10.1007/s10482-008-9295-2

O'Malley, M. A. (2008). Everything is everywhere: but the environment selects: ubiquitous distribution and ecological determinism in microbial biogeography. *Stud. Hist. Philos. Sci. Part C Stud. Hist. Philos. Biol. Biomed. Sci.* 39, 314–325. doi: 10.1016/j.shpsc.2008.06.005

Penrose, D. M., and Glick, B. R. (2003). Methods for isolating and characterizing ACC deaminase-containing plant growth-promoting rhizobacteria. *Physiol. Plant.* 118, 10–15. doi: 10.1034/j.1399-3054.2003.00086.x

Philippot, L., Raaijmakers, J. M., Lemanceau, P., and van der Putten, W. H. (2013). Going back to the roots: the microbial ecology of the rhizosphere. *Nat. Rev. Microbiol.* 11, 789–799. doi: 10.1038/nrmicro3109

Piacentini, R. D., Cede, A., and Bárcena, H. (2003). Extreme solar total and UV irradiances due to cloud effect measured near the summer solstice at the high-altitude desertic plateau Puna of Atacama (Argentina). *J. Atmos. Solar-Terrestrial Phys.* 65, 727–731. doi: 10.1016/S1364-6826(03)00084-1

Pointing, S. B., Chan, Y., Lacap, D. C., Lau, M. C. Y., Jurgens, J. A., and Farrell, R. L. (2010). Highly specialized microbial diversity in hyper-arid polar desert. *Proc. Natl. Acad. Sci. U.S.A.* 107, 1254–1254. doi: 10.1073/pnas.0913882107

Quast, C., Pruesse, E., Yilmaz, P., Gerken, J., Schweer, T., Yarza, P., et al. (2012). The SILVA ribosomal RNA gene database project: improved data processing

and web-based tools. *Nucleic Acids Res.* 41, D590–D596. doi: 10.1093/nar/gks1219

Rateb, M. E., Houssen, W. E., Harrison, W. T., Deng, H., Okoro, C. K., Asenjo, J. A., et al. (2011). Diverse metabolic profiles of a Streptomyces strain isolated from a hyper-arid environment. *J. Nat. Prod.* 74, 1965–1971. doi: 10.1021/np200470u

Risacher, F., Alonso, H., and Salazar, C. (1999). *Geoquímica de Aguas En Cuencas Cerradas I,II y III Regiones - Chile*. Tech Rep SIT 51, Conv de Coop DGA-UCN-IRD, Santiago.

Schloss, P. D., Westcott, S. L., Ryabin, T., Hall, J. R., Hartmann, M., Hollister, E. B., et al. (2009). Introducing mothur: open-source, platform-independent, community-supported software for describing and comparing microbial communities. *Appl. Environ. Microbiol.* 75, 7537–7541. doi: 10.1128/AEM.01541-09

Schulz, D., Beese, P., Ohlendorf, B., Erhard, A., Zinecker, H., Dorador, C., et al. (2011). Abenquines A-D: Aminoquinone derivatives produced by Streptomyces sp. strain DB634. *J. Antibiot.* 64, 763–768. doi: 10.1038/ja.2011.87

Schwyn, B., and Neilands, J. B. (1987). Universal chemical assay for the detection and determination of siderophore. *Anal. Biochem.* 160, 47–56.

Tarlachkov, S. V., and Starodumova, I. P. (2017). TaxonDC : calcularing the similarity value of the 16S rRNA gene sequences of prokaryotes or ITS regions of fungi. *J. Bioinforma. Genomics* 3, 3–5. doi: 10.18454/jbg.2017.3.5.1

Tassi, F., Aguilera, F., Vaselli, O., Medina, E., Tedesco, D., Delgado Huertas, A., et al. (2009). The magmatic- and hydrothermal-dominated fumarolic system at the Active Crater of Lascar volcano, northern Chile. *Bull. Volcanol.* 71, 171–183. doi: 10.1007/s00445-008-0216-z

Timmusk, S., Paalme, V., Pavlicek, T., Bergquist, J., Vangala, A., Danilas, T., et al. (2011). Bacterial distribution in the rhizosphere of wild barley under contrasting microclimates. *PLoS ONE* 6:e17968. doi: 10.1371/journal.pone.0017968

Torsvik, V., and Øvreås, L. (2002). Microbial diversity and function in soil: from genes to ecosystems. *Curr. Opin. Microbiol.* 5, 240–245. doi: 10.1016/S1369-5274(02)00324-7

Tse, C., and Ma, K. (2016). "Growth and Metabolism of Extremophilic Microorganisms," in *Biotechnology of Extremophiles*, ed. P. H. Rampelotto (Cham: Springer), 1–47.

Vartoukian, S. R., Palmer, R. M., and Wade, W. G. (2010). Strategies for culture of "unculturable" bacteria. *FEMS Microbiol. Lett.* 309, 1–7. doi: 10.1111/j.1574-6968.2010.02000.x

Yadav, A. N., Sachan, S. G., Verma, P., Tyagi, S. P., Kaushik, R., and Saxena, A. K. (2015). Culturable diversity and functional annotation of psychrotrophic bacteria from cold desert of Leh Ladakh (India). *World J. Microbiol. Biotechnol.* 31, 95–108. doi: 10.1007/s11274-014-1768-z

Zhou, J., Bruns, M. A., and Tiedje, J. M. (1996). DNA recovery from soils of diverse composition. *Appl. Environ. Microbiol.* 62, 316–322.

**Conflict of Interest Statement:** The authors declare that the research was conducted in the absence of any commercial or financial relationships that could be construed as a potential conflict of interest.

frontiers in Bioengineering and Biotechnology

ORIGINAL RESEARCH
published: 05 February 2019
doi: 10.3389/fbioe.2019.00012

# Airborne Microbial Communities at High-Altitude and Suburban Sites in Toyama, Japan Suggest a New Perspective for Bioprospecting

*Daisuke Tanaka*[1]*, *Kei Sato*[1], *Motoshi Goto*[1], *So Fujiyoshi*[2,3], *Fumito Maruyama*[3,4], *Shunsuke Takato*[1], *Takamune Shimada*[1], *Akihiro Sakatoku*[1], *Kazuma Aoki*[1] and *Shogo Nakamura*[1]

[1] Graduate School of Science and Engineering, University of Toyama, Toyama, Japan, [2] Graduate School of Human and Environmental Studies, Kyoto University, Kyoto, Japan, [3] JST/JICA, Science and Technology Research Partnership for Sustainable Development Program, Tokyo, Japan, [4] Department of Microbiology, Graduate School of Medicine, Kyoto University, Kyoto, Japan

OPEN ACCESS

**Edited by:**
*Thomas Bartholomäus Brück, Technische Universität München, Germany*

**Reviewed by:**
*David Anthony Pearce, Northumbria University, United Kingdom*
*Ashok K. Dubey, Netaji Subhas Institute of Technology, India*

***Correspondence:**
*Daisuke Tanaka*
*tanakada@sci.u-toyama.ac.jp*

**Specialty section:**
*This article was submitted to Bioprocess Engineering, a section of the journal Frontiers in Bioengineering and Biotechnology*

**Received:** *15 October 2018*
**Accepted:** *17 January 2019*
**Published:** *05 February 2019*

**Citation:**
*Tanaka D, Sato K, Goto M, Fujiyoshi S, Maruyama F, Takato S, Shimada T, Sakatoku A, Aoki K and Nakamura S (2019) Airborne Microbial Communities at High-Altitude and Suburban Sites in Toyama, Japan Suggest a New Perspective for Bioprospecting. Front. Bioeng. Biotechnol. 7:12. doi: 10.3389/fbioe.2019.00012*

Airborne microorganisms, especially those at high altitude, are exposed to hostile conditions, including ultraviolet (UV) radiation, desiccation, and low temperatures. This study was conducted to compare the composition and abundance of airborne microorganisms at a high-altitude site, Mt. Jodo [2,839 m above mean sea level (AMSL)] and a suburban site (23 m AMSL) in Toyama, Japan. To our knowledge, this is the first study to investigate microbial communities in air samples collected simultaneously at two sites in relatively close proximity, from low and high altitude. Air samples were collected over a period of 3 years during 2009–2011. We then examined the bacterial and eukaryotic communities and estimated the abundance of bacteria and fungi with real-time TaqMan PCR. The airborne bacterial and eukaryotic communities differed between high-altitude and suburban sites on each sampling day. Backward trajectory analysis of air masses that arrived at high-altitude and suburban sites on each sampling day displayed almost the same paths. The bacterial communities were dominated by Actinobacteria, Firmicutes, and Proteobacteria, while the eukaryotic communities included Ascomycota, Basidiomycota, and Streptophyta. We also predicted some application of such microbial communities. The airborne bacterial and fungal abundance at the high-altitude site was about two times lower than that at the suburban site. These results showed that each airborne microbial communities have locality even if they are collected close location.

**Keywords: atmosphere, bacteria, eukaryote, community, bioaerosol, bioprospecting**

## INTRODUCTION

Airborne microbes are ubiquitous in the atmosphere, being present at a density of $10^3$–$10^6$ cells per cubic meter of air. These microbes are emitted from terrestrial, soil, forest, desert, agricultural, and composting activities as well as urban, wetland, coastal, and marine environments (Jaenicke, 2005; Gandolfi et al., 2013). These organisms are exposed to hostile conditions, including scarcity of nutrients, UV radiation, desiccation, temperature and pH shifts, and the presence of reactive oxygen species. Physical and chemical characteristics of aerosols in the atmospheric boundary layer

(ABL; from surface to about 1–2 km high) are distinct from those in the free troposphere just above the ABL. Airborne microbes play an important role in agriculture, the biosphere, cloud formation, global climate, and atmospheric dynamics (Jaenicke, 2005; Brodie et al., 2007; Després et al., 2007; Christner et al., 2008; Burrows et al., 2009). Moreover, these microbes provide a medium for the spread of diseases (Bowers et al., 2012; Cao et al., 2014; Fujiyoshi et al., 2017).

Studies of airborne bacteria at high altitudes conducted to date have mainly focused on bacterial ice nucleation activity (Matthias-Maser et al., 2000; Marinoni et al., 2004; Bowers et al., 2009; Vaïtilingom et al., 2012; Xu et al., 2017; Tandon et al., 2018). Bowers et al. (2012) presented the seasonal variability of airborne bacterial communities sampled from a pristine high-elevation atmospheric research site at Mt. Werner (3,220 m above sea level), CO, USA. DeLeon-Rodriguez et al. (2013) reported 17 bacterial taxa in the middle to upper troposphere across the United States, including taxa known to use C1–C4 carbon compounds present in the atmosphere. Recently, some studies have characterized airborne fungi occurring at high-altitude sites, focusing on those that are pathogens for humans and plants (Kumar and Attri, 2016; Pusz et al., 2017; Xu et al., 2017).

Here, we describe the bacterial and eukaryotic communities in air samples collected simultaneously from high-altitude and suburban sites in Toyama, central Japan, at five time points from September 2009 to September 2011 during late summer to early autumn. We previously reported seasonal variations in airborne bacterial community over a 1-year period at a suburban site in Toyama based on PCR-DGGE (Tanaka et al., 2015). In this study, we analyzed 16S and 18S rRNA gene hypervariable regions to characterize airborne microbial communities. Furthermore, quantitative PCR was used to estimate the total number of airborne bacteria and fungi in each sample. Finally, we discussed the potential for use of airborne microorganisms as a source for bioprospecting.

## MATERIALS AND METHODS

### Air Samples

Air samples were collected at five time points from 2009 to 2011 on August or September at two different sites in Toyama Prefecture, Japan. Toyama prefecture is surrounded by steep mountains on three sides and spreading fields. The size of the prefecture is 4,248 $km^2$ (90 km east-west, 76 km north-south). The Toyama sampling sites include a suburban site on the roof of the three-story building of the Faculty of Science, University of Toyama (36°41′54″N, 137°11′13″E, 23 m above mean sea level, AMSL) and a high-altitude site at the peak of Mt. Jodo (36°34′00″N, 137°36′21″E, 2,839 m AMSL) (**Figure 1**). The two sites are located ∼40 km apart from one another. Prior to the test, we evaluated the filtration efficiency using 0.2 or 0.4 μm pore size polycarbonate filters. Then, we decided to use 0.4 μm pore size filters. Similar pore size filter (pore size 0.45 μm) was also used in air sampling according to the procedure of Kobayashi et al. (2016). Air samples were collected by a vacuum pump using 47 mm diameter, 0.4 μm pore size polycarbonate filters (Advantec, Tokyo, Japan) at a flow rate of 5 L $min^{-1}$ over 3 h (mostly 10:00–13:00). A total volume of 900 L of air was collected. All samples were collected when there was no precipitation. After sampling, the filters were stored at −20°C until DNA extraction. The duration of each sampling period and the corresponding weather conditions are presented in **Table 1**.

### DNA Extraction and Illumina MiSeq Sequencing

The filtered samples were processed using an UltraClean Soil DNA isolation kit (MO BIO Laboratories, Carlsbad, CA, USA) according to the manufacturer's instructions. This kit uses a vigorous bead-beating method to effectively disrupt bacterial and fungal cells (Peccia and Hernandez, 2006). The purity and concentration of the extracted DNA was measured using a NanoDrop ND-1000 spectrophotometer (Nanodrop Technologies, Wilmington, DE, USA).

Subsequently, the V3–V4 region of the bacterial 16S rRNA gene was amplified using the 341F (5′-CCTACGGGNGGC WGCAG-3′) and 805R (5′-GACTACHVGGGTATCTAATCC-3′) primers (Klindworth et al., 2013). The V8 region of the eukaryotic 18S rRNA gene was amplified using the 1422–1440f (5′-ATAACAGGTCTGTGATGCC-3′) and 1624–1642r (5′-CGG GCGGTGTGTACAAAGG-3′) primers (Wang et al., 2014). For amplification of the 16S and 18S rRNA genes, samples were subjected to initial denaturation at 94°C for 2 min, followed by 35 cycles of denaturation at 94°C for 30 s, annealing at 55°C for 30 s, and extension at 72°C for 30 s, and then final extension at 72°C for 5 min (Klindworth et al., 2013). The amplified products were purified using Agencourt AMPure XP (Beckman Coulter, Brea, CA, USA) then, DNA quantification was conducted using Synergy H1 (Bio Tek, Tokyo, Japan) and a QuantiFluor dsDNA System (Promega, Madison, WI, USA). Purified amplicons were pooled in equimolar concentrations, then paired-end sequenced on an Illumina MiSeq instrument (Illumina, San Diego, CA, USA). The obtained sequence data were then processed using USEARCH version 10.0.240 and analyzed with the software package Quantitative Insights into Microbial Ecology (QIIME) version 1.9.1 (Caporaso et al., 2010). Sequences were clustered into operational taxonomic units (OTUs) using the Greengenes 13_8 reference OTU database (97% similarity). For 16S rRNA gene fragment analysis, chloroplast and mitochondrial OTUs were removed. Statistical analysis was conducted using the R software, version 3.2.0 (www.r-project.org). All sequences have been deposited in the DNA Data Bank of Japan (DDBJ) under the accession number DRA007352.

### Real-Time TaqMan PCR

Quantification of the bacterial 16S rRNA gene and fungal 18S rRNA gene was accomplished using real-time PCR. Bacterial DNA was quantified using the primers 1055f and 1392r and the TaqMan probe 16Staq1115 (Harms et al., 2003). Fungal DNA quantification was conducted using the primers FungiQuant-F and FungiQuant-R and the TaqMan probe FungiQuant-Prb (Liu et al., 2012). For fungi, universal fungal primers, and TaqMan probes covered the 1,199–1,549 *S. cerevisiae* numbering region of the 18S rRNA-encoding gene. Each reaction mixture was prepared in a total volume of 25 μL with 12.5 μL Premix Ex

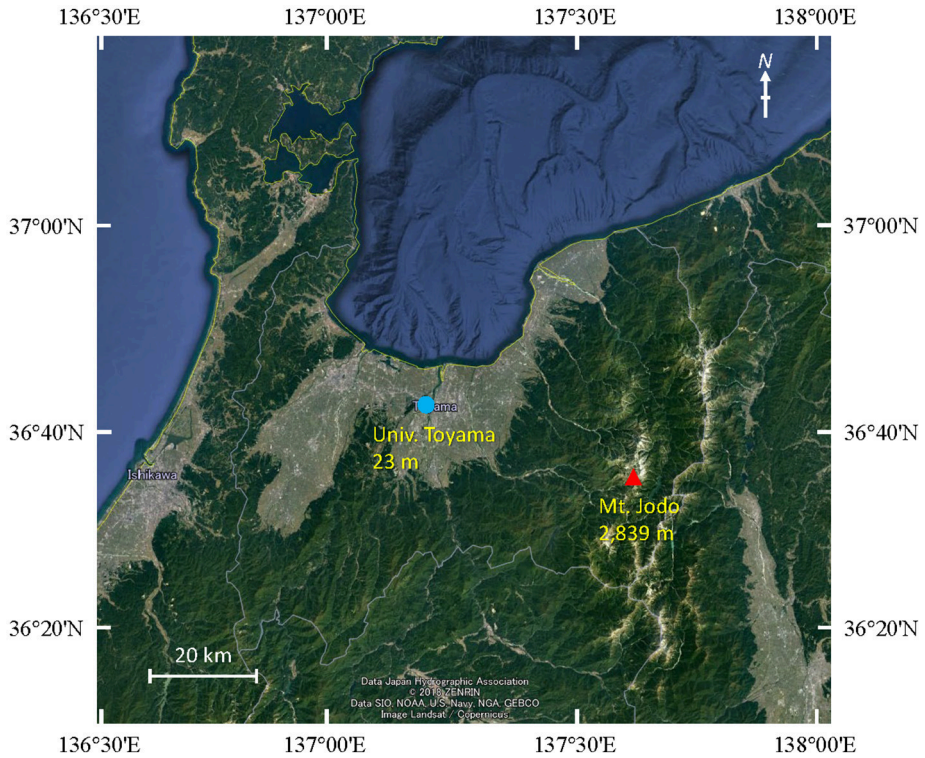


**FIGURE 1 |** Map showing the sampling locations at Mt. Jodo (high-altitude) and Univ. Toyama (suburban) in Toyama, Japan.

**TABLE 1 |** Meteorological conditions during sampling.

| Date of collection | Location | Sample ID | Average temperature (°C) | Average relative humidity (%) | Average wind velocity (m/s) | Predominant wind direction |
|---|---|---|---|---|---|---|
| 9/16/2009 | Mt. Jodo | 20090916H | 2.4 | 100 | 4.3 | N |
| | Univ. Toyama | 20090916S | 22.9 | 64.5 | 2.2 | NNE |
| 8/20/2010 | Mt. Jodo | 20100820H | 13.3 | 87.5 | 2.4 | NNE |
| | Univ. Toyama | 20100820S | 33.3 | 65.1 | 2.1 | NNE |
| 9/24/2010 | Mt. Jodo | 20100924H | 6.4 | 20.6 | 1.9 | ESE |
| | Univ. Toyama | 20100924S | 21.1 | 63.6 | 6.1 | NE |
| 8/27/2011 | Mt. Jodo | 20110827H | 11.4 | 95.3 | 2 | W |
| | Univ. Toyama | 20110827S | 27.7 | 72.4 | 5.2 | NNE |
| 9/14/2011 | Mt. Jodo | 20110914H | 13.2 | 85.5 | 1.3 | SE |
| | Univ. Toyama | 20110914S | 30.7 | 59.5 | 3.1 | NNE |

Taq (Probe qPCR, Takara Bio), 0.2 μM of each primer, 0.25 μM TaqMan probe, and 2 μL of standard or extracted DNA. For the assay, PCR amplification was performed in a Thermal Cycler Dice Real Time System (TP-850, Takara Bio, Otsu, Japan) under the conditions of initial denaturation for 30 s at 95°C followed by 40 cycles of 5 s at 95°C and 30 s at 60°C. DNA standards for bacteria and fungi were prepared from serial dilutions of the pGEM-T Easy Vector (Promega) containing the 16S rRNA gene from *Escherichia coli* and the 18S rRNA gene from *Cladosporium* sp., respectively. Duplicate aliquots of the standards and the samples were included in each PCR run and all assays included a negative control without template DNA.

## Backward Trajectory Analysis

To evaluate the process of air mass transport to the sample locations, backward trajectory analysis was conducted using the HYSPLIT model (https://www.ready.noaa.gov/HYSPLIT.php) developed by the National Oceanic and Atmospheric Administration (NOAA; Stein et al., 2015) with archived data from the Global Data Assimilation System (GDAS) meteorological dataset. Three-day backward trajectories were calculated for air masses arriving at the University of Toyama at heights of 500 m and 1,000 m and at the summit of Mt. Jodo at heights of 3,000 m and 3,500 m, respectively.

# RESULTS AND DISCUSSION

## Meteorological Conditions and Backward Trajectories

As shown in **Table 1**, the temperature at the University of Toyama site was higher than that at Mt. Jodo. With the exception of September 24, 2010, the relative humidity at the high-altitude site was higher than that at the suburban site. The wind velocity at the high-altitude site and the suburban site was 1.3–4.3 and 2.1–6.1 m $s^{-1}$, respectively. Additionally, the predominant wind direction was mainly north-northeast (NNE) and northeast (NE) at the suburban site, while no such tendency was observed at the high-altitude site. The predominant wind direction observed at the suburban site is concordant with our previous observations (Tanaka et al., 2015). There was no precipitation at each sampling time.

Three-day backward trajectories were calculated for air masses arriving at the high-altitude site at 3,000 and 3,500 m and at the suburban site at 500 and 1,000 m (**Supplementary Figure 1**). The two different trajectories for each site were similar on each sampling day except August 27, 2011. This similarity may have arisen because the two sites are not that far away from each other.

## Characterization of Airborne Bacterial Communities

During analysis of the bacterial community (bacterial 16S rRNA gene/V3–V4 region), we obtained 406,035 raw sequence reads from 10 samples (**Table S1**). The number of clean reads ranged from 2,404 to 20,794 (8,967/sample on average) in the high-altitude site samples and 19,888 to 33,701 (25,478/sample on average) in the suburban site samples, with a read length of 420 bp. There was a difference in the number of clean reads between high-altitude and suburban sites (*t*-test, $P = 0.02$). The number of OTUs ranged from 20 to 779 with an average of 266 OTUs per sample, and the number of OTUs in the suburban site samples was higher than in the high-altitude site samples (*t*-test, $P = 0.03$). The Chao1 index, Shannon index, and Simpson index were also higher in the suburban site samples (*t*-test, $P = 0.003$ for Chao1; $P = 0.006$ for Shannon; $P = 0.04$ for Simpson). Our results are possibly concordant with those reported by DeLeon-Rodriguez et al. (2013), who found that the upper troposphere harbors less complex communities than several other environments such as soils.

The bacterial community was largely dominated by three phyla: Proteobacteria (49.1%), Actinobacteria (26.3%), and Firmicutes (14.0%) (**Figure 2A**). At the class level, the dominant groups were Actinobacteria (26.1%), Alphaproteobacteria (25.4%), Gammaproteobacteria (16.0%), Bacilli (12.9%), and Betaproteobacteria (7.5%) (**Figure 2B**). These findings are congruent with those reported in other air studies (Brodie et al., 2007; Fahlgren et al., 2010; Lee et al., 2010; Bowers et al., 2012; Maki et al., 2013; Tanaka et al., 2015; Xu et al., 2017), and hierarchical clustering of bacterial community did not show any clear trend (**Supplementary Figures 2A**, **3A**).

## Characterization of Airborne Eukaryotic Communities

During analysis of the eukaryotic community (eukaryotic 18S rRNA gene/V8 region), we obtained 595,100 raw sequence reads from 10 samples (**Table S2**). The number of clean reads ranged from 36,467 to 53,771 (45,888/sample on average) in the high-altitude site samples and 40,124 to 70,933 (59,949/sample on average) in the suburban site samples, with a read length of 220 bp. There was a significant difference in the number of clean reads between high-altitude and suburban sites (*t*-test, $P = 0.03$). The number of OTUs ranged from 566 to 1,200 with an average of 825 OTUs per sample. Unlike the bacterial community, there were no significant differences in the number of OTUs, Chao1 index, Shannon index, or Simpson index of the eukaryotic community between the high-altitude and suburban site samples (*t*-test, $P = 0.59$ for OTUs; $P = 0.68$ for Chao1; $P = 0.38$ for Shannon; $P = 0.08$ for Simpson).

The eukaryotic community was largely dominated by three phyla, Basidiomycota (41.7%), Ascomycota (30.9%), and Streptophyta (14.9%) (**Figure 3A**). This result is remarkably similar to previous work using a multidomain PCR primer set that was designed to capture a portion of the small-subunit rRNA gene from Archaea, Bacteria, and Eukarya (Bowers et al., 2013). At the class level, the dominant groups were Agaricomycetes (37.9%), Dothideomycetes (19.4%), Magnoliopsida (14.9%), Ascomycetes (5.3%), and Sordariomycetes (4.6%) (**Figure 3B**). It is widely accepted that Dothideomycetes is the most represented taxa in Ascomycetes, while Agaricomycetes is within the Basidiomycetes group (Yamamoto et al., 2012; Dannemiller et al., 2014; Shin et al., 2015; Núñez et al., 2016; Woo et al., 2018). Dothideomycetes, which includes genera associated with allergenic fungi such as *Alternaria*, *Epicoccum*, *Curvularia*, and *Cladosporium*, comprised almost half of the Ascomycota (Shin et al., 2015). Agaricomycetes includes many types of mushroom species, and generally do not contain described allergenic or pathogenic members, with the exception of some Agaricales (Yamamoto et al., 2012; Haga et al., 2014). In this study, differences in the eukaryotic community composition between high-altitude and suburban sites were observed (**Figure 3B**, **Supplementary Figures 2B**, **3B**). Agaricomycetes (Basidiomycota) was richer in the high-altitude samples than the suburban samples, while Dothideomycetes (Ascomycota) was more abundant at the suburban site samples (**Figure 4**).

## Quantification of Airborne Microorganisms

Enumeration of total bacteria and total fungi was conducted using quantitative real-time TaqMan PCR analysis of the bacterial 16S rRNA gene and the fungal 18S rRNA gene (**Figure 5**). The number of bacteria in air samples collected from Mt. Jodo and the University of Toyama ranged from $3.8 \times 10^4$ to $6.1 \times 10^4$ copies $m^{-3}$ ($4.6 \times 10^4$ copies $m^{-3}$ on average) and from $5.1 \times 10^4$ to $1.3 \times 10^5$ copies $m^{-3}$ ($7.4 \times 10^4$ copies $m^{-3}$ on average), respectively (**Figure 5A**). The number of fungi in air samples from the high-altitude site and the suburban site ranged from

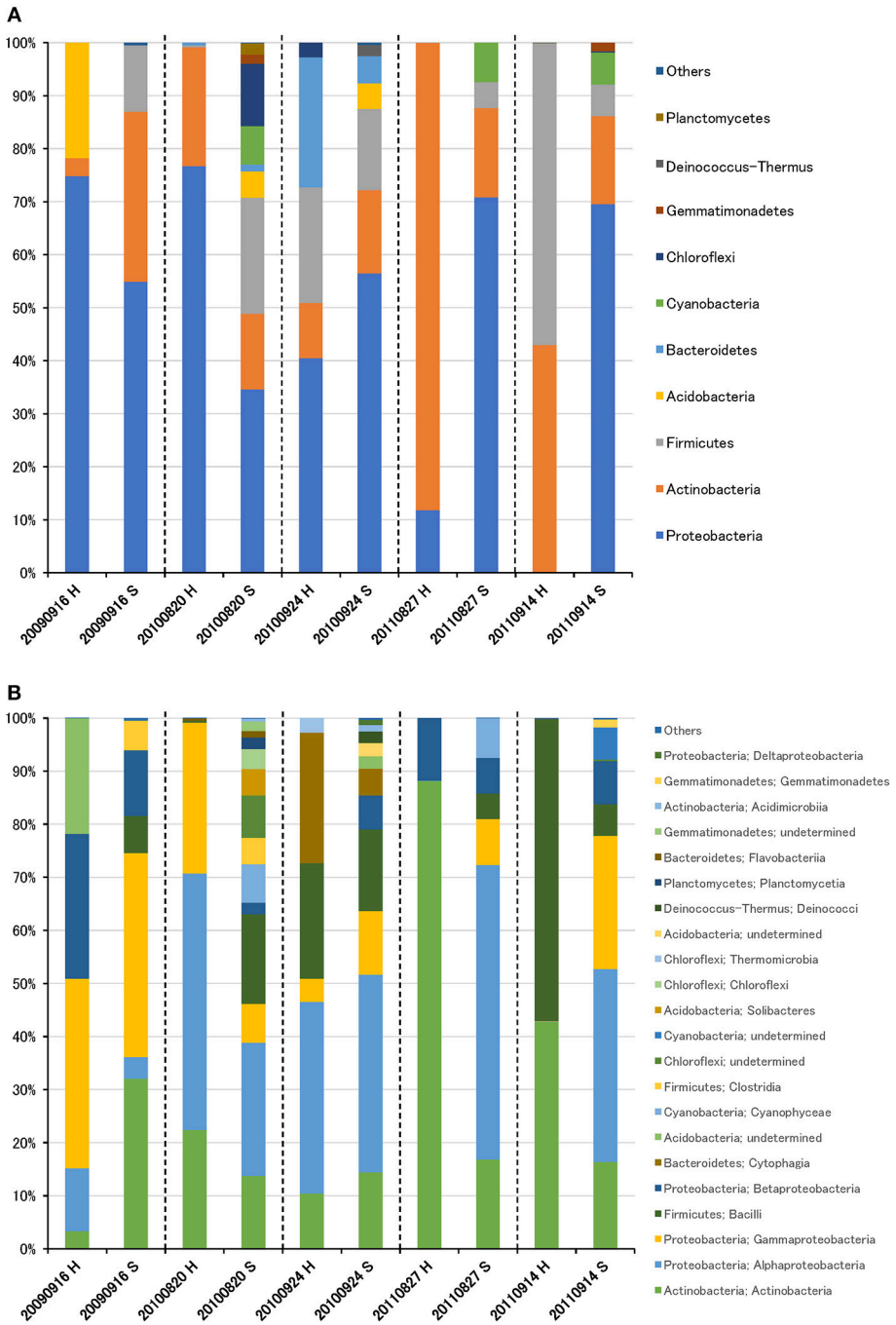


**FIGURE 2 |** Taxonomic composition of bacterial reads at the phylum **(A)** and class **(B)** levels in air samples collected at high-altitude (H) and suburban (S) sites in Toyama.

$2.5 \times 10^3$ to $8.6 \times 10^4$ copies $m^{-3}$ ($2.8 \times 10^4$ copies $m^{-3}$ on average) and from $1.8 \times 10^4$ to $1.5 \times 10^5$ copies $m^{-3}$ ($6.0 \times 10^4$ copies $m^{-3}$ on average), respectively (**Figure 5B**). This study showed that airborne bacterial and fungal abundance at the high-altitude site was about two times lower than that at the suburban site. The total bacteria and total fungi observed in this study are similar to those reported in other airborne microbial studies (Lee et al., 2010; Li et al., 2010; Bertolini et al., 2013; DeLeon-Rodriguez et al., 2013; Dannemiller et al., 2014; Gandolfi et al., 2015). Assuming an average rRNA gene copy number of four per bacterial genome and 30–100 per fungal genome (DeLeon-Rodriguez et al., 2013), our results suggest

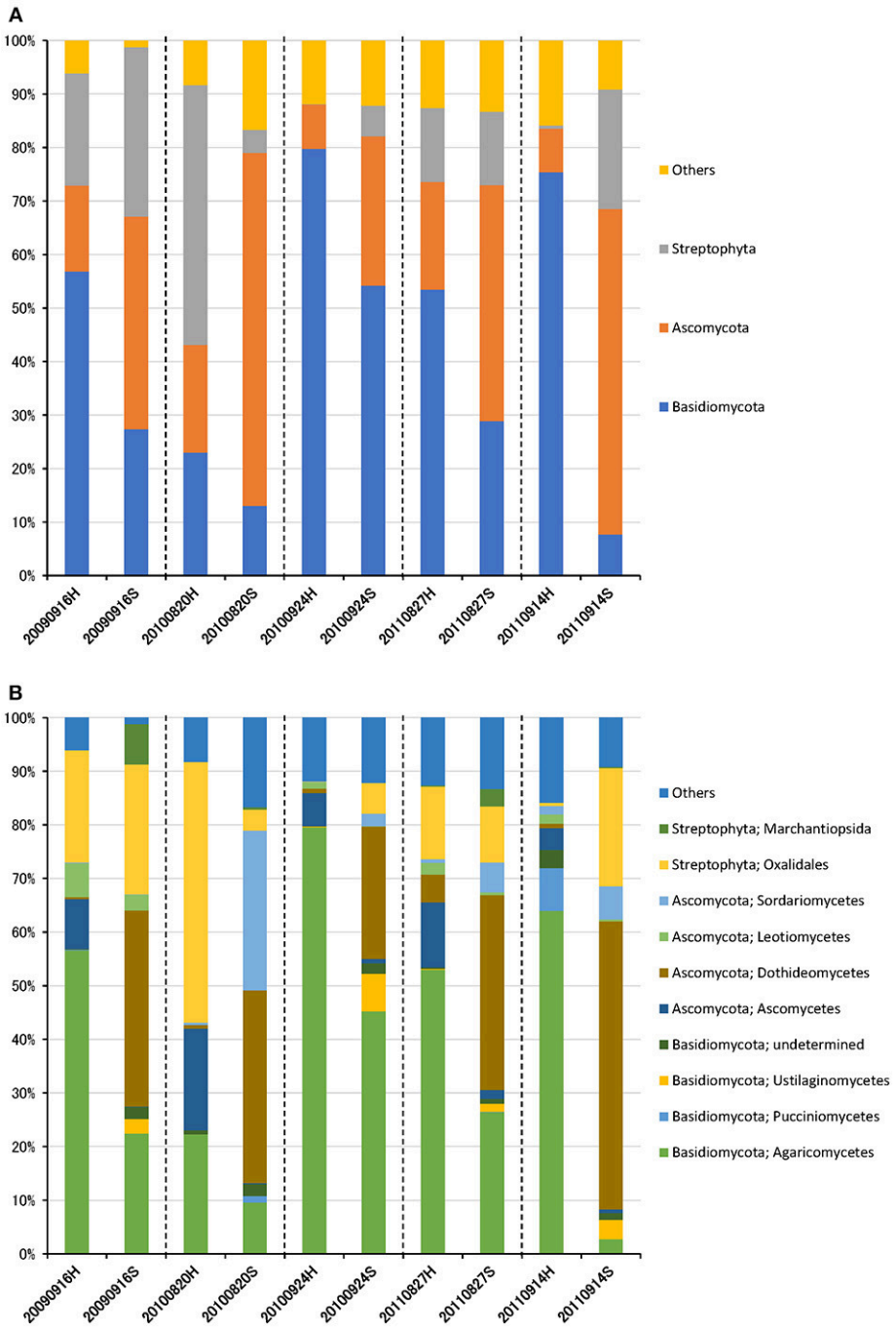


**FIGURE 3 |** Taxonomic composition of eukaryotic reads at the phylum **(A)** and class **(B)** levels in air samples collected at high-altitude (H) and suburban (S) sites in Toyama.

that bacterial abundance is one or two orders of magnitude greater than that of fungi at the high-altitude and suburban sites. These results are concordant with previous quantitative measurements using molecular and microscopic approaches (Bauer et al., 2002; DeLeon-Rodriguez et al., 2013; Gabey et al., 2013).

## Differences of High-Altitude and Suburban Microbial Community

Although there was no significant difference in bacterial communities between the high-altitude and suburban sites, different taxons were detected in the eukaryotic community such as Agaricomycetes (Basidiomycota) at the high-altitude site and

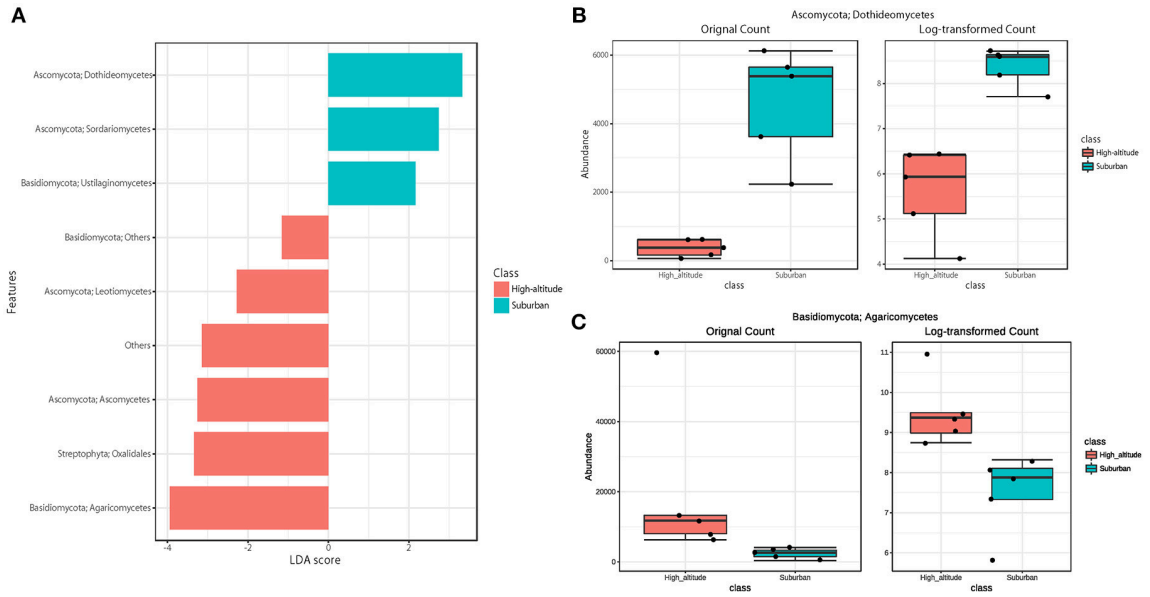


**FIGURE 4 |** Linear discriminant analysis (LDA) effect size (LEfSe), a method for biomarker discovery, was used to determine eukaryotic taxa that best characterize each location. Differences in eukaryotic taxa between suburban and high-altitude ($P < 0.05$). **(A)** More abundant taxa in suburban are shown in blue, and in high-altitude are shown in red. The most different taxa in suburban **(B)** and in high-altitude **(C)** detected by the LEfSe analytic method.

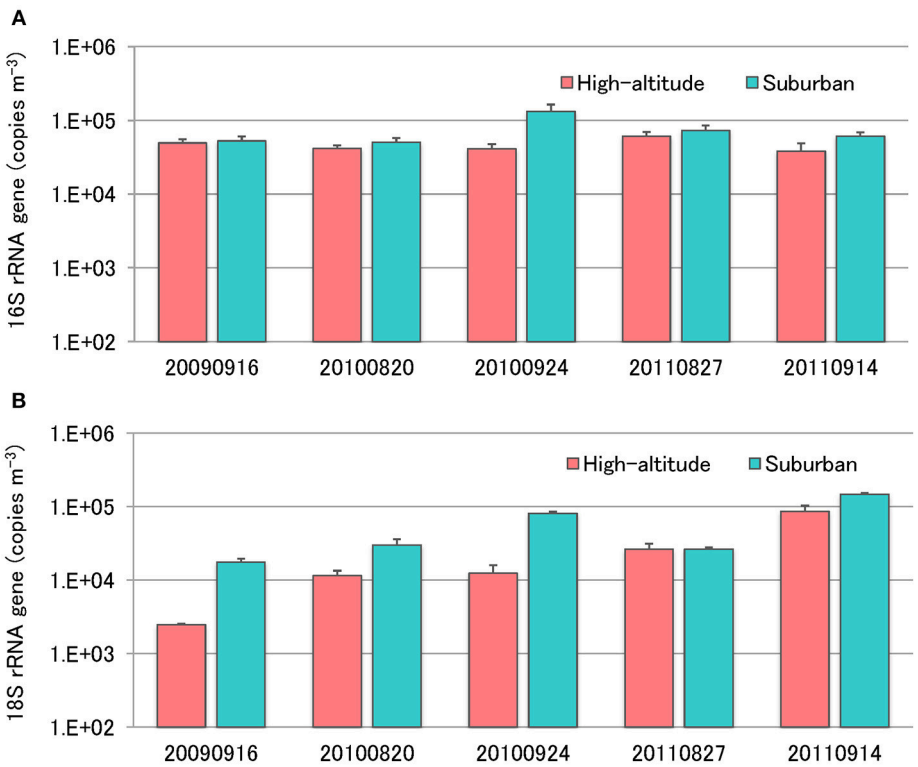


**FIGURE 5 |** Quantification of total bacterial 16S rRNA genes **(A)** and fungal 18S rRNA genes **(B)** using real-time TaqMan PCR.

Dothideomycetes (Ascomycota) at the suburban site (**Figures 2–4**, **Supplementary Figures 2B**, **3B**). Among abundant 18S OTUs, the dominant genera in Dothideomycetes included *Cladosporium* sp. (6.3–41.2% in the suburban samples and 0.1–2.4% in the high-altitude samples; 11.6% on average) and *Dothideomycetes* sp. (2.4–19.9% in the suburban samples and 0.1–1.5% in the

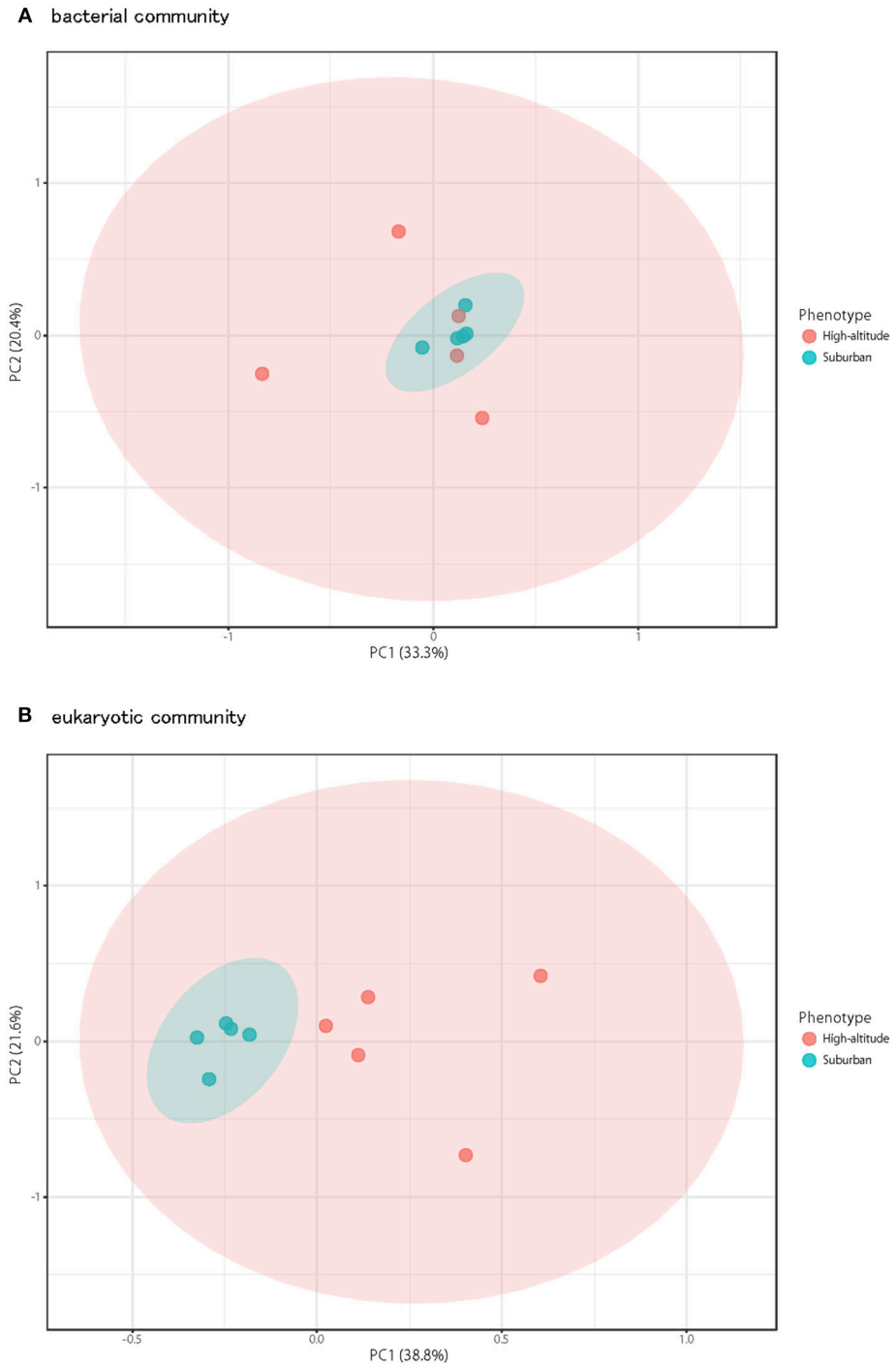


**FIGURE 6 |** Principal coordinates plot shows overall variation in bacterial community **(A)** and eukaryotic community **(B)**. Five samples from the high-altitude (red) and suburban (blue) groups were plotted with two coordinates. The mean and standard deviation in each axis are indicated by an ellipse for each located group.

high-altitude samples; 5.4% on average) (**Table S4**). Although *Cladosporium* is generally considered the most common outdoor genus in temperate climates (Gonçalves et al., 2010; Núñez et al., 2016; Lin et al., 2018), this fungus was only detected in low percentages from the high-altitude sites. In addition, the two different trajectories for each site were similar on each sampling day except August 27, 2011. The main cause may be related to vegetation type and weather conditions (Awad, 2005; Lin et al., 2018). Therefore, these findings suggest that the influence of local environmental factors on the airborne eukaryotic community are

more important than those on the airborne bacterial community. Relationships between bacterial communities in samples from the two locations were shown by principal coordinates analysis (**Figure 6A**). Bacterial communities at the suburban site were more clustered than at the high-altitude site. These results were also observed in eukaryotic communities (**Figure 6B**). These findings suggest that the bacterial and eukaryotic communities at the high-altitude site fluctuate more than at the suburban site.

### Potential Applications of Airborne Microorganisms

The top 30 abundant 16S rRNA OTUs found during analysis of the airborne bacterial community made up more than 70.9% of all sequences (**Table S3**). Among these OTUs, bacteria in the order Actinomycetales (3 OTUs) and *Bacillus* sp. (1 OTUs) can be considered a useful source for antimicrobial compounds (Motta et al., 2007; Weber and Werth, 2015). The cosmopolitan distribution of Actinomycetales and *Bacillus* sp. may be partly a result of their ability to form spores, which can travel long distances in the air (Hervàs et al., 2009). *Methylobacterium* sp. (3 OTUs) can be used to reduce environmental contamination because they are able to degrade toxic compounds, tolerate high heavy metal concentrations, and increase plant tolerance to these compounds (Dourado et al., 2015). Moreover, these bacteria have genes related to plant-bacteria interactions that may be important for developing strains able to promote plant growth and protection against phytopathogens, showing its agricultural importance. Additionally, *Pseudomonas* sp. (3 OTUs), *Streptomyces* sp. (1 OTUs), *Bradyrhizobium* sp. (1 OTU), and *Hymenobacter* sp. (1 OTU) can be a source of natural pigments (Narsing Rao et al., 2017). On the other hand, the 30 most abundant 18S OTUs found upon analysis of the airborne eukaryotic community made up more than 88.2% of all sequences (**Table S4**). *Aspergillus* sp. (1 OUT) can be a source of natural pigments (Narsing Rao et al., 2017). Smets et al. (2016) found that airborne bacteria were useful for biotechnological applications because of their unique metabolic enzymes and metabolites as well as their ability to resist typical airborne conditions such as drought, UV irradiation, specific pollutants, and low temperatures. As described above, detected airborne microorganisms showed differences between high-altitude and suburban sites. These situations should be considered at the time of screening of beneficial airborne microorganisms.

## AUTHOR CONTRIBUTIONS

DT conceived and designed the experiments. DT, KS, and ST performed the experiments. DT, MG, SF, and FM analyzed and interpreted the data. DT, SF, and FM wrote the paper. DT, SF, FM, MG, TS, AS, KA, and SN reviewed drafts of the manuscript.

## FUNDING

This work was supported by the Japan Society for the Promotion of Science KAKENHI (Grant Number 17K00579, awarded to DT) and a research grant from the Toyama First Bank Scholarship Foundation to DT.

## ACKNOWLEDGMENTS

We thank Dr. Atsushi Kume, Dr. Masanori Watahiki, and Dr. Shunsuke Matsuoka for scientific advice and Yohei Terada, Takuro Kayashima, Toyo Takahashi, Syoko Tamura, Satoru Yoneda, Muneaki Endoh, and Tatsuma Masuta for their support during sampling.

## SUPPLEMENTARY MATERIAL

The Supplementary Material for this article can be found online at: https://www.frontiersin.org/articles/10.3389/fbioe.2019.00012/full#supplementary-material

## REFERENCES

Awad, A. H. A. (2005). Vegetation: a source of air fungal bio-contaminant. *Aerobiologia* 21, 53–61. doi: 10.1007/s10453-004-5878-1

Bauer, H., Kasper-Giebl, A., Löflund, M., Giebl, H., Hitzenberger, R., Zibuschka, F., et al. (2002). The contribution of bacteria and fungal spores to the organic carbon content of cloud water, precipitation and aerosols. *Atmos. Res.* 64, 109–119. doi: 10.1016/S0169-8095(02)00084-4

Bertolini, V., Gandolfi, I., Ambrosini, R., Bestetti, G., Innocente, E., Rampazzo, G., et al. (2013). Temporal variability and effect of environmental variables on airborne bacterial communities in an urban area of Northern Italy. *Appl. Microbiol. Biotechnol.* 97, 6561–6570. doi: 10.1007/s00253-012-4450-0

Bowers, R. M., Clements, N., Emerson, J. B., Wiedinmyer, C., Hannigan, M. P., and Fierer, N. (2013). Seasonal variability in bacterial and fungal diversity of the near-surface atmosphere. *Environ. Sci. Technol.* 47, 12097–12106. doi: 10.1021/es402970s

Bowers, R. M., Lauber, C. L., Wiedinmyer, C., Hamady, M., Hallar, A. G., Fall, R., et al. (2009). Characterization of airborne microbial communities at a high-elevation site and their potential to act as atmospheric ice nuclei. *Appl. Environ. Microbiol.* 75, 5121–5130. doi: 10.1128/AEM.00447-09

Bowers, R. M., McCubbin, I. B., Hallar, A. G., and Fierer, N. (2012). Seasonal variability in airborne bacterial communities at a high-elevation site. *Atmos. Environ.* 50, 41–49. doi: 10.1016/j.atmosenv.2012.01.005

Brodie, E. L., DeSantis, T. Z., Parker, J. P., Zubietta, I. X., Piceno, Y. M., and Andersen, G. L. (2007). Urban aerosols harbor diverse and dynamic bacterial populations. *Proc. Natl. Acad. Sci. U.S.A.* 104, 299–304. doi: 10.1073/pnas.0608255104

Burrows, S. M., Elbert, W., Lawrence, M. G., and Pöschl, U. (2009). Bacteria in the global atmosphere–part 1: review and synthesis of literature data for different ecosystems. *Atmos. Chem. Phys.* 9, 9263–9280. doi: 10.5194/acp-9-9263-2009

Cao, C., Jiang, W., Wang, B., Fang, J., Lang, J., Tian, G., et al. (2014). Inhalable microorganisms in Beijing's PM2.5 and PM10 pollutants during a severe smog event. *Environ. Sci. Technol.* 48, 1499–1507. doi: 10.1021/es4048472

Caporaso, J. G., Kuczynski, J., Stombaugh, J., Bittinger, K., Bushman, F. D., Costello, E. K., et al. (2010). QIIME allows analysis of high-throughput community sequencing data. *Nat. Methods* 7, 335–336. doi: 10.1038/nmeth.f.303

Christner, B. C., Morris, C. E., Foreman, C. M., Cai, R., and Sands, D. C. (2008). Ubiquity of biological ice nucleators in snowfall. *Science* 319:1214. doi: 10.1126/science.1149757

Dannemiller, K. C., Lang-Yona, N., Yamamoto, N., Rudich, Y., and Peccia, J. (2014). Combining real-time PCR and next-generation DNA sequencing to provide quantitative comparisons of fungal aerosol populations. *Atmos. Environ.* 84, 113–121. doi: 10.1016/j.atmosenv.2013.11.036

DeLeon-Rodriguez, N., Lathem, T. L., Rodriguez-R, L. M., Barazesh, J. M., Anderson, B. E., Beyersdorf, A. J., et al. (2013). Microbiome of the upper troposphere: species composition and prevalence, effects of tropical storms, and atmospheric implications. *Proc. Natl. Acad. Sci U.S.A.* 110, 2575–2580. doi: 10.1073/pnas.1212089110

Després, V. R., Nowoisky, J. F., Klose, M., Conrad, R., Andreae, M. O., and Pöschl, U. (2007). Characterization of primary biogenic aerosol particles in urban, rural, and high-alpine air by DNA sequence and restriction fragment analysis of ribosomal RNA genes. *Biogeosciences* 4, 1127–1141. doi: 10.5194/bg-4-1127-2007

Dourado, M. N., Camargo Neves, A. A., Santos, D. S., and Araújo, W. L. (2015). Biotechnological and agronomic potential of endophytic pink-pigmented methylotrophic *Methylobacterium* spp. *Biomed Res. Int.* 2015:909016. doi: 10.1155/2015/909016

Fahlgren, C., Hagström, A., Nilsson, D., and Zweifel, U. L. (2010). Annual variations in the diversity, viability, and origin of airborne bacteria. *Appl. Environ. Microbiol.* 76, 3015–3025. doi: 10.1128/AEM.02092-09

Fujiyoshi, S., Tanaka, D., and Maruyama, F. (2017). Transmission of airborne bacteria across built environments and its measurement standards: a review. *Front. Microbiol.* 8:2336. doi: 10.3389/fmicb.2017.02336

Gabey, A. M., Vaitilingom, M., Freney, E., Boulon, J., Sellegri, K., Gallagher, M. W., et al. (2013). Observations of fluorescent and biological aerosol at a high-altitude site in central France. *Atmos. Chem. Phys.* 13, 7415–7428. doi: 10.5194/acp-13-7415-2013

Gandolfi, I., Bertolini, V., Ambrosini, R., Bestetti, G., and Franzetti, A. (2013). Unravelling the bacterial diversity in the atmosphere. *Appl. Microbiol. Biotechnol.* 97, 4727–4736. doi: 10.1007/s00253-013-4901-2

Gandolfi, I., Bertolini, V., Bestetti, G., Ambrosini, R., Innocente, E., Rampazzo, G., et al. (2015). Spatio-temporal variability of airborne bacterial communities and their correlation with particulate matter chemical composition across two urban areas. *Appl. Microbiol. Biotechnol.* 99, 4867–4877. doi: 10.1007/s00253-014-6348-5

Gonçalves, F. L. T., Bauer, H., Cardoso, M. R. A., Pukinskas, S., Matos, D., Melhem, M., et al. (2010). Indoor and outdoor atmospheric fungal spores in the São Paulo metropolitan area (Brazil): species and numeric concentrations. *Int. J. Biometeorol.* 54, 347–355. doi: 10.1007/s00484-009-0284-6

Haga, D. I., Burrows, S. M., Iannone, R., Wheeler, M. J., Mason, R. H., Chen, J., et al. (2014). Ice nucleation by fungal spores from the classes *Agaricomycetes*, *Ustilaginomycetes*, and *Eurotiomycetes*, and the effect on the atmospheric transport of these spores. *Atmos. Chem. Phys.* 14, 8611–8630. doi: 10.5194/acp-14-8611-2014

Harms, G., Layton, A. C., Dionisi, H. M., Gregory, I. R., Garrett, V. M., Hawkins, S. A., et al. (2003). Real-time PCR quantification of nitrifying bacteria in a municipal wastewater treatment plant. *Environ. Sci. Technol.* 37, 343–351. doi: 10.1021/es0257164

Hervàs, A., Camarero, L., Reche, I., and Casamayor, E. O. (2009). Viability and potential for immigration of airborne bacteria from Africa that reach high mountain lakes in Europe. *Environ. Microbiol.* 11, 1612–1623. doi: 10.1111/j.1462-2920.2009.01926.x

Jaenicke, R. (2005). Abundance of cellular material and proteins in the atmosphere. *Science* 308:73. doi: 10.1126/science.1106335

Klindworth, A., Pruesse, E., Schweer, T., Peplies, J., Quast, C., Horn, M., et al. (2013). Evaluation of general 16S ribosomal RNA gene PCR primers for classical and next-generation sequencing-based diversity studies. *Nucleic Acids Res.* 41:e1. doi: 10.1093/nar/gks808

Kobayashi, F., Maki, T., Kakikawa, M., Noda, T., Mitamura, H., Takahashi, A., et al. (2016). Atmospheric bioaerosols originating from Adélie penguins (*Pygoscelis adeliae*): ecological observations of airborne bacteria at Hukuro Cove, Langhovde, Antarctica. *Polar Sci.* 10, 71–78. doi: 10.1016/j.polar.2015.12.002

Kumar, A., and Attri, A. K. (2016). Characterization of fungal spores in ambient particulate matter: a study from the Himalayan region. *Atmos. Environ.* 142, 182–193. doi: 10.1016/j.atmosenv.2016.07.049

Lee, S. H., Lee, H. J., Kim, S. J., Lee, H. M., Kang, H., and Kim, Y. P. (2010). Identification of airborne bacterial and fungal community structures in an urban area by T-RFLP analysis and quantitative real-time PCR. *Sci. Total Environ.* 408, 1349–1357. doi: 10.1016/j.scitotenv.2009.10.061

Li, K., Dong, S., Wu, Y., and Yao, M. (2010). Comparison of the biological content of air samples collected at ground level and at higher elevation. *Aerobiologia* 26, 233–244. doi: 10.1007/s10453-010-9159-x

Lin, W. R., Wang, P. H., Tien, C. J., Chen, W. Y., Yu, Y. A., and Hsu, L. Y. (2018). Changes in airborne fungal flora along an urban to rural gradient. *J. Aerosol Sci.* 116, 116–123. doi: 10.1016/j.jaerosci.2017.11.010

Liu, C. M., Kachur, S., Dwan, M. G., Abraham, A. G., Aziz, M., Hsueh, P. R., et al. (2012). FungiQuant: a broad-coverage fungal quantitative real-time PCR assay. *BMC Microbiol.* 12:255. doi: 10.1186/1471-2180-12-255

Maki, T., Kakikawa, M., Kobayashi, F., Yamada, M., Matsuki, A., Hasegawa, H., et al. (2013). Assessment of composition and origin of airborne bacteria in the free troposphere over Japan. *Atomos. Environ.* 74, 73–82. doi: 10.1016/j.atmosenv.2013.03.029

Marinoni, A., Laj, P., Sellegri, K., and Mailhot, G. (2004). Cloud chemistry at the Puy de Dôme: variability and relationships with environmental factors. *Atmos. Chem. Phys.* 4, 715–728. doi: 10.5194/acp-4-715-2004

Matthias-Maser, S., Bogs, B., and Jaenicke, R. (2000). The size distribution of primary biological aerosol particles in cloud water on the mountain Kleiner Feldberg/Taunus (FRG). *Atmos. Res.* 54, 1–13. doi: 10.1016/S0169-8095(00)00039-9

Motta, A. S., Cannavan, F. S., Tsai, S. M., and Brandelli, A. (2007). Characterization of a broad range antibacterial substance from a new *Bacillus* species isolated from Amazon basin. *Arch. Microbiol.* 188, 367–375. doi: 10.1007/s00203-007-0257-2

Narsing Rao, M. P., Xiao, M., and Li, W. J. (2017). Fungal and bacterial pigments: secondary metabolites with wide applications. *Front. Microbiol.* 8:1113. doi: 10.3389/fmicb.2017.01113

Núñez, A., Amode Paz, G., Rastrojo, A., García Ruiz, A. M., Alcamí, A., Gutiérrez-Bustillo, A. M., et al. (2016). Monitoring of airborne biological particles in outdoor atmosphere. Part 2: metagenomics applied to urban environments. *Int. Microbiol.* 19, 69–80. doi: 10.2436/20.1501.01.265

Peccia, J., and Hernandez, M. (2006). Incorporating polymerase chain reaction-based identification, population characterization, and quantification of microorganisms into aerosol science: a review. *Atmos. Environ.* 40, 3941–3961. doi: 10.1016/j.atmosenv.2006.02.029

Pusz, W., Weber, R., Dancewicz, A., and Kita, W. (2017). Analysis of selected fungi variation and its dependence on season and mountain range in southern Poland-key factors in drawing up trial guidelines for aeromycological monitoring. *Environ. Monit. Assess.* 189:526. doi: 10.1007/s10661-017-6243-5

Shin, S. K., Kim, J., Ha, S. M., Oh, H. S., Chun, J., Sohn, J., et al. (2015). Metagenomic insights into the bioaerosols in the indoor and outdoor environments of childcare facilities. *PLoS ONE* 10:e0126960. doi: 10.1371/journal.pone.0126960

Smets, W., Moretti, S., Denys, S., and Lebeer, S. (2016). Airborne bacteria in the atmosphere: presence, purpose, and potential. *Atmos. Environ.* 139, 214–221. doi: 10.1016/j.atmosenv.2016.05.038

Stein, A. F., Draxler, R. R., Rolph, G. D., Stunder, B. J. B., Cohen, M. D., and Ngan, F. (2015). NOAA's HYSPLIT atmospheric transport and dispersion modeling system. *Bull. Am. Meteorl. Soc.* 96, 2059–2077. doi: 10.1175/BAMS-D-14-00110.1

Tanaka, D., Terada, Y., Nakashima, T., Sakatoku, A., and Nakamura, S. (2015). Seasonal variations in airborne bacterial community structures at a suburban site of central Japan over a 1-year time period using PCR-DGGE method. *Aerobiologia* 31, 143–157. doi: 10.1007/s10453-014-9353-3

Tandon, K., Yang, S. H., Wan, M. T., Yang, C. C., Baatar, B., Chiu, C. Y., et al. (2018). Bacterial community in water and air of two sub-alpine lakes in Taiwan. *Microbes Environ.* 33, 120–126. doi: 10.1264/jsme2.ME17148

Vaïtilingom, M., Attard, E., Gaiani, N., Sancelme, M., Deguillaume, L., Flossmann, A. I., et al. (2012). Long-term features of cloud microbiology at the puy de Dôme (France). *Atmos. Environ.* 56, 88–100. doi: 10.1016/j.atmosenv.2012.03.072

Wang, Y., Tian, R. M., Gao, Z. M., Bougouffa, S., and Qian, P. Y. (2014). Optimal eukaryotic 18S and universal 16S/18S ribosomal RNA primers and their application in a study of symbiosis. *PLoS ONE* 9:e90053. doi: 10.1371/journal.pone.0090053

Weber, C. F., and Werth, J. T. (2015). Is the lower atmosphere a readily accessible reservoir of culturable, antimicrobial compound-producing Actinomycetales? *Front. Microbiol.* 6:802. doi: 10.3389/fmicb.2015.00802

Woo, C., An, C., Xu, S., Yi, S. M., and Yamamoto, N. (2018). Taxonomic diversity of fungi deposited from the atmosphere. *ISME J.* 12, 2051–2060. doi: 10.1038/s41396-018-0160-7

Xu, C., Wei, M., Chen, J., Sui, X., Zhu, C., Li, J., et al. (2017). Investigation of diverse bacteria in cloud water at Mt. Tai, China. *Sci. Total Environ.* 580, 258–265. doi: 10.1016/j.scitotenv.2016.12.081

Yamamoto, N., Bibby, K., Qian, J., Hospodsky, D., Rismani-Yazdi, H., Nazaroff, W. W., et al. (2012). Particle-size distributions and seasonal diversity of allergenic and pathogenic fungi in outdoor air. *ISME J.* 6, 1801–1811. doi: 10.1038/ismej.2012.30

**Conflict of Interest Statement:** The authors declare that the research was conducted in the absence of any commercial or financial relationships that could be construed as a potential conflict of interest.

frontiers in Bioengineering and Biotechnology

ORIGINAL RESEARCH
published: 19 February 2019
doi: 10.3389/fbioe.2019.00022

# Antarctic Extremophiles: Biotechnological Alternative to Crop Productivity in Saline Soils

*Ian S. Acuña-Rodríguez[1], Hermann Hansen[2], Jorge Gallardo-Cerda[1], Cristian Atala[3] and Marco A. Molina-Montenegro[1,4]**

[1] Center for Molecular and Functional Ecology (CEMFE), Instituto de Ciencias Biológicas, Universidad de Talca, Talca, Chile, [2] Facultad de Ciencias Agrarias, Universidad de Talca, Talca, Chile, [3] Laboratorio de Anatomía y Ecología Funcional de Plantas (AEF), Instituto de Biología, Pontificia Universidad Católica de Valparaíso, Valparaiso, Chile, [4] Centro de Estudios Avanzados en Zonas Áridas (CEAZA), Facultad de Ciencias del Mar, Universidad Católica del Norte, Coquimbo, Chile

Salinization of soils is one of the main sources of soil degradation worldwide, particularly in arid and semiarid ecosystems. High salinity results in osmotic stress and it can negatively impact plant grow and survival. Some plant species, however, can tolerate salinity by accumulating osmolytes like proline and maintaining low $Na^+$ concentrations inside the cells. Another mechanism of saline stress tolerance is the association with symbiotic microorganism, an alternative that can be used as a biotechnological tool in susceptible crops. From the immense diversity of plant symbionts, those found in extreme environments such as Antarctica seems to be the ones with most potential since they (and their host) evolved in harsh and stressful conditions. We evaluated the effect of the inoculation with a consortium of plant growth-promoting rhizobacteria (PGPB) and endosymbiotic fungi isolated from an Antarctic plant on saline stress tolerance in different crops. To test this we established 4 treatments: (i) uninoculated plants with no saline stress, (ii) uninoculated plants subjected to saline stress (200 mM NaCl), (iii) plants inoculated with the microorganism consortium with no saline stress, and (iv) inoculated plants subjected to saline stress. First, we assessed the effect of symbiont consortium on survival of four different crops (cayenne, lettuce, onion, and tomato) in order to obtain a more generalized response of this biological interaction. Second, in order to deeply the mechanisms involved in salt tolerance, in lettuce plants we measured the ecophysiological performance ($F_v/F_m$) and lipid peroxidation to estimate the impact of saline stress on plants. We also measured proline accumulation and *NHX1* antiporter gene expression (involved in $Na^+$ detoxification) to search for possible mechanism of stress tolerance. Additionally, root, shoot, and total biomass was also obtained as an indicator of productivity. Overall, plants inoculated with microorganisms from Antarctica increased the fitness related traits in several crops. In fact, three of four crops selected to assess the general response increased its survival under salt conditions compared with those uninoculated plants. On the other hand, saline stress negatively impacted all measured trait, but inoculated plants were significantly less affected. In control osmotic conditions, there were no differences in proline accumulation and lipid peroxidation between inoculation treatments. Interestingly, even in control salinity, $F_v/F_m$ was higher in inoculated plants after 30 and 60 days. Under osmotic stress, $F_v/F_m$,

OPEN ACCESS

**Edited by:**
*Milko Alberto Jorquera, Universidad de La Frontera, Chile*

**Reviewed by:**
*Dirk Tischler, Ruhr-Universität Bochum, Germany*
*Ashok K. Dubey, Netaji Subhas Institute of Technology, India*

***Correspondence:**
*Marco A. Molina-Montenegro*
*marco.molina@utalca.cl*

**Specialty section:**
*This article was submitted to Bioprocess Engineering, a section of the journal Frontiers in Bioengineering and Biotechnology*

**Received:** *18 October 2018*
**Accepted:** *29 January 2019*
**Published:** *19 February 2019*

**Citation:**
*Acuña-Rodríguez IS, Hansen H, Gallardo-Cerda J, Atala C and Molina-Montenegro MA (2019) Antarctic Extremophiles: Biotechnological Alternative to Crop Productivity in Saline Soils. Front. Bioeng. Biotechnol. 7:22. doi: 10.3389/fbioe.2019.00022*

proline accumulation and *NHX1* expression was significantly higher and lipid peroxidation lower in inoculated plants compared to uninoculated individuals. Moreover, inoculated plants exposed to saline stress had a similar final biomass (whole plant) compared to individuals under no stress. We conclude that Antarctic extremophiles can effectively reduce the physiological impact of saline stress in a salt-susceptible crops and also highlight extreme environments such as Antarctica as a key source of microorganism with high biotechnological potential.

**Keywords: extremophiles, Antarctica, functional symbiosis, crops, food security, salt tolerance**

## INTRODUCTION

As a result of the global demand for processed food, intensive agricultural practices had altered the natural dynamics of the soil around the world, leading in many cases to the degradation of edaphic properties that are fundamental for crop productivity (Godfray et al., 2010). Rainfall and evapotranspiration dynamics, like those experienced by soils from arid and semiarid regions, could naturally produce a high concentration of diluted salts in the edaphic plant-rooting zone (Zhu, 2001; Zheng et al., 2009). However, several key aspects of intensive agricultural systems, like assisted irrigation, are actually one of the main drivers of soil saline accumulation (Allbed and Kumar, 2013). This process, known as soil salinization, represents one of the major forms of land degradation and was proposed to be a global problem for food security in the upcoming decades (Food and Agriculture Organization of the United Nations, 2009).

Today, agricultural productivity of arid and semiarid regions has become the most affected by salinity around the world (Rozema and Flowers, 2008), and traditional agricultural practices are already being challenged to maintain crop productivity. The pressure on agricultural soils will likely increase at a global scale in the future. This mainly due to the increased food demand as the world's population increases (Godfray et al., 2010), and the expected restrictions in water use as predicted by climate change models. Thus, alternative practices that allow the utilization of degraded soils for crop production could became necessary in the near future. One of these practices, plant-microbe symbiosis, is highlighted as one of the most promising tools in such context (Paul and Lade, 2014; Joshi et al., 2015). For this reason, the mechanistic analysis of this kind of interactions, and their evaluation for crop production, must be of primary interest in the upcoming years.

Whereas a consequence of low osmotic potential (Munns and James, 2003), specific saline ion stress (Tester and Davenport, 2003) or nutritional imbalances derived from saline edaphic accumulation (Ashraf and Harris, 2004), salinity on soils can cause strong adverse effects on plant growth and development in several crop species (Glenn et al., 1999). Nevertheless, plants have developed a wide variety of mechanisms to cope with high saline concentrations in the environment (Munns, 1993; Forni et al., 2017). For example, at the cellular scale, the accumulation of organic osmolytes (e.g., proline, glycine, betaine, sugar alcohols, or polyamines), play a key role in preventing the harmful effects of salinity stress by maintaining a low intracellular osmotic potential (Pandey et al., 2015; Reddy et al., 2015; Saha et al., 2015). This was clearly demonstrated in the *Arabidopsis thaliana* knockout variety P5CS1, which fails to encode Δ-1-pyrroline-5-carboxylate synthetase, impairing proline synthesis, which resulted in a salt hypersensitive plant (Székely et al., 2008; Szabados and Savoure, 2010). Other mechanisms of saline-stress control are related to the maintenance of low cytoplasmic $Na^+$ concentrations. This could be achieved by the augmentation of the tonoplast-localized $Na^+/H^+$ exchanger protein NHX1, which detoxifies the cells via sequestration of $Na^+$ cations within the vacuole (Sun et al., 2017). In this sense, strategies at the genetic scale, as the constitutive over-expression of the *AtNHX1* gene have shown increases on plant tolerance to salinity in *Arabidopsis* sp., but also in important crops like tomato and rice (Assaha et al., 2017; Sun et al., 2017).

Despite significant efforts (Munns and Tester, 2008; Dodd and Pérez-Alfocea, 2012; Coleman-Derr and Tringe, 2014; Krishna et al., 2015), traditional breeding and genetic engineering approaches have had only limited successes in developing salinity-resistant plants. However, the utilization of microbial symbionts has arisen as a successful (and relatively simple) biotechnological tool to achieve this goal (Bianco and Defez, 2009; Karlidag et al., 2013; Kang et al., 2014; Radhakrishnan et al., 2015; Forni et al., 2017). In fact, due to their active role in the regulation of a wide variety of plant physiological responses, the inoculation of specific microbial species on different plant hosts has been linked to enhance stress-tolerance responses against both biotic and abiotic factors (Cocking, 2003; Redman et al., 2011; Kang et al., 2015; Rho et al., 2017). However, despite the wide diversity of microbial symbionts that are present on almost all plant species; those associated with plant hosts from extreme environments appear to be the most promising in developing biological alternatives to assist crop production (Molina-Montenegro et al., 2016; Orhan, 2016; Qin et al., 2016). This could be consequence, at least in part, of the adaptive nature supposed for asymptomatic plant-microbe interaction in extreme environments (Saikkonen et al., 1998); but also because the selective pressure that these kinds of ecosystems imposes on plants demands specific biological responses, in this case, via symbiotic interactions (Redman et al., 2011).

Consequently, the Antarctic terrestrial ecosystem appears as a promising place to find plant-associated microorganisms that could confer plants protection against abiotic stress (Upson et al., 2009; Santiago et al., 2017; Gallardo-Cerda et al., 2018; Ramos et al., 2018). Besides its isolation, Antarctica is characterized

by harsh environmental conditions like low temperatures, low water content, low nutrient availability and saline soils (Convey et al., 2008; Gallardo-Cerda et al., 2018). In such conditions, only two native vascular plants grow: *Colobanthus quitensis* and *Deschampsia antarctica* (Alberdi et al., 2002). In the last 10 years, the interest in microorganisms associated to these vascular plants has greatly increased, finding promising bacterial and fungal strains with a wide spectrum of applications (Parnikoza et al., 2011; Fardella et al., 2014; Molina-Montenegro et al., 2016; Santiago et al., 2017).

Related to the saline stress tolerance, the microbial symbionts of both Antarctic vascular plant species appeared as great candidates to explore this role, since at the local scale these plants can be found primarily along the ice-free zones close to the coast, where their populations are constantly subjected to saline spray influence (Convey et al., 2008). For example, Gallardo-Cerda et al. (2018) showed the beneficial effect of various Antarctic rhizospheric bacteria (e.g., *Arthrobacter* sp.) in the physiology and survival of both native plants under controlled conditions of salt stress (200 mM of NaCl). Similarly, Torres-Díaz et al. (2016) found a strong functional role of the microbial symbionts of *C. quitensis*, particularly its root-fungal endophytes, in the ecophysiological improvement of plant individuals under osmotic stress. Interestingly, some of these Antarctic microorganisms (i.e., root-fungal endophytes and halotolerant rhizobacteria) have also shown the potential to improve the physiological performance of non-native host plants (Fardella et al., 2014), which could be quite important for a future use as biotechnological tool. Nevertheless, beyond the positive effects observed in some crops as a consequence of a manipulative symbiosis, there is still a lack of understanding regarding the mechanisms behind these positive effects under stressful conditions. For example, for most crop-microbial symbiosis, it is not clear if the observed benefits are a direct consequence of counteracting specific abiotic stressors (i.e., increased tolerance; Kim et al., 2014; López-Gómez et al., 2014), or an indirect effect derived, for example, from an enhanced nutritional status (Upson et al., 2009; Dodd and Pérez-Alfocea, 2012). On the other hand, some studies have been conducted to test the effect of microorganisms associated to Antarctic plants on stress tolerance in others plants, but all of them have been addressed using only an specific functional group (i.e., rhizobacteria or fungal), but neither has assessed the "consortium." This is surprising, because in a realistic scenario these functional groups are interacting in a determined way, exerting an inhibitory, neutral or synergic effect among then. In fact, the effect of isolated specific functional group can exert a different effect compared when is considered as part of the microbiome (Vandenkoornhuyse et al., 2015). In this sense, to determine the biotechnological potential of a given crop-microbe functional symbiosis against a particular stressor like saline soils, it is important to identify which response mechanisms are triggered in the host plant as a consequence of the microbial presence as well as to determinate the effects of functional groups acting as part of the microbiome of a given plant species rather than as isolated symbionts.

Hence, to evaluate the potential of a selected group of Antarctic extremophiles to ameliorate the stressful effect of soil salinization on susceptible crops, we monitored the physiological (individual) and biochemical (cellular) performances of inoculated and non-inoculated lettuce plants exposed for 60 days to saline stress. Furthermore, to determine the potential mechanisms involved in the observed stress-response enhancement, we analyzed the foliar accumulation of proline and the relative expression of saline-stress related genes like *NHX1*. Finally, we established the overall effect of the interaction between saline stress and symbiosis on the final biomass of lettuce individuals as an indicator of crop productivity.

# MATERIALS AND METHODS

## Generation of the Symbiont Consortium

The consortium of microorganisms used in our study was composed by two halotolerant plant growth-promoting rhizobacteria (PGPR) of the genus *Arthrobacter* sp. and *Planoccocus* sp. and two root-fungal endophytes; identifies as *Penicillium chrysogenum* and *Penicillium brevicompactum*. In brief, both rhizobacteria used for this study were selected because are one of the most abundant in the rhizosphere of antarctic plants, ease to cultivate and has been demonstrated to growth under high salt concentrations (Gallardo-Cerda et al., 2018). In addition, these rhizobacteria has been showed to improve the ecophysiological performance of their native hosts in Antarctica (Gallardo-Cerda et al., 2018). On the other hand, root fungal endophytes selected to use in this study were selected because are the two most abundant in the root of Antarctic plants and can be grown at different temperatures and abiotic conditions in the laboratory (Molina-Montenegro et al., 2016). In addition, these endophytes have been demonstrated to improve the ecophysiological performance and productivity in crops under osmotic stress (Molina-Montenegro et al., 2016). Both rhizobacteria and fungal endophytes were identifies and its sequences deposited in the gene-bank. These inoculums are maintained as part of the collection of microorganisms of the Plant Ecology Laboratory, Universidad de Talca, Chile. The inoculums were separated in different Petri dishes and then frozen until to be used in the experiments.

For more details of isolation, inoculation, and the gene-bank code (see Molina-Montenegro et al., 2016; Gallardo-Cerda et al., 2018).

Plant inoculation was performed according to the procedure describe by Hadi et al. (2010) with the selected consortium of microorganisms. Briefly, the rhizosphere of each crop individual was injected with ∼2 ml of distilled water containing a concentrated mix of spores (5,000 spores $ml^{-1}$) from each fungal endophyte, and about $10^8$ cells $ml^{-1}$ of the bacterial species. A posterior validation of the effectiveness of the inoculation was conducted using a light microscope in a subsample of roots (10% of the experimental individuals) 1 week after inoculation, and at the end of the experiment (60 days).

Fresh inoculums were obtained during March 2017 from single-conidia of fungal endophytes cultured on potato dextrose agar (PDA) medium diluted eight times and supplemented with 50 mg/ml of streptomycin. Cultures with endophytes were incubated at 22 ± 2°C with a photoperiod 14/10 day/night.

After 2 weeks of incubation, conidia were harvested from plates by adding 10 ml of sterile water and gently scraping off conidia with a sterile glass slide. The conidia suspension was adjusted to 100 ml of 0.05% Tween-100, sterilized solution, filtered through three layers of sterile cotton cheesecloth gauze. Conidia concentration was estimated by using a Neubauer chamber and adjusted to $1 \times 10^5$ conidia/ml and its viability was tested according to methodology described by Greenfield et al. (2016) and the mean conidia viability was >95%. In addition, rhizobacteria used in this assays were cultured in Laura Bertani broth (LB). Later, they were mixed on an orbital shaker with a speed of 120 rpm and incubated at 10°C for 72 h. The incubated broth cultures were then centrifuged for 15 min at 3,000 rpm. Pelleted cells were suspended in sterile distilled water and its optical density was adjusted to about $10^8$ cells $*ml^{-1}$. Symbiont consortium (fungal endophytes + rhizobacteria) was injected in the rhizosphere, according the procedure describe by Hadi et al. (2010).

## Overall Assessment of Symbiont Consortium in Crops

To test the overall effect of symbiont consortium on salt tolerance in crops, we compared the survival percentage of individuals of cayenne (*Capsicum annuum*), lettuce (*Lactuca sativa*), onion (*Allium cepa*), and tomato (*Solanum lycopersicum*) inoculated and un-inoculated with microorganisms as well as exposed to salt-stressed and control condition. The plant inoculation was repeated two times to ensure the consortium to establish an effective association. Before the beginning of the experiment, three plants of each species/treatment were sacrificed to check microscopically for the presence and/or absence of microorganisms by routine staining of roots.

Seedlings of these crop species were obtained from seeds germinated in glasshouse located at the Universidad de Talca, Talca, Chile (35.4°S), under semi-controlled environmental conditions of light and temperature ($730 \pm 77$ μmol $m^{-2}s^{-1}$; $23 \pm 5$°C, respectively). For treatment setup, crop seedlings were transplanted into the field when individuals presented at least four expanded leaves and/or 3-cm roots. One-hundred seedlings of each species were randomly assigned to one of the following treatments: (i) *Saline stress*: control individuals watered without salt addition, and stressed individuals watered with a 0.2 M saline water solution; (ii) *Symbiont inoculation*: control plants (S–) without the set of Antarctic extremophile microorganisms, and infected plants (S+) which were inoculated with the symbiont consortium described above. Thus, the four treatments corresponded to S+ plants with and without salt stress and S– plants with and without salt stress, with a sample size of 25 plants per treatment per crop species (total $n = 400$ individuals). Finally, each group of 25 individuals was grouped in five group with five individuals each one. Survival percentage was recorded at 60 days on each group of five seedlings per treatment in the field.

## Experimental Arrangement to Evaluate Salt Tolerance in Crops

We decided to use lettuce as a model crop to deeply the understanding about mechanisms and consequences of microorganisms to confer environmental tolerance in crops. This crop has been shown to be highly sensitive and dependent on water at all developmental stages (Sánchez, 2000; Molina-Montenegro et al., 2011), and demands constant watering to maintain high photosynthetic rates and a fresh biomass of high commercial value (Nissen and San martín, 2004). Complementarily, lettuce has also shown the ability to accept non-native microbial symbionts and moreover, to respond positively to these new partners (Molina-Montenegro et al., 2016). Consequently, during April 2017, 500 lettuce seeds (var. Romaine) were germinated in greenhouse conditions. After 3 weeks, 125 seedlings were transplanted to individual pots containing 500 ml of a peat: perlite: sand mix (35%: 35%: 30%) as substrate. Their successful establishment was verified for 1 more week previous to any experimental treatment.

From the set of 114 successfully established seedlings, 100 individuals were selected for the experiments and were then randomly divided into four groups of 25 to fulfill the factorial combination of the two experimental variables of saline stress and effective symbiosis ($2 \times 2$ full factorial design). The respective treatments were (i) *Saline stress*: control individuals watered without salt addition, and stressed individuals watered with a 0.2 M saline water solution; (ii) *Symbiont inoculation*: control plants (S–) without the set of Antarctic extremophile microorganisms, and infected plants (S+) which were inoculated with the symbiont consortium. Thus, the four treatments corresponded to S+ plants with and without salt stress and S– plants with and without salt stress, with a sample size of 25 plants per treatment. The referred consortium of microorganisms was the same to those used to assess the overall effect on survival of several crops indicated above. Similarly, a posterior validation of the effectiveness of the inoculation was conducted using a light microscope in a subsample of roots (10% of the experimental individuals) 1 week after inoculation, and at the end of the experiment (60 days).

## Estimation of the Saline Stress Effect

Having validated the symbiosis by re-inoculation and visual assessment in root samples of experimental plants, half of the 4-weeks old inoculated seedlings, started their saline-stress treatment included in the watering routine. We estimated the photochemical efficiency and the membrane lipid peroxidation state as two physiological/biochemical proxies of osmotic stress (Egert and Tevini, 2002; Molina-Montenegro et al., 2013). To measure chlorophyll fluorescence we obtain the minimum ($F_0$) and maximum ($F_m$) fluorescence yields per individual ($n = 10$) using a pulse modulated-amplitude fluorimeter (FMS 2, Hansatech, Instrument Ltd, and Norfolk, UK). The baseline ($t_0$) measurements were taken previous to the saline addition and were also estimated after 30 ($t_{30}$) and 60 ($t_{60}$) days. In each case we calculated the maximum quantum yield of photosystem-II ($F_v/F_m$), where $F_v$ refers to $F_0 - F_m$ (Maxwell and Johnson, 2000). To ensure maximum photochemical efficiency, the chosen leaves from each individual were dark-adapted for 30 min previous to the measurements.

Complementary to the individual level of response denoted by the photochemical efficiency, we estimated the state of

lipid oxidative degradation by the thiobarbituric acid reactive substances (TBARS) assay (Egert and Tevini, 2002), which measures the concentration of malondialdehyde (MDA) at the cellular level as a proxy of cell damage. For each experimental group, the lipid peroxidation state in 0.5 g of fresh foliar tissue samples from five random individuals was estimated at each time (i.e., $t_0$, $t_{30}$, and $t_{60}$). Samples were prepared and homogenized with 2 ml of TCA (1%) to be later centrifuged at 10,000 G for 5 min. For each sample, the supernatant was mixed with 1 ml of 0.5% thiobarbituric acid in TCA (20%) and then incubated for 30 min in boiling water. Once cooled to room temperature, the absorbance of each sample was determined at 532 nm and non-specific absorbance at 600 nm (Hodges et al., 1999). The MDA content was determined by its molar extinction coefficient of 155 $mM^{-1}$ $cm^{-1}$.

## Mechanisms of Saline-Stress Tolerance

To determine the proline accumulation in the foliar tissues of the experimental plants we followed most of the Bate's method (Bates et al., 1973). Samples of fresh healthy leaves (∼250 mg) were frozen at each time (i.e., $t_0$, $t_{30}$, and $t_{60}$) from the same individuals selected for the TBARS assay. From each individual, a sample of 100 mg was grinded in 1.2 ml of 3% sulfosalicylic acid. The resulting homogenate was then centrifuged at 16,000 G for 20 min to obtain 1 ml of the supernatant, which was added to 2 ml of ninhydrin reagent (2.5% ninhydrin in glacial acetic acid: distilled water: 85% orthophosphoric acid [6:3:1]). Each reaction mix was kept for 1 h in water bath at 90°C to develop color. After cooling the test tubes in an ice-bath, 2 ml of toluene was added to separate the chromophores in the sample. Finally, the toluene phase absorbance was read in a spectrophotometer at 525 nm to further estimate proline concentration by comparing sample absorbances with the standard proline curve.

In addition to the biochemical mechanisms mentioned above, genetic responses of lettuce to saline stress were assessed at each time (i.e., $t_0$, $t_{30}$, and $t_{60}$) through the expression of the *NHX1* antiporter gene among a subsample of individuals ($n = 5$) from each experimental group. To achieve this, total RNA was extracted from foliar samples according to Chang et al. (1993). DNA was removed from aliquots of total RNA using TURBO DNA-free (Applied Biosystems, USA). Synthesis of the cDNA strand was performed according to Ruíz-Carrasco et al. (2011). The quantitative PCR (qPCR) reaction contained the cDNA, 5 *p*mol of each primer, and 12.5 ml of the Fast SYBR Green PCR master mix (Applied Biosystems. USA). The sequences used to amplify *LsNHX1* amplicons (∼200 bp) were: 5′-GCACTTCTGTTGCTGTGAGTTCCA-3′ (forward); 5′-TGTGCCCTGACCTCGTAAACTGAT-3′ (reverse). PCRs were performed on a Step-One Plus 7500 thermocycler (Applied Biosystems, USA). The process includes an initial cycle of 30 min at 45°C and 2 min at 95°C, and then 40 cycles as follows: 95°C for 30 s, 60°C for 30 s, 72°C for 2 min, and finally one cycle at 72°C for 10 min. Cycle threshold (Ct) values were obtained and analyzed with the $2^{-\Delta\Delta CT}$ method (Livak and Schmittgen, 2001). The Elongation Factor 1a (EF1a) housekeeping gene was used as reference gene to normalize, and estimate up- or down-regulation of the target genes for all qPCR analyses: 5′-GTACGCATGGGTGCTTGACAAACTC-3′ (forward); 5′-ATCAGCCTGGGAGGTACCAGTAAT-3′ (reverse). The relative expression ratio ($log_2$) between the target gene and EF1a, as well as the fold changes (FC) between controls plants (non-inoculated and without salt stress) and experimentally manipulated individuals were calculated from the qRT-PCR efficiencies and the crossing point deviation using the mathematical model proposed by Pfaffl (2001).

## Symbiont Consortium on Crops Productivity

As a commercial crop, the individual final yield of the monitored lettuce plants was averaged in each experimental group. At the end of the experiment (day 60), all remaining lettuces in the experiment were carefully harvested and their roots gently washed with tap water to separate above (leaves) and belowground (roots) tissues in each individual. After 1 h of drying in the shade, their respective fresh weights were obtained using a digital scale (Boeco BBL-52; 0.01 g-precision). Finally, total dry biomass was measured after whole lettuce individuals were over-dried at 62°C for 96 h and the constant weight of biomass was achieved.

## Statistical Analysis

To evaluate the effect of symbiont consortium on the average survival percentage in different crops was used a two-way ANOVA with inoculation and salt as independent variables. The effect of microbial inoculation and saline stress on lettuce plants traits was assessed by repeated measures (rm) ANOVAs on the following variables: proline accumulation, lipid peroxidation (TBARS), *NHX1* relative gene expression, and photochemical efficiency ($F_v/F_m$). Non-parametric mixed model fitting was performed with the *lme* function on the *nlme* R-package using the individual nested in time as the random error structure (Pinheiro et al., 2017). *A posteriori* comparisons for the mixed models between experimental groups were performed by the comparison of their Estimated Marginal Means (EMMs), as supported by the pair function in the *emmeans* R-package (Lenth et al., 2018). Differences in final fresh biomass were analyzed by independent two-way standard ANOVAs for each kind of tissue (root, shoot or the whole plant). We used the presence of the microbial symbionts (inoculated: S+ or non-inoculated: S–) and stress status (no stress: control; saline-stress: stressed) as explanatory variables. When significant results were obtained, *a posteriori* differences between experimental groups were analyzed by the Honest Significant Differences (HSD) Tukey test (Rohlf and Sokal, 1981).

# RESULTS

## Overall Assessment of Symbiont Consortium in Crops

Average survival was greater in all crop species assessed under control compared with salt-stressed treatment (**Figure 1**). Similarly, symbiont consortium increase the survival in the majority of crops, with the exception of onion where survival

**TABLE 1 |** Repeated measures ANOVA for the effect of saline stress (S) and microbial symbiosis (Sy) on two variables of physiological performance (**a**: photosynthetic efficiency; **b**: lipid peroxidation) and two specific stress-response mechanisms (**c**: proline concentration; **d**: *NHX1* relative expression).

| Response variable | Source of variation | $df_{num}$ | $df_{den}$ | *F* | *p* |
|---|---|---|---|---|---|
| Photochemical efficiency (Fv/Fm) | Stress (S) | 1 | 72 | 908445.8 | <0.0001 |
| | Symbiont (Sy) | 1 | 36 | 1226.8 | <0.0001 |
| | Time (T) | 1 | 36 | 547.8 | <0.0001 |
| | Stress × Symbiont | 2 | 72 | 366.3 | <0.0001 |
| | Stress × Time | 1 | 36 | 149.1 | <0.0001 |
| | Symbiont × Time | 2 | 72 | 396.4 | <0.0001 |
| | S × Sy × T | 2 | 72 | 165.6 | <0.0001 |
| Lipid peroxidation (TBARS [MDA]) | Stress (S) | 1 | 32 | 16724.88 | <0.0001 |
| | Symbiont (Sy) | 1 | 16 | 816.535 | <0.0001 |
| | Time (T) | 1 | 16 | 382.987 | <0.0001 |
| | Stress × Symbiont | 2 | 32 | 487.53 | <0.0001 |
| | Stress × Time | 1 | 16 | 330.013 | <0.0001 |
| | Symbiont × Time | 2 | 32 | 452.058 | <0.0001 |
| | S × Sy × T | 2 | 32 | 207.78 | <0.0001 |
| Proline concentration (mmol/g FW) | Stress (S) | 1 | 16 | 901.146 | <0.0001 |
| | Symbiont (Sy) | 1 | 16 | 137.093 | <0.0001 |
| | Time (T) | 2 | 32 | 185.671 | <0.0001 |
| | Stress × Symbiont | 1 | 16 | 117.031 | <0.0001 |
| | Stress × Time | 2 | 32 | 171.692 | <0.0001 |
| | Symbiont × Time | 2 | 32 | 30.934 | <0.0001 |
| | S × Sy × T | 2 | 32 | 29.946 | <0.0001 |
| *NHX1* gene expression (Relative fold change) | Stress (S) | 1 | 32 | 513.41 | <0.0001 |
| | Symbiont (Sy) | 1 | 16 | 90.69 | <0.0001 |
| | Time (T) | 1 | 16 | 1065.19 | <0.0001 |
| | Stress × Symbiont | 2 | 3.2 | 23.23 | 0.0002 |
| | Stress × Time | 1 | 16 | 755.79 | <0.0001 |
| | Symbiont × Time | 2 | 32 | 92.31 | <0.0001 |
| | S × Sy × T | 2 | 32 | 31.47 | <0.0001 |

*The table shows the probability value (p) obtained for the significance of each factor in the fitted linear mixed model, which was obtained by maximizing the restricted log-likelihood for the data.*

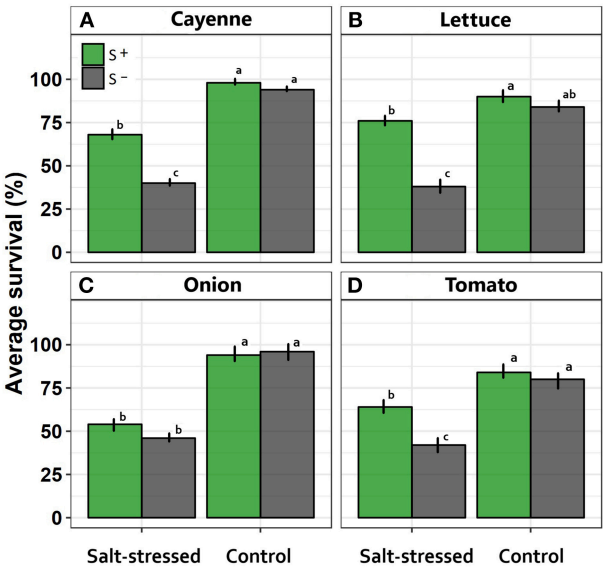


**FIGURE 1 |** Effects of saline treatment (control vs. salt-stressed) and inoculation with a mix of Antarctic microorganisms (S– vs. S+ plants) on survival probability along time, in **(A)** cayenne, **(B)** lettuce, **(C)** onion, and **(D)** tomato crops. Different lowercase letters indicate significant differences between treatments (Tukey HSD tests; $\alpha = 0.05$) independently for each species. Error bars represent ± SE values.

percentage in salt-stress treatment was not different between inoculated vs. uninoculated individuals (**Figure 1**).

Specifically, symbiont consortium significantly increased the survival percentage in cayenne crop [$F_{(1, 16)} = 30.12$; $p = 0.004$; **Figure 1A**]. Contrarily, salt treatment significantly decreased the survival percentage in cayenne crop [$F_{(1, 16)} = 207.53$; $p < 0.0001$]. Interaction between inoculation x salt was significant [$F_{(1, 16)} = 16.94$; $p = 0.008$] since salt treatment decreased the survival with greater intensity in the treatment without symbiont consortium (**Figure 1A**). In the same way, interaction between inoculation x salt in lettuce crop was significant [$F_{(1, 16)} = 28.44$; $p = 0.0067$] because the survival average decrease under salt condition, being more evident in uninoculated condition (**Figure 1B**). On the other hand, onion crop showed a significant decrease in survival under salt-stress condition [$F_{(1, 16)} = 337.50$; $p < 0.0001$], but was not different among inoculated vs. uninoculated condition [$F_{(1, 16)} = 4.17$; $p = 0.238$; **Figure 1C**]. Finally, tomato crop showed a significative interaction between inoculation vs. salt [$F_{(1, 16)} = 9.01$; $p = 0.0083$] since those uninoculated individuals showed a more evident decrease in the survival percentage under salt-stress treatment (**Figure 1D**).

## Effects of the Saline-Stress

Photochemical efficiency, measured as $F_v/F_m$, showed the expected trend in plants under saline stress in both S– and S+ individuals, since their photosynthetic performance along time appeared to be negatively affected compared with control individuals without salt addition (**Table 1**). However, as it could be seen in stressed individuals after 30 and 60 days of saline treatment, the presence of the microbial symbionts significantly ameliorated the negative impact of saline stress. Symbiont appeared to stabilize the decrease of $F_v/F_m$ with time (**Figure 2A**). By contrast, among non-inoculated individuals under salt stress, the values of $F_v/F_m$ showed a continuous decrease along time, being the $F_v/F_m$ value at end of the experiment significantly lower than those recorded at day 30 (**Figure 2A**). Interestingly, the symbiotic interaction significantly enhanced the $F_v/F_m$ values of lettuce plants, even if they were not under saline stress; S+ individuals where already 3.8% more efficient in their photochemical performance than S– plants by the 30th day, and this difference was maintained in time (**Figure 2A**). On the other hand, the amount of TBARS showed a substantial increase for both S+ and S– plants under saline stress. Nevertheless, among S+ individuals, this increase was less than a half of what was observed for their S– counterparts (**Figure 2B**). Conversely, TBARS concentrations showed no differences at any time in plants without saline stress, despite their symbiotic status (**Figure 2B**).

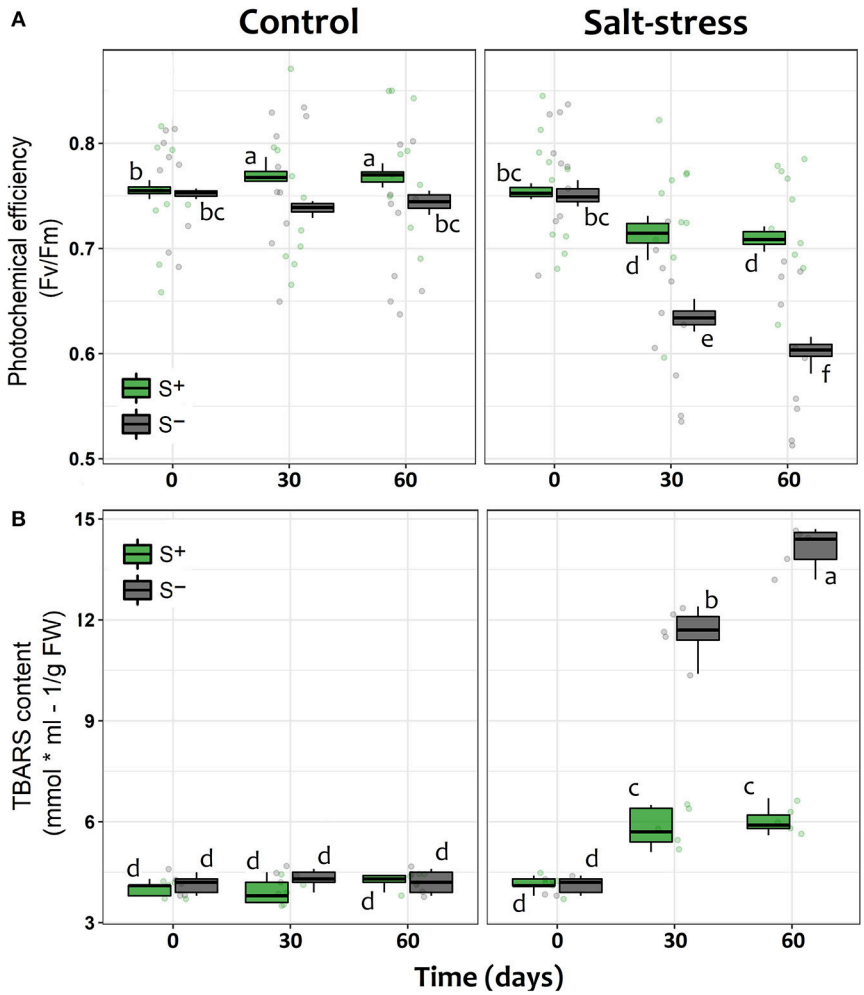


**FIGURE 2 |** Physiological performance of lettuce individuals measured as **(A)** the individual photochemical efficiency ($F_v$ /$F_m$) of photosystem II (PSII) and **(B)** the level of lipid cell membrane peroxidation (TBARS) measured in leaves at 0, 30, and 60 days after exposed to salt stress (200 mM NaCl for "stressed" individuals) and inoculated with the Antarctic microbial consortium (S+ plants). Control groups for both conditions (non-stressed and non-inoculated, S–) are also showed. The box-plot represents the interquartile distribution of the data for each experimental group. Different letters indicate significant *a posteriori* differences (Tukey test, $\alpha < 0.05$).

## Mechanisms of Saline-Stress Tolerance

The concentration of proline significantly increased after 30 and 60 days in salt-stressed individuals compared to non-stressed plants (**Figure 3A**). However, whilst S– individuals under saline stress showed an increase in proline concentration of 32% (day 30) and 48% (day 60), plants inoculated with the antarctic symbiotic consortium this increase achieved a 96 and 98%, respectively, during the same period (**Figure 3A**). As expected, among individuals without salt addition the mean proline concentrations were observed to be independent of time and symbiotic interaction (**Table 1**). In addition, described as a genetic response to saline-stress (Khan et al., 2013), the relative expression of *NHX1* showed larger changes in time among salt-stressed individuals compared with non-stressed S– and S+ plants. Furthermore, under saline stress, major increases appeared to be related with the presence of the symbiotic consortium; at day 30 its increase with respect to the reference value (S– day 0) was 32% for S– but 59% for S+ plants, a difference that was maintained at day 60 (**Figure 3B**). Interestingly, the symbiotic interaction also changes the *NHX1* relative expression under non-stressed conditions, although small (9%), a significant increase was observed at day 30 among S+ plants. By contrast, the *NHX1* expression of S– individuals do not present changes along time (**Figure 3B**).

## Symbiont Consortium on Crops Productivity

Overall, those lettuce individuals exposed to salt-stress treatment showed a smaller size than those allocated to control treatment or even those exposed to salt-stress but inoculated with the symbiont consortium (**Figure 4**). The two-way ANOVA on the final fresh biomass values showed a general negative impact of the saline growth conditions on productivity (factor salt-stress: *df*

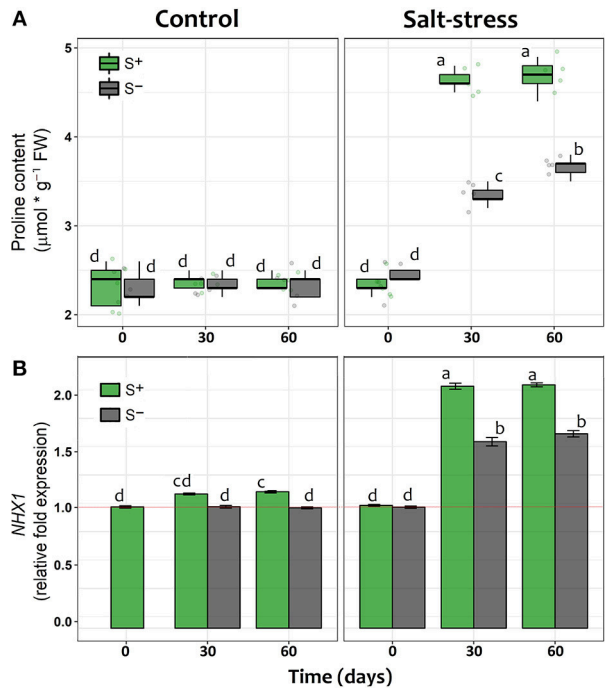


**FIGURE 3 | (A, B)** Proline concentration (mmol/g FW) and, relative fold gene expression of *NHX1* in shoot tissue of lettuce plants measured at 0, 30, and 60 days after exposed to salt stress (200 mM NaCl for "stressed" individuals) and inoculated with the Antarctic microbial consortium (S+ plants). Control groups for both conditions (non-stressed and non-inoculated, S–) are also showed. The relative expression increases are referred to the mean levels of expression in control lettuce plants (i.e., non-stressed and non-inoculated) at time 0, indicated by a red line. The box-plot represents the interquartile distribution of the data for each experimental group. Error bars at the *NHX1* plot represent ± SE values. Different letters indicate significant a posteriori differences (Tukey test, $\alpha < 0.05$).

$= 1.49$; $F = 5.502$; $p = 0.023$, **Figure 3**); however, the significance of the ANOVA interaction term (i.e., inoculation x salt-stress: $df = 1.49$; $F = 4.981$; $p = 0.031$) suggests that this negative effect depends on the symbiotic status. In this sense, the root biomass reduction was only noticed among S– individuals, as could be observed on the a posteriori HSD-Tukey results (**Figure 5**). In lettuce plants under salt stress, the absence of microorganisms resulted in a decrease of 38% in the fresh biomass weight of roots respect to non-stressed plants. The same trend that was observed on the aboveground biomass, with a 31% mean shoot decrease among S– plants under saline stress and, consequently, on the whole plants (**Figure 5**). Interestingly, the two-way ANOVA for shoot tissues alone and for the whole individuals, despite shown significant *p*-values for "inoculation" and "salt-stress" as separate terms, do not presented a significant interaction in term of "inoculation x salt-stress" (shoot: $df = 1.49$; $F = 1.777$; $p = 0.188$; entire plant: $df = 1,49$; $F = 3.047$; $p = 0.0871$). This suggests a role of both factors in the observed results, however, with an apparent independence between them. Despite this, a-posteriori significant differences on either biomass variables could only be observed between stressed and non-stresses S– plants (**Figure 5**). By contrast, between both, salt-stressed and non-stressed S+ lettuce plants, we did not find any statistical differences between mean fresh weight of neither root or shoot tissues, nor for the whole plant.

## DISCUSSION

In our study we showed evidence suggesting the importance of symbiont microorganisms from Antarctica improving salt tolerance in crops. In fact, under salt-stress condition the symbiont consortium significantly enhanced the survival in three of four crops assessed here. Hence, selected microorganisms from Antarctic plants could be a successful tool to avoid the negative effect of salt stress to others plant species as crops.

Beyond confirming that Antarctic environments are a fructiferous source of microbial extremophiles with potential applications, the results obtained in this work also unveil part of the mechanisms by which these symbiotic partners could benefit their host-plants. Compared with non-inoculated individuals, an enhanced proline accumulation and increased expression of the *NHX1* gene was observed among inoculated lettuces when they were subjected to salt-stress. Additionally, plants that were carrying the symbiotic consortium showed lower levels of cellular damage by lipid peroxidation and higher photosynthetic efficiencies.

Regarding the concentration of osmolytes, as a reported stres S–tolerance mechanism (e.g., glutamate, threalose, peptides, and other N-acetylated amino acids), proline appears to be particularly relevant to reduce the stressful effects of salinity (Hayat et al., 2012; López-Gómez et al., 2014; Reddy et al., 2015; Forni et al., 2017). The derived benefits of proline accumulation for a plant exposed to adverse environmental conditions (i.e., saline soils), could be related with the prevention of electrolyte leakage (Shahid et al., 2014), maintenance of the cell turgor (Ben Ahmed et al., 2011), and/or oxidative burst prevention (Hayat et al., 2012). In our work, the content of proline increased in both inoculated and non-inoculated individuals under salt stress. However, its accumulation in the later appeared to be slower, suggesting a role of the inoculated microorganisms in this process. In this sense, despite it is not possible with our design to differentiate the effects of the fungal and bacterial components of the microbial consortium, the proline-related response observed among inoculated lettuce plants may be originated by rhizobacterial symbionts, as other authors have shown (Kohler et al., 2009; Kumari et al., 2015). According to Creus et al. (2004), the plant-PGPR interaction frequently involves the control of the plant–water dynamics, facilitating the consequent enhanced potential for osmotic adjustment. Thus, it is not surprising that PGPR inoculation has been reported to result in enhanced tolerance to salt stress in several crops (Glick et al., 1997; Mayak et al., 2004; Yildirim and Taylor, 2005; Barassi et al., 2006; Egamberdieva et al., 2013; Forni et al., 2017).

Root-fungal endophytes could also have profound effects on plant performance as they can impact several components of their fitness; for example, by facilitating the uptake of essential nutrients like Potassium, Nitrogen or Phosphorus (Barka et al., 2002; Tanaka et al., 2005). This may have a direct impact in

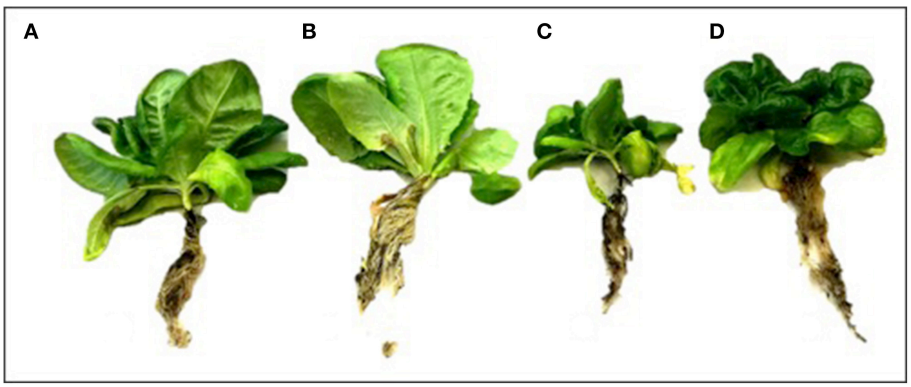


**FIGURE 4 |** Morphology of lettuce plants after 90 day in each treatment. Uninoculated (S–) plant without salt stress **(A)**; Plants inoculated with a mix of Antarctic microorganisms (S+) not subjected to salt stress **(B)**; S– plants under salt stress (200 mM NaCl) **(C)**; S+ plant under salt stress (200 mM NaCl) **(D)**. Image credit: H. Hansen.


**FIGURE 5 |** Final mean fresh biomass weight for roots, shoots and whole individuals of lettuce plants after being subjected for 60 days to saline stress (200 mM NaCl for "stressed" individuals) and inoculated with the Antarctic microbial consortium (S+ plants). Control groups for both conditions (non-stressed and non-inoculated, S–) are also shown. The box-plot represents the interquartile distribution of the data for each experimental group. Different letters indicate significant *a posteriori* differences (Tukey test, $\alpha < 0.05$).

the physiological processes of the plant that are N-limited like carbon assimilation, and ultimately, growth, especially in soils with low degradation rates of organic matter in the rhizosphere (Jumpponen and Trappe, 1998; Upson et al., 2009). In this regard, diverse enzymes from root-fungal endophytes have been observed to degrade organic molecules like cellulose, lipids, starch, and complex proteins (Petrini et al., 1993; Caldwell et al., 2000; Suryanarayanan et al., 2012). For this reason, it has been proposed that the metabolic activity of these endophytes propitiates the nutritional enhancement of the rhizosphere in which their plant-host is developing (Newsham, 2011).

More similar to the proline response, the augmentation of the *NHX1* gene expression observed among inoculated individuals represents a direct effect of the interaction on the response capacity of the host-plant against saline stress. Linked with the synthesis of the NHX antiporter proteins, the expression of the *NHX1* gene has been associated with pH control and $Na^+$/ $K^+$ homeostasis (Leidi et al., 2010; Bassil and Blumwald, 2014), cell expansion (Apse et al., 2003) and salt tolerance (Hernández et al., 2009; Bassil and Blumwald, 2014). A generally accepted mode of operation of this protein is the transport of either $K^+$ or $Na^+$ into vacuoles in exchange of an $H^+$efflux to the cytosol (Bassil and Blumwald, 2014). These antiporters also contribute to $K^+$ uptake which is stored in specific vacuoles for turgor-generation and cell pH regulation (Leidi et al., 2010). This prevents toxic $Na^+$: $K^+$ ratios in the cytosol while accruing solutes for osmotic balance (McCubbin et al., 2014), for which the vacuolar accumulation of these elements is an especially crucial feature for plants under osmotic stress (Jiang et al., 2010).

For example, the PGPR *B. subtilis* can also decrease the absorption of excessive amounts of $Na^+$ by the roots of plants by down-regulating the expression of the high affinity $K^+$ transporter (*HKT1*) in the roots of salt-affected plants (Zhang et al., 2008; Qin et al., 2016). In addition, the effect of *B. subtilis* also was related with the shoot-to-root $Na^+$ recirculation by triggering the induction of *HKT1* in shoots (Zhang et al., 2008). On the other hand, inoculation with fungal endohytes like *Piriformospora indica* have also resulted in increases in the expression of *NHX1* in salt-grown *Arabidopsis* compared to non-inoculated individuals (Abdelaziz et al., 2017). In our study, inoculated lettuce plants induced high levels of *NHX1* transcripts both under control and salt-stress conditions. However, it is under saline conditions where the relative expression increase appeared to be relevant, reaching almost a two-fold increase in the expression compared with non-inoculated plants.

In conclusion, we could determine that the selected consortium of Antarctic extremophiles effectively reduces the physiological impact of saline stress in a salt-susceptible crop like lettuce, as observed at both the individual and cellular levels. Interestingly, in terms of photochemical efficiency, the

studied symbiosis leads to increases in plant performance even in the absence of saline stress. Nevertheless, under saline-stress, the responses of inoculated lettuce plants largely exceed those of non-inoculated individuals, both in terms of proline concentration and *NHX1* relative expression. Furthermore, as a consequence of this enhanced saline-stress tolerance, inoculated plants finalize their productivity cycle with a higher size than their non-inoculated counterparts. This may respond to the higher levels of photosynthetic efficiency sustained over time even under saline conditions, complemented with the decrease in the oxidative effects derived from saline-related ions, which appeared to be controlled by great amounts of NHX antiporters. The role of proline in stabilizing the cellular membranes under salt stress was also evident from the reduced lipid peroxidation measured as TBARS in inoculated plants, which showed almost a three-fold reduction compared with non-inoculated but stressed individuals.

Finally, the use of microorganisms associated with plants from stressful sites appears as a powerful tool for improving salt stress tolerance in intolerant (susceptible) crops. A variety of symbiotic microorganisms are now being used worldwide with the aim of enhancing plant productivity, especially on agricultural crops under saline stress conditions (Kim et al., 2014; Kaushal and Wani, 2016; Orhan, 2016; Qin et al., 2016; Singh and Jha, 2016; Etesami and Beattie, 2018). However, while most studies analyzed the effect of a single symbiotic partner, the high diversity of occurring microorganisms also implies a wide spectrum of physiological and biochemical effects. In this sense, while it is expected that we should aim to fully understand the nature of each plant-microbe relation, broad benefits for a potential plant-host could arise from the "consortium" approach to its symbiotic interactions (Sturz and Nowak, 2000; Faust, 2019).

## AUTHOR CONTRIBUTIONS

MM-M, IA-R, and HH designed the experiments. MM-M, JG-C, and HH performed the experiments. MM-M, IA-R, HH, and CA analyzed the data. IA-R and MM-M wrote the paper along with HH, JG-C, and CA. All authors reviewed the manuscript.

## FUNDING

MM-M was funded by FONDECYT regular 1181034.

## ACKNOWLEDGMENTS

We thank Instituto Antártico Chileno (INACH) and the Chilean Navy for logistics and field support. All sampling was performed in accordance to international permits and authorizations given by INACH. MM-M thanks to Milko Jorquera for the invitation to participate of this special issue.

## REFERENCES

Abdelaziz, M. E., Kim, D., Ali, S., Fedoroff, N. V., and Al-Babili, S. (2017). The endophytic fungus *Piriformospora indica* enhances *Arabidopsis thaliana* growth and modulates Na+/K+ homeostasis under salt stress conditions. *Plant Sci.* 263, 107–115. doi: 10.1016/j.plantsci.2017.07.006

Ahmed, C. B., Magdich, S., Rouina, B. B., Sensoy, S., Boukhris, M., and Abdullah, F. B. (2011). Exogenous proline effects on water relations and ions contents in leaves and roots of young olive. *Amino Acids* 40, 565–573. doi: 10.1007/s00726-010-0677-1

Alberdi, M., Bravo, L. A., Gutiérrez, A., Gidekel, M., and Corcuera, L. J. (2002). Ecophysiology of Antarctic vascular plants. *Physiol. Plant.* 115, 479–486. doi: 10.1034/j.1399-3054.2002.1150401.x

Allbed, A., and Kumar, L. (2013). Soil Salinity mapping and monitoring in arid and semi-arid regions using remote sensing technology: a review. *Adv. Remote Sens.* 2, 373–385. doi: 10.4236/ars.2013.24040

Apse, M. P., Sottosanto, J. B., and Blumwald, E. (2003). Vacuolar cation/H+ exchange, ion homeostasis, and leaf development are altered in a T-DNA insertional mutant of AtNHX1, the Arabidopsis vacuolar Na+/H+ antiporter. *Plant J.* 36, 229–239. doi: 10.1046/j.1365-313X.2003.01871.x

Ashraf, M. P. J. C., and Harris, P. J. C. (2004). Potential biochemical indicators of salinity tolerance in plants. *Plant Sci.* 166, 3–16. doi: 10.1016/j.plantsci.2003.10.024

Assaha, D. V., Ueda, A., Saneoka, H., Al-Yahyai, R., and Yaish, M. W. (2017). The role of Na+ and K+ transporters in salt stress adaptation in glycophytes. *Front. Physiol.* 8:509. doi: 10.3389/fphys.2017.00509

Barassi, C. A., Ayrault, G., Creus, C. M., Sueldo, R. J., and Sobrero, M. T. (2006). Seed inoculation with *Azospirillum* mitigates NaCl effects on lettuce. *Sci. Hortic.* 109, 8–14. doi: 10.1016/j.scienta.2006.02.025

Barka, E. A., Gognies, S., Nowak, J., Audran, J. C., and Belarbi, A. (2002). Inhibitory effect of endophyte bacteria on *Botrytis cinerea* and its influence to promote the grapevine growth. *Biol. Control* 24, 135–142. doi: 10.1016/S1049-9644(02)00034-8

Bassil, E., and Blumwald, E. (2014). The ins and outs of intracellular ion homeostasis: NHX-type cation/H+ transporters. *Curr. Opin. Plant Biol.* 22, 1–6. doi: 10.1016/j.pbi.2014.08.002

Bates, L. S., Waldren, R. P., and Teare, I. D. (1973). Rapid determination of free proline for water-stress studies. *Plant Soil* 39, 205–207. doi: 10.1007/BF00018060

Bianco, C., and Defez, R. (2009). *Medicago truncatula* improves salt tolerance when modulated by an indole-3-acetic acid-overproducing *Sinorhizobium meliloti* strain. *J. Exp. Bot.* 60, 3097–3107. doi: 10.1093/jxb/erp140

Caldwell, B. A., Jumpponen, A., and Trappe, J. M. (2000). Utilization of major detrital substrates by dark-septate, root endophytes. *Mycologia* 92, 230–232. doi: 10.2307/3761555

Chang, S., Puryear, J., and Cairney, J. (1993). A simple and efficient method for isolating RNA from pine trees. *Plant Mol. Biol. Rep.* 11, 113–116. doi: 10.1007/BF02670468

Cocking, E. C. (2003). Endophytic colonization of plant roots by nitrogen-fixing bacteria. *Plant Soil* 252, 169–175. doi: 10.1023/A:1024106605806

Coleman-Derr, D., and Tringe, S. G. (2014). Building the crops of tomorrow: advantages of symbiont-based approaches to improving abiotic stress tolerance. *Front. Microbiol.* 5:283. doi: 10.3389/fmicb.2014.00283

Convey, P., Gibson, J. A., Hillenbrand, C. D., Hodgson, D. A., Pugh, P. J., Smellie, J. L., et al. (2008). Antarctic terrestrial life–challenging the history of the frozen continent? *Biol. Rev.* 83, 103–117. doi: 10.1111/j.1469-185X.2008.00034.x

Creus, C. M., Sueldo, R. J., and Barassi, C. A. (2004). Water relations and yield in *Azospirillum*-inoculated wheat exposed to drought in the field. *Can. J. Bot.* 82, 273–281. doi: 10.1139/b03-119

Dodd, I. C., and Pérez-Alfocea, F. (2012). Microbial amelioration of crop salinity stress. *J. Exp. Bot.* 63, 3415–3428. doi: 10.1093/jxb/ers033

Egamberdieva, D., Berg, G., Lindström, K., and Räsänen, L. A. (2013). Alleviation of salt stress of symbiotic *Galega officinalis* L. *(goat's rue)* by co-inoculation of Rhizobium with root-colonizing Pseudomonas. *Plant Soil* 369, 453–465. doi: 10.1007/s11104-013-1586-3

Egert, M., and Tevini, M. (2002). Influence of drought on some physiological parameters symptomatic for oxidative stress in leaves of chives (*Allium schoenoprasum*). *Environ. Exp. Bot.* 48, 43–49. doi: 10.1016/S0098-8472(02)00008-4

Etesami, H., and Beattie, G. A. (2018). Mining halophytes for plant growth-promoting halotolerant bacteria to enhance the salinity tolerance of non-halophytic crops. *Front. Microbiol.* 9:148. doi: 10.3389/fmicb.2018.00148

Fardella, C., Oses, R., Torres-Díaz, C., and Molina-Montenegro, M. A. (2014). Antarctic fungal endophytes as tool for the reintroduction of native plant species in arid zones. *Bosque* 35, 235–239. doi: 10.4067/S0717-92002014000200011

Faust, K. (2019). Microbial consortium design benefits from metabolic modeling. *Trends Biotechnol.* 37, 123–125. doi: 10.1016/j.tibtech.2018.11.004

Food and Agriculture Organization of the United Nations (2009). *State of Food Insecurity in the World 2009*. Rome: FAO.

Forni, C., Duca, D., and Glick, B. R. (2017). Mechanisms of plant response to salt and drought stress and their alterations by rhizobacteria. *Plant Soil* 410, 335–356. doi: 10.1007/s11104-016-3007-x

Gallardo-Cerda, J., Levihuan, J., Lavín, P., Oses, R., Atala, C., Torres-Díaz, C., et al. (2018). Antarctic rhizobacteria improve salt tolerance and physiological performance of the Antarctic vascular plants. *Polar Biol.* 41, 1973–1982. doi: 10.1007/s00300-018-2336-z

Glenn, E. P., Brown, J. J., and Blumwald, E. (1999). Salt tolerance and crop potential of halophytes. *Crit. Rev. Plant Sci.* 18, 227–255. doi: 10.1080/07352689991309207

Glick, B. R., Liu, C., Ghosh, S., and Dumbroff, E. B. (1997). Early development of canola seedlings in the presence of the plant growth-promoting rhizobacterium *Pseudomonas putida* GR12-2. *Soil Biol. Biochem.* 29, 1233–1239. doi: 10.1016/S0038-0717(97)00026-6

Godfray, H. C. J., Beddington, J. R., Crute, I. R., Haddad, L., Lawrence, D., Muir, J. F., et al. (2010). Food security: the challenge of feeding 9 billion people. *Science* 327, 812–818. doi: 10.1126/science.1185383

Greenfield, M., Gómez-Jiménez, M. I., Ortiz, V., Vega, F. E., Kramer, M., and Parsa, S. (2016). *Beauveria bassiana* and *Metarhizium anisopliae* endophytically colonize cassava roots following soil drench inoculation. *Biol. Control* 95, 40–48. doi: 10.1016/j.biocontrol.2016.01.002

Hadi, F., Bano, A., and Fuller, M. P. (2010). The improved phytoextraction of lead (Pb) and the growth of maize (*Zea mays* L.): the role of plant growth regulators (GA3 and IAA) and EDTA alone and in combinations. *Chemosphere* 80, 457–462. doi: 10.1016/j.chemosphere.2010.04.020

Hayat, S., Hayat, Q., Alyemeni, M. N., Wani, A. S., Pichtel, J., and Ahmad, A. (2012). Role of proline under changing environments: a review. *Plant Signal. Behav.* 7, 1456–1466. doi: 10.4161/psb.21949

Hernández, A., Jiang, X., Cubero, B., Nieto, P. M., Bressan, R. A., Hasegawa, P. M., et al. (2009). Mutants of the *Arabidopsis thaliana* cation/H+ antiporter AtNHX1 conferring increased salt tolerance in yeast. The endosome/prevacuolar compartment is a target for salt toxicity. *J. Biol. Chem.* 284, 14276–14285. doi: 10.1074/jbc.M806203200

Hodges, D. M., DeLong, J. M., Forney, C. F., and Prange, R. K. (1999). Improving the thiobarbituric acid-reactive-substances assay for estimating lipid peroxidation in plant tissues containing anthocyanin and other interfering compounds. *Planta* 207, 604–611. doi: 10.1007/s004250050524

Jiang, X., Leidi, E. O., and Pardo, J. M. (2010). How do vacuolar NHX exchangers function in plant salt tolerance? *Plant Signal. Behav.* 5, 792–795. doi: 10.4161/psb.5.7.11767

Joshi, R., Mangu, V. R., Bedre, R., Sanchez, L., Pilcher, W., Zandkarimi, H., et al. (2015). "Salt adaptation mechanisms of halophytes: improvement of salt tolerance in crop plants" in *Elucidation of Abiotic Stress Signaling in Plants*, ed K. P. Girdhar (New York, NY: Springer), 243–279.

Jumpponen, A. R. I., and Trappe, J. M. (1998). Dark septate endophytes: a review of facultative biotrophic root-colonizing fungi. *N. Phytol.* 140, 295–310. doi: 10.1046/j.1469-8137.1998.00265.x

Kang, S. M., Radhakrishnan, R., Khan, A. L., Kim, M. J., Park, J. M., Kim, B. R., et al. (2014). Gibberellin secreting rhizobacterium, *Pseudomonas putida* H-2-3 modulates the hormonal and stress physiology of soybean to improve the plant growth under saline and drought conditions. *Plant Physiol. Biochem.* 84, 115–124. doi: 10.1016/j.plaphy.2014.09.001

Kang, S. M., Radhakrishnan, R., You, Y. H., Khan, A. L., Park, J. M., Lee, S. M., et al. (2015). Cucumber performance is improved by inoculation with plant growth-promoting microorganisms. *Acta Agric. Scand.* 65, 36–44. doi: 10.1080/09064710.2014.960889

Karlidag, H., Yildirim, E., Turan, M., Pehluvan, M., and Donmez, F. (2013). Plant growth-promoting rhizobacteria mitigate deleterious effects of salt stress on strawberry plants (*Fragaria* × *ananassa*). *Hortscience* 48, 563–567. doi: 10.21273/HORTSCI.48.5.563

Kaushal, M., and Wani, S. P. (2016). Rhizobacterial-plant interactions: strategies ensuring plant growth promotion under drought and salinity stress. *Agric. Ecosyst. Environ.* 231, 68–78. doi: 10.1016/j.agee.2016.06.031

Khan, A. L., Waqas, M., Khan, A. R., Hussain, J., Kang, S. M., Gilani, S. A., et al. (2013). Fungal endophyte *Penicillium janthinellum* LK5 improves growth of ABA-deficient tomato under salinity. *World J. Microbiol. Biotechnol.* 29, 2133–2144. doi: 10.1007/s11274-013-1378-1

Kim, K., Jang, Y. J., Lee, S. M., Oh, B. T., Chae, J. C., and Lee, K. J. (2014). Alleviation of salt stress by *Enterobacter sp*. EJ01 in tomato and *Arabidopsis* is accompanied by up-regulation of conserved salinity responsive factors in plants. *Mol. Cells* 37:109. doi: 10.14348/molcells.2014.2239

Kohler, J., Hernández, J. A., Caravaca, F., and Roldán, A. (2009). Induction of antioxidant enzymes is involved in the greater effectiveness of a PGPR versus AM fungi with respect to increasing the tolerance of lettuce to severe salt stress. *Environ. Exp. Bot.* 65, 245–252. doi: 10.1016/j.envexpbot.2008.09.008

Krishna, G., Singh, B. K., Kim, E. K., Morya, V. K., and Ramteke, P. W. (2015). Progress in genetic engineering of peanut (*Arachis hypogaea* L.)—A review. *Plant Biotechnol. J.* 13, 147–162. doi: 10.1111/pbi.12339

Kumari, S., Vaishnav, A., Jain, S., Varma, A., and Choudhary, D. K. (2015) Bacterial-mediated induction of systemic tolerance to salinity with expression of stress alleviating enzymes in soybean (*Glycine max* L. Merrill). *J. Plant Growth Regul.* 34, 558–573. doi: 10.1007/s00344-015-9490-0

Leidi, E. O., Barragán, V., Rubio, L., El-Hamdaoui, A., Ruiz, M. T., Cubero, B., et al. (2010). The AtNHX1 exchanger mediates potassium compartmentation in vacuoles of transgenic tomato. *Plant J.* 61, 495–506. doi: 10.1111/j.1365-313X.2009.04073.x

Lenth, R., Love, J., and Hervé, M. (2018). *'emmeans': Estimated Marginal Means, aka Least-Squares Means.* R-package, version 1.2.2. Available online at: https://CRAN.R-project.org/package=emmeans

Livak, K. J., and Schmittgen, T. D. (2001). Analysis of relative gene expression data using real-time quantitative PCR and the 2– ΔΔCT method. *Methods* 25, 402–408. doi: 10.1006/meth.2001.1262

López-Gómez, M., Hidalgo-Castellanos, J., Iribarne, C., and Lluch, C. (2014). Proline accumulation has prevalence over polyamines in nodules of *Medicago sativa* in symbiosis with *Sinorhizobium meliloti* during the initial response to salinity. *Plant Soil* 374, 149–159. doi: 10.1007/s11104-013-1871-1

Maxwell, K., and Johnson, G. N. (2000). Chlorophyll fluorescence a practical guide. *J. Exp. Bot.* 51, 659–668. doi: 10.1093/jexbot/51.345.659

Mayak, S., Tirosh, T., and Glick, B. R. (2004). Plant growth-promoting bacteria confer resistance in tomato plants to salt stress. *Plant Physiol. Biochem.* 42, 565–572. doi: 10.1016/j.plaphy.2004.05.009

McCubbin, T., Bassil, E., Zhang, S., and Blumwald, E. (2014). Vacuolar Na+/H+ NHX-type antiporters are required for cellular K+ homeostasis, microtubule organization and directional root growth. *Plants* 3, 409–426. doi: 10.3390/plants3030409

Molina-Montenegro, M. A., Oses, R., Torres-Díaz, C., Atala, C., Zurita-Silva, A., and Ruiz-Lara, S. (2016). Root-endophytes improve the ecophysiological performance and production of an agricultural species under drought condition. *AoB Plants* 8:plw062. doi: 10.1093/aobpla/plw062

Molina-Montenegro, M. A., Salgado-Luarte, C., Oses, R., and Torres-Díaz, C. (2013). Is physiological performance a good predictor for fitness? Insights from an invasive plant species. *PLoS ONE* 8:e76432. doi: 10.1371/journal.pone.0076432

Molina-Montenegro, M. A., Zurita-Silva, A., and Oses, R. (2011). Effect of water availability on physiological performance and lettuce crop yield (*Lactuca sativa*). *Ciencia e Investigación Agraria* 38, 65–74. doi: 10.4067/S0718-16202011000100006

Munns, R. (1993). Physiological processes limiting plant growth in saline soils: some dogmas and hypotheses. *Plant Cell Environ.* 16, 15–24. doi: 10.1111/j.1365-3040.1993.tb00840.x

Munns, R., and James, R. A. (2003). Screening methods for salinity tolerance: a case study with tetraploid wheat. *Plant Soil* 253, 201–218. doi: 10.1023/A:1024553303144

Munns, R., and Tester, M. (2008). Mechanisms of salinity tolerance. *Annu. Rev. Plant Biol.* 59, 651–681. doi: 10.1146/annurev.arplant.59.032607.092911

Newsham, K. K. (2011). A meta-analysis of plant responses to dark septate root endophytes. *N. Phytol.* 190, 783–793. doi: 10.1111/j.1469-8137.2010.03611.x

Nissen, J., and San martín, K. (2004). Uso de poliacrilamidas y el riego en el manejo hídrico de lechugas (*Lactuca sativa* L.). *Agro Sur.* 32, 1–12. doi: 10.4206/agrosur.2004.v32n2-01

Orhan, F. (2016). Alleviation of salt stress by halotolerant and halophilic plant growth-promoting bacteria in wheat (*Triticum aestivum*). *Braz. J. Microbiol.* 47, 621–627. doi: 10.1016/j.bjm.2016.04.001

Pandey, G. K., Kanwar, P., Singh, A., Steinhorst, L., Pandey, A., Yadav, A. K., et al. (2015). CBL-interacting protein kinase, CIPK21, regulates osmotic and salt stress responses in Arabidopsis. *Plant Physiol.* 169, 780–792. doi: 10.1104/pp.15.00623

Parnikoza, I., Kozeretska, I., and Kunakh, V. (2011). Vascular plants of the Maritime Antarctic: origin and adaptation. *Am. J. Plant Sci.* 2, 381–395. doi: 10.4236/ajps.2011.23044

Paul, D., and Lade, H. (2014). Plant-growth-promoting rhizobacteria to improve crop growth in saline soils: a review. *Agron. Sustain. Dev.* 34, 737–752. doi: 10.1007/s13593-014-0233-6

Petrini, O., Sieber, T. N., Toti, L., and Viret, O. (1993). Ecology, metabolite production, and substrate utilization in endophytic fungi. *Nat. Toxins* 1, 185–196. doi: 10.1002/nt.2620010306

Pfaffl, M. W. (2001). A new mathematical model for relative quantification in real-time RT–PCR. *Nucleic Acids Res.* 29, e45–e45. doi: 10.1093/nar/29.9.e45

Pinheiro, J., Bates, D., DebRoy, S., Sarkar, D., Heisterkamp, S., Van Willigen, B., et al. (2017). *'nlme': Linear and Nonlinear Mixed Effects Models*. R-package version 3.1. Available online at: https://cran.r-project.org/web/packages/nlme/nlme.pdf

Qin, Y., Druzhinina, I. S., Pan, X., and Yuan, Z. (2016). Microbially mediated plant salt tolerance and microbiome-based solutions for saline agriculture. *Biotechnol. Adv.* 34, 1245–1259. doi: 10.1016/j.biotechadv.2016.08.005

Radhakrishnan, R., Khan, A. L., Kang, S. M., and Lee, I. J. (2015). A comparative study of phosphate solubilization and the host plant growth promotion ability of *Fusarium verticillioides* RK01 and *Humicola sp.* KNU01 under salt stress. *Ann. Microbiol.* 65, 585–593. doi: 10.1007/s13213-014-0894-z

Ramos, P., Rivas, N., Pollmann, S., Casati, P., and Molina-Montenegro, M. A. (2018). Hormonal and physiological changes driven by fungal endophytes increase Antarctic plant performance under UV-B radiation. *Fungal Ecol.* 34, 76–82. doi: 10.1016/j.funeco.2018.05.006

Reddy, P. S., Jogeswar, G., Rasineni, G. K., Maheswari, M., Reddy, A. R., Varshney, R. K., et al. (2015). Proline over-accumulation alleviates salt stress and protects photosynthetic and antioxidant enzyme activities in transgenic sorghum [*Sorghum bicolor* (L.) Moench]. *Plant Physiol. Biochem.* 94, 104–113. doi: 10.1016/j.plaphy.2015.05.014

Redman, R. S., Kim, Y. O., Woodward, C. J., Greer, C., Espino, L., Doty, S. L., et al. (2011). Increased fitness of rice plants to abiotic stress via habitat adapted symbiosis: a strategy for mitigating impacts of climate change. *PLoS ONE* 6:e14823. doi: 10.1371/journal.pone.0014823

Rho, H., Hsieh, M., Kandel, S. L., Cantillo, J., Doty, S. L., and Kim, S. H. (2017). Do endophytes promote growth of host plants under stress? A meta-analysis on plant stress mitigation by endophytes. *Microb. Ecol.* 75, 407–418. doi: 10.1007/s00248-017-1054-3

Rohlf, F. J., and Sokal, R. R. (1981). *Biometry: The Principles and Practice of Statistics in Biological Research*. New York, NY: WH Freeman.

Rozema, J., and Flowers, T. (2008). Crops for a salinized world. *Science* 322, 1478–1480. doi: 10.1126/science.1168572

Ruíz-Carrasco, K., Antognoni, F., Coulibaly, A. K., Lizardi, S., Covarrubias, A., Martínez, E. A., et al. (2011). Variation in salinity tolerance of four lowland genotypes of quinoa (*Chenopodium quinoa* Willd.) as assessed by growth, physiological traits, and sodium transporter gene expression. *Plant Physiol. Biochem.* 49, 1333–1341. doi: 10.1016/j.plaphy.2011.08.005

Saha, J., Brauer, E. K., Sengupta, A., Popescu, S. C., Gupta, K., and Gupta, B. (2015). Polyamines as redox homeostasis regulators during salt stress in plants. *Front. Environ. Sci.* 3:21. doi: 10.3389/fenvs.2015.00021

Saikkonen, K., Faeth, S. H., Helander, M., and Sullivan, T. J. (1998). Fungal endophytes: a continuum of interactions with host plants. *Annu. Rev. Ecol. Systemat.* 29, 319–343. doi: 10.1146/annurev.ecolsys.29.1.319

Sánchez, C. H. A. (2000). Response of lettuce to water and nitrogen on sand and the potential for leaching of nitrate-N. *Hortic. Sci.* 35, 73–75. doi: 10.21273/HORTSCI.35.1.73

Santiago, I. F., Rosa, C. A., and Rosa, L. H. (2017). Endophytic symbiont yeasts associated with the Antarctic angiosperms *Deschampsia antarctica* and *Colobanthus quitensis*. *Polar Biol.* 40, 177–183. doi: 10.1007/s00300-016-1940-z

Shahid, M. A., Balal, R. M., Pervez, M. A., Abbas, T., Aqeel, M. A., Javaid, M. M., et al. (2014). Exogenous proline and proline-enriched *Lolium perenne* leaf extract protects against phytotoxic effects of nickel and salinity in *Pisum sativum* by altering polyamine metabolism in leaves. *Turk. J. Bot.* 38, 914–926. doi: 10.3906/bot-1312-13

Singh, R. P., and Jha, P. N. (2016). The multifarious PGPR *Serratia marcescens* CDP-13 augments induced systemic resistance and enhanced salinity tolerance of wheat (*Triticum aestivum* L.). *PLoS ONE* 11:e0155026. doi: 10.1371/journal.pone.0155026

Sturz, A. V., and Nowak, J. (2000). Endophytic communities of rhizobacteria and the strategies required to create yield enhancing associations with crops. *Appl. Soil Ecol.* 15, 183–190. doi: 10.1016/S0929-1393(00)00094-9

Sun, M. H., Ma, Q. J., Liu, X., Zhu, X. P., Hu, D. G., and Hao, Y. J. (2017). Molecular cloning and functional characterization of MdNHX1 reveals its involvement in salt tolerance in apple calli and Arabidopsis. *Sci. Hortic.* 215, 126–133. doi: 10.1016/j.scienta.2016.11.031

Suryanarayanan, T. S., Thirunavukkarasu, N., Govindarajulu, M. B., and Gopalan, V. (2012). Fungal endophytes: an untapped source of biocatalysts. *Fungal Divers.* 54, 19–30. doi: 10.1007/s13225-012-0168-7

Szabados, L., and Savoure, A. (2010). Proline: a multifunctional amino acid. *Trends Plant Sci.* 15, 89–97. doi: 10.1016/j.tplants.2009.11.009

Székely, G., Ábrahám, E., Csépl,o, Á., Rigó, G., Zsigmond, L., Csiszár, J., et al. (2008). Duplicated P5CS genes of Arabidopsis play distinct roles in stress regulation and developmental control of proline biosynthesis. *Plant J.* 53, 11–28. doi: 10.1111/j.1365-313X.2007.03318.x

Tanaka, A., Tapper, B. A., Popay, A., Parker, E. J., and Scott, B. (2005). A symbiosis expressed non-ribosomal peptide synthetase from a mutualistic fungal endophyte of perennial ryegrass confers protection to the symbiotum from insect herbivory. *Mol. Microbiol.* 57, 1036–1050. doi: 10.1111/j.1365-2958.2005.04747.x

Tester, M., and Davenport, R. (2003). Na+ tolerance and Na+ transport in higher plants. *Ann. Bot.* 91, 503–527. doi: 10.1093/aob/mcg058

Torres-Díaz, C., Gallardo-Cerda, J., Lavin, P., Oses, R., Carrasco-Urra, F., Atala, C., et al. (2016). Biological interactions and simulated climate change modulates the ecophysiological performance of *Colobanthus quitensis* in the Antarctic ecosystem. *PLoS ONE* 11:e0164844. doi: 10.1371/journal.pone.0164844

Upson, R., Read, D. J., and Newsham, K. K. (2009). Nitrogen form influences the response of *Deschampsia antarctica* to dark septate root endophytes. *Mycorrhiza* 20, 1–11. doi: 10.1007/s00572-009-0260-3

Vandenkoornhuyse, P., Quaiser, A., Duhamel, M., Le Van, A., and Dufresne, A. (2015). The importance of the microbiome of the plant holobiont. *N. Phytol.* 206, 1196–1206. doi: 10.1111/nph.13312

Yildirim, E., and Taylor, A. G. (2005). Effect of biological treatments on growth of bean plants under salt stress. *Annu. Rep. Been Improvement Cooperat.* 48, 176–177. Available online at: http://arsftfbean.uprm.edu/bic/wp-content/uploads/2018/05/BIC_2005_volume_48.pdf

Zhang, H., Kim, M. S., Sun, Y., Dowd, S. E., Shi, H., and Paré, P. W. (2008). Soil bacteria confer plant salt tolerance by tissue-specific regulation of the sodium transporter *HKT1*. *Mol. Plant Microbe Interact.* 21, 737–744. doi: 10.1094/MPMI-21-6-0737

Zheng, Y. H., Xu, X. B., Wang, M. Y., Zheng, X. H., Li, Z. J., and Jiang, G. M. (2009). Responses of salt-tolerant and intolerant wheat genotypes to sodium chloride: photosynthesis, antioxidants activities, and yield. *Photosynthetica* 47, 87–94. doi: 10.1007/s11099-009-0014-7

Zhu, J. K. (2001). Plant salt tolerance. *Trends Plant Sci.* 6, 66–71. doi: 10.1016/S1360-1385(00)01838-0

**Conflict of Interest Statement:** The authors declare that the research was conducted in the absence of any commercial or financial relationships that could be construed as a potential conflict of interest.

frontiers in Bioengineering and Biotechnology

ORIGINAL RESEARCH
published: 21 February 2019
doi: 10.3389/fbioe.2019.00030

# Identification and Characterization of Five Cold Stress-Related Rhododendron Dehydrin Genes: Spotlight on a FSK-Type Dehydrin With Multiple F-Segments

*Hui Wei*[1,2*†], *Yongfu Yang*[3†], *Michael E. Himmel*[1], *Melvin P. Tucker*[4], *Shi-You Ding*[5,6], *Shihui Yang*[3*] and *Rajeev Arora*[2*]

[1] National Renewable Energy Laboratory, Biosciences Center, Golden, CO, United States, [2] Department of Horticulture, Iowa State University, Ames, IA, United States, [3] State Key Laboratory of Biocatalysis and Enzyme Engineering, Hubei Collaborative Innovation Center for Green Transformation of Bio-Resources, Environmental Microbial Technology Center of Hubei Province, Hubei Key Laboratory of Industrial Biotechnology, School of Life Sciences, Hubei University, Wuhan, China, [4] National Renewable Energy Laboratory, National Bioenergy Center, Golden, CO, United States, [5] DOE-Great Lakes Bioenergy Research Center, Michigan State University, East Lansing, MI, United States, [6] Department of Plant Biology, Michigan State University, East Lansing, MI, United States

OPEN ACCESS

**Edited by:**
Steffen P. Graether,
University of Guelph, Canada

**Reviewed by:**
George Richard Strimbeck,
Norwegian University of Science and Technology, Norway
Juan F. Jimenez,
Instituto Potosino de Investigación Científica y Tecnológica (IPICYT), Mexico

***Correspondence:**
Hui Wei
hui.wei@nrel.gov
Shihui Yang
shihui.yang@hubu.edu.cn
Rajeev Arora
rarora@iastate.edu

[†] These authors have contributed equally to this work

**Specialty section:**
This article was submitted to Bioprocess Engineering, a section of the journal Frontiers in Bioengineering and Biotechnology

**Received:** 13 October 2018
**Accepted:** 05 February 2019
**Published:** 21 February 2019

**Citation:**
Wei H, Yang Y, Himmel ME, Tucker MP, Ding S-Y, Yang S and Arora R (2019) Identification and Characterization of Five Cold Stress-Related Rhododendron Dehydrin Genes: Spotlight on a FSK-Type Dehydrin With Multiple F-Segments. Front. Bioeng. Biotechnol. 7:30. doi: 10.3389/fbioe.2019.00030

Dehydrins are a family of plant proteins that accumulate in response to dehydration stresses, such as low temperature, drought, high salinity, or during seed maturation. We have previously constructed cDNA libraries from *Rhododendron catawbiense* leaves of naturally non-acclimated (NA; leaf $LT_{50}$, temperature that results in 50% injury of maximum, approximately −7°C) and cold-acclimated (CA; leaf $LT_{50}$ approximately −50°C) plants and analyzed expressed sequence tags (ESTs). Five ESTs were identified as dehydrin genes. Their full-length cDNA sequences were obtained and designated as *RcDhn 1-5*. To explore their functionality vis-à-vis winter hardiness, their seasonal expression kinetics was studied at two levels. Firstly, in leaves of *R. catawbiense* collected from the NA, CA, and de-acclimated (DA) plants corresponding to summer, winter and spring, respectively. Secondly, in leaves collected monthly from August through February, which progressively increased freezing tolerance from summer through mid-winter. The expression pattern data indicated that *RcDhn 1-5* had 6- to 15-fold up-regulation during the cold acclimation process, followed by substantial down-regulation during deacclimation (even back to NA levels for some). Interestingly, our data shows RcDhn 5 contains a histidine-rich motif near N-terminus, a characteristic of metal-binding dehydrins. Equally important, RcDhn 2 contains a consensus 18 amino acid sequence (i.e., ETKDRGLFDFLGKKEEEE) near the N-terminus, with two additional copies upstream, and it is the most acidic (pI of 4.8) among the five RcDhns found. The core of this consensus 18 amino acid sequence is a 11-residue amino acid sequence (DRGLFDFLGKK), recently designated in the literature as the F-segment (based on the pair of hydrophobic F residues it contains). Furthermore, the 208 orthologs of F-segment-containing RcDhn 2 were identified across a broad range of species in GenBank database. This study expands our knowledge about the types of F-segment

from the literature-reported single F-segment dehydrins ($FSK_n$) to two or three F-segment dehydrins: *Camelina sativa* dehydrin ERD14 as $F_2S_2K_n$ type; and RcDhn 2 as $F_3SK_n$ type identified here. Our results also indicate some consensus amino acid sequences flanking the core F-segment in dehydrins. Implications for these cold-responsive RcDhn genes in future genetic engineering efforts to improve plant cold hardiness are discussed.

**Keywords: expressed sequence tags (EST), gene expression profiling, cold hardiness, *Rhododendron*, cold acclimation, deacclimation, FSK-type dehydrins, dehydrin F-segment**

## INTRODUCTION

Survival and growth of woody plants in cold climate is important for traditional sectors of horticulture and forestry. One advantage of using Rhododendron as a material to study cold-hardiness physiology is the wide range of leaf and bud cold (freezing) tolerance among species (Sakai, 1986). *Rhododendron,* like many other woody perennials, can adapt to harsh winter through a process called cold acclimation (CA), by which they develop tolerance to low temperature and freezing seasonally, with hardiness increasing through the autumn, peaking in midwinter, declining during the spring, and reaching the lowest in summer (Arora and Taulavuori, 2016).

Cold acclimation is considered to be an active process that involves a wide range of physiological and biochemical reprogramming, including altered membrane structure and function (Yamada et al., 2002), as well as myriad of changes in primary and secondary metabolisms (Guy, 1990; Thomashow, 1990, 1998); most of these are also accompanied by related changes in protein/gene expression. As the D-11 subgroup of late embryogenesis abundant proteins (Dure, 1993), dehydrins have been found to play an important role in plant defense against dehydration stresses, including freeze-desiccation stress (Lin and Thomashow, 1992; Close, 1996; Wisniewski et al., 2003; Kaplan et al., 2004; Kosová et al., 2007; Tunnacliffe and Wise, 2007). The defining characteristic of plant dehydrins is the existence of a putative amphipathic α-helix-forming domain, called the conserved K-segment (Close, 1997; Malik et al., 2017). It has been shown that dehydrins are located in the nucleus or cytoplasm of the cell (Close, 1997), specifically in the vicinity of the plasma membrane (Danyluk et al., 1998), cytoplasmic endomembrane (Egerton-Warburton et al., 1997), and plasmodesmata (Karlson et al., 2003). In addition, their high concentrations in cells (Baker et al., 1988), add to the appeal as engineering targets for enhancing plant stress defense capacity.

We had previously generated 862 5′-end high-quality ESTs from cold acclimated (CA) and non-acclimated (NA; non-cold-hardened) leaves of field grown plants of *Rhododendron catawbiense*, a cold-hardy North American rhododendron species (Wei et al., 2005a). NA (summer-collected) and CA (winter-collected) leaves were also evaluated for cold-hardiness in a laboratory-based freeze-thaw assay which indicated their leaf-freezing tolerance (defined as $LT_{50}$, temperature that results in 50% injury of maximum) to be approximately −7° and −50°C, respectively. Comparative analysis of NA- and CA-EST data sets revealed cDNAs for five dehydrins that were more abundant in the more cold-hardy CA tissues (Wei et al., 2005a), and are thus of interest for further characterization. In the present study, sequence analyses of these five rhododendron dehydrins were performed to characterize their conserved motif features. In addition, the seasonal gene expression of individual dehydrins was characterized using northern blot and RT-PCR, providing experimental information on their cold-acclimation-response. Furthermore, a thorough bioinformatic analysis was carried out for an identified 18 amino acid sequence (ETKDRGLFDFLGKKEEEE) located in one of the rhododendron dehydrins. Interestingly, the center part of this consensus 18 amino acid sequence is a 11-residue amino acid sequence (DRGLFDFLGKK) that has been recently identified and named as the "F-segment" based on the pair of hydrophobic F residues it contains (Strimbeck, 2017). This present study, however, expands our knowledge regarding the types of F-segment peptides found in the known single copy ($FSK_n$) dehydrins to the $F_2S_2K_n$ or $F_3SK_n$ dehydrins which contain two or three F-segments (this study). Our bioinformatic analysis also indicates some consensus amino acid sequences flanking the core F-segment in at least some of the F-segment containing dehydrins. Potential use of the identified cold stress-related rhododendron dehydrins for plant engineering is also discussed.

**Abbreviations:** ABA, abscisic acid; CA, cold-acclimated; DA, de-acclimated; Dhn, dehydrin; EST, expressed sequence tag; NA, non-acclimated; RcDhn, *Rhododendron catawbiense* dehydrin.

## MATERIALS AND METHODS

The overall experimental and analysis approaches are illustrated in **Figure 1**.

### Sample Collection

Field-grown plants of *R. catawbiense*, maintained at The Holden Arboretum's David G. Leach Research Station in Madison, Ohio, were used for this study. Two sets of leaf samples were collected from these plants to determine the changes of dehydrin expression profiles. The first set of leaf samples was the seasonal collection representing summer (July), winter (January), and the following spring (May). Summer and winter-collected samples represent NA and CA leaves, respectively; whereas the spring collection is for tissues that are expected to have lost their previously acquired (during fall/winter) cold hardiness in a process called deacclimation (DA) upon the return of warmer temperatures in spring (Kalberer et al., 2006).

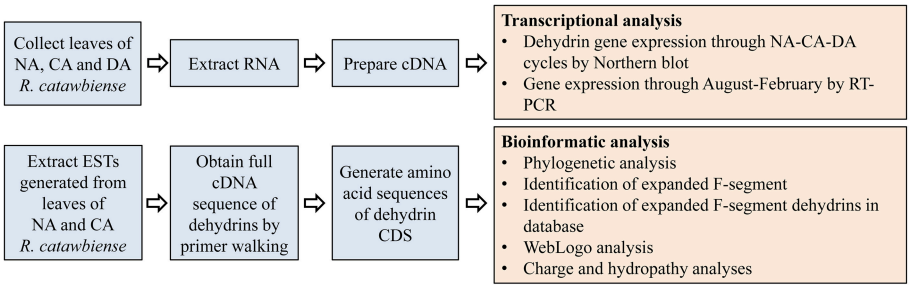


**FIGURE 1 |** Diagram of the outline for the experimental design and analyses.: CA, cold-acclimated; DA, de-acclimated; EST, expressed sequence tag; NA, non-acclimated.

Together, this sampling represented annual cycle of NA-CA-DA tissues. Leaf freezing tolerance, defined as $LT_{50}$, of NA and CA leaves, was found to be −7° and −53°C, respectively (Wei et al., 2005a). Whereas precise freezing tolerance of deacclimated leaves (May collection) could not be ascertained for this study, it can be safely assumed to be substantially lower than cold acclimated levels (from January) and closer to that of non-acclimated tissues (Kalberer et al., 2006). The second set of leaf samples was approximately monthly collections from August through February, representing the period of gradual/seasonal development of cold acclimation from summer (August) through the fall/early winter (September, October, November) reaching close to maximal cold-hardiness by January. For all the samplings, leaf tissues were flash frozen in liquid nitrogen and stored at −80°C until RNA and cDNA preparations.

## RNA Extraction

Total RNA was extracted according to the modified hot-borate method of Wilkins and Smart (Wilkins and Smart, 1996). The prepared RNA was dissolved in DEPC treated water and store at −80°C until use.

## Northern Blot

Equal amounts of total RNA (8 μg) extracted from leaf tissues were denatured and fractionated on 1% (w/v) formaldehyde-agarose gels for electrophoresis, followed by viewing and photographing under UV light to confirm RNA quality and equal sample loading. The transfer of RNA to nylon membranes, the preparation of DNA probes corresponding to cDNA inserts of interest, and the hybridization conditions were described previously (Wei et al., 2005a). After the northern blotting, the intensity of positive bands was analyzed by densitometry using imaging software (NIH Image version 1.41, National Institutes of Health, Bethesda, MD).

## Reverse Transcription

For each sample's reverse transcription (RT), RNA was treated with DNase I (amplification grade; Invitrogen, Carlsbad, CA) to avoid contamination with genomic DNA. First-strand cDNA was synthesized using 3 μg of total RNA with the Superscript RT III kit (Invitrogen, Carlsbad, CA) and random hexamer primers for 18S and *R. catawbiense* ubiquitin-like (*RcUbql*) genes (used for initial reference gene screening), or oligo(dT)18 for *RcUbql* gene and dehydrin genes (used in formal functional gene screening) according to the manufacturer's instructions. The total RT reaction volume was 20 μL and was further diluted to 80 μL by adding DEPC-treated water (thus each μL contained "first-strand cDNA" derived from approximately 40 ng of initial total RNA). This was used as "first-strand cDNA" for regular RT-PCR and real-time RT-PCR as described below. A second aliquot of total RNA (also 3 μg) was treated using $ddH_2O$ instead of reverse transcriptase and used as minus reverse transcriptase (–RT) controls for monitoring any genomic DNA contamination or nonspecific DNA amplification.

## Selection and Validation of *RcUbql* as Reference Genes for Regular and Real-Time RT-PCR

As in our EST dataset, we have identified the EST for *RcUbql* (GenBank accession No. CV015651), which allowed us to design a pair of primers for both regular RT-PCR and real-time RT-PCR with an amplicon size of 254 bp (**Table 1**). To validate the suitability of *RcUbql* as the reference gene, the Quantum RNA Universal 18S Internal Standards primers (amplicon size of 315 bp; Ambion, Austin, TX, USA) were used as an internal standard with 18S primers-to-competimers ratio of 3:7. As described by the manufacturer's manual, the 18S rRNA and our target gene (*RcUbql*) were amplified in a multiplex reaction using the above-mentioned random hexamer primers-reverse transcribed cDNA as templates.

## Regular RT-PCR and Real-Time RT-PCR

The primers used for both regular and real-time RT-PCR are listed in **Table 1**. Whereas, the regular RT-PCR with three different cycle numbers provided a visual, traditional means to examine the expression level of target genes, the real-time RT-PCR allowed a more accurate, quantitative assessment of the gene expressions.

For regular RT-PCR, which was used in parallel to real-time RT-PCR (as described below) to detect the expression level of dehydrin genes and *RcUbql* gene, the "first-strand cDNA" (derived from approximately 40 ng of initial total RNA) was used in a final reaction of 20 μL containing 0.2 mM dNTP, 2 mM $MgCl_2$, 625 nM of each forward and reverse primers and 1 unit

**TABLE 1 |** Primer sequences for regular and real-time RT-PCR.

| *Dhn* genes | Forward primer | Amplicon size (bp) |
|---|---|---|
| *RcDhn* 1 | F: CCACCAGTCCCACGACACTA<br>R: TACCCACCACCTGCTCCAG | 57 |
| *RcDhn* 2 | F: AAGGATGGGTTGTTGACGAAGT<br>R: TTCCTCCGAAGAGCTTGAGC | 51 |
| *RcDhn* 3 | F: ATCGCCCCGTCCTAATCTTCT<br>R: CCCTCGAGACTCCGTCCAC | 71 |
| *RcDhn* 4 | F: CGTGGACAAGGTGAAGGACAA<br>R: ACTAGCGGCGGAAAAGAAGAT | 111 |
| *RcDhn* 5 | F: AAGTTCCACCGTTCCGATAGC<br>R: ATTCGTGTCCTCCTCGTGCT | 128 |
| *RcUbql* | F: AGAGGTGGTGTTGAACGATCG<br>R: TCTCGCACTTATTACCGCACA | 254 |

*GenBank accession No. for RcDhn 1-5 can be found in* ***Table 2****, while that for RcUbql is CV015651.*

of Taq. The setup reaction mixture was subjected to regular RT-PCR at three different cycle numbers empirically determined for amplification at non-saturation levels (28, 32, and 36 cycles for most transcripts). This setup ensured that the amount of amplified products stayed in the linear proportion to the initial template amount present in the reaction under at least one of these three cycle numbers. The PCR products were separated and analyzed on agarose gels.

For real-time RT-PCR, the "first-strand cDNA" (equivalent to approximately 10 ng of initial total RNA extracted from leaf tissues) was used in a final reaction of 20 μL containing 1X SYBR Master Mix, 625 nM forward primer and 625 nM reverse primer, using ABI optical tube and caps. All reactions were performed in triplicate and repeated in two independent experiments. The real-time RT-PCR were performed in ABI model 7000 sequence detection system (Applied Biosystems, Foster City, CA). Thermal cycling conditions consisted of 2 min at 94°C for denaturation and 40 cycles of amplification (15 s at 94°C, 30 s at 59°C, 20 s at 72°C), followed by standard dissociation procedure. PCR data were analyzed with the sequence detection software version 1.2.3.

PCR amplification efficiency of real-time RT-PCR was determined using the absolute fluorescence method (Ramakers et al., 2003), in which a serial cDNA template dilutions were conducted to obtain the standard curves. The resultant PCR efficiency for each gene's primers was calculated. Expression level of test gene (i.e., *RcDhn 1-4*) relative to reference gene (*RcUbql*) was calculated using the comparative CT method, i.e., by subtracting the CT of reference gene from the test gene CT according to the function ΔCT = CT (test gene)—CT (reference gene). To obtain the seasonal changes in expression levels of a certain *RcDhn* gene, the function ΔΔCT was determined using the equation ΔΔCT = ΔCT(test gene in a specific month's sample)—ΔCT(test gene in August sample). The final fold change of a specific month against August was then calculated by the formula $2^{-\Delta\Delta Ct}$ in accordance with ABI sequence detection system user manual, with the gene expression level in August set as 1. For statistical analysis, the *p*-values were calculated using a Student's *t*-test on the fold change values, and the analyses were performed using Excel; significance was defined as $p<0.05$, whereas high significance was defined as $p < 0.01$.

## ESTs Source and Primer Walk to Obtain Full cDNA Sequence of Dehydrins

Previously, 423 and 439 5′ ESTs were generated from cold acclimated (CA) and non-acclimated (NA) leaves, respectively, of *R. catawbiense* (Wei et al., 2005a). These ESTs (GenBank accession nos. CV014938– CV015799) were clustered to produce a list of unique transcripts, which were annotated using PIR-NREF protein database (Protein Information Resource: Non-Redundant Reference) and BLASTX (Wei et al., 2005a). The study annotation led to the identification of five dehydrins, which were labeled as *RcDhn* 1-5, wherein "*Rc*" represents *R. catawbiense*, *Dhn* for dehydrin, and each gene has a unique number.

Sequences of full length dehydrin genes were obtained by primer-walking sequencing of the 5 *RcDhn* cDNA clones. The primers used were either the universal primers or designed based on the sequences of ESTs that also existed for cDNA clones. DNA multiple sequence alignments were conducted by using the Genetics Computer Group (GCG) PILEUP program (University of Wisconsin, Madison, WI, USA) to determine the full-length sequences of the cDNA clones.

## Open Reading Frame (ORF) of the Nucleotide Sequences and Protein Sequence Alignment

The full-length sequences of the *RcDhn* clones were input into the NCBI's ORF to deduce the amino acid sequences of the dehydrin genes. The most feasible ORF was determined by comparing the deduced amino acid sequence with the sequences in GenBank databases using the BLAST server. The resultant amino acid sequences were used to (1) identify the potential YSK segments of dehydrins, (2) identify the expanded F-segment (see below), and (3) align specific dehydrins of interest from other plant sources.

## Identification and Clustering of the Expanded F-Segment Containing Ortholog Proteins and Bioinformatics Analysis

The procedure for BlastP analyses to identify the homolog proteins that contain the conserved F-segment in protein database is outlined in **Figure 2**. The *R. catawbiense* dehydrin 2 (RcDhn 2) amino acid sequence obtained from NCBI (AGI36547) was used to search for other similar dehydrins using the local Protein-protein BLAST (BlastP) program against the non-redundant (NR) protein database. The e-value was set to 0.01 and other parameters kept at default. Consequently, 270 sequences were retained to do the next analysis after removing the 10 repeats in all 280 hits. Another local BlastP was performed to search for the similar amino acid consensus sequence using the 18 amino acid sequence initially identified in RcDhn 2 (ETKDRGLFDFLGKKEEEE) as the query and the 270 sequences as database. The e-value was set to 0.01

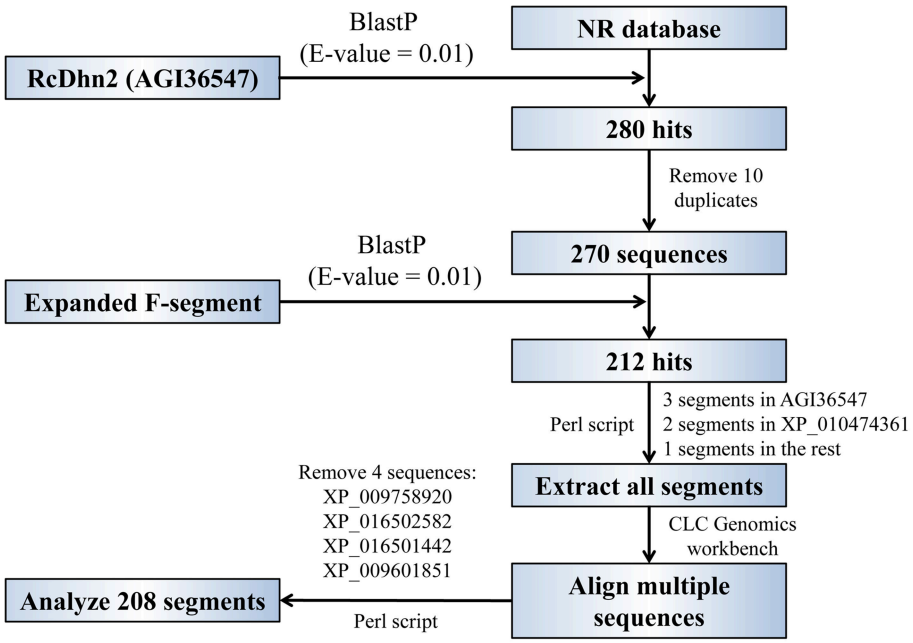


**FIGURE 2 |** Flowchart for global and local BlastP analyses to identify the homologous proteins that contain the conserved, expanded F-segment in protein database. See the Materials and Methods section for details.

and other parameters kept at default. There were 212 hits with AGI36547 (i.e., RcDhn 2 deposited into GenBank by our group) containing three F-segments, XP_010474361 containing two F-segments (*Camelina sativa* dehydrin ERD14; $F_2S_2K_n$ as illustrated in **Figure 3**, bottom panel), and the rest containing one F-segment.

The start and end positions of the 212 F-segments in the BlastP result was extracted using a customized Perl script, which were then used for multiple sequence alignment. Four segments containing two amino acid "CG" insertions may belong to another family and were removed for alignment, as illustrated in **Supplemental Figure S1**. The rest 208 segments were used for consensus sequence analysis and the unrooted evolutionary tree construction by using CLC Genomics workbench 9. The consensus sequence Logo was then constructed by WebLogo online server (http://weblogo.berkeley.edu/logo.cgi) (Schneider and Stephens, 1990; Crooks et al., 2004).

## Charge and Hydropathy Analyses of Conserved Segments of Dehydrins

For conserved segments, Peptide Analyzer (http://haubergs.com/peptide) was used to calculate the charge and hydropathy scores, and to generate hydropathy plot.

# RESULTS

## Sequence Analyses of *Rhododendron* Dehydrin Genes

BLASTX search of PIR-NREF protein database revealed that several ESTs from the CA library were identified as dehydrin transcripts encoding five distinct dehydrins (**Table 2**). Five corresponding cDNA clones from the cold-acclimated cDNA library (Wei et al., 2005a) were picked and cultured for plasmid extraction. The extracted plasmid DNA was sent to the DNA facility of Iowa State University for Primer Walking service to obtain the full-length sequence of these clones. The resultant sequence analysis showed that each cDNA contains the 3′ untranslated region, the start codon, stop codon, and the poly(A)+ tail, confirming that they represent the full-length genes (data not shown). The deduced amino acid sequences from these genes are shown in **Figure 3**.

As noted before, the distinct Dhn genes were referred by a nomenclature composed of five-letter (*RcDhn*) plus a sequential number (1 to 5), in which "*Rc*" represents *R. catawbiense*, *Dhn* for dehydrin. The dehydrin protein names follow the same convention, except that the letters are capitalized and not italicized. Based on the presence of certain consensus regions of amino acids in their sequence, dehydrins are conventionally described by the "YSK" shorthand, according to which plant dehydrins can be categorized into five distinct structural types: (1) $Y_nSK_n$, (2) $SK_n$, (3) $Y_nK_n$, (4) $K_n$, and (5) $K_nS$ (Close, 1996, 1997). Except for the type 5 ($K_nS$), other four types, 1 to 4, have been identified in *Rhododendron* in this study (**Table 2**). The predicted size of dehydrins identified was from 81 to 303 in amino acids (**Table 2**), which fits within the reported wide range of dehydrins (82-648 amino acids) (Close, 1996). Variation in isoelectric point is in the range of 4.8 to 6.9. It is suggested that each YSK structure type may bear a distinctive functional role (Svensson et al., 2002), thus we characterized each identified dehydrin as below.

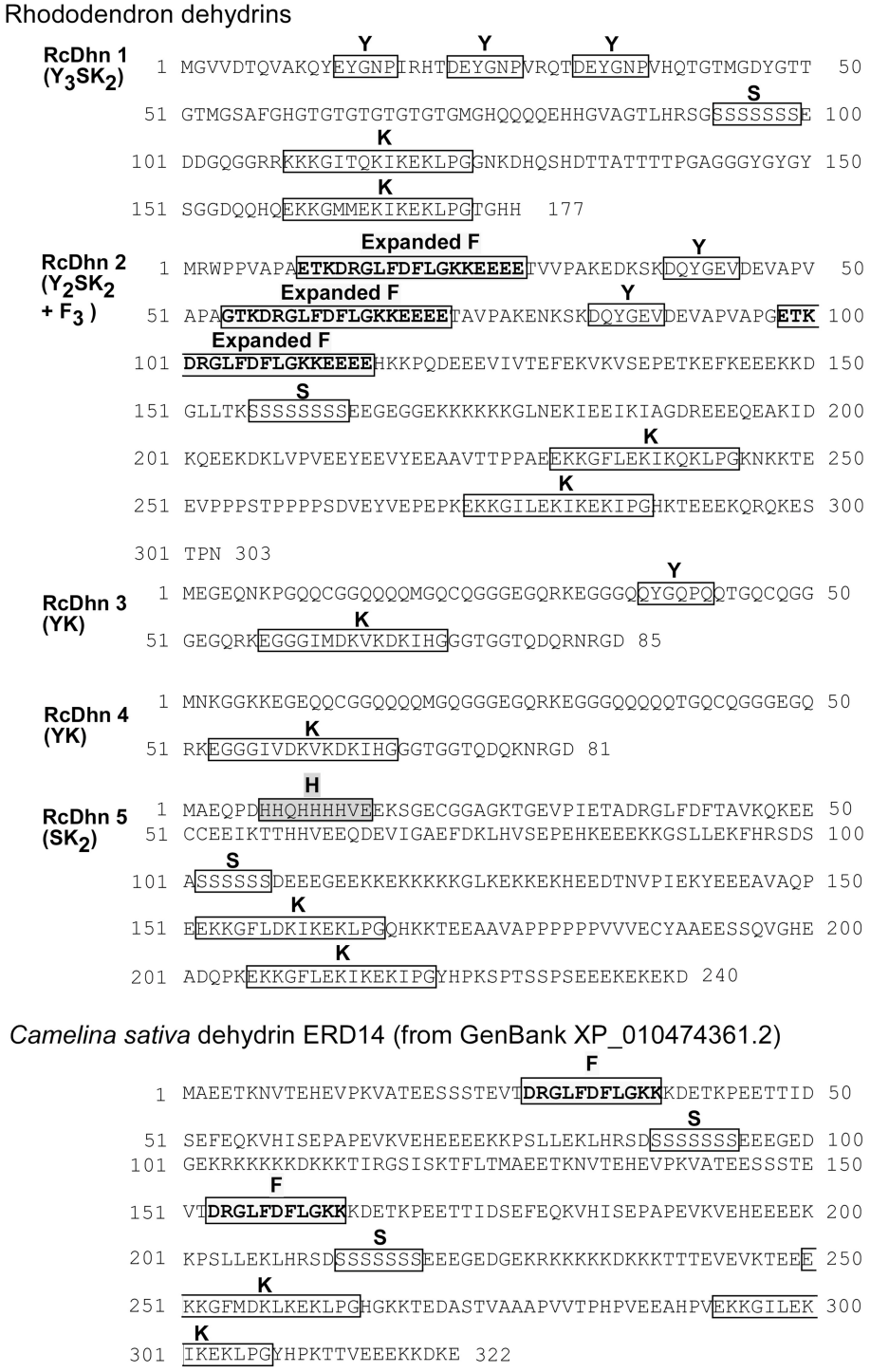


**FIGURE 3 |** Deduced amino acid sequences for *Rhododendron* dehydrins RcDhn 1-5 and *C. sativa* dehydrin ERD14. Amino-acid residues are designated in single-letter code. The Y-, S-, and K-segments are boxed. The defined expanded F-segments in RcDhn 2 are boxed and in boldface and yellow; the histidine-rich (H) segment are boxed and in pink. *C. sativa* dehydrin ERD14 was identified by our BlastP analysis hit against the NCBI protein database.

(1) **$Y_3SK_2$ type RcDhn 1**

$Y_3SK_2$ has been found widely across diverse plant species some of which include sunflower (*Helianthus annuus*), radish (*Raphanus sativus*) (Campbell and Close, 1997), *Arabidopsis thaliana* (Nylander et al., 2001; Svensson et al., 2002), *Brassica juncea* and *B. napus* (Yao et al., 2005).

**TABLE 2 |** Characteristics of *Rhododendron Dhn* genes and their protein products.

| *Dhn* genes | GenBank Protein No. (cDNA clone No.) | Dehydrin type | Amino acid number | MW | PI (kDa) | Picked times[a] |
|---|---|---|---|---|---|---|
| *RcDhn 1* | KC425881 (CA3A12) | $Y_3SK_2$ potato type | 177 | 20 | 6.5 | 1 |
| *RcDhn 2* | KC417479 (CA5B04) | $Y_2SK_2 + F_3$ | 303 | 34 | 4.8 | 1 |
| *RcDhn 3* | KC425882 (CA1F12) | $Y_1K_1$ | 85 | 10 | 6.9 | 4 |
| *RcDhn 4* | KC425883 (CA3E05) | $K_1$ blueberry type | 81 | 10 | 6.9 | 1 |
| *RcDhn 5* | ACB41781 (CA2D12) | $SK_2$ kidney bean type | 240 | 29 | 5.2 | 1 |

[a]*Number of times that a particular cDNA was picked from cDNA library (containing 423 5′ end ESTs) of rhododendron cold acclimated (CA) leaf tissues (Wei et al., 2005a).*

The transcript of sunflower $Y_3SK_2$ type dehydrin (*HaDhn1*) increased in abundance under water deficit stress (Cellier et al., 2000), while this type of dehydrins in *B. juncea* and *B. napus* were found to be expressed in germinating seeds and with enhanced cold tolerance during seedling emergence (Yao et al., 2005).

(2) **$Y_2SK_2 + F_3$ type RcDhn 2 ($F_3SK_2$)**
RcDhn 2 (Z05B04) belongs to the $Y_2SK_2$ type and can be distinguished from the other four rhododendron dehydrins because it has three copies of an unusual, expanded F-segment (ETKDRGLFDFLGKKEEEE), one of which is always present near the N-terminus (**Figure 3**; **Table 2**). Dehydrins with all three consensus segments, Y, S, and K, have been widely reported to occur in plants (Close, 1996; Wisniewski et al., 2006).

(3) **RcDhn 3 and RcDhn 4: the blueberry-type dehydrins**
RcDhn 3 (CA1F12; $Y_1K_1$) belongs to $Y_1K_1$ type (**Figure 3** and **Table 2**). Although $Y_nK_n$ dehydrins have been found in other species, such as $Y_2K_2$ (*Pisum sativum*) (Haider, 2012), and $Y_2K_9$ (*Prunus persica*) (Wisniewski et al., 2006), $Y_1K_1$ type has not been reported in literature based on our knowledge. RcDhn 4 (CA3E05; $K_1$) belongs to $K_1$ type (**Figure 3** and **Table 2**); unlike RcDhn 3, it lacks Y-segment. $K_n$ type dehydrins have been found in many other species, including $K_2$ in *Pseudotsuga menziesii*, $K_3$ in *Medicago falcata*, $K_6$ in *Triticum aestivum* and *A. thaliana*, and $K_9$ in *Hordeum vulgare* (Campbell and Close, 1997). In addition, $K_2$ type dehydrins also exist in *Pinus sylvestris* (GenBank accession No. CAD54624.1, CAD54623.1, and CAD54621.1). However, $K_1$ type has not been reported in other species so far. Since the defining feature of dehydrins is the conserved K-segment, the $K_1$ type RcDhn 4 is among the groups of a few simplest dehydrins reported so far with regard to deduced amino acid sequences(Lee et al., 2005). Except for the Y-segment, both RcDhns 3 and 4 have $K_1$ and also show considerable similarity to each other in their deduced amino acid sequences. BLAST search against NR-PIR database identified five blueberry (*Vaccinium corymbosum*) dehydrin orthologs (Dhanaraj et al., 2005). Since *Rhododendron* and blueberries both belong to the health family (*Ericaceae*), RcDhns 3 and 4 were thus labeled as blueberry-type dehydrins.

(4) **RcDhn 5: the kidney bean-type dehydrins**
RcDhn 5 (CA2D12; $SK_2$) is an acidic, $SK_2$ type dehydrin (**Figure 3** and **Table 2**); it lacks the Y-segment. It also contains a histidine-rich segment (HHQHHHHVE) close to N-terminus. $SK_2$ dehydrins have also been found in other woody plants like peach (*Prunus persica*) (GenBank accession No. AAZ83586) (Bassett et al., 2009) and birch in which the pre-exposure to short-day followed by low-temperature treatment led to a significant increase in the expression of a SK2 type dehydrin gene, compared with low-temperature-treated plants grown at long-day photoperiod (Puhakainen et al., 2004). Heterologous expression of this birch SK2 type dehydrin in *Arabidopsis* indicated that this short-day potentiation of gene expression could be tree-specific (Puhakainen et al., 2004).

## Seasonal Expression Profiling of RcDhn Genes by Northern Blot: Approach I to Identify Quantitative Expression of *RcDhns* vis-à-vis Seasonal Changes in Freezing Tolerance

To further investigate seasonal changes of *RcDhn*s during NA-CA-DA seasonal cycle, we used the respective gene probes to hybridize with the RNA extracted from the non-acclimated (NA), cold acclimated (CA), and deacclimated (DA) *Rhododendron* leaf tissues as described in the Materials and Methods. The northern blot results showed that the transcript levels of all five *RcDhns* followed a distinct seasonal cycle, i.e., relatively low levels in less-hardy tissues in summer followed by ∼5–14-fold accumulation (densitometric analysis) in much cold-hardier tissues in winter and then substantial decline in concert with a seasonal transition to spring with the expected loss of freezing tolerance (**Figure 4**; Peng et al., 2008). The magnitudes of fold-change of these genes among NA CA, and DA tissues indicate that they were all cold-responsive dehydrin genes.

It is noteworthy that northern blot analysis using *RcDhn 4* EST probe revealed three hybridizing mRNA bands of 2.0, 1.1, and 0.5 kb (**Figure 4**). The predominant band was 0.5 kb, corresponding to the expected size of the *RcDhn 4* EST, which had been previously deposited to GenBank by our group (accession no. CV015159, with mRNA length 491 bp) (Wei et al., 2005a). This *RcDhn 4* EST sequence was used to design primers (as listed in **Table 1**) for real-time RT-PCR analysis for its monthly expression profiling as described below. The occurrence of three bands on northern blot of *RcDhn 4* indicates the presence of three mature *RcDhn 4* transcripts, which could arise by either alternative splicing, and/or due to alternative transcription initiation or polyadenylation sites.

## Monthly Expression Profiling of *RcDhns* by RT-PCR: Approach II to Identify Cold Acclimation-Responsive Dehydrin Genes

The very hardy species, *R. catawbiense*, has the remarkable ability to increase their leaf freezing tolerance to cope

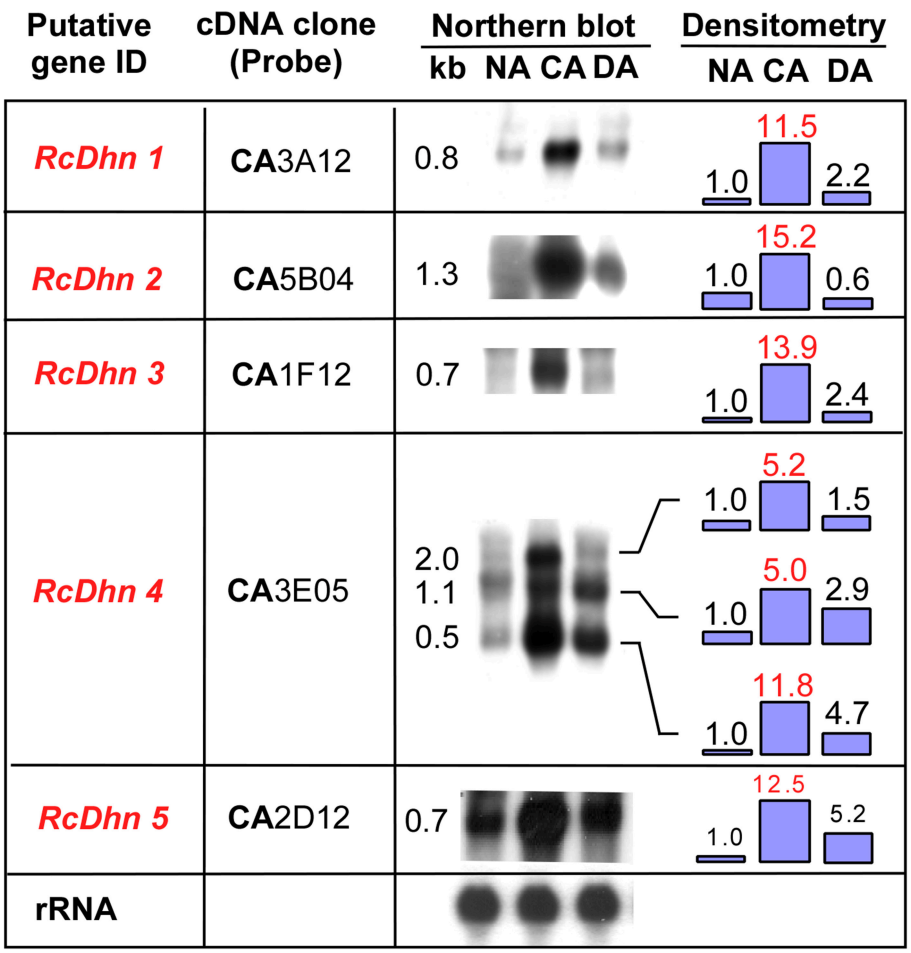


**FIGURE 4 |** Northern blot analysis for the seasonal expression levels of *RcDhn 1-5* in NA, CA, and DA leaf tissues. Total RNA (8 μg) was isolated and hybridized with respective cDNA probes. Lower panel shows control hybridization of the filters to rRNA using a blueberry cDNA probe confirming equal loadings among the lanes. Fold change in the expression level during cold acclimation and deacclimation relative to non-acclimated state (defined as '1') was estimated by densitometry. The putative genes in red text showed at least 5-fold differences in the intensity of bands of northern blot between NA and CA, thus defined as highly cold-responsive genes. *RcDhn 5*'s northern blot data were adapted from a previous study (Peng et al., 2008). CA, cold-acclimated; DA, de-acclimated; NA, non-acclimated.

with cold winters (Wei et al., 2005a; Wang et al., 2009). This study examined the monthly gene expression of five *RcDhns* using the samples collected monthly between August (summer) and January (winter); as well as late February. This work provides cold-acclimation-responsive dehydrin gene expression patterns with greater resolution than before, showing that leaf tissues progressively increase their freezing tolerance from summer through fall (Peng et al., 2008). Gene expression profiling was conducted using both regular RT-PCR and real-time RT-PCR. The relative expression levels in each cDNA sample were normalized by comparing the data to the reference gene (e.g., ubiquitin-like protein) in the same sample, which remained constant throughout the season changes. The threshold cycle (Ct) values and calculation worksheets for the fold changes of dehydrin gene expression are provided in **Additional File 2**, following the data presentation examples for semi-quantitative RT-PCR published in recent literature (Nguyen et al., 2014; Xiong et al., 2016; Feng et al., 2017; Sharma et al., 2017). The statistical analysis process and results are also included in the worksheets (**Additional File 2**).

The transcript levels of *RcDhns 1, 2, 3, 4,* and *5* followed an incremental accumulation pattern from late August (summer), through October (autumn) till January (winter). The accumulation of transcript began in early autumn (October), and reached a peak in January (**Figures 5**, **6**). Such accumulation pattern mirrors the monthly increase in leaf freezing tolerance from August through January in this species (Peng et al., 2008). Overall, the magnitude of changes of *RcDhns 1-5* genes in *R. catawbiense* between August and January, estimated by real-time RT-PCR, were in the range of 6- to 15-fold, confirming the results observed in the above Approach I for gene expression profiling and supported that they were all cold-acclimation-response dehydrins, which was also similar to the seasonal expression pattern of *RcDhn* 5 previously reported by our group (Peng et al., 2008).

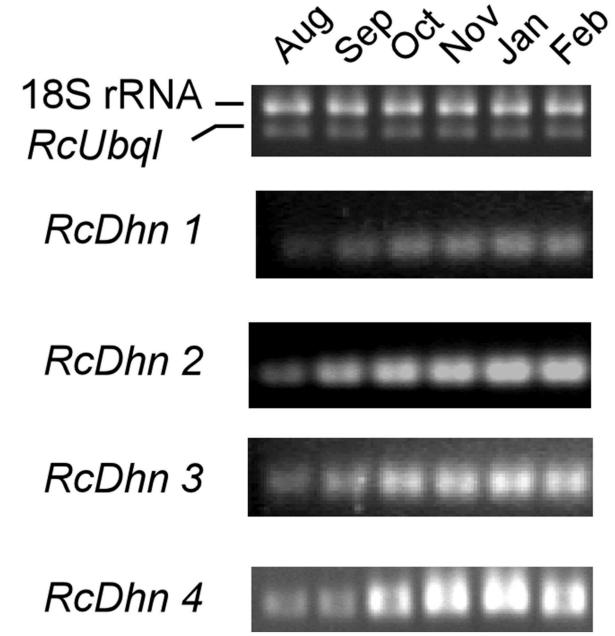


**FIGURE 5 |** Regular RT-PCR DNA gel images for monthly expression patterns of dehydrin genes in leaf tissues of field-grown *R. catawbiense* collected in August, September, October, November, January, and February. Total RNA extracted from leaf tissues were used for cDNA synthesis. Regular RT-PCR was conducted by using each dehydrin's primers, while the Universal 18S Internal Standards primers (Ambion) and gene-specific primers of rhododendron ubiquitin-like (*RcUbql*) gene were used as the mixed primers for the reference genes; the cycle numbers were 32, which was in the exponential phase of the PCR amplification.

## Orthologous Proteins of Cold-Responsive RcDhn 2 and Distribution of Expanded F-Segment in Protein Database

To investigate if an expanded F-segment found in RcDhn 2 is conserved in amino acid sequences relative to other dehydrins from other plant species, a bioinformatic study was conducted by two rounds of BlastP search as described in the Materials and Methods and outlined in **Figure 2**. Briefly, the first round of search was conducted by using the RcDhn 2 amino acid sequence to search for other similar dehydrins using the local BlastP program against the non-redundant protein database (NR), which generated 270 hits. The second round of local BlastP was performed to search for the expanded F-segment consensus sequence using the expanded F-segment initially identified in RcDhn 2 (ETKDRGLFDFLGKKEEEE) as the query and the 270 hits as the database, which led to 208 hits containing the expanded F-segments. Accordingly, the start and end positions of the 208 expanded F-segments in the BlastP result was extracted, and the NCBI accession numbers of resultant hit protein sequences and their contained expanded F-segment sequences are listed in **Supplemental Table S1**. These 208 expanded F-segment sequences were used to generate the unrooted evolutionary tree using CLC Genomics Workbench 9. Expanded F-segments can be arranged into classes 1, 2, 3, 4, and 5, among which the expanded F-segment in RcDhn 2 belongs to class 3 based on sequence similarity, as illustrated in **Figure 7**.

Furthermore, the 208 expanded F-segment sequences listed in **Supplemental Table S1** were used to generate the expanded F-segment consensus sequence, which is presented in two forms. The first form is the WebLogo graphic form (**Figure 8**, upper panel), which reveals the consensus sequence with a stack of amino acid letters, with the height of each letter representing the observed frequency of the corresponding amino acid at each position. The second form is the conventional form, which is illustrated in **Figure 8**, lower panel. Whereas, the original expanded F-segment identified in RcDhn 2 is ETKDRGLFDFLGKKEEEE, the expanded F-segment consensus sequence generated from 208 F-segment sequences is $E_{197}T_{67}K_{92}D_{188}R_{207}G_{207}L_{150}F_{200}D_{198}F_{204}L_{123}G_{167}K_{142}K_{149}E_{93}E_{114}E_{105}$.

## Comparison of the Expanded F-Segment With K-Segment

As listed in the **Supplemental Table S1**, the 208 expanded F-segment containing dehydrins were found to exist broadly across a range of species.

Bioinformatics analyses of charge and hydropathy were conducted for the expanded F-segment and the K-segment, the signature sequence of all dehydrins (Campbell and Close, 1997). The results show that the expanded F-segment, explored in this study, contains $K_3E_5D_2R_1$; whereas the K-segment consensus contains $K_5E_2D_1$, as illustrated in **Figure 9**. It is interesting to note that among the four most hydrophilic amino acids—glutamic acid (E), glutamine (Q), aspartic acid (D) and asparagine (N)—two of them (E and D) are present in the expanded F-segment and the K-segment, which lead to the overall hydrophilic nature of these two motifs. For these two motifs, the expanded F-segment has a more negative net charge (with a value of−3.0) (**Figure 9A**).

The hydropathy plots are shown in **Figure 9B**, in which the Kyte–Doolittle scale (Kyte and Doolittle, 1982) was used to compare hydrophobicity by which a positive score indicating hydrophobic and negative score indicating hydrophilic residues. The expanded F-segment has an unique hydropathy plot, which is significantly different from the K-segment (**Figure 9B**) and may have an implication for its role in interacting with other molecules and subcellular structures, differentiating it from the K-segment motif, as further explored below.

# DISCUSSION

## Possible Function for F-Segment Domain in Dehydrins

Although there is a general acceptance about a broad range of functions of dehydrins, a question still arises as to the fundamental biochemical role of F-segments in dehydrins. Strimbeck (2017) proposed that the F segment may form a

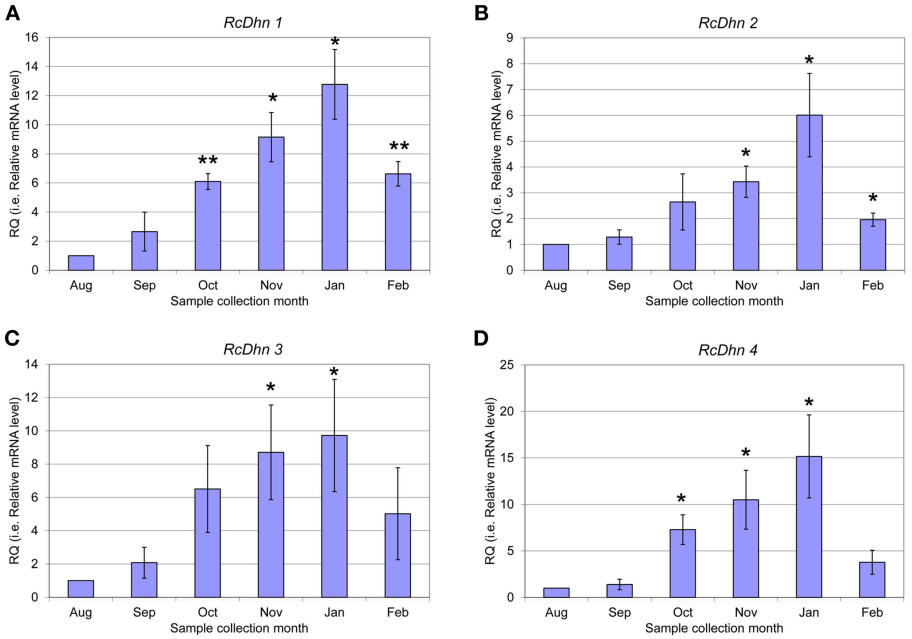


**FIGURE 6 |** Real-time RT-PCR analysis for monthly expression patterns of dehydrin genes in leaf tissues of field-grown *R. catawbiense* collected in August, September, October, November, January, and February **(A-D)** *RcDhn 1-4*. Total RNA extracted from leaf tissues were used for cDNA synthesis. Real-time RT-PCR was conducted by using each dehydrin's primers, while the gene-specific primers of rhododendron ubiquitin-like (*RcUbql*) gene for the reference gene. The monthly expression of each dehydrin gene was presented as the expression levels relative to its expression level in August (which was set at 1). * and ** indicate statistical significance of $p < 0.05$ and $p < 0.01$, respectively, comparing with the expression level in August.

short, amphipathic helix capable of binding with membranes or proteins (Strimbeck, 2017). Further biochemical characterization of the F-segments will provide more clues to its structural and functional roles, if any.

It is known that a group of calcium-binding proteins, including calreticulin, calsequestrin, calnexin, and calmegin, use the negatively charged, acidic amino acid region near the C-terminus to bind calcium at high capacity and low affinity (Corbett and Michalak, 2000; Alsheikh et al., 2003). Similarly, an acidic *Arabidopsis* dehydrin was also found to have the ion binding properties (Alsheikh et al., 2003). As described above, the expanded F-segment consensus contains $K_3E_5D_2R_1$, and has the lowest net charge (with a value of – 3.0) among three compared motifs. Not surprisingly, the expanded F-segment containing RcDhn 2 is an acidic dehydrin, with the lowest pI of all five RcDhns (a value of 4.8), and it is reasonable to speculate that RcDhn 2 and its orthologs in other species are also likely able to bind with ions, thus may play a role in water retention and/or directly replacing water for the "solvation" of the membrane.

## Implications for the Genetic Engineering of Plants

Dehydrins are a group of intrinsically disordered proteins (lacking secondary and tertiary structure) (Graether and Boddington, 2014) with multiple potential roles, such as cryoprotection, antifreeze proteins (Wisniewski et al., 1999; Reyes et al., 2008), metal binding/ion sequestration, antioxidants (Svensson et al., 2000; Alsheikh et al., 2003; Hara et al., 2005, 2013), and chaperone properties (Kovacs et al., 2008). Current study identified five *RcDhn* genes related to stress tolerance traits. These can be used for genetic engineering of plants to enhance their cold adaptation capacity. A previous study conducted by co-authors and collaborators supports the feasibility of this approach, demonstrating that *Arabidopsis* plants overexpressing RcDhn 5 were significantly more freeze-tolerant than the wild-type controls (Peng et al., 2008); same dehydrin also was shown to provide cryoprotection and dehydration-stress tolerance, *in vitro*, to cold labile lactate dehydrogenase protein (Peng et al., 2008; Reyes et al., 2008).

Based on the amino acid sequence data (**Figure 3**), we propose here that RcDhn 5 may also have a metal/ion-binding property. This SK2-type acidic dehydrin contains a histidine-rich sequence. Published research suggests that metal/ion binding property may be restricted to acidic, SK-type dehydrins (Alsheikh et al., 2005) and that histidine-rich motif is characteristic of metal binding proteins (Hernández-Sánchez et al., 2014). Hernández-Sánchez et al. (2015) reported that the deletion of histidine-rich motif in cactus dehydrin OpsDHN1 restricted its localization to cytoplasm, and the deletion of its S-segment also affected its nuclear localization (Hernández-Sánchez et al., 2015). We speculate that the histidine-rich motif of RcDhn5 may also be involved in the similar function as both histidine- and serine-rich motifs exist in RcDhn5, and further studies are needed to test this proposal.

It has also been shown for several SK-type dehydrins (ERD14, ERD10, and COR47 of *A. thaliana*) that activation of their ion-binding ($Ca^{2+}$—binding) property may require phosphorylation and that this phosphorylation site is contained within the serine

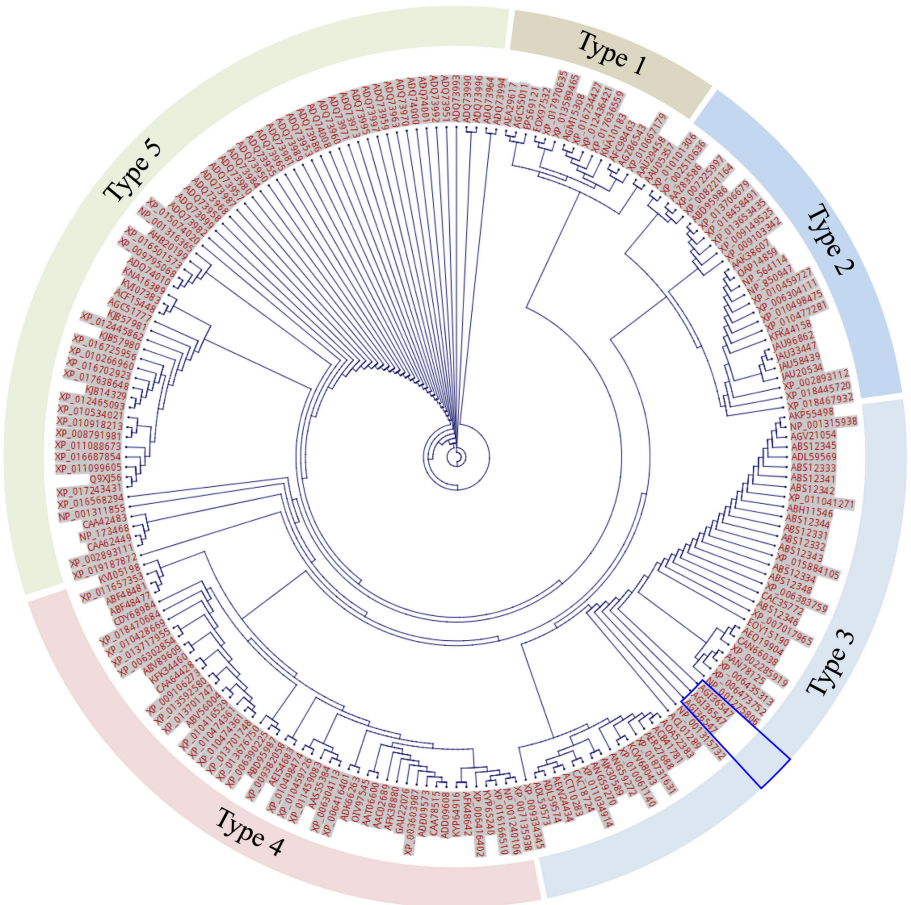


**FIGURE 7 |** Unrooted tree of total 208 expanded F-segment sequences using CLC Genomics Workbench. The labels beside each dot are protein NCBI accession numbers. The segments are arranged into 5 classes based on the genetic distance. The unique expanded F-segment (three copies from RcDhn 2) is highlighted by the blue box. All are eukaryotes.

(S) motif (Alsheikh et al., 2005). Presence of a serine tract in RcDhn 5 sequence (**Figure 3**) is in line with this proposition.

In addition, the transcript levels of all five RcDhns genes increased throughout the autumn and reached a peak in the middle of winter season (January), as illustrated in **Figures 5**, **6**. This prompts us to further propose that the sequences of *RcDhns* promoters can be explored for the temporal control of expressing heterologous cold-hardiness related genes aiming to enhance cold acclimation of plants. Literature shows that promoters selected from highly expressed genes are effective to build expression vector for expressing heterologous genes in eukaryotic organisms (Poulsen et al., 2006).

## Future Studies for Gene Structure Analysis of *RcDhn4* and Its Variants

It is interesting that we identified three mature transcripts of the *RcDhn 4* gene, which could arise by alternative splicing, and alternative transcription initiation or polyadenylation sites. Furthermore, it is noteworthy that SKn-type dehydrins are known to typically contain one intron sequence within the S-segment (Jiménez-Bremont et al., 2013). It would be interesting to determine, by obtaining and comparing the genomic sequence with the cDNA sequence of *RcDhn 4* gene, whether this gene also contains intron(s). If the presence of intron is indeed confirmed, it can be used to design the intron-flanking PCR molecular markers for rhododendron genetic mapping, since it is assumed that intronic regions have richer polymorphism than exonic regions (Wei et al., 2005b).

## CONCLUSION

Multiple approaches were taken to identify and characterize five RcDhns and examine their transcriptional profiling over the course of NA, CA and DA spanning from summer, autumn, winter, and spring. Their transcript expression patterns indicated that *RcDhn 1-5* had 5- to 10-fold upregulation during the cold acclimation process, followed by a significant downregulation in spring as plants lose their previously

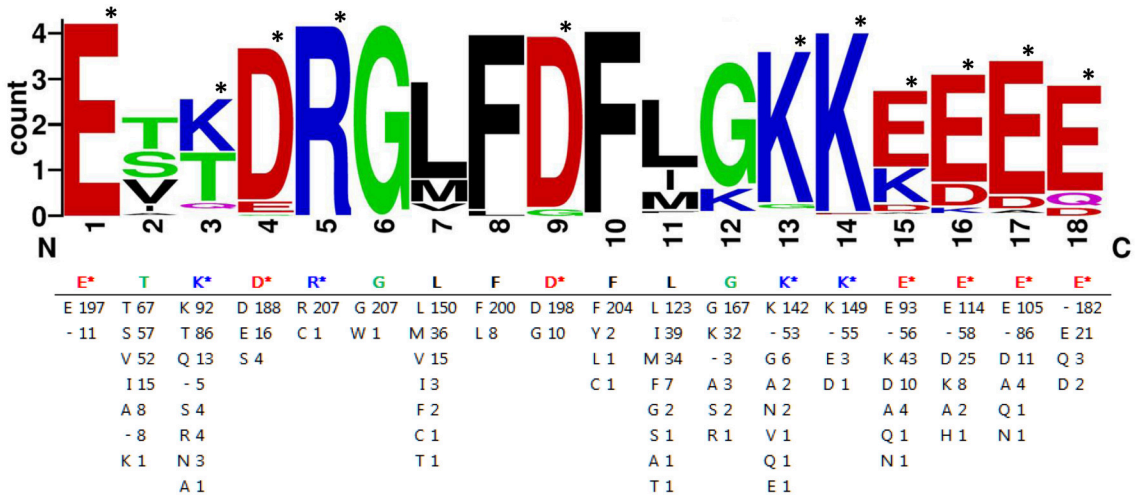


| | | | | | | | | | | | | | | | | | |
|---|---|---|---|---|---|---|---|---|---|---|---|---|---|---|---|---|---|
| E* | T | K* | D* | R* | G | L | F | D* | F | L | G | K* | K* | E* | E* | E* | E* |
| E 197 | T 67 | K 92 | D 188 | R 207 | G 207 | L 150 | F 200 | D 198 | F 204 | L 123 | G 167 | K 142 | K 149 | E 93 | E 114 | E 105 | - 182 |
| - 11 | S 57 | T 86 | E 16 | C 1 | W 1 | M 36 | L 8 | G 10 | Y 2 | I 39 | K 32 | - 53 | - 55 | - 56 | - 58 | - 86 | E 21 |
| | V 52 | Q 13 | S 4 | | | V 15 | | | L 1 | M 34 | - 3 | G 6 | E 3 | K 43 | D 25 | D 11 | Q 3 |
| | I 15 | - 5 | | | | I 3 | | | C 1 | F 7 | A 3 | A 2 | D 1 | D 10 | K 8 | A 4 | D 2 |
| | A 8 | S 4 | | | | F 2 | | | | G 2 | S 2 | N 2 | | A 4 | A 2 | Q 1 | |
| | - 8 | R 4 | | | | C 1 | | | | S 1 | R 1 | V 1 | | Q 1 | H 1 | N 1 | |
| | K 1 | N 3 | | | | T 1 | | | | A 1 | | Q 1 | | N 1 | | | |
| | | A 1 | | | | | | | | T 1 | | E 1 | | | | | |

**FIGURE 8 |** Consensus amino acids of expanded F-segment in dehydrin protein hits from BLASTP search against rhododendron expanded F-segment containing RcDhn2. The sequence graphics in the upper panel was created using WebLogo program. Single letters are abbreviations for amino acids. The number after the letters in the lower panel indicates the occurrence of each amino acid residue at each position. "-" represents a gap in alignment. The most hydrophilic amino acids lysine (K), glutamate (E), aspirate (D) and arginine (R) are indicated by the star marks (*), and counted as $K_3E_5D_2R_1$.

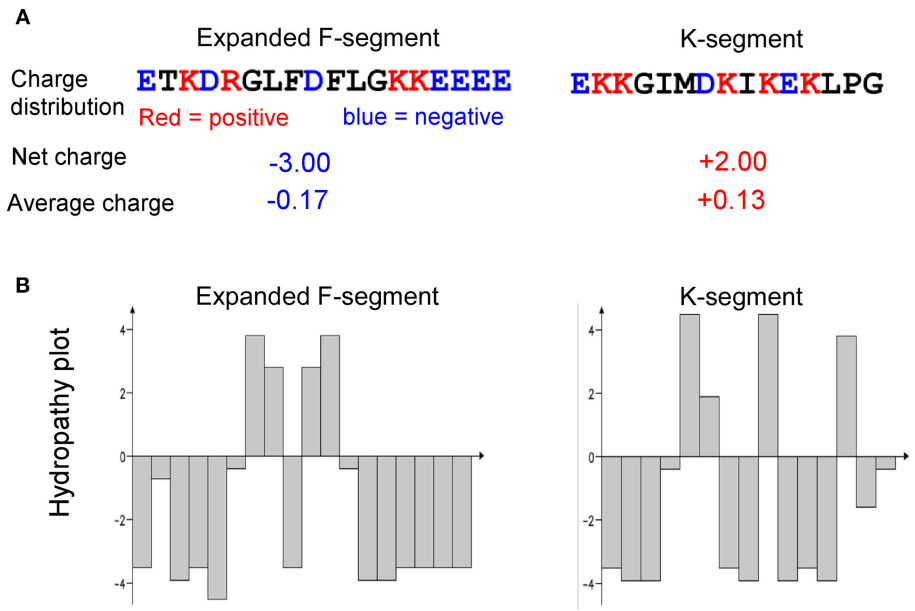


**FIGURE 9 |** Comparison of charge and hydropathy between the expanded F-segment and K-segment. **(A)** Charge profiling. **(B)** Hydropathy plot. K-segment was reported in literature as described in the text.

acquired freezing tolerance, supporting the roles of these cold-responsive genes in plant freezing tolerance. The identification of an unique expanded F-segment consensus sequence in RcDhn 2 and its orthologs across a broad range of species, together with their negative charge and hydrophilic nature, highlight their potential to be used for genetic engineering of crops and bioenergy plants for improved cold tolerance.

## AUTHOR CONTRIBUTIONS

RA and HW lead the project and coordinated the study, conceived designed and executed the experiments related to the transcriptional analysis. S-YD designed and YY executed the bioinformatic analysis. HW coordinated the manuscript preparation. All authors contributed to the data analyses, read, revised and approved the final manuscript.

## FUNDING

This journal paper of the Iowa Agriculture and Home Economics Experiment Station, Ames, Iowa, Project no. 3601 was supported by Hatch Act and State of Iowa funds to the research program of RA that also supported HW as a postdoctoral fellow. HW, MH, and MT were supported by the funding provided by U.S. Department of Energy Office of Energy Efficiency and Renewable Energy, Bioenergy Technologies Office (BETO), and by the Center for Direct Catalytic Conversion of Biomass to Biofuels (C3Bio), an Energy Frontier Research Center funded by the DOE Office of Science, Office of Basic Energy Sciences (Award Number DE-SC0000997). The National Renewable Energy Laboratory (NREL) is operated for the U.S. Department of Energy under Contract No. DE-AC36-08-GO28308. YY and SY acknowledge the support from State Key Laboratory of Biocatalysis and Enzyme Engineering and Technical Innovation Special Fund of Hubei Province (2018ACA149). S-YD was supported in part by the Great Lakes Bioenergy Research Center, U.S. Department of Energy, Office of Science, Office of Biological and Environmental Research under Award Number DE-SC0018409. The views expressed in the article do not necessarily represent the views of the DOE or the U.S. Government. The U.S. Government retains and the publisher, by accepting the article for publication, acknowledges that the U.S. Government retains a nonexclusive, paid-up, irrevocable, worldwide license to publish or reproduce the published form of this work, or allow others to do so, for U.S. Government purposes.

## SUPPLEMENTARY MATERIAL

The Supplementary Material for this article can be found online at: https://www.frontiersin.org/articles/10.3389/fbioe.2019.00030/full#supplementary-material

### Additional File 1

**Supplemental Figure S1 |** Diagram showing four BlastP search hits that were not included in the consensus sequence analysis of the F-segment.

**Supplemental Table S1 |** List of 208 putative proteins identified as the orthologs for the expanded F–segment containing RcDhn 2.

### Additional File 2

Threshold cycle (Ct) values and fold change calculation worksheets for the monthly expression of rhododendron dehydrin genes.

## REFERENCES

Alsheikh, M., Heyen, B., and Randall, S. (2003). Ion binding properties of the dehydrin ERD14 are dependent upon phosphorylation. *J. Biol. Chem.* 278, 40882–40889. doi: 10.1074/jbc.M307151200

Alsheikh, M. K., Svensson, J. T., and Randall, S. K. (2005). Phosphorylation regulated ion-binding is a property shared by the acidic subclass dehydrins. *Plant Cell Environ.* 28, 1114–22. doi: 10.1111/j.1365-3040.2005.01348.x

Arora, R., and Taulavuori, K. (2016). Increased risk of freeze damage in woody perennials VIS-À-VIS climate change: Importance of deacclimation and dormancy response. *Front. Environ. Sci.* 4:44. doi: 10.3389/fenvs.2016.00044

Baker, J., Steele, C., and Dure, L. (1988). Sequence and characterization of 6 Lea proteins and their genes from cotton. *Plant Mol. Biol.* 11, 277–291. doi: 10.1007/BF00027385

Bassett, C. L., Wisniewski, M. E., Artlip, T. S., Richart, G., Norelli, J. L., and Farrell, R. E. (2009). Comparative expression and transcript initiation of three peach dehydrin genes. *Planta* 230, 107–118. doi: 10.1007/s00425-009-0927-1

Campbell, S., and Close, T. (1997). Dehydrins: genes, proteins, and associations with phenotypic traits. *New Phytol.* 137, 61–74. doi: 10.1046/j.1469-8137.1997.00831.x

Cellier, F., Conéjéro, G., and Casse, F. (2000). Dehydrin transcript fluctuations during a day/night cycle in drought-stressed sunflower. *J. Exp. Bot.* 51, 299–304. doi: 10.1093/jexbot/51.343.299

Close, T. (1996). Dehydrins: emergence of a biochemical role of a family of plant dehydration proteins. *Physiol. Plant.* 97, 795–803. doi: 10.1111/j.1399-3054.1996.tb00546.x

Close, T. J. (1997). Dehydrins: a commonality in the response of plants to dehydration and low temperature. *Physiol. Plant.* 100, 291–296. doi: 10.1111/j.1399-3054.1997.tb04785.x

Corbett, E. F., and Michalak, M. (2000). Calcium, a signaling molecule in the endoplasmic reticulum? *Trends Biochem. Sci.* 25, 307–311. doi: 10.1016/S0968-0004(00)01588-7

Crooks, G. E., Hon, G., Chandonia, J. M., and Brenner, S. E. (2004). WebLogo: a sequence logo generator. *Genome Res.* 14, 1188–1190. doi: 10.1101/gr.849004

Danyluk, J., Perron, A., Houde, M., Limin, A., Fowler, B., Benhamou, N., et al. (1998). Accumulation of an acidic dehydrin in the vicinity of the plasma membrane during cold acclimation of wheat. *Plant Cell Online* 10:623. doi: 10.1105/tpc.10.4.623

Dhanaraj, A. L., Slovin, J. P., and Rowland, L. J. (2005). Isolation of a cDNA clone and characterization of expression of the highly abundant, cold acclimation-associated 14 kDa dehydrin of blueberry. *Plant Sci.* 168, 949–957. doi: 10.1016/j.plantsci.2004.11.007

Dure, L. (1993). "Structuralmotifs in Lea proteins," in *Plant Responses to Cellular Dehydration during Environmental Stress*, eds T. J. Close, and E. A. Bray (Rockville, MD: American Society of Plant Physiologists), 91–104.

Egerton-Warburton, L., Balsamo, R., and Close, T. (1997). Temporal accumulation and ultrastructural localization of dehydrins in Zea mays. *Physiol. Plant.* 101, 545–555. doi: 10.1111/j.1399-3054.1997.tb01036.x

Feng, Y., Yin, Y., and Fei, S. (2017). BdVRN1 expression confers flowering competency and is negatively correlated with freezing tolerance in *Brachypodium distachyon*. *Front. Plant Sci.* 8:1107. doi: 10.3389/fpls.2017.01107

Graether, S. P., and Boddington, K. F. (2014). Disorder and function: a review of the dehydrin protein family. *Front. Plant Sci.* 5:576. doi: 10.3389/fpls.2014.00576

Guy, C. (1990). Cold accelimation and freezing stress tolerance: role of protein metabolism. *Annu. Rev. Plant Biol.* 41, 187–223. doi: 10.1146/annurev.pp.41.060190.001155

Haider, A. H. (2012). Characterization and expression of dehydrins in wild Egyptian pea (*Pisum sativum L.*). *Afr. J. Biotechnol.* 11, 11789–11796. doi: 10.5897/AJB11.1707

Hara, M., Fujinaga, M., and Kuboi, T. (2005). Metal binding by citrus dehydrin with histidine-rich domains. *J. Exp. Bot.* 56, 2695–2703. doi: 10.1093/jxb/eri262

Hara, M., Kondo, M., and Kato, T. (2013). A KS-type dehydrin and its related domains reduce Cu-promoted radical generation and the histidine residues contribute to the radical-reducing activities. *J. Exp. Bot.* 64, 1615–1624. doi: 10.1093/jxb/ert016

Hernández-Sánchez, I. E., Martynowicz, D. M., Rodríguez-Hernández, A. A., Pérez-Morales, M. B., Graether, S. P., and Jiménez-Bremont, J. F. (2014). A dehydrin-dehydrin interaction: the case of SK3 from Opuntia streptacantha. *Front. Plant Sci.* 5:520. doi: 10.3389/fpls.2014.00520

Hernández-Sánchez, I. E., Maruri, I., Ferrando, A., Carbonell, J., Graether, S. P., and Jimenez Bremont, J. F. (2015). Nuclear localization of the dehydrin OpsDHN1 is determined by histidine-rich motif. *Front. Plant Sci.* 6:702. doi: 10.3389/fpls.2015.00702

Jiménez-Bremont, J. F., Maruri-López, I., Ochoa-Alfaro, A. E., Delgado-Sánchez, P., Bravo, J., and Rodríguez-Kessler, M. (2013). LEA gene introns: is the intron of dehydrin genes a characteristic of the serine-segment? *Plant Mol. Biol. Rep.* 31, 128–140. doi: 10.1007/s11105-012-0483-x

Kalberer, S. R., Wisniewski, M., and Arora, R. (2006). Deacclimation and reacclimation of cold-hardy plants: current understanding and emerging concepts. *Plant Sci.* 171, 3–16. doi: 10.1016/j.plantsci.2006.02.013

Kaplan, F., Kopka, J., Haskell, D. W., Zhao, W., Schiller, K. C., Gatzke, N., et al. (2004). Exploring the temperature-stress metabolome of Arabidopsis. *Plant Physiol.* 136, 4159–4168. doi: 10.1104/pp.104.052142

Karlson, D. T., Fujino, T., Kimura, S., Baba, K., Itoh, T., and Ashworth, E. N. (2003). Novel plasmodesmata association of dehydrin-like proteins in cold-acclimated red-osier dogwood (*Cornus sericea*). *Tree Physiol.* 23, 759–767. doi: 10.1093/treephys/23.11.759

Kosová, K., Vítámvás, P., and Prášil, I. (2007). The role of dehydrins in plant response to cold. *Biol. Plant.* 51, 601–617. doi: 10.1007/s10535-007-0133-6

Kovacs, D., Kalmar, E., Torok, Z., and Tompa, P. (2008). Chaperone activity of ERD10 and ERD14, two disordered stress-related plant proteins. *Plant Physiol.* 147, 381–390. doi: 10.1104/pp.108.118208

Kyte, J., and Doolittle, R. F. (1982). A simple method for displaying the hydropathic character of a protein. *J. Mol. Biol.* 157, 105–132. doi: 10.1016/0022-2836(82)90515-0

Lee, S. C., Lee, M. Y., Kim, S. J., Jun, S. H., An, G., and Kim, S. R. (2005). Characterization of an abiotic stress-inducible dehydrin gene, OsDhn1, in rice (Oryza sativa L.). *Mol Cells.* 19, 212–218. Available online at: http://www.molcells.org/journal/view.html?year=2005&volume=19&number=2&spage=212

Lin, C., and Thomashow, M. (1992). A cold-regulated Arabidopsis gene encodes a polypeptide having potent cryoprotective activity. *Biochem. Biophys. Res. Commun.* 183, 1103–1108. doi: 10.1016/S0006-291X(05)80304-3

Malik, A. A., Veltri, M., Boddington, K. F., Singh, K. K., and Graether, S. P. (2017). Genome analysis of conserved Dehydrin motifs in vascular plants. *Front. Plant Sci.* 8:709. doi: 10.3389/fpls.2017.00709

Nguyen, N. N., Ranwez, V., Vile, D., Soulié, M. C., Dellagi, A., Expert, D., et al. (2014). Evolutionary tinkering of the expression of PDF1s suggests their joint effect on zinc tolerance and the response to pathogen attack. *Front. Plant Sci.* 5:70. doi: 10.3389/fpls.2014.00070

Nylander, M., Svensson, J., Palva, E. T., and Welin, B., V. (2001). Stress-induced accumulation and tissue-specific localization of dehydrins in *Arabidopsis thaliana*. *Plant Mol. Biol.* 45, 263–279. doi: 10.1023/A:1006469128280

Peng, Y., Reyes, J. L., Wei, H., Yang, Y., Karlson, D., Covarrubias, A. A., et al. (2008). RcDhn5, a cold acclimation-responsive dehydrin from *Rhododendron catawbiense* rescues enzyme activity from dehydration effects in vitro and enhances freezing tolerance in RcDhn5-overexpressing Arabidopsis plants. *Physiol. Plant.* 134, 583–597. doi: 10.1111/j.1399-3054.2008.01164.x

Poulsen, N., Chesley, P. M., and Kroger, N. (2006). Molecular genetic manipulation of the diatom *Thalassiosira pseudonana* (*Bacillariophyceae*). *J. Phycol.* 42, 1059–1065. doi: 10.1111/j.1529-8817.2006.00269.x

Puhakainen, T., Li, C., Boije-Malm, M., Kangasjärvi, J., Heino, P., and Palva, E., T. (2004). Short-day potentiation of low temperature-induced gene expression of a C-repeat-binding factor-controlled gene during cold acclimation in silver birch. *Plant Physiol.* 136, 4299–4307. doi: 10.1104/pp.104.047258

Ramakers, C., Ruijter, J., K. Deprez, R., H. and Moorman, A., F. (2003). Assumption-free analysis of quantitative real-time polymerase chain reaction (PCR) data. *Neurosci. Lett.* 339, 62–66. doi: 10.1016/S0304-3940(02)01423-4

Reyes, J. L., Campos, F., Wei, H., Arora, R., Yang, Y., Karlson, D. T., et al. (2008). Functional dissection of hydrophilins during in vitro freeze protection. *Plant Cell Environ.* 31, 1781–1790. doi: 10.1111/j.1365-3040.2008.01879.x

Sakai, A. (1986). Cold hardiness in the genus Rhododendron. *J. Amer. Soc. Hort. Sci.* 111, 273–280.

Schneider, T. D., and Stephens, R. M. (1990). Sequence logos: a new way to display consensus sequences. *Nucleic Acids Res.* 18, 6097–6100. doi: 10.1093/nar/18.20.6097

Sharma, A., Bendre, A., Mondal, A., Muzumdar, D., Goel, N., and Shiras, A. (2017). Angiogenic gene signature derived from subtype specific cell models segregate proneural and Mesenchymal glioblastoma. *Front. Oncol.* 7:146. doi: 10.3389/fonc.2017.00146

Strimbeck, G. R. (2017). Hiding in plain sight: the F segment and other conserved features of seed plant SK n dehydrins. *Planta* 245, 1061–1066. doi: 10.1007/s00425-017-2679-7

Svensson, J., Ismail, A., Palva, E., and Close, T. (2002). *Dehydrins: Sensing, Signaling and Cell Adaptation*. Amsterdam: Elsevier, 155–171.

Svensson, J., Palva, E. T., and Welin, B. (2000). Purification of recombinant Arabidopsis thaliana dehydrins by metal ion affinity chromatography. *Protein Expr. Purif.* 20, 169–178. doi: 10.1006/prep.2000.1297

Thomashow, M. (1990). Molecular genetics of cold acclimation in higher plants. *Adv. Genet.* 28, 99–131. doi: 10.1016/S0065-2660(08)60525-8

Thomashow, M. (1998). Role of cold-responsive genes in plant freezing tolerance. *Plant Physiol.* 118, 1–8. doi: 10.1104/pp.118.1.1

Tunnacliffe, A., and Wise, M. (2007). The continuing conundrum of the LEA proteins. *Naturwissenschaften* 94, 791–812. doi: 10.1007/s00114-007-0254-y

Wang, X., Peng, Y., Singer, J. W., Fessehaie, A., Krebs, S. L., and Arora, R. (2009). Seasonal changes in photosynthesis, antioxidant systems and ELIP expression in a thermonastic and non-thermonastic Rhododendron species: a comparison of photoprotective strategies in overwintering plants. *Plant Sci.* 177, 607–617. doi: 10.1016/j.plantsci.2009.08.009

Wei, H., Dhanaraj, A. L., Rowland, L. J., Fu, Y., Krebs, S. L., and Arora, R. (2005a). Comparative analysis of expressed sequence tags from cold-acclimated and non-acclimated leaves of *Rhododendron catawbiense* Michx. *Planta* 221, 406–416. doi: 10.1007/s00425-004-1440-1

Wei, H., Fu, Y., and Arora, R. (2005b). Intron-flanking EST–PCR markers: from genetic marker development to gene structure analysis in Rhododendron. *Theor. Appl. Genet.* 111, 1347–1356. doi: 10.1007/s00122-005-0064-6

Wilkins, T., and Smart, L. (1996). "Isolation of RNA from plant tissue," in *A Laboratory Guide to RNA: Isolation, Analysis, and Synthesis*, ed P. A. Krieg (New York, NY: Wiley-Liss Inc.), 21–41.

Wisniewski, M., Bassett, C., and Gusta, L. V. (2003). An overview of cold hardiness in woody plants: seeing the forest through the trees. *HortScience* 38, 952–959. doi: 10.21273/HORTSCI.38.5.952

Wisniewski, M., Webb, R., Balsamo, R., Close, T. J., Yu, X. M., and Griffith, M. (1999). Purification, immunolocalization, cryoprotective, and antifreeze activity of PCA60: a dehydrin from peach (*Prunus persica*). *Physiol. Plant.* 105, 600–608. doi: 10.1034/j.1399-3054.1999.105402.x

Wisniewski, M. E., Bassett, C. L., Renaut, J., Farrell R., Tworkoski, T., and Artlip, T. S. (2006). Differential regulation of two dehydrin genes from peach (*Prunus persica*) by photoperiod, low temperature and water deficit. *Tree Physiol.* 26, 575–584. doi: 10.1093/treephys/26.5.575

Xiong, D., Wang, Y., Tian, L., and Tian, C. (2016). MADS-Box transcription factor VdMcm1 regulates conidiation, microsclerotia formation, pathogenicity, and secondary metabolism of Verticillium dahliae. *Front. Microbiol.* 7:1192. doi: 10.3389/fmicb.2016.01192

Yamada, T., Kuroda, K., Jitsuyama, Y., Takezawa, D., Arakawa, K., and Fujikawa, S. (2002). Roles of the plasma membrane and the cell wall in the responses of plant cells to freezing. *Planta* 215, 770–778. doi: 10.1007/s00425-002-0814-5

Yao, K., Lockhart, K. M., and Kalanack, J., J. (2005). Cloning of dehydrin coding sequences from *Brassica juncea* and *Brassica napus* and their low temperature-inducible expression in germinating seeds. *Plant Physiol. Biochem.* 43, 83–89. doi: 10.1016/j.plaphy.2004.12.006

**Conflict of Interest Statement:** The authors declare that the research was conducted in the absence of any commercial or financial relationships that could be construed as a potential conflict of interest.

frontiers in Bioengineering and Biotechnology

ORIGINAL RESEARCH
published: 26 February 2019
doi: 10.3389/fbioe.2019.00032

# Anadromous Arctic Char Microbiomes: Bioprospecting in the High Arctic

*Erin F. Hamilton[1], Geraint Element[1], Peter van Coeverden de Groot[1], Katja Engel[2], Josh D. Neufeld[2], Vishal Shah[3] and Virginia K. Walker[1]**

[1] Department of Biology, Queen's University, Kingston, ON, Canada, [2] Department of Biology, University of Waterloo, Waterloo, ON, Canada, [3] College of the Sciences and Mathematics, West Chester University, West Chester, PA, United States

OPEN ACCESS

**Edited by:**
*Steffen P. Graether, University of Guelph, Canada*

**Reviewed by:**
*Ashok K. Dubey, Netaji Subhas Institute of Technology, India*
*Nadia Solovieva, University College London, United Kingdom*

***Correspondence:**
*Virginia K. Walker*
*walkervk@queensu.ca*

**Specialty section:**
*This article was submitted to Bioprocess Engineering, a section of the journal Frontiers in Bioengineering and Biotechnology*

**Received:** *15 October 2018*
**Accepted:** *05 February 2019*
**Published:** *26 February 2019*

**Citation:**
*Hamilton EF, Element G, van Coeverden de Groot P, Engel K, Neufeld JD, Shah V and Walker VK (2019) Anadromous Arctic Char Microbiomes: Bioprospecting in the High Arctic. Front. Bioeng. Biotechnol. 7:32. doi: 10.3389/fbioe.2019.00032*

Northern populations of Arctic char (*Salvelinus alpinus*) can be anadromous, migrating annually from the ocean to freshwater lakes and rivers in order to escape sub-zero temperatures. Such seasonal behavior demands that these fish and their associated microbiomes adapt to changes in salinity, temperature, and other environmental challenges. We characterized the microbial community composition of anadromous *S. alpinus,* netted by Inuit fishermen at freshwater and seawater fishing sites in the high Arctic, both under ice and in open water. Bacterial profiles were generated by DNA extraction and high-throughput sequencing of PCR-amplified 16S ribosomal RNA genes. Results showed that microbial communities on the skin and intestine of Arctic char were statistically different when sampled from freshwater or saline water sites. This association was tested using hierarchical Ward's linkage clustering, showing eight distinct clusters in each of the skin and intestinal microbiomes, with the clusters reflecting sampling location between fresh and saline environments, confirming a salinity-linked turnover. This analysis also provided evidence for a core composition of skin and intestinal bacteria, with the phyla Proteobacteria, Firmicutes, and Cyanobacteria presenting as major phyla within the skin-associated microbiomes. The intestine-associated microbiome was characterized by unidentified genera from families Fusobacteriaceae, Comamonadaceae, Pseudomonadaceae, and Vibrionaceae. The salinity-linked turnover was further tested through ordinations that showed samples grouping based on environment for both skin- and intestine-associated microbiomes. This finding implies that core microbiomes between fresh and saline conditions could be used to assist in regulating optimal fish health in aquaculture practices. Furthermore, identified taxa from known psychrophiles and with nitrogen cycling properties suggest that there is additional potential for biotechnological applications for fish farm and waste management practices.

**Keywords: Arctic char, salmonid fish, anadromous, microbiomes, bioprospecting, aquaculture, Arctic Ocean, aquatic biotechnology**

# INTRODUCTION

Fish carry a mucous layer on their epithelial surfaces that consists of mucins, immunoglobulins, antimicrobial peptides, and commensal bacteria, which serve roles in friction reduction, waste removal, osmoregulation, as well as an early line of defense against pathogens (Esteban and Cerezuela, 2015). In addition, variations in mucous layer microbiome composition occur across different life stages, among different species, and across distinct geographies in amphibians and marine mammals, which are known to share certain microbial species with the surrounding water (Boutin et al., 2013; Apprill et al., 2014; Kueneman et al., 2014; Chiarello et al., 2015). Indeed, in farmed Atlantic salmon (*Salmo salar*), the abundance of certain bacterial phyla in skin- and intestine-associated microbiomes changed depending on the water source (Lokesh and Kiron, 2016; Dehler et al., 2017). Structural changes to the microbiota, however, have not been well-described in wild fish populations. This research is noteworthy because it indicates that deliberate shifts in community structure could potentially hinder the development of dysbiosis.

Arctic char (*Salvelinus alpinus*), a salmonid species, is of particular interest given the increased popularity of the farmed product in temperate regions. Wild *S. alpinus* stocks from high latitude waters with an anadromous life history, such that they spend the winter in freshwater lakes to avoid freezing and subsequently migrate to the more nutrient-rich Arctic sea in the summer, could provide insight into the purported turnover in char microbiomes and be of interest to aquaculture biotechnologists.

Although relatively unexploited commercially, Arctic char stocks in the lower Northwest Passage of the Kitikmeot region of Nunavut, Canada represent an essential subsistence fishery to indigenous Inuit communities. With recent altered sea ice patterns as a consequence of climate change, and the potential for increasing stress of pollutants associated with future industrialization, we considered it important to undertake genomic, demographic, physiological and microbial analyses on these fish populations. At present, the stocks are considered healthy due a general lack of commercial fisheries in this region, as well as the relatively long-life span of individual fish, which has been reported as up to 33 years in our samples. As part of this effort, an assessment of the mucosa-associated microbiomes of the skin and intestines of *S. alpinus* from the area in, and surrounding, King William Island Nunavut, has been undertaken. We further explored whether this increased understanding of the microbial communities could inform future biotechnological applications in the management of commercially farmed fish, in addition to other biotechnologies.

# MATERIALS AND METHODS

## Study Area

Fishing was done within the Kitikmeot region of Nunavut, Canada in the Western Arctic, at seven distinct sites within 200 km of King William Island, located along the lower Northwest Passage (**Figure 1**; **Table 1**). Fishing sites were chosen based on Traditional Ecological Knowledge shared by local Inuit elders and in association with the Hunters and Trappers Association of Gjoa Haven, NU, as part of a large-scale fisheries project (Towards; www.arcticfishery.ca). At each fishing site, specific conductance of surface water was obtained with a conductivity meter (Traceable Fisherbrand, Fisher Scientific) to record conductivity and determine our site designations as either freshwater or saline sites (**Table 1**). The southern region of the study area is unique due to large freshwater influence from major river systems, including Murchison River, Legendary River, Back River, and Hayes River. Therefore, the major sea-water bodies within the region, namely Rasmussen Basin and Chantrey Inlet, are characterized by brackish salinities as defined by Watling (2007), with conductivities between 1,500 and 15,000 $\mu S\ cm^{-1}$, diverging from sea salinities more characteristic of the Pacific and Atlantic Oceans (Carmack, 2007). Fishing sites within these locations are referred to as "saline" sites.

## Fish Collection

Commercial (140 mm mesh) and multi-mesh subsistence (5 or 8 panels of 38–140 mm) fishing nets were set during December-June (freshwater lakes under thick ice) and August-September (at open water river estuaries during sea-ice formation and char migration) at distinct geographic sites over a period of 3 years. After setting for several hours, nets were retrieved, and fish were pulled from the nets with nitrile gloves. Using either sterile cotton swabs or an ethanol-sterilized scalpel, the surface mucosal layer of each fish was sampled once per fish with the swabs, or skin scrapings, taken from above the lateral line. The fish were then photographed, weighed, and measured, followed by dissection in an on-site mobile lab. Full intestines were removed using sterile technique, and both skin and intestinal samples were placed in sterile sample tubes or bags, respectively, and frozen at −20°C in a freezer on-site. Samples were shipped frozen and subsequently stored at −20°C until further processing. In addition to the skin and intestine samples, water samples were also taken at each fishing site, in which up to 2 L of water was filtered through sterile 0.22 μm PALL filters in triplicate. The filters were then frozen at −20°C and were subsequently transported and stored at −80°C until further processing.

Fish were sampled in accordance with issued licenses to fish for scientific purposes in the waters of the Northwest Territories, Yukon north slope, and Nunavut (in accordance with section 52 of the general fishery regulations of the fisheries act, Fisheries and Oceans, Canada) along with an associated animal care permit issued by the Fresh Water Institute Animal Care Committee of the Department of Fisheries and Oceans (current permit numbers S-18/19-1045-NU and FWI-ACC AUP-2018-63).

## Sample Processing and DNA Extraction

After initial optimization experimentation to determine the selection of appropriate DNA extraction kits for each sample type, DNA from the skin samples was extracted using a NucleoSpin Soil Extraction Kit (Machery-Nagel, Bethlehem, PA), with modifications following the procedures of Kueneman et al. (2014) in which samples were incubated at 65°C for 10 min before mechanical lysis. In order to maximize

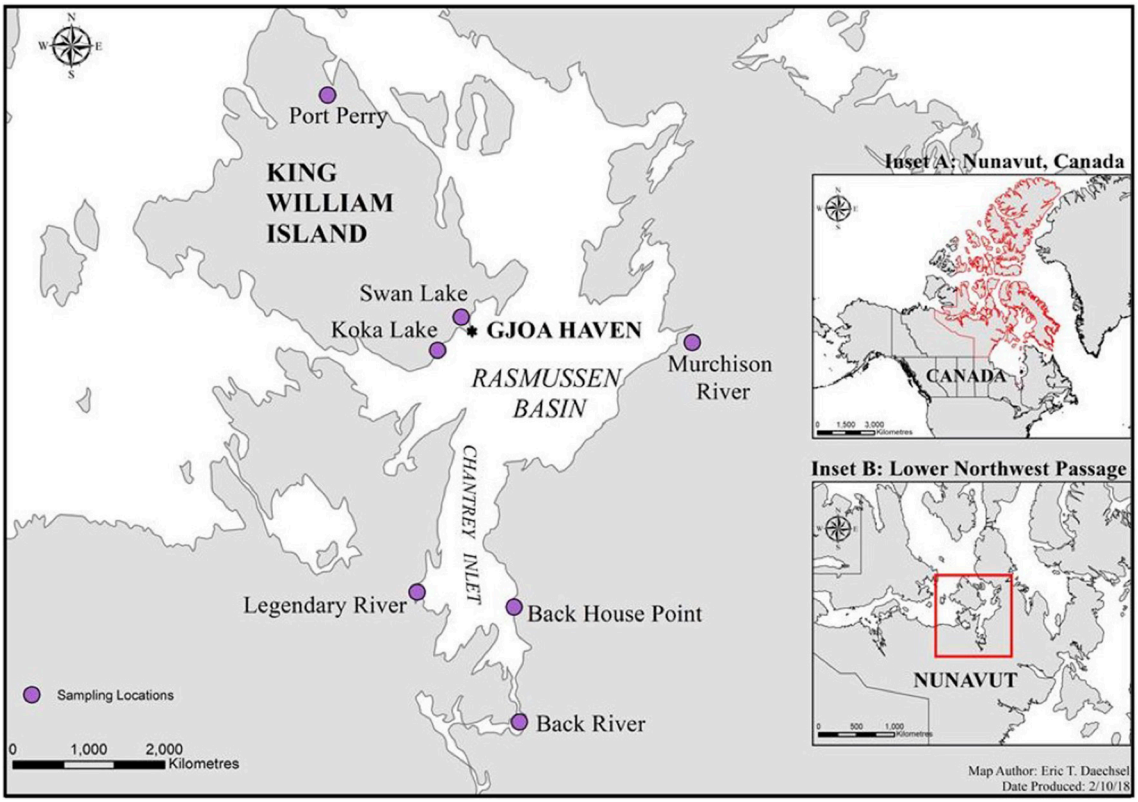


**FIGURE 1 |** A map of the lower Northwest Passage in Nunavut, Canada and the location of seven distinct fishing sites initially chosen based on Inuit Traditional Ecological Knowledge. The sites fished include five freshwater sites (Port Perry, Swan Lake, Koka Lake, Murchison River, and Back River); and two saltwater sites (Back House Point and Legendary River estuary). Inset A outlines Nunavut, Canada, in red, while inset B showcases the lower Northwest Passage, in red.

yield, the initial lysis step was conducted twice, and double-distilled sterile water was left on the filter for 5 min prior to elution. Extracted DNA concentrations were assessed using an Invitrogen Qubit 4 Fluorometer and a QuantiFluor ONE dsDNA system (Promega Corporation, Madison, WI, USA), followed by qualitative analysis with agarose gel electrophoresis and a NanoDrop One Microvolume spectrophotometer (Thermo Scientific) set to $A_{260/280}$ absorbance. High concentration samples were diluted to 50 ng $\mu L^{-1}$ prior to PCR amplification, in which starting material for PCR templates ranged from 1 to 50 ng $\mu L^{-1}$. These skin-associated microbiome samples underwent a pre-amplification PCR step using primers 8F and 1406R (Lane, 1991; Coolen et al., 2005) to amplify the variable V1–V9 region of the bacterial 16S ribosomal RNA (rRNA) gene. The PCR mix for each reaction (50 µL total volume) contained 1X ThermoFisher DreamTaq Buffer (with 2 mM $MgCl_2$), 0.4 µM forward and reverse primers, 200 µM dNTPs, 400 ng BSA, 2.5 U ThermoFisher DreamTaq DNA Polymerase, and 2 µL of template. The PCR was performed as follows: 95°C for 5 min, 25 cycles of 95°C for 1 min, 52°C for 1 min, 72°C for 1 min, with a final extension of 72°C for 7 min.

Intestinal samples were partially thawed to excise three slices within the distal intestine (~2 cm from the vent), comprising a total of 5–100 mg epithelial tissue, avoiding feces and connective tissue. The slices were pooled and DNA was extracted using MOBIO UltraClean Tissue and Cells DNA Isolation Kit (QIAGEN Inc., Toronto, ON) following the manufacturer's instructions, except that elution was achieved with double-distilled sterile water rather than EDTA. The DNA concentrations for the intestine-associated microbiome samples were estimated as described for the skin-associated microbiome preparations, but adjusted to 30 ng $\mu L^{-1}$. Pre-amplified PCR products were also prepared as described above.

**TABLE 1 |** Location and GPS coordinates for each fishing site, followed by designated water source categories and specific conductance measurements shown as conductivity that were determined by a conductivity meter on-site.

| Location and GPS coordinates | Water source | Conductivity ($\mu S\ cm^{-1}$) |
|---|---|---|
| Port Perry (N69°33′28.764″, W97°26′13.884″) | Fresh | 286 |
| Swan Lake (N68°40′13.62, W95°56′57.408″) | Fresh | 880 |
| Koka Lake (N68°32′5.1″, W96°12′45.899″) | Fresh | 670 |
| Back House Point (N67°27′27.2″, W95°21′38.6″) | Saline | 8,240 |
| Legendary River (N67°31′17.8″, W96°26′21.8″) | Saline | 3,450 |
| Murchison River (N68°34′1.2″, W 93°22′37.452″) | Fresh | 225 |
| Back River (N66°57′30.70″, W95°18′5.20″) | Fresh | 19 |

In addition, the V4 region of the 16S rRNA gene was amplified on an Illumina sequence platform from DNA isolated from the triplicate water filters using primers 515F and 806R (Caporaso et al., 2011).

## 16S rRNA Gene Sequencing of Mucosal Microbiomes

The V4-V5 region of the 16S rRNA gene was amplified from each of the skin and intestinal amplification products using primers 515F-Y (Parada et al., 2016) and 926R (Quince et al., 2011). Each primer contained a 6-base index sequence for sample multiplexing as well as Illumina flow cell binding and sequencing sites (Bartram et al., 2011). The PCR mix (25 μL total volume) contained 1X ThermoPol Buffer, 0.2 μM forward and reverse primers, 200 μM dNTPs, 15 μg BSA, 0.625 U Hot Start *Taq* DNA polymerase, and 1 μL of template. The PCR was performed as follows: 95°C for 3 min, 35 cycles of 95°C for 30 s, 50°C for 30 s, 68°C for 1 min, and a final extension of 68°C for 7 min. Each amplification reaction was done in triplicate. Equal quantities of each amplicon were pooled. Samples that did not yield a PCR product were not included. No-template controls were added to the Illumina sequencing pool (5 μL), even when amplicons were not detected. Pooled 16S rRNA gene amplicons were subsequently excised from an agarose gel and purified using the Wizard SV Gel and PCR Clean-Up System (Promega, WI, USA). A 5 pM library containing 15% PhiX Control v3 (Illumina Canada Inc, NB, Canada) was sequenced on a MiSeq instrument (Illumina Inc, CA, USA) using a 2 × 250 cycle MiSeq Reagent Kit v2 (Illumina Canada Inc., BC, Canada).

## Sequence Data Analysis, OTU Tables, and Statistics

Sequence reads were demultiplexed using Illumina MiSeq Reporter software version 2.5.0.5. Reads were assembled using the paired-end assembler for Illumina sequences (PANDAseq version 2.8, Masella et al., 2012) with a quality threshold of 0.9, an 8 nucleotide minimum overlap, and 32 nucleotide minimum assembled read length. Assembled reads were analyzed using Quantitative Insights Into Microbial Ecology (QIIME version 1.9.0, Caporaso et al., 2010). Sequences were clustered into operational taxonomic units (OTUs) using UPARSE algorithm USEARCH version 7.0.1090 (Edgar, 2013) at 97% identity and aligned with the Python Nearest Alignment Space Termination tool (PyNAST version 1.2.2, Caporaso et al., 2010). All representative sequences were classified using the Ribosomal Database Project (RDP version 2.2, Wang et al., 2007) with a stringent confidence threshold (0.8) and the Greengenes database (McDonald et al., 2012) was used to assign taxonomy. Chimeric sequences were filtered with UCHIME (Edgar et al., 2011). Before performing statistical analysis, OTUs observed in no-template PCR controls for a sample type were filtered from all samples of that type. OTUs with three or fewer reads within negative PCR controls were retained within the samples, since their low representation in the negative controls rendered them viable representatives in the samples. The OTUs were then rarefied to ∼2,000 reads for skin and intestinal microbiome samples. Alpha and beta diversity for samples were analyzed based on rarified OTU tables generated using QIIME with principal coordinate analysis (PCoA). Additional visualizations were done using EMPeror (Vázquez-Baeza et al., 2013). Primer 7 software version 7.0.13 was used for analysis of similarity (ANOSIM) and similarity percentages (SIMPER) analyses (Clarke et al., 2014). Clustering analysis was performed using Statistica 13.0 Academic software.

The hypothesis that skin microbial community composition was linked to salinity was tested by performing hierarchical Ward's linkage clustering (Dillner et al., 2005). Tree cluster analysis was carried out using Ward's method as the amalgamation rule and the distance measured as Euclidean units (Dillner et al., 2005). Using K-means clustering, the samples were divided into K clusters by selecting the number of iterations as 10, and the initial cluster centers chosen to maximize initial between-cluster distances. The output of this step is the list of fish samples that are present in each cluster. The sequence data is publicly available in the European Nucleotide Archive within the European Bioinformatics Institute, under the study: Characterization and Analysis of Skin- and Intestine-associated Microbiomes in the Lower Northwest Passage (Nunavut, Canada) with the following accession number, PRJEB29173.

# RESULTS

## Comparisons of Skin and Intestinal Microbiota Within Individual Fish

Based on fish sampled at seven distinct sites on or within 200 km of King William Island, located along the lower Northwest Passage (**Figure 1**; **Table 1**), microbiome sequences were successfully obtained for 118 skin mucosal samples and 202 intestinal samples. Grouping the skin microbiome consortia by environment showed that the freshwater samples contained significantly more Shannon diversity overall than those from saline water ($R^2 = 0.11$, $F = 16.0$, $p < 0.05$), whereas $\log_{10}$ Chao1 OTU richness was not significantly different between the two environment types ($R^2 = 0.00$, $F = 0.1$, $p > 0.05$). In contrast, when intestinal microbiomes were grouped by environment, the saline water samples were more diverse overall than freshwater samples when $\log_{10}$ Chao1 OTU richness was considered, though this difference was small ($R^2 = 0.03$, $F = 4.7$, $p < 0.05$). A significant difference was not observed in the intestinal microbiomes between the two environment types when Shannon diversity was considered ($R^2 = 0.00$, $F = 0.1$, $p > 0.05$). Of the 320 skin and intestine samples combined, 60 individual Arctic char had both sets of microbiome data, allowing a comparison of skin and intestinal flora from the same fish (**Figure 2**). When comparing across these 60 fish, skin-associated microbiomes were significantly more diverse than intestine-associated microbiomes when both $\log_{10}$ Chao1 OTU richness ($R^2 = 0.60$, $F = 180.0$, $p < 0.05$) and Shannon diversity ($R^2 = 0.52$, $F = 127.4$, $p < 0.05$) were considered. In addition, though the skin and intestine communities were

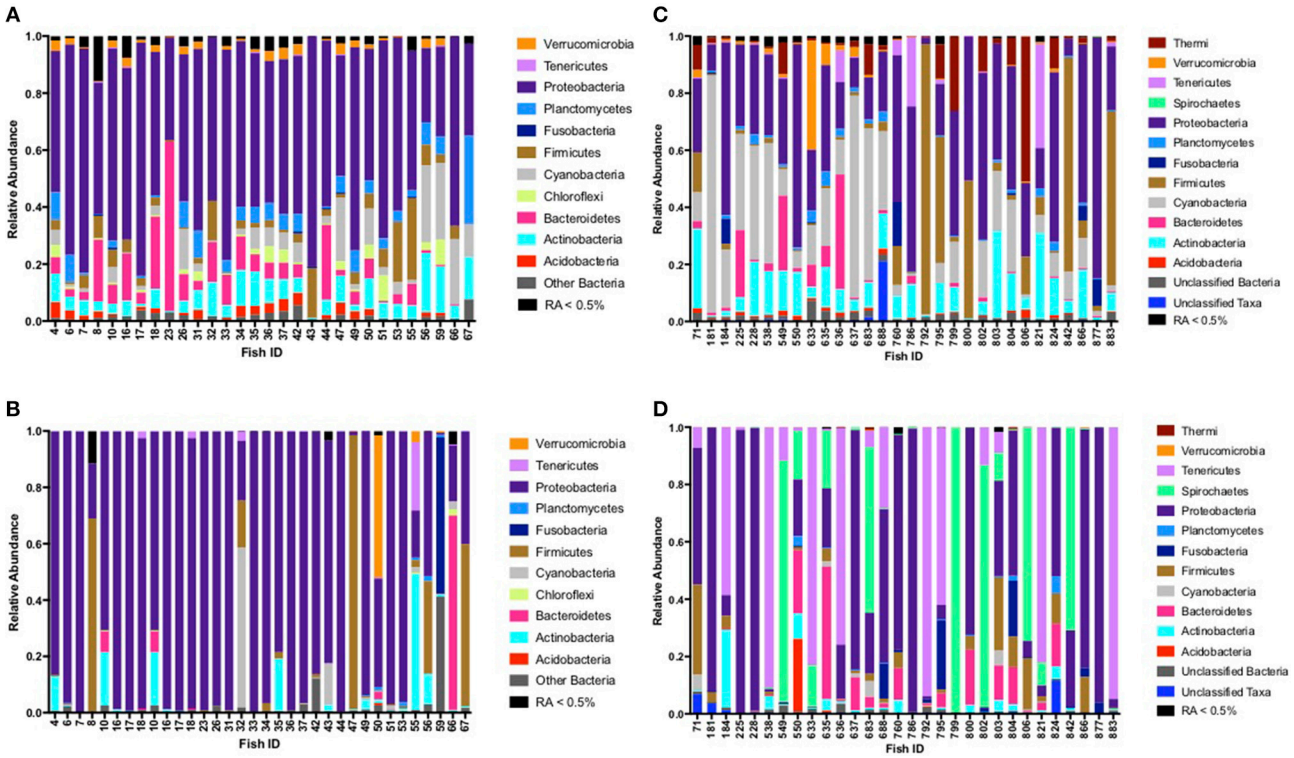


**FIGURE 2 |** Phyla comparison of skin and intestinal complementary microbiomes for individual fish, shown for samples collected at **(A)** freshwater sites Port Perry, Swan Lake, and Koka Lake for skin-associated microbiomes, **(B)** freshwater sites Port Perry, Swan Lake, and Koka Lake for intestine-associated microbiomes, **(C)** saltwater sites, Back House Point and Legendary River for skin-associated microbiomes, and **(D)** saltwater sites, Back House Point and Legendary River for intestine-associated microbiomes. Phyla with relative abundances (RA) $\geq$ 0.5% are shown. Phyla present at RA $<$ 0.5% were pooled together.

distinct, the skin- and intestine-associated microbiomes among individual fish appeared to be more similar at freshwater sites (**Figures 2A,B**) compared to saline water sites (**Figures 2C,D**).

The relative abundance of rarified OTUs identified to the genus level, if known, for each of the total 320 skin and intestinal microbiome samples is presented in supplemental tables (**Tables S1**, **S2**, respectively).

## Skin and Intestinal Microbiota Compositions Linked to Salinity

At freshwater sites, most taxa from skin- and intestine-associated microbiome sequence data were affiliated with Proteobacteria, but many also classified to Actinobacteria, Cyanobacteria, and Firmicutes (**Figures 2A,B**; **Tables S1**, **S2**). Although fish skin from saline environments was also colonized by Proteobacteria and Actinobacteria (**Figure 2C**), other phyla, such as Acidobacteria and Bacteroidetes, were also prominent. Intestines derived from fish sampled in saline waters were similarly characterized by Proteobacteria, Actinobacteria, and Bacteroidetes, but also by Firmicutes, Spirochaetes and Tenericutes, with considerable variation across individual fish (**Figure 2D**). Given these observations, depending on whether fish were sampled from fresh or saline waters, skin or intestinal bacterial communities appeared to change. For example, relative abundance based on rarified data of the psychrophile *Photobacterium* increased 200-fold in relative abundance in skin-associated microbiomes from saline sites, compared to freshwater sites (**Table 2A**). Similarly, relative abundance for *Deinococcus,* known for its ability to resist a variety of environmental stresses, increased 150-fold between fresh- and saline-caught skin microbiome fish samples. Taxa in the intestinal bacterial communities were also shown to change between fresh and saline-caught fish, with similar increases, but to a lesser magnitude including those belonging to the order Vibrionales (18-fold), the genus *Photobacterium* (14-fold), and an unknown genus in the class Mollicutes (14-fold; **Table 2B**).

Overall, PCoA combined with ANOSIM showed a statistically significant separation between samples obtained from freshwater and saline sites for both skin microbiomes ($p < 0.001$; **Figure 3A**), and intestinal microbiomes ($p < 0.001$; **Figure 3B**). This indicates that salinity is a primary factor in defining these microbial communities. For the 60 skin and intestinal microbiome samples used for within-fish comparisons where possible, ANOSIM showed that the communities obtained from the two sample types were significantly different ($p < 0.001$; **Figure 4**).

In addition, preliminary results show that the community structure of identified bacteria from water samples at sites corresponding to where fish were caught (excluding Back River) differs from that of the fish, suggesting that the

**TABLE 2 | (A)** SIMPER analysis (Primer 7) output showing relative abundances and impact ratio of environmental change between freshwater and saline locations across 118 skin-associated microbiome samples **(B)** SIMPER analysis (Primer 7) output showing relative abundances and impact ratio of environmental change between freshwater and saline locations across 202 intestine-associated samples.

| Taxonomy | Relative abundance | | Impact ratio (Saline: Fresh) |
|---|---|---|---|
| | Saline | Fresh | |
| **(A)** | | | |
| p: Proteobacteria c: Gammaproteobacteria o: Vibrionales f: Vibrionaceae g: *Photobacterium* | 4.22 | 0.02 | 211 |
| p: Deinococcus c: Deinococci o: Deinococcales f: Deinococcaceae g: *Deinococcus* | 7.72 | 0.05 | 154 |
| p: Proteobacteria c: Alphaproteobacteria o: Rhodospirillales f: Acetobacteraceae g: Unknown | 8.58 | 1.52 | 5.64 |
| p: Firmicutes c: Clostridia o: Clostridiales f: Clostridiaceae g: *Clostridium* | 3.84 | 2.50 | 1.54 |
| p: Proteobacteria c: Betaproteobacteria o: Burkholderiales f: Comamonadaceae g: Other | 2.97 | 8.01 | 0.37 |
| p: Proteobacteria c: Alphaproteobacteria o: Sphingomonadales f: Sphingomonadaceae g: *Sphingomonas* | 1.69 | 5.00 | 0.34 |
| p: Bacteroidetes c: Saprospirae o: Saprospirales f: Chitinophagaceae g: Unknown | 1.23 | 4.90 | 0.25 |
| p: Proteobacteria c: Alphaproteobacteria o: Rhodospirillales f: Rhodospirillaceae g: Unknown | 0.90 | 5.69 | 0.16 |
| p: Proteobacteria c: Alphaproteobacteria o: Caulobacterales f: Caulobacteraceae g: Other | 0.69 | 4.39 | 0.16 |
| p: Proteobacteria c: Betaproteobacteria o: Other f: Other g: Other | 0.73 | 5.27 | 0.14 |
| p: Proteobacteria c: Alphaproteobacteria o: Sphingomonadales f: Sphingomonadaceae g: *Novosphingobium* | 0.75 | 6.42 | 0.12 |
| p: Proteobacteria c: Gammaproteobacteria o: Xanthomonadales f: Sinobacteraceae g: Unknown | 0.40 | 6.76 | 0.06 |
| p: Proteobacteria c: Betaproteobacteria o: Burkholderiales f: Oxalobacteraceae g: *Cupriavidus* | 0.12 | 4.90 | 0.02 |
| p: Cyanobacteria c: Nostocophycideae o: Stigonematales f: Rivulariaceae g: *Rivularia* | 4.80 | 0.00 | 0.00 |
| p: Cyanobacteria c: Oscillatoriophycideae o: Oscillatoriales f: Phormidiaceae g: *Phormidium* | 7.27 | 0.00 | 0.00 |
| **(B)** | | | |
| p: Proteobacteria c: Gammaproteobacteria o: Vibrionales f: Other g: Other | 3.10 | 0.17 | 18.23 |
| p: Tenericutes c: Mollicutes o: Unknown f: Unknown g: Unknown | 7.32 | 0.52 | 14.08 |
| p: Proteobacteria c: Gammaproteobacteria o: Vibrionales f: Vibrionaceae g: *Photobacterium* | 20.8 | 1.48 | 14.03 |
| p: Spirochaetes c: Brevinematae o: Brevinematales f: Brevinemataceae g: Unknown | 4.54 | 0.54 | 8.41 |
| p: Proteobacteria c: Gammaproteobacteria o: Vibrionales f: Vibrionaceae g: Other | 6.06 | 1.09 | 5.56 |
| p: Proteobacteria c: Gammaproteobacteria o: Vibrionales f: Vibrionaceae g: *Aliivibrio* | 5.08 | 1.22 | 4.16 |
| p: Proteobacteria c: Alphaproteobacteria o: Sphingomonadales f: Sphingomonadaceae g: *Sphingomonas* | 5.91 | 4.06 | 1.46 |
| p: Tenericutes c: Mollicutes o: Mycoplasmatales f: Mycoplasmataceae g: *Mycoplasma* | 4.17 | 4.42 | 0.94 |
| p: Fusobacteria c: Fusobacteriia o: Fusobacteriales f: Fusobacteriaceae g: *u114* | 2.77 | 4.12 | 0.67 |
| p: Proteobacteria c: Gammaproteobacteria o: Pseudomonadales f: Pseudomonadaceae g: *Pseudomonas* | 1.65 | 3.50 | 0.47 |
| p: Proteobacteria c: Betaproteobacteria o: Burkholderiales f: Comamonadaceae g: Other | 2.50 | 5.96 | 0.42 |
| p: Proteobacteria c: Gammaproteobacteria o: Pseudomonadales f: Pseudomonadaceae g: Other | 2.23 | 7.91 | 0.28 |
| Unclassified Taxa | 1.23 | 7.65 | 0.16 |
| p: Proteobacteria c: Alphaproteobacteria o: Caulobacterales f: Caulobacteraceae g: *Phenylobacterium* | 0.40 | 5.71 | 0.07 |
| p: Proteobacteria c: Betaproteobacteria o: Neisseriales f: Neisseriaceae g: *Deefgea* | 0.05 | 2.86 | 0.02 |

*Taxonomy from phylum (p) to clade (c) to order (o) to family (f) to genus (g) is shown.*

distribution of microbiota identified on the fish are influenced by physiological processes inherent to the fish (**Figure S1**). However, the phyla Proteobacteria, Bacteroidetes, and Actinobacteria are represented in both the water microbiomes and in both skin- and intestine-associated microbiota. Across water samples, no significant difference was observed between freshwater and saline sites overall for either Chao1 OTU richness ($R^2 = 0.01$, $F = 0.2$, $p > 0.05$), or Shannon diversity ($R^2 = 0.07$, $F = 1.6$, $p > 0.05$). The most similarity was observed between samples from similar geographic regions. For example, Port Perry, Swan Lake, and Koka Lake were from freshwater sites on King William Island whereas the saline sites Back House Point, Legendary River, and the freshwater site Murchison River were from Chantrey Inlet.

## Characterization of the Skin Microbiota

When the 118 skin-associated microbiome samples were analyzed using hierarchical Ward's linkage clustering (Dillner et al., 2005), eight distinct clusters were apparent in the amalgamation schedule graph (**Figure 5A**), with the decreasing linkage distance after the seventh fusion step indicating a minimal difference for any newly formed clusters. Euclidean distances between the centers of clusters confirmed the distinct nature of each cluster, with all clusters largely apart from each other (**Table S3**). Subsequent K-means clustering was then carried out to identify members of each of the clusters (**Table 3A**). The largest cluster (#6) contained 98% of the freshwater (54/55) and 52% of the saline (32/62) samples, supporting the distinct grouping of saline and freshwater samples observed in the PCoA

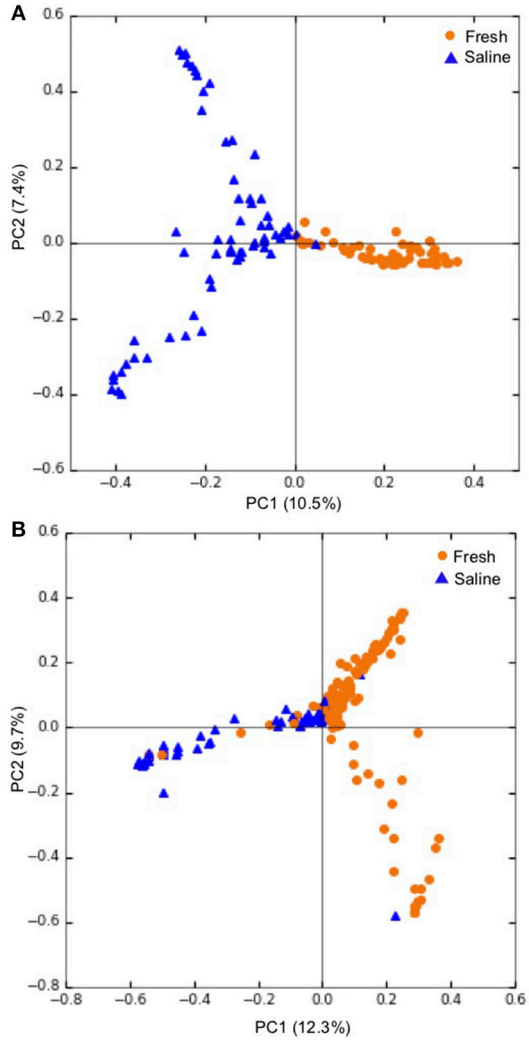


**FIGURE 3 |** Principal coordinate analysis (PCoA) showing grouping of **(A)** individual skin microbiomes at fresh ($n = 55$), and saline ($n = 63$) sites and **(B)** individual intestinal microbiomes at fresh ($n = 144$) and saline ($n = 58$) sites. PCoA ordinations are based on the Bray-Curtis dissimilarity metric. Freshwater sites include lake and river sites sampled in winter and spring while saline sites refer to sea shoreline locations sampled in autumn during the annual char run.

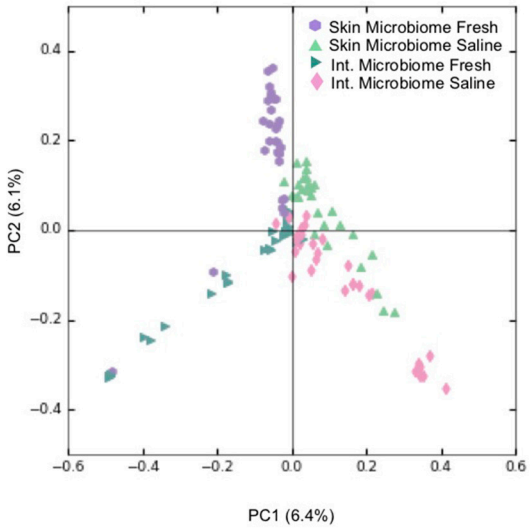


**FIGURE 4 |** Principal coordinate analysis (PCoA) showing clustering of individual skin and intestinal microbiome communities based on Bray-Curtis dissimilarity. For every skin-associated community represented, a counterpart intestine-associated community from the same *S. alpinus* individual is shown. Legend refers to the sample type and environment of where an *S. alpinus* individual was caught and includes skin microbiomes from freshwater sites ($n = 30$), and from saline sites ($n = 30$), as well as intestinal microbiomes from freshwater sites ($n = 30$) and from saline sites ($n = 30$). Fresh refers to lake and river sites sampled in winter and spring while saline refers to sea shoreline locations sampled in autumn during the annual char run.

ordinations (**Figure 3**). Because many of the fish were netted in autumn, during the annual char migration, it is probable that some saline-associated microbiota could remain in the same cluster as the microbiota from freshwater fish. The ANOVA results show that of the 899 taxa used in the clustering analysis, 56 have a *p*-value below 0.05. These results also indicated that Proteobacteria, Cyanobacteria, and Firmicutes contributed most to the clustering analysis (**Table S4**). As an approach to identify a core microbiome for Arctic char skin, bacteria present across the eight clusters were identified (**Table 4A**). The fact that none of the nine taxa, except for *Clostridium*, matched to any known genus likely emphasizes the paucity of research for this wild species. For example, an unknown genus from the Acetobacteraceae family represents over 5% of the total microbiota. In contrast to the clustering based on a saline environment, no correlation was obtained between the presence of any of the microbial genus species and the sex, age, or size of the Arctic char samples ($p > 0.05$; data not shown).

## Characterization of the Intestinal Microbiota

The 202 intestinal microbiome samples were tested by hierarchical Ward's linkage clustering (Dillner et al., 2005) to investigate the link between salinity and intestine-associated microbiota. The amalgamation schedule graph again showed seven major fusion steps, resulting in eight distinct clusters (**Figure 5B**) with Euclidean distances between clusters showing their distinctive nature (**Table S5**). Of the 59 intestinal microbiome samples from freshwater and 143 from saline sites, two clusters (#6 and #8) were dominated by samples from saline water sites whereas another two clusters (#2 and #5) only showed samples from freshwater (**Table 3B**). Therefore, these clusters provide further support to the PCoA analysis (**Figure 3**) that salinity is a statistically significant variable defining the Arctic char intestine-associated microbiome. The ANOVA results indicate that of the 507 taxa used in the clustering analysis, 50 have a *p*-value below 0.05. The phylum Proteobacteria accounted for 25 of these taxa (**Table S6**). Members defined as belonging to an "unidentified kingdom" represented over 6% of the microbial community in two clusters (#4 and #5). Overall, the intestinal core microbiome appears more diverse

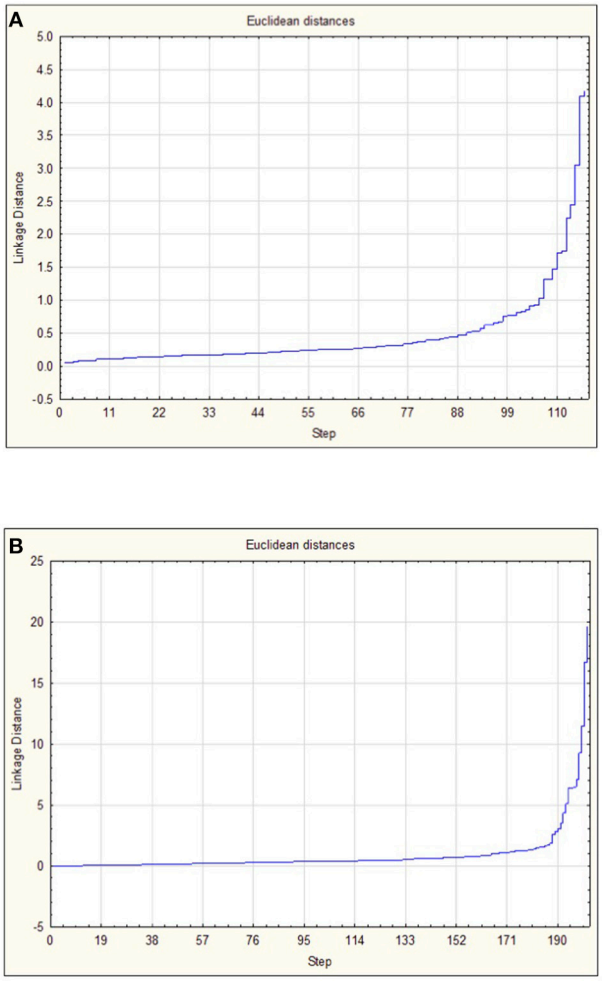


**FIGURE 5 |** Amalgamation schedule used to identify the number of major clusters (K) for **(A)** OTUs from skin-associated microbiomes and **(B)** OTUs from intestine-associated microbiomes. Linkage distance is shown in addition to the visualization of steps.

than that of the skin, with 14 taxa present in all eight clusters (**Table 4B**). Clusters (#1–#7) included taxa that represented ∼8% or more of the community, with 4 and 8 clusters with a single genus occupying over 50% of the entire intestinal microbiome. The taxa included unidentified genera from families Fusobacteriaceae, Comamonadaceae, Pseudomonadaceae, and Vibrionaceae. Other members of the intestinal-associated microbiome include *Streptococcus, Sphingomonas, Shewanella, Pseudomonas, Aliivibrio, Photobacterium*, and *Mycoplasma* (**Table 4B**). Again, no correlation was obtained between the presence of any of the microbial genus species and the sex, age, or size of the Arctic char ($p > 0.05$; not shown). Additionally, since hierarchical Ward's linkage clustering was implemented on skin and intestine samples without regard to fishing site, we postulate that the following results provide further evidence that the changes in microbiome between fish caught in saline and freshwater environments are strongly linked to salinity.

**TABLE 3 | (A)** Sample counts of each cluster, showing number of samples either caught in a saline or freshwater environment, as obtained using K mean clustering analysis using the skin microbiome data at genus level and **(B)** Sample counts of each cluster, showing number of samples either caught in a saline or fresh environment, as obtained using K mean clustering analysis using the intestinal microbiome data at genus level.

| Cluster | Saline | Fresh |
|---|---|---|
| **(A)** | | |
| 1 | 9 | 0 |
| 2 | 12 | 0 |
| 3 | 3 | 0 |
| 4 | 1 | 1 |
| 5 | 1 | 0 |
| 6 | 31 | 54 |
| 7 | 1 | 0 |
| 8 | 3 | 0 |
| **(B)** | | |
| 1 | 2 | 7 |
| 2 | 0 | 8 |
| 3 | 1 | 11 |
| 4 | 21 | 82 |
| 5 | 0 | 14 |
| 6 | 19 | 2 |
| 7 | 1 | 19 |
| 8 | 8 | 1 |

# DISCUSSION

## Microbial Structure in the Skin and Intestinal Mucous

The commensal microbes contributing to these Arctic char skin- and intestine-associated microbiome communities were found to be distinct from one another (**Table 2**; **Figure 2**; **Tables S1**, **S2**). There have been few published reports on skin-associated microbiomes, especially in wild fish, possibly because of the challenges associated with ensuring aseptic collection practices and optimal preservation techniques (Kueneman et al., 2014). Microbiome analysis on the skin of anadromous Atlantic salmon, *S. salar,* showed that Proteobacteria was the dominant phylum (Lokesh and Kiron, 2016), and it was also dominant in the majority of our skin samples taken from freshwater Arctic char (**Figure 2A**). Significant differences in the microbiome from fish caught in fresh and saline waters suggests that the skin microbial community changes as the fish swim from one environment to another. Part of the challenge, and likely reflecting the generally unstudied field, is the large proportion of unknown genera in the skin-associated microbiome; 8 of 9 organisms making up the putative core microbiome are currently unknown, and in addition, over 1% of the microbial community belonged to unknown phyla (**Table 4A**). Some of these currently unknown members likely serve important roles in the skin mucous, suggesting that metagenomic analysis could perhaps be used to assign putative roles in waste removal, osmoregulation, glycoprotein-mediated drag reduction, and in immune function, and would be of interest for future experiments.

**TABLE 4 | (A)** Microorganisms, classified to genus where possible, present in eight clusters along with the percentage within the skin microbiome of Arctic char and **(B)** Microorganisms, classified to genus where possible, present in eight clusters along with the percentage within the intestinal microbiome of Arctic char.

| Taxonomy | Cluster number and percent abundance | | | | | | | |
|---|---|---|---|---|---|---|---|---|
| | 1 | 2 | 3 | 4 | 5 | 6 | 7 | 8 |
| **(A)** | | | | | | | | |
| Other bacteria | 0.96 | 1.61 | 2.04 | 0.28 | 0.52 | 1.93 | 0.81 | 0.74 |
| p: Actinobacteria c: Actinobacteria o: Actinomycetales f: Other g: Other | 0.30 | 0.81 | 0.85 | 0.05 | 0.19 | 0.80 | 0.05 | 0.30 |
| p: Proteobacteria c: Other o: Other f: Other g: Other | 0.07 | 0.20 | 0.03 | 0.17 | 0.09 | 0.55 | 0.05 | 0.03 |
| p: Proteobacteria c: Alphaproteobacteria o: Rhodospirillales f: Acetobacteraceae g: Unknown | 0.45 | 4.14 | 4.73 | 0.05 | 1.52 | 5.15 | 0.14 | 0.03 |
| p: Cyanobacteria c: Other o: Other f: Other g: Other | 0.41 | 3.99 | 0.19 | 0.00 | 0.19 | 0.32 | 0.05 | 0.06 |
| p: Firmicutes c: Bacilli o: Lactobacillales f: Other g: Other | 2.67 | 0.20 | 0.02 | 0.02 | 0.00 | 0.17 | 3.94 | 57.1 |
| p: Firmicutes c: Clostridia o: Clostridiales f: Clostridiaceae g: *Clostridium* | 2.42 | 0.22 | 72.0 | 0.00 | 0.14 | 0.78 | 0.09 | 0.27 |
| p: Proteobacteria c: Alphaproteobacteria o: Rhodobacterales f: Rhodobacteraceae g: Other | 0.11 | 0.30 | 0.14 | 0.02 | 70.2 | 0.94 | 0.00 | 0.09 |
| p: Proteobacteria c: Betaproteobacteria o: Burkholderiales f: Comamonadaceae g: Other | 0.13 | 0.21 | 0.08 | 87.42 | 0.47 | 2.73 | 0.00 | 0.03 |
| **(B)** | | | | | | | | |
| Unclassified | 2.16 | 2.17 | 1.48 | 8.20 | 6.26 | 0.21 | 1.28 | 0.15 |
| Other Bacteria | 0.39 | 0.38 | 3.62 | 1.37 | 1.03 | 0.38 | 0.16 | 1.09 |
| p: Actinobacteria c: Actinobacteria o: Actinomycetales f: Other g: Other | 3.59 | 0.01 | 0.02 | 0.14 | 0.01 | 0.03 | 0.05 | 0.16 |
| p: Firmicutes c: Bacilli o: Lactobacillales f: Streptococcaceae g: *Streptococcus* | 0.03 | 0.28 | 1.02 | 2.35 | 1.81 | 0.08 | 0.34 | 0.44 |
| p: Fusobacteria c: Fusobacteriia o: Fusobacteriales f: Fusobacteriaceae g: *u114* | 0.03 | 0.04 | 84.2 | 0.79 | 0.02 | 1.64 | 0.01 | 2.70 |
| p: Proteobacteria c: Alphaproteobacteria o: Sphingomonadales f: Sphingomonadaceae g: *Sphingomonas* | 9.56 | 0.02 | 0.17 | 10.5 | 0.23 | 0.62 | 0.06 | 0.46 |
| p: Proteobacteria c: Betaproteobacteria o: Burkholderiales f: Comamonadaceae g: Other | 0.07 | 0.11 | 0.01 | 2.48 | 52.5 | 0.61 | 1.01 | 0.17 |
| p: Proteobacteria c: Gammaproteobacteria o: Alteromonadales f: Shewanellaceae g: *Shewanella* | 2.74 | 0.57 | 0.03 | 1.29 | 1.50 | 0.57 | 0.04 | 0.03 |
| p: Proteobacteria c: Gammaproteobacteria o: Pseudomonadales f: Pseudomonadaceae g: Other | 0.08 | 8.23 | 2.46 | 1.27 | 1.32 | 0.45 | 85.0 | 0.20 |
| p: Proteobacteria c: Gammaproteobacteria o: Pseudomonadales f: Pseudomonadaceae g: *Pseudomonas* | 0.01 | 0.70 | 0.14 | 2.66 | 1.47 | 0.31 | 3.80 | 0.15 |
| p: Proteobacteria c: Gammaproteobacteria o: Vibrionales f: Vibrionaceae g: Other | 0.11 | 0.01 | 0.17 | 2.43 | 0.47 | 6.11 | 0.01 | 0.09 |
| p: Proteobacteria c: Gammaproteobacteria o: Vibrionales f: Vibrionaceae g: *Alivibrio* | 0.20 | 0.01 | 0.13 | 3.20 | 0.80 | 3.47 | 0.01 | 0.04 |
| p: Proteobacteria c: Gammaproteobacteria o: Vibrionales f: Vibrionaceae g: *Photobacterium* | 0.24 | 0.27 | 0.68 | 1.78 | 0.02 | 71.0 | 0.38 | 4.49 |
| p: Tenericutes c: Mollicutes o: Mycoplasmatales f: Mycoplasmataceae g: *Mycoplasma* | 73.8 | 0.20 | 1.37 | 2.11 | 0.36 | 1.19 | 0.42 | 2.14 |

*Taxonomy from phylum (p) to clade (c) to order (o) to family (f) to genus (g) is shown.*

In contrast to the paucity of information on skin-associated microbiomes, intestine-associated microbiomes have been better studied, although not extensively in wild, ocean-going fish (Egerton et al., 2018). Previously reported microorganisms present in the Arctic char gut include *Aeromonas*, *Flavobacterium*, *Pseudomonas*, *Lactobacillus*, and *Vibrio* (Ringø and Strøm, 1994; Ringø et al., 1995; Nyman et al., 2017). Lactic acid bacteria (phylum Firmicutes), Fusobacteria, Bacteroidetes, Gammaproteobacteria, Planctomycetes, Clostridia, Verrumicrobia and Bacilli have all been reported as a normal part of the intestine-associated microbiomes in several fish species (Ringø and Gatesoupe, 1998; Befring-Hovda, 2007; Ingerslev et al., 2014; Ghanbari et al., 2015). The results reported here are therefore consistent with the previous literature, demonstrating that the community found in wild adult *S. alpinus* intestine-associated microbiomes is not fundamentally different from other fish.

The core intestine-associated microbiome in Arctic char includes taxa from the Gammaproteobacteria class as well as three genera within the Vibrionaceae family (**Table 4B**), similar to observations from Antarctic notothenioid fish species (Ward et al., 2009). We also noted the presence of *Streptococcus* and *Mycoplasma*. *Mycoplasma* have been reportedly abundant in Antarctic fish and Atlantic salmon (Holben et al., 2002; Song et al., 2016; Dehler et al., 2017). Unlike in humans where *Mycoplasma* and certain *Streptococcus* are associated with dysbiosis, these genera are proposed to be important for lipid and sugar metabolism and are therefore included in the core intestinal microbiome for Atlantic salmon (Dehler et al., 2017). In vertebrates, *Sphingomonas* have been associated with the early-life education of the immune system (Olszak et al., 2012; Wingender et al., 2012; Caballero and Pamer, 2015; Gensollen et al., 2016), and therefore may play a similar role in the gut of Arctic char.

Notwithstanding the distinct profiles of the skin- and intestine-associated microbiomes, they appear to share certain taxa, including psychrophilic genera, such as *Psychrobacter*, *Shewanella*, *Flavobacterium*, *Acinetobacter*, *Photobacterium*,

*Planctomyces*, and *Psychromonas*, and including bacteria belonging to the phyla Firmicutes and Cyanobacteria, which could contribute to geochemical cycles, including the nitrogen cycle. Certainly, both microbial community compositions were significantly influenced by the environment in which the fish were caught (**Figure 3**; **Table 3**), with *Photobacterium* and *Deinococcus* increasing over 1–2 orders of magnitude when intestine- and skin-associated microbiomes, respectively, were recovered from saline water samples. There was no apparent correlation with other measured biotic factors. Our results on wild Arctic char populations are in accord with previous reports including Atlantic salmon, in that they showed salinity-mediated turnover in microbial distributions across the skin and intestines (Schmidt et al., 2015; Lokesh and Kiron, 2016; Dehler et al., 2017). Manipulation of the skin and intestinal microbiomes by deliberate salinity changes in aquaculture has not yet been explored, but our results suggest that a directed turnover in taxa might be achieved by such a protocol, and should be considered to prevent or inhibit dysbiosis. Although there has been some examination of the survival of farmed *S. alpinus* at higher salinities, consensus has not yet been reached on best practices for inland recirculating systems (Jørgensen et al., 1993; Larsson and Berglund, 1998; Summerfelt et al., 2004; Duston et al., 2007). To date, existing aquaculture studies have focused on the osmoregulatory consequences of keeping stocks at low salinity or the transfer of young fish from freshwater to a potential saltwater grow-out phase (Arnesen et al., 1993; Aarset, 1999; Duston et al., 2007), but there has been little consideration of the Arctic char skin-associated microbiome, nor of skin- and intestine-associated microbiomes together, and yet the biotechnological applications for manipulation of the microbiota by probiotics is of considerable interest.

## Bioprospecting in the Skin and Intestinal Microbiomes

Anadromous Arctic char from this high Arctic region grow more rapidly than other local salmonids and live several decades (McPhedran et al., unpublished data). Therefore, we posit that knowledge of the microbiota could be helpful in the development of sustainable and efficient aquaculture practices and to provide an alternate modality to overcome the adverse effects of antibiotics and drugs (Nayak, 2010). As suggested above, consideration could be given to the manipulation of salt concentrations in Arctic char aquaculture to deliberately direct bacterial communities and possibly bypass dysbiotic episodes. Alternatively, individual isolates may prove valuable. Previously, lactic acid bacteria including *Streptococcus* have been used as probiotics and specifically for furunculosis in rainbow trout, *Oncorhynchus mykiss* (Balcázar et al., 2007; Pandiyan et al., 2013). This is a serious infection of farmed fish causing skin lesions, hemorrhaging, intestinal tissue damage, and death (Ringø et al., 2004). Other studies have reported the beneficial effect of *Shewanella* and *Vibrio* probiotics (Kamei et al., 1988; Irianto and Austin, 2002; Díaz-Rosales et al., 2006a,b). The bacteria that we detected in Arctic char skin- and intestine-associated microbiomes, especially those identified as part of the core microbiome, therefore have potential in probiotic applications for aquaculture where they could play a role in immune development and promote the health and growth of farmed fish.

Many OTUs in the skin and intestinal microbiomes represented unidentified microorganisms, and it suggests that the microbial diversity associated with these wild Arctic char provides fertile ground for bioprospecting for psychrophiles and osmotolerant organisms. For example, some known organisms that are psychrophilic and halophilic are a good source for polyunsaturated fatty acids (PUFA) (Russell and Nichols, 1999). Russell (1998) proposed that PUFA in marine psychrophiles allows them to balance the requirement for a fluid membrane at low temperatures with the retention of a requisite level of order. Given these functions, PUFA-producing bacteria may represent an alternate source for human use, with the added advantage of containing only one long-chain PUFA rather than the multiple components present in fish or algal oils (de Pascale et al., 2012).

As indicated, taxa involved in nitrogen fixation (Cyanobacteria and Rhizobiales), nitrate oxidation (Nitrospirales), and nitrite oxidization (*Nitrospira*) are present in the skin- and intestine-associated microbiomes (**Tables S1**, **S2**). Their presence suggests that they may provide an inorganic source of nitrogen when organic nitrogen is low, such as when prey may not be as readily available during the winter under ice. Similar results have been observed by Lee and Childress (1994) and Shah et al. (in press) in marine invertebrates. Isolates of Nitrospirales, *Nitrospira*, and *Paracoccus,* identified in Arctic char that are adapted to low temperature conditions might be employed in municipal and domestic wastewater treatment facilities where wastewater temperatures fall below 10 °C in winter, and when microbial activity is normally severely depressed (Xu et al., 2018). Similarly, isolates of *Pseudomonas, Shewanella, Bacillus, Arthrobacter,* and *Sphingobacterium* in the intestine-associated microbiome (**Table 4B**) could play an important role in degradation of pollutants during wastewater treatment. Some bacteria (e.g., members of the Rhizobiales) could even find utility as nitrogen fixers if used for agricultural applications under low temperature conditions.

Bioprospecting need not be restricted to probiotics, however. Further exploration of identified extremophiles may be useful for other applications. For example, between 6 and 8 million tons of waste crab, shrimp, and lobster shells are produced globally, with the chitin-rich wastes dumped in landfills or the sea (Yan and Chen, 2015). The presence of OTUs representing *Photobacterium,* in the intestine-associated microbiome of Arctic char (**Table 2B**), with members of this taxon known to aid in chitin digestion (MacDonald et al., 1986; Ramesh and Venugopalan, 1989; Itoi et al., 2006) is noteworthy. It suggests that in the future, chitin-containing seafood waste could be used as supplements for fish food in aquaculture facilities, and also used as a probiotic supplement for Arctic char and other fish.

In general, our results highlight the need to further explore structural and functional aspects of the microbial communities that naturally inhabit *S. alpinus*. The turnover of both the skin- and intestine-associated communities together during

migration represents a previously underappreciated stressor for the species that could be exploited for biotechnological applications including advanced aquaculture systems. The specific taxa observed suggest the potential for isolating useful probiotics, whilst the number of undefined taxa exposes a lack of understanding of this ecosystem, the resolution of which could benefit our understanding of Arctic marine ecosystems as a whole.

## DATA AVAILABILITY

The datasets generated for this study can be found in European Nucleotide Archive, ERP111452.

## ETHICS STATEMENT

Fish were sampled in accordance with an approved and issued license to fish for scientific purposes in the waters of the Northwest Territories, Yukon north slope, and Nunavut (in accordance with section 52 of the general fishery regulations of the fisheries act, Fisheries and Oceans, Canada; current permit number S-18/19-1045-NU) along with an associated animal care permit approved and issued by the Fresh Water Institute Animal Care Committee of the Department of Fisheries and Oceans (current permit number FWI-ACC AUP-2018-63).

## AUTHOR CONTRIBUTIONS

PvCdG organized the fish collection. JDN and KE undertook sequencing and provided bioinformatics analysis. EFH and GE isolated the DNA and conducted statistical analyses. VS did additional statistical analyses. VKW designed the study. EFH, VS, and VKW drafted the manuscript. All authors have read and accepted the final manuscript.

## FUNDING

This work was funded by the Government of Canada through Genome Canada and the Ontario Genomics Institute (OGI-096). We also acknowledge funding from the Natural Sciences and Engineering Research Council (Canada), the Ontario Ministry of Research and Innovation, CanNor, the Government of Nunavut, and the Northern Scientific Training Program (Polar Knowledge Canada).

## ACKNOWLEDGMENTS

We thank the Gjoa Haven, NU community residents, the Hunters and Trappers Association (HTA), and all of the associated supporters of the Towards a Sustainable Fishery for Nunavummiut. We would like to thank all sampling personnel that provided invaluable help in the field, and particularly the Gjoa Haven fishermen who were integral to the fish sampling efforts. We would also like to thank Eric T. Daechsel for producing the map for this publication, Kristy Moniz for her valuable technical support throughout the sampling and processing efforts, and Dr. Charles W. Greer (National Research Council) for facilitating and providing the initial water microbiome analyses with alternative primers.

## SUPPLEMENTARY MATERIAL

The Supplementary Material for this article can be found online at: https://www.frontiersin.org/articles/10.3389/fbioe.2019.00032/full#supplementary-material

## REFERENCES

Aarset, B. (1999). Aquacultural development, institution building and research and development policy: Norwegian salmon and Arctic char farming as cases. *Aquacult. Econ. Manage.* 3, 177–191. doi: 10.1080/13657309909380244

Apprill, A., Robbins, J., Eren, A. M., Pack, A. A., Reveillaud, J., Mattila, D., et al. (2014). Humpback whale populaions share a core skin bacterial community: towards a health index for marine mammals? *PLoS ONE*. 9:e90785. doi: 10.1371/journal.pone.0090785

Arnesen, A. M., Jørgensen, E. H., and Jobling, M. (1993). Feed intake, growth and osmoregulation in Arctic charr, *Salvelinus alpinus* (L.), transferred from freshwater to saltwater at 8 °C during summer and winter. *FISH.* 12, 281–292.

Balcázar, J. L., De Blas, I., Ruiz-Zarzuela, I., Vendrell, D., Gironés, O., and Muzquiz, J. L. (2007). Enhancement of the immune response and protection induced by probiotic lactic acid bacteria against furuncolosis in rainbow trout (*Oncorhynchus mykiss*). *FEMS Immunol. Med. Microbiol.* 51, 185–193. doi: 10.1111/j.1574-695X.2007.00294.x

Bartram, A. K., Lynch, M. D. J., Stearns, J. C., Moreno-Hagelsieb, G., and Neufeld, J. D. (2011). Generation of multimillion-sequence 16S rRNA gene libraries from complex microbial communities by assembling paired-end Illumina reads. *Appl. Environ. Microbiol.* 77, 3846–3852. doi: 10.1128/AEM.02772-10

Befring-Hovda, M. (2007). *Application of PCR and DGGE to Characterize the Microflora of Farmed Fish*. Bergen: Doctoral Disseration, University of Bergen.

Boutin, S., Bernatchez, L., Audet, C., and Derôme, N. (2013). Network analysis highlights complex interactions between pathogen, host and commensal microbiota. *PLoS ONE* 8:e84772. doi: 10.1371/journal.pone.0084772

Caballero, S., and Pamer, E. G. (2015). Microbiota-mediated inflammation and antimicrobial defense in the intestine. *Annu. Rev. Immunol.* 33, 227–256. doi: 10.1146/annurev-immunol-032713-120238

Caporaso, J. G., Kuczynski, J., Stombaugh, J., Bittinger, K., Bushman, F. D., Costello, E. K., and Knight R (2010). QIIME allows analysis of high-throughput community sequencing data. *Nat. Methods.* 7, 335–336. doi: 10.1038/nmeth.f.303

Caporaso, J. G., Lauber, C. L., Walters, W. A., Berg-Lyons, D., Lozupone, C. A., Turnbaugh, P. J., et al. (2011). Global patterns of 16S rRNA diversity at a depth of millions of sequences per sample. *PNAS* 108, 4516–4522. doi: 10.1073/pnas.1000080107

Carmack, E. C. (2007). The alpha/beta ocean distinction: a perspective on freshwater fluxes, convection, nutrients and productivity in high-latitude seas. *Deep Sea Res. Part II: Top Stud. Oceanogr.* 54, 2578–2598. doi: 10.1016/j.dsr2.2007.08.018

Chiarello, M., Villéger, S., Bouvier, C., Bettarel, Y., and Bouvier, T. (2015). High diversity of skin-associated bacterial communities of marine fishes is promoted by their high variability among body parts, individuals and species. *FEMS Microbiol. Ecol.* 91:fiv061. doi: 10.1093/femsec/fiv061

Clarke, K. R., Gorely, R. N., Somerfield, P. J., and Warwick, R. M. (2014). *Change in Marine Communities: An Approach to Statistical Analysis and Interpretation*, 3rd edition. Plymouth: PRIMER-E.

Coolen, M. J., Post, E., Davis, C. C., and Forney, L. J. (2005). Characterization of microbial communities found in the human vagina by analysis of terminal restriction fragment length polymorphisms of 16S rRNA genes. *Appl. Environ. Microbiol.* 71, 8729–8737. doi: 10.1128/AEM.71.12.8729-8737.2005

de Pascale, D., De Santi, C., Fu, J., and Landfald, B. (2012). The microbial diversity of Polar environments is a fertile ground for bioprospecting. *Mar. Genom.* 8, 15–22. doi: 10.1016/j.margen.2012.04.004

Dehler, C. E., Secombes, C. J., and Martin, S. A. M. (2017). Seawater transfer alters the intestinal microbiota profiles of Atlantic salmon (*Salmo salar* L.). *Sci. Rep.* 7:13877. doi: 10.1038/s41598-017-13249-8

Díaz-Rosales, P., Chabrillón, M., Arijo, S., Martinez-Manzanares, E., Moriñigo, M. A., and Balebona, M. C. (2006b). Superoxide dismutase and catalase activities in photobacterium *Damselae* ssp. *piscicida. J. Fish Dis.* 29, 355–364. doi: 10.1111/j.1365-2761.2006.00726.x

Díaz-Rosales, P., Salinas, I., Rodriguez, A., Cuesta, A., Chabrillon, M., Balebona, M. C., et al. (2006a). Gilthead seabream (*Sparus aurata* L.) innate immune response after dietary administration of heat-inactivated potential probiotics. *Fish Shellfish Immun.* 20, 482–492. doi: 10.1016/j.fsi.2005.06.007

Dillner, A. M., Schauer, J. J., Christensen, W. F., and Cass, G. R. (2005). A quantitiative method for clustering size distributions of elements. *Atmos. Environ.* 39, 1525–1537. doi: 10.1016/j.atmosenv.2004.11.035

Duston, J., Astatkie, T., and Murray, S. B. (2007). Effect of salinity at constant 10 °C on grow-out of anadromous Arctic charr from Labrador. *Aquaculture*. 273, 679–686. doi: 10.1016/j.aquaculture.2007.10.035

Edgar, R. C. (2013). UPARSE: highly accurate OTU sequences from microbial amplicon reads. *Nat. Methods*. 10, 996–998. doi: 10.1038/nmeth.2604

Edgar, R. C., Haas, B. J., Clemente, J. C., Quince, C., and Knight, R. (2011). UCHIME improves sensitivity and speed of chimera detection. *Bioinformatics* 27, 2194–2200. doi: 10.1093/bioinformatics/btr381

Egerton, S., Culloty, S., Whooley, J., Stanton, C., and Ross, R. P. (2018). The gut microbiota of marine fish. *Front. Microbiol.* 9:873. doi: 10.3389/fmicb.2018.00873

Esteban, M., and Cerezuela, R. (2015). "4-Fish mucosal immunity: skin A2," in *Mucosal Health in Aquaculture*, eds H.B. Beck and E. Peatman (London, UK: Elsevier Inc.), 67–92. doi: 10.1016/B978-0-12-417186-2.00004-2

Gensollen, T., Iyer, S. S., Kasper, D. L., and Blumberg, R. S. (2016). How colonization by microbiota in early life shapes the immune system. *Science* 352, 539–544. doi: 10.1126/science.aad9378

Ghanbari, M., Kneifel, W., and Domig, K. J. (2015). A new view of the fish gut microbiome: advances from next-generation sequencing. *Aquaculture* 448, 464–475. doi: 10.1016/j.aquaculture.2015.06.033

Holben, W. E., Williams, P., Saarinen, M., Särkilahti, L. K., and Apajalahti, J. H. A. (2002). Phylogenetic analysis of intestinal microflora indicates a novel *Mycoplasma* phylotype in farmed and wild salmon. *Microb. Ecol.* 44, 175–185. doi: 10.1007/s00248-002-1011-6

Ingerslev, H. C., von Gersdorff Jørgensen, L., Strube, M. L., Larsen, N., Dalsgaard, I., Boye, M., et al. (2014). The development of the gut microbiota in rainbow trout (*Oncorhynchus mykiss*) is affected by first feeding and diet type. *Aquaculture* 424, 24–34. doi: 10.1016/j.aquaculture.2013.12.032

Irianto, A., and Austin, B. (2002). Use of probiotics to control furunculosis in rainbow trout, *Oncorhynchus mykiss* (Walbaum). *J. Fish Dis.* 25, 333–342. doi: 10.1046/j.1365-2761.2002.00375.x

Itoi, S., Okamura, T., Koyama, Y., and Sugita, H. (2006). Chitinolytic bacteria in the intestinal tract of Japanese coastal fishes. *Can. J. Microbiol.* 52, 1158–1163. doi: 10.1139/w06-082

Jørgensen, E. H., Christiansen, J. S., and Jobling, M. (1993). Effects of stocking density on food intake, growth performance and oxygen consumption in Arctic charr (*Salvelinus alpinus*). *Aquaculture* 110, 191–204. doi: 10.1016/0044-8486(93)90272-Z

Kamei, Y., Yoshimizu, M., Ezura, Y., and Kimura, T. (1988). Screening of bacteria with antiviral activity from fresh water salmonid hatcheries. *Microbiol. Immunol.* 32, 67–73. doi: 10.1111/j.1348-0421.1988.tb01366.x

Kueneman, J. G., Parfrey, L. W., Woodhams, D. C., Archer, H. M., Knight, R., and McKenzie, V. J. (2014). The amphibian skin-associated microbiome across species, space and life history stages. *Mol. Ecol.* 23, 1238–1250. doi: 10.1111/mec.12510

Lane, D. J. (1991). "16S/23S rRNA sequencing". *Nucl. Acid Techniq. Bact. Systemat.* 115–175.

Larsson, S., and Berglund, I. (1998). Growth and food consumption of 0+ Arctic charr fed pelleted or natural food at six different temperatures. *J. Fish Biol.* 52, 230–242. doi: 10.1111/j.1095-8649.1998.tb00795.x

Lee, R. W., and Childress, J. J. (1994). Assimilation of inorganic nitrogen by marine invertebrates and their chemoautotrophic and methanotrophic symbionts. *Appl. Environ. Microbiol.* 60, 1852–1858.

Lokesh, J., and Kiron, V. (2016). Transition from freshwater to seawater reshapes the skin-associated microbiota of Atlantic salmon. *Sci. Rep.* 6:19707. doi: 10.1038/srep19707

MacDonald, N. L., Stark, J. R., and Austin, B. (1986). Bacterial microflora in the gastro-intestinal tract of Dover sole (*Solea solea* L.), with emphasis on the possible role of bacteria in the nutrition of the host. *FEMS Microbiol. Lett.* 35, 107–111. doi: 10.1111/j.1574-6968.1986.tb01508.x

Masella, A. P., Bartram, A. K., Truszkowski, J. M., Brown, D. G., and Neufeld, J. D. (2012). PANDAseq: paired-end assembler for Illumina sequences. *BMC Bioinformat.* 13:31. doi: 10.1186/1471-2105-13-31

McDonald, D., Price, M. N., Goodrich, J., Nawrocki, E. P., DeSantis, T. Z., Probst, A., et al. (2012). An improved Greengenes taxonomy with explicit ranks for ecological and evolutionary analyses of bacteria and archaea. *ISME J.* 6:610–618. doi: 10.1038/ismej.2011.139

Nayak, S. K. (2010). Probiotics and immunity: a fish perspective. *Fish Shellfish Immun.* 29, 2–14. doi: 10.1016/j.fsi.2010.02.017

Nyman, A., Huyben, D., Lundh, T., and Dicksved, J. (2017). Effects of microbe-and mussel-based diets on the gut microbiota in Arctic charr (*Salvelinus alpinus*). *Aquacult. Rep.* 5, 34–40. doi: 10.1016/j.aqrep.2016.12.003

Olszak, T., An, D., Zeissig, S., Vera, M. P., Richter, J., Franke, A., et al. (2012). Microbial exposure during early life has persistent effects on natural killer T cell function. *Science* 336, 489–493. doi: 10.1126/science.1219328

Pandiyan, P., Balaraman, D., Thirunavukkarasu, R., George, E. G. J., Subaramaniyan, K., Manikkam, S., et al. (2013). Probiotics in aquaculture. *Drug Invent. Today* 5, 55–59. doi: 10.1016/j.dit.2013.03.003

Parada, A. E., Needham, D. M., and Fuhrman, J. A. (2016). Every base matters: assessing small subunit rRNA primers for marine microbiomes with mock communities, time series and global field samples. *Environ. Microbiol.* 18, 1403–1414. doi: 10.1111/1462-2920.13023

Quince, C., Lanzen, A., Davenport, R. J., and Turnbaugh, P. J. (2011). Removing noise from pyrosequenced amplicons. *BMC Bioinformat.* 12:38. doi: 10.1186/1471-2105-12-38

Ramesh, A., and Venugopalan, V. K. (1989). Response of enteric luminous bacteria to environmental conditions in the gut of the fish. *J. Appl. Bacteriol.* 67, 529–533. doi: 10.1111/j.1365-2672.1989.tb02536.x

Ringø, E., and Gatesoupe, F. J. (1998). Lactic acid bacteria in fish: a review. *Aquaculture.* 160, 177–203. doi: 10.1016/S0044-8486(97)00299-8

Ringø, E., Jutfelt, F., Kanapathippillai, P., Bakken, Y., Sundell, K., Glette, J., et al. (2004). Damaging effect of the fish pathogen *Aeromonas salmonicida* ssp. *salmonicida* on intestinal enterocytes of Atlantic salmon *(Salmo salar L.). Cell Tissue Res*. 318, 305–311. doi: 10.1007/s00441-004-0934-2

Ringø, E., and Strøm, E. (1994). Microflora of Arctic charr, *Salvelinus alpinus* (L.): gastrointestinal microflora of free-living fish and effect of diet and salinity on intestinal microflora. *Aquacult. Res.* 25, 623–629. doi: 10.1111/j.1365-2109.1994.tb00726.x

Ringø, E., Strøm, E., and Tabachek, J. A. (1995). Intestinal microflora of salmonids: a review. *Aquacult Res*. 26, 773–789. doi: 10.1111/j.1365-2109.1995.tb00870.x

Russell, N. J. (1998). "Molecular adaptations in psychrophilic bacteria: potential for biotechnological applications," in *Biotechnology of Extremophiles. Advances in Biochemical Engineering/Biotechnology*, Vol 61, ed H Antranikian (Heidelberg: Springer), 1–21. doi: 10.1007/BFb0102287

Russell, N. J., and Nichols, D. S. (1999). Polyunsaturated fatty acids in marine bacteria- a dogma rewritten. *Microbiology* 145, 767–779. doi: 10.1099/13500872-145-4-767

Schmidt, V. T., Smith, K. F., Melvin, D. W., and Amaral-Zettler, L. A. (2015). Community assembly of a euryhaline fish microbiome during salinity acclimation. *Mol. Ecol.* 24, 2537–2550. doi: 10.1111/mec.13177

Shah, V., Tanacredi, J., and Joshi, V. (in press). "Microbial flora associated with laboratory breed horseshoe crabs," in *The Conservation and Biology of Horseshoe Crabs: Social and Ecological Global Perspectives*. ed J. T. Tanacredi,

M. Botton, P. Shin, S. G. Cheung, R. Carmichael and Y. Iwasaki. (Dordrecht: Springer Publishers).

Song, W., Li, L., Huang, H., Jiang, K., Zhang, F., Chen, X., et al. (2016). The gut microbial community of antarctic fish detected by 16S rRNA gene sequence analysis. *Biomed Res. Int.*.2016, 1–7. doi: 10.1155/2016/3241529

Summerfelt, S. T., Wilton, G., Roberts, D., Rimmer, T., and Fonkalsrud, K. (2004). Developments in recirculating systems for Arctic char culture in North America. *Aquacult. Eng.* 30, 31–71. doi: 10.1016/j.aquaeng.2003.09.001

Vázquez-Baeza, Y., Pirrung, M., Gonzalez, A., and Knight, R. (2013). EMPeror: a tool for visualizing high-throughput microbial community data. *Gigascience* 2:16. doi: 10.1186/2047-217X-2-16

Wang, Q., Garrity, G. M., Tiedje, J. M., and Cole, J. R. (2007). Naive Bayesian classifier for rapid assignment of rRNA sequences into the new bacterial taxonomy. *Appl. Environ. Microbiol.* 73, 5261–5267. doi: 10.1128/AEM.00062-07

Ward, N. L., Steven, B., Penn, K., Meth,é, B. A., and Detrich, W. H. (2009). Characterization of the intestinal microbiota of two Antarctic notothenioid fish species. *Extremophiles* 13, 679–685. doi: 10.1007/s00792-009-0252-4

Watling, K. (2007). *Queensland Government Natural Resources and Water*. Measuring salinity. (Report No. L137).

Wingender, G., Stepniak, D., Krebs, P., Lin, L., McBride, S., Wei, B., et al. (2012). Intestinal microbes affect phenotypes and functions of invariant natural killer T cells in mice. *Gastroenterology* 143, 418–428. doi: 10.1053/j.gastro.2012.04.017

Xu, S., Yao, J. Q., Ainiwaer, M., and Zhang, Y. J. (2018). Analysis of bacterial community structure of activated sludge from wastewater treatment plants in winter. *Biomed Res. Int.* 2018, 1–8. doi: 10.1155/2018/8278970

Yan, N., and Chen, X. (2015). Sustainability: don't waste seafood waste. *Nature News*. 524:7155. doi: 10.1038/524155a

**Conflict of Interest Statement:** The authors declare that the research was conducted in the absence of any commercial or financial relationships that could be construed as a potential conflict of interest.

frontiers in Bioengineering and Biotechnology

ORIGINAL RESEARCH
published: 07 March 2019
doi: 10.3389/fbioe.2019.00028

# Occurrence of Soil Fungi in Antarctic Pristine Environments

*Paola Durán[1,2]*, Patricio J. Barra[1], Milko A. Jorquera[1,3], Sharon Viscardi[4], Camila Fernandez[2], Cristian Paz[1], María de la Luz Mora[1] and Roland Bol[5]*

*[1] Scientific and Technological Bioresource Nucleus, Universidad de La Frontera, Temuco, Chile, [2] Biocontrol Research Laboratory, Universidad de La Frontera, Temuco, Chile, [3] Laboratorio de Ecología Microbiana Aplicada, Departamento de Ciencias Químicas y Recursos Naturales, Universidad de la Frontera, Temuco, Chile, [4] Departamento de Procesos Diagnósticos y Evaluación, Facultad de Ciencias de la Salud, Universidad Católica de Temuco, Temuco, Chile, [5] Agrosphere (IBG-3), Institute of Bio- and Geosciences, Forschungszentrum Jülich, Jülich, Germany*

OPEN ACCESS

**Edited by:**
*Thomas Bartholomäus Brück, Technische Universität München, Germany*

**Reviewed by:**
*Sunil Khare, Indian Institute of Technology Delhi, India*
*Johannes Kabisch, Darmstadt University of Technology, Germany*
*Wolfram Manuel Brück, University of Applied Sciences and Arts of Western Switzerland, Switzerland*

***Correspondence:**
*Paola Durán*
*paola.duran@ufrontera.cl*

**Specialty section:**
*This article was submitted to Bioprocess Engineering, a section of the journal Frontiers in Bioengineering and Biotechnology*

**Received:** *15 October 2018*
**Accepted:** *31 January 2019*
**Published:** *07 March 2019*

**Citation:**
*Durán P, Barra PJ, Jorquera MA, Viscardi S, Fernandez C, Paz C, Mora ML and Bol R (2019) Occurrence of Soil Fungi in Antarctic Pristine Environments. Front. Bioeng. Biotechnol. 7:28. doi: 10.3389/fbioe.2019.00028*

The presence of fungi in pristine Antarctic soils is of particular interest because of the diversity of this microbial group. However, the extreme conditions that coexist in Antarctica produce a strong selective pressure that could lead to the evolution of novel mechanisms for stress tolerance by indigenous microorganisms. For this reason, in recent years, research on cold-adapted microorganisms has increased, driven by their potential value for applications in biotechnology. Cold-adapted fungi, in particular, have become important sources for the discovery of novel bioactive secondary metabolites and enzymes. In this study, we studied the fungal community structure of 12 soil samples from Antarctic sites, including King George Island (including Collins Glacier), Deception Island and Robert Island. Culturable fungi were isolated and described according to their morphological and phenotypical characteristics, and the richness index was compared with soil chemical properties to describe the fungal community and associated environmental parameters. We isolated 54 fungal strains belonging to the following 19 genera: *Penicillium*, *Pseudogymnoascus*, *Lambertella*, *Cadophora*, *Candida*, *Mortierella*, *Oxygenales*, *Geomyces*, *Vishniacozyma*, *Talaromyces*, *Rhizopus*, *Antarctomyces*, *Cosmospora*, *Tetracladium*, *Leptosphaeria*, *Lecanicillium*, *Thelebolus*, *Bjerkandera* and an uncultured Zygomycete. The isolated fungi were comprised of 70% Ascomycota, 10% Zygomycota, 10% Basidiomycota, 5% Deuteromycota and 5% Mucoromycota, highlighting that most strains were associated with similar genera grown in cold environments. Among the culturable strains, 55% were psychrotrophic and 45% were psychrophilic, and most were Ascomycetes occurring in their teleomorph forms. Soils from the Collins Glacier showed less species richness and greater species dominance compared with the rest of the sites, whereas samples 4, 7, and 10 (from Fildes Bay, Coppermine Peninsula and Arctowski Station, respectively) showed greater species richness and less species dominance. Species richness was related to the C/N ratio, whereas species dominance was inversely related to C and N content. Thus, the structure of the fungal community was mainly related to soil chemical parameters more than sample location and altitude.

**Keywords: Antarctica, fungal community, biodiversity index, extreme environment, cold desert**

## INTRODUCTION

Antarctica is considered the "Land of Peace and Science" because it is the most extreme environment on the planet and represents an interesting and unique habitat for the colonization and survival of natural life. For these reasons, Antarctica is considered an "outdoor laboratory" where we can study different life forms subjected to multiple extreme conditions. The prevalent extreme conditions in Antarctic are low temperature, lack of water availability (cold desert) and precipitation, numerous freeze–thaw cycles, strong wind levels and high sublimation, evaporation and ultraviolet radiation (Selbmann et al., 2007). For this reason, it is very likely that strong selective pressures may have led to the evolution of still unknown mechanisms for stress tolerance by indigenous microorganisms.

Similar to other environments, among the biota present in Antarctica, the microbial life is mainly represented by archaea, bacteria, and fungi (Teixeira et al., 2013; Purves et al., 2016). However, fungi are the most diverse group in the different Antarctic ecosystems, including the soils (Godinho et al., 2015). The survival of fungi in extreme environments is a consequence of both ecological selection and evolutionary adaptations expressed at physiologic, metabolic, structural and genetic levels (Cowan et al., 2014). Selbmann et al. (2007) stated that Antarctic fungi could be cosmopolitan, where some propagules could be transported externally but are unable to grow under Antarctic conditions, while other indigenous well-adapted fungi, mainly psychrotolerants, are able to grow and reproduce even at low temperatures. Both psychotrophic and psychrophilic fungi have the ability to grow at 0°C. Psychotrophic fungi have a maximum growth temperature above 20°C, whereas psychrophilic fungi have an optimum growth temperature of 15°C or lower and a maximum growth temperature of 20°C (Robinson, 2001).

Some studies have determined that these specialized microorganisms are able to tolerate a wide range of stresses, including desiccation, hypersalinity, solar radiation, and low temperatures, by developing functional strategies, such as the production of bioactive compounds (Godinho et al., 2013), cold-active enzymes and antifreeze proteins (Robinson, 2001; Krishnan et al., 2011, 2018). In fact, Pacelli et al. (2017) characterized the effects of spaceflight-relevant radiation on the cryptoendolithic black fungus *Cryomyces antarcticus,* noting that the fungus maintained high survival and metabolic activity with no detectable DNA and ultrastructural damage, even after the highest dose of radiation. To date, the *Cryomyces* genus is considered one of the best eukaryotic models for astrobiological studies and has been used as a model for space experiments over the last decade (Coleine et al., 2018). However, although fungi represent the main microbial group in Antarctica, they are rarely studied (Selbmann et al., 2007).

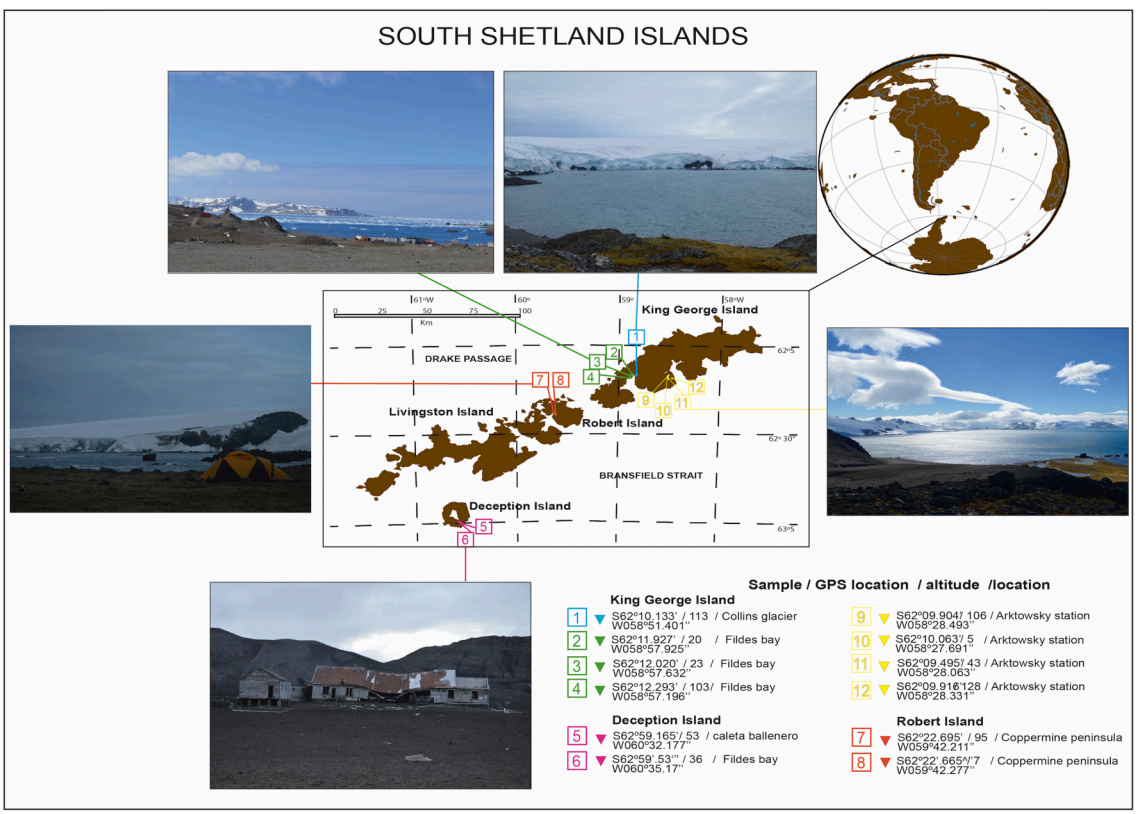


**FIGURE 1 |** Antarctic soil sampling from the South Shetland Islands during expedition ECA53.

In this context, Ding et al. (2016) studied the diversity and biological activities of 150 cultivable fungal strains isolated from Fildes Bay (King George Islands), where 18 isolates produced biologically active compounds. In contrast, Siciliano et al. (2014) characterized fungal and bacterial communities from a broader range of soil conditions, highlighting the importance of edaphic factors in controlling microbial communities, especially fungal communities. Because the vast majority of studies about microbial communities have been confined to bacteria (Maida et al., 2015; Cid et al., 2016; Tedesco et al., 2016; Sannino et al., 2017), very little is currently known about the ecology of fungi inhabiting the Antarctic continent.

Therefore, in this study, we focus on determining, analyzing, and comparing the fungal community structure and composition of twelve Antarctic soils from King George Island (including the Collins Glacier), Deception Island and Robert Island. In addition, culturable fungi were isolated and described according their morphological and phenotypical characteristics.

**TABLE 1 |** Chemical parameters of Antarctic soil samples.

| Soil | C (%) | N (%) | C/N | pH |
|---|---|---|---|---|
| Soil 1 | $2.65 \pm 0.29^{a}$ | $0.36 \pm 0.001^{a}$ | $7.36 \pm 0.81^{c}$ | $6.13 \pm 0.30^{g}$ |
| Soil 2 | $1.03 \pm 0.04^{b}$ | $0.08 \pm 0.000^{d}$ | $12.5 \pm 0.48^{bc}$ | $6.53 \pm 0.08^{f}$ |
| Soil 3 | $0.27 \pm 0.01^{d}$ | $0.02 \pm 0.001^{g}$ | $15.8 \pm 1.53^{b}$ | $6.73 \pm 0.13^{c}$ |
| Soil 4 | $0.46 \pm 0.05^{cd}$ | $0.01 \pm 0.002^{h}$ | $42.1 \pm 4.46^{a}$ | $7.23 \pm 0.22^{a}$ |
| Soil 5 | $0.34 \pm 0.04^{d}$ | $0.04 \pm 0.001^{e}$ | $8.63 \pm 1.05^{bc}$ | $6.74 \pm 0.14^{c}$ |
| Soil 6 | $0.21 \pm 0.01^{d}$ | $0.04 \pm 0.001^{e}$ | $5.92 \pm 0.15^{c}$ | $5.88 \pm 0.18^{j}$ |
| Soil 7 | $1.13 \pm 0.05^{b}$ | $0.20 \pm 0.001^{b}$ | $6.23 \pm 0.30^{c}$ | $5.46 \pm 0.23^{k}$ |
| Soil 8 | $0.25 \pm 0.01^{d}$ | $0.04 \pm 0.001^{e}$ | $6.96 \pm 0.33^{c}$ | $5.61 \pm 0.25^{j}$ |
| Soil 9 | $0.79 \pm 0.01^{bc}$ | $0.11 \pm 0.001^{c}$ | $7.42 \pm 0.18^{c}$ | $5.98 \pm 0.02^{h}$ |
| Soil 10 | $0.10 \pm 0.00^{d}$ | $0.01 \pm 0.001^{h}$ | $7.47 \pm 0.44^{c}$ | $6.58 \pm 0.15^{e}$ |
| Soil 11 | $0.14 \pm 0.01^{d}$ | $0.03 \pm 0.001^{f}$ | $5.53 \pm 0.64^{c}$ | $6.62 \pm 0.04^{d}$ |
| Soil 12 | $0.26 \pm 0.01^{d}$ | $0.04 \pm 0.000^{e}$ | $7.21 \pm 0.62^{c}$ | $6.77 \pm 0.13^{b}$ |

*Tukey test to compare different soil samples, values followed by the same letter do not differ at $P < 0.05$ ($n = 3$).*

# MATERIALS AND METHODS

## Sampling

Bulk soil (without plant influence) samples were collected from South Shetland Island (62°00′S, 59°30′W) during the Antarctic campaign ECA-53, during the austral summer (2017) (**Table 1**). Twelve samples were collected from the top 0–20 cm without the presence of plants (bulk soil). Sample 1 corresponds to the Collins Glacier; samples 2, 3 and 4 correspond to Fildes Bay; samples 5 and 6 correspond to Deception Island; samples 7 and 8 correspond to Coppermine; and samples 9, 10, 11, and 12 correspond to Arctowski Station (**Figure 1**). The samples were transported in coolers (∼4°C) and processed at the Laboratory of Research in Biocontrol located in Universidad de la Frontera.

The chemical properties of the soil samples were determined as follows: carbon and nitrogen concentrations were determined by combustion in a Vario MicroCube elemental analyzer (DIN ISO 10694; Elementar Analysen systeme, Hanau, Germany) according to DIN ISO 10694 (1996). Samples were air dried and finely ground with a mortar and pestle before measurement. Samples did not contain inorganic C; hence, TC equals OC. Soil pH was measured in 1:2.5 soil/deionized water suspensions.

## Isolation of Culturable Fungi

Fungi were isolated from each soil sample according to Gonc et al. (2015). Briefly, 1 g of each sample was added to 9 mL of sterile saline solution (0.85% NaCl) in triplicate and vortexed. One hundred microliters of homogenized soil dilutions at $10^{0}$ and $10^{-2}$ were spread onto YM media (0.3% yeast extract, 0.3% malt extract, 0.5% peptone, 2% glucose, 2% agar, pH 6.2 ± 2). Plates were supplemented with chloramphenicol (100 μg $mL^{-1}$) to prevent bacterial growth. The plates were incubated at 4, 15, and 25°C for 30 days to evaluate the optimal growth temperature of each fungal strain to determinate the existence of psychrophilic and/or psychrotrophic fungi. Pure cultures were visualized by scanning electron microscopy (VP-SEM) with an energy dispersive X-ray spectrometer detector (EDX, Hitachi, Japan).

## Identification of Fungal Strains

Genotypic characterization of selected fungal strains was performed based on sequencing of the ribosomal internal transcribed spacer 2 (ITS2) region. ITS2 was amplified by touchdown polymerase chain reaction (PCR) with the primer set fITS9 (5′-GAACGCAGCRAAIIGYG-3′) and ITS4 (5-′TCC TCCGCTTATTGATATGC-3′) as described by Ihrmark et al. (2016), using the following conditions: an initial denaturation at 95°C for 3 min; followed by 25 cycles each at 95°C for 30 sec; an annealing step with a 0.5°C decrease each cycle from 65 to 52.5°C; and extension at 72°C for 30 sec. Twenty-five additional cycles were carried out with denaturation at 95°C for 30 sec; a 55 °C annealing step; and primer extension at 72°C for 30 sec; with a final extension step of 7 min at 72°C. The PCR products were purified and sequenced by Austral-Omics (Universidad Austral of Valdivia-Chile). The sequence was compared with those present in the GenBank database and were deposited in the GenBank nucleotide sequence data library under the accession numbers in **Table 2**.

## Fungal Community Structures by PCR-DGGE

Total DNA was extracted from both fungal and soil samples using the PowerPlant® DNA isolation kit for plants and the PowerSoil® DNA Isolation Kit for soil (MO BIO Laboratories, Inc., CA) according to the manufacturer's instructions.

The fungal community composition was evaluated by denaturing gradient gel electrophoresis (PCR-DGGE) according to Iwamoto et al. (2000). First, touchdown PCR was performed with reagents supplied with GoTaq® Flexi DNA Polymerase (Promega, Co.) using the primer sets NS1 (5′-GTA GTC ATA TGC TTG TCT C-3′)/NS8 (5′-TCC GCA GGT TCA CCT ACG GA-3′). A second PCR with the primer sets NS7-GC (5′-GAG GCA ATA ACA GGT CTG TGA TGC-3, GC-clamp: CGC CCG GGG CGC GCC CCG GGC GGG GCG GGG GCA CGG GGG)/F1Ra (5′-CTT TTA CTT CCT CTA AAT GAC C-3′) was performed with 94°C for 1 min; followed by 30 cycles of 55°C

**TABLE 2 |** Fungal strains isolated from South Shetland Island.

| Strain | Closest relatives or cloned sequences (accession N°) | Similarity (%) | Accesion N° |
|---|---|---|---|
| *Penicillium* sp.SA1.3 | *Penicillium commune* , wine cellar fungi (KT316690) | 91 | MG754011 |
| *Pseudogymnoascus* sp.SA1.4 | *Pseudogymnoascus pannorum*, cave bear bones (KY465766) | 97 | MG754012 |
| *Penicillium* sp.SA2.2 | *Penicillium brevicompactum*, cold environments of Western Himalaya (AM948959) | 96 | MG845129 |
| *Lambertella* sp.SA3.1 | *Lambertella viburni*, molecular phylogenetic studies (AB926098) | 98 | MG845130 |
| *Cadophora* sp.SA3.2 | *Cadophora malorum*, King George Island, Antarctic (MG813381) | 99 | MG754013 |
| *Cadophora* sp.SA3.3 | *Cadophora* sp. King George Island, Antarctic (MG813382) | 99 | MG754014 |
| *Candida* sp.SA3.5 | *Candida zeylanoides*, Pomegranate Fruits (KY366245) | 95 | MG754015 |
| Uncultured Zygomycete SA3.6 | *Fungal* sp, Antarctic Peninsula (FJ236010) | 100 | MG845131 |
| *Mortierella* sp.SA3.7 | *Mortierellaceae* sp, Antarctic Peninsula (HM589297) | 100 | MG754016 |
| *Cadophora* sp.SA3.8 | *Cadophora* sp., roots of *Populus deltoids* (KF428355) | 88 | MG754017 |
| *Mortierella* sp.SA4.1 | *Mortierella* sp., Antarctic Peninsula (MG00140) | 88 | MG754018 |
| *Onygenales* sp.SA4.4 | *Onygenales* sp., altitude lakes in the Indian trans-Himalayas (MF326613) | 99 | MG754019 |
| *Geomyces* sp.SA4.5 | *Geomyces* sp. King George Island, Antarctic (MG813416) | 96 | MG754020 |
| *Vishniacozyma* sp.SA4.6 | *Vishniacozyma victoriae,* Antarctic Peninsula (LC203739) | 99 | MG754021 |
| *Talaromyces* sp.SA4.7 | *Talaromyces radicus*, cooling tower systems (KX090340) | 99 | MG754022 |
| *Mortierella* sp.SA5.1 | *Mortierella amoeboidea*, Indian Himalaya(MF467879) | 99 | MG754023 |
| *Mortierella* sp.SA5.2 | *Mortierella* sp., King George Island, Antarctic (JQ670951) | 100 | MG754024 |
| *Mortierella* sp.SA5.3 | *Mortierella* sp., Deception Island Antarctica (KC514910) | 97 | MG754025 |
| *Peudogymnoascus* sp.SA5.5 | *Peudogymnoascus* sp., Antarctic Peninsula (LC085196) | 89 | MG754026 |
| *Rhizopus* sp.SA5.6 | *Rhizopus microsporus,* Indonesian Tempeh Inoculant (KF709998) | 99 | MG845132 |
| *Mortierella* sp.SA5.7 | *Mortierella* sp., Ross Sea Antarctica region (DQ317354) | 97 | MG754027 |
| *Rhizopus* sp.SA5.8 | *Rhizopus microsporus,* maize rhizosphere soil (MF945552) | 92 | MG754028 |
| *Ascomycota* sp.SA5.10 | *Ascomycota* sp., Deception Island Antarctica (KC514882) | 99 | MG754029 |
| *Mortierella* sp.SA6.1 | *Mortierella* sp., Deception Island Antarctica (KC514910) | 99 | MG754030 |
| *Rhizopus* sp.SA6.2 | *Rhizopus microsporus,* maize rhizosphere soil (MF945552) | 99 | MG754031 |
| *Antarctomyces* sp.SA6.3 | *Antarctomyces pellizariae,* Antarctic Peninsula (KX576510) | 99 | MG845133 |
| *Rhizopus* sp.SA6.4 | *Rhizopus microsporus,* maize rhizosphere soil (MF945552) | 76 | MG754032 |
| Uncultured fungus SA6.8 | Uncultured fungus, Antarctic soil fungal (KU559753) | 99 | MG754033 |
| *Mortierella* sp.SA7.1 | *Mortierella* sp., Antarctic Peninsula (MG001404) | 99 | MG754034 |
| *Peudogymnoascus* sp.SA7.3 | *Pseudogymnoascus pannorum*, Arctic soil (MG000968) | 99 | MG754035 |
| *Onygenales* sp.SA8.1 | *Onygenales* sp., altitude lakes in the Indian trans-Himalayas (MF326613) | 99 | MG754036 |
| *Rhizopus* sp.SA8.4 | *Rhizopus microsporus,* maize rhizosphere soil (MF945552) | 99 | MG754060 |
| *Mortierella* sp.SA8.5 | *Mortierella* sp., *Humulus lupulus* (AY842393) | 100 | MG845134 |
| *Mortierella* sp.SA8.7 | *Mortierella* sp., Deception Island Antarctic (KC514910) | 99 | MG754037 |
| *Cosmospora* sp.SA8.8 | *Cosmospora* sp., King George Island, Antarctic (MG813394) | 96 | MG754038 |
| *Cosmospora* sp.SA8.9 | *Cosmospora viridescens*, King George Island, Antarctic (MG813394) | 85 | MG754039 |
| *Rhizopus* sp.SA8.13 | *Rhizopus microsporus,* maize rhizosphere soil (MF945552) | 99 | MG754055 |
| *Pseudogymnoascus* sp.SA9.2 | *Pseudogymnoascus* sp., King George Island, Antarctic (MG813409) | 99 | MG754042 |
| *Mortierella* sp.SA9.3 | *Mortierella* sp., forest soil of Poland (EF152521) | 100 | MG845135 |
| *Geomyces* sp.SA9.4 | *Geomyces* sp., Arctic soil (JN630629) | 99 | MG845138 |
| *Pseudogymnoascus* sp.SA9.6 | *Pseudogymnoascus* sp., King George Island, Antarctic (MG813409) | 98 | MG754043 |
| *Rhizopus* sp.SA9.7 | *Rhizopus microsporus,* maize rhizosphere soil, (MF945552) | 100 | MG754058 |
| *Rhizopus* sp.SA9.8 | *Rhizopus microsporus,* maize rhizosphere soil, (MF945552) | 99 | MG754044 |
| *Rhizopus* sp.SA9.9 | Biogas plant, Hydrolysis tank sludge (MF919345) | 99 | MG754045 |
| *Tetracladium* sp.SA10.1 | *Tetracladium* sp., Glacier National Park, British Columbia (KP411581) | 94 | MG754046 |
| *Leptosphaeria* sp.SA10.2 | *Leptosphaeria veronicae*, from *Veronica austriaca* plants (JF740255) | 99 | MG754047 |
| *Lecanicidium* sp.SA10.3 | *Lecanicillium attenuatum*, seawater gradients Antarctica Peninsula (KY786076) | 98 | MG754057 |
| *Mortierella* sp.SA10.4 | *Mortierella polygonia*, soil from Pit Clave Glacier National Park (KP411578) | 100 | MG845136 |
| *Thelebolus* sp.SA10.7 | *Thelebolus* sp., King George Island, Antarctic (MG813440) | 99 | MG754051 |

*(Continued)*

**TABLE 2 |** Continued

| Strain | Closest relatives or cloned sequences (accession N°) | Similarity (%) | Accesion N° |
|---|---|---|---|
| *Pseudogymnoascus* sp.SA11.1 | *Pseudogymnoascus* sp. , King George Island, Antarctic (MG813409) | 100 | MG754052 |
| *Pseudogymnoascus* sp.SA11.2 | *Pseudogymnoascus* sp. , King George Island, Antarctic (MG813409) | 99 | MG754053 |
| *Rhizopus* sp.SA11.3 | *Rhizopus microsporus,* maize rhizosphere soil (MF945552) | 85 | MG754054 |
| *Bjerkandera* sp.SA12.1 | *Bjerkandera adusta,* National park of Chiloe (KF562019) | 99 | MG754059 |
| *Geomyces* sp.SA12.2 | *Geomyces* sp., Antarctic Peninsula (JN630629) | 99 | MG845137 |

*Blue rows indicate sequence isolated from cold environment.*

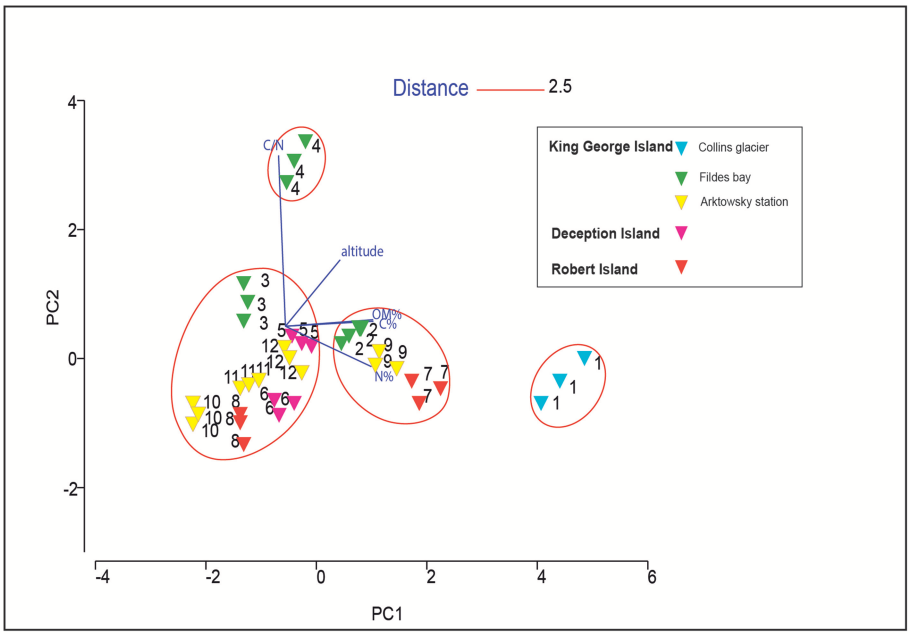


**FIGURE 2 |** Principal component analysis (PCA) analysis based on the chemical properties of 12 Antarctic soil samples.

for 1 min; and 72°C for 3 min; with a final extension at 72°C for 7 min. The primer set NS1/NS8 amplifies a 1700 bp fragment of the 18S rRNA gene and NS7-GC/F1Ra amplifies a 400 bp fragment nested within the NS1/ NS8 target. The DGGE analysis was performed using a DCode system (Bio-Rad Laboratories, Inc.). Twenty-five μL of PCR product was loaded onto a 6% (w/v) polyacrylamide gel with a 40–70% gradient (urea and formamide). The electrophoresis was run for 16 h at 75 V. The gel was then stained with SYBR Gold (Molecular Probes, Invitrogen Co.) for 30 min and photographed on a UV transilluminator. Clustering of DGGE banding profiles using a dendrogram was carried out using Phoretix 1D analysis software (TotalLab Ltd., UK). The *in silico* analysis was also used to estimate the bacterial diversity by richness (S) and the Shannon-Wiener index and dominance by the Simpson Index (D) represented by 1- D or 1- λ (Sagar and Sharma, 2012).

## Statistical Analyses

Data normality was analyzed according to Kolmogorov's test. Data were analyzed by a one-way analysis of variance (ANOVA) and compared by Tukey's test using SPSS software (SPSS, Inc.). Values are given as the means ± standard errors. Differences were considered significant when the *P*-value was lower than or equal to 0.01. For chemical soil parameters, all tests were performed in triplicate. For the fungal community composition, data normality was analyzed according to Kolmogorov's test. The similarity between bacterial communities was visualized with distance-based redundancy analyses (dbRDA) using Primer 7 software (Primer-E Ltd., Ivybridge, UK), which showed a Bray–Curtis similarity index at 60 and 30% and stress values <0.14 (Clarke, 1993). Values are given as the means ± standard errors. Differences were considered significant when the *P*-value was lower than or equal to 0.01.

# RESULTS

## Chemical Parameters of Antarctic Soils

To determine the chemical composition of the 12 collected Antarctic soils, chemical analyses (C, N, and pH) were performed using triplicate samples of each soil (**Table 1**). In general, soil samples showed total C values from 0.10 (soil 10) to 2.65% (soils

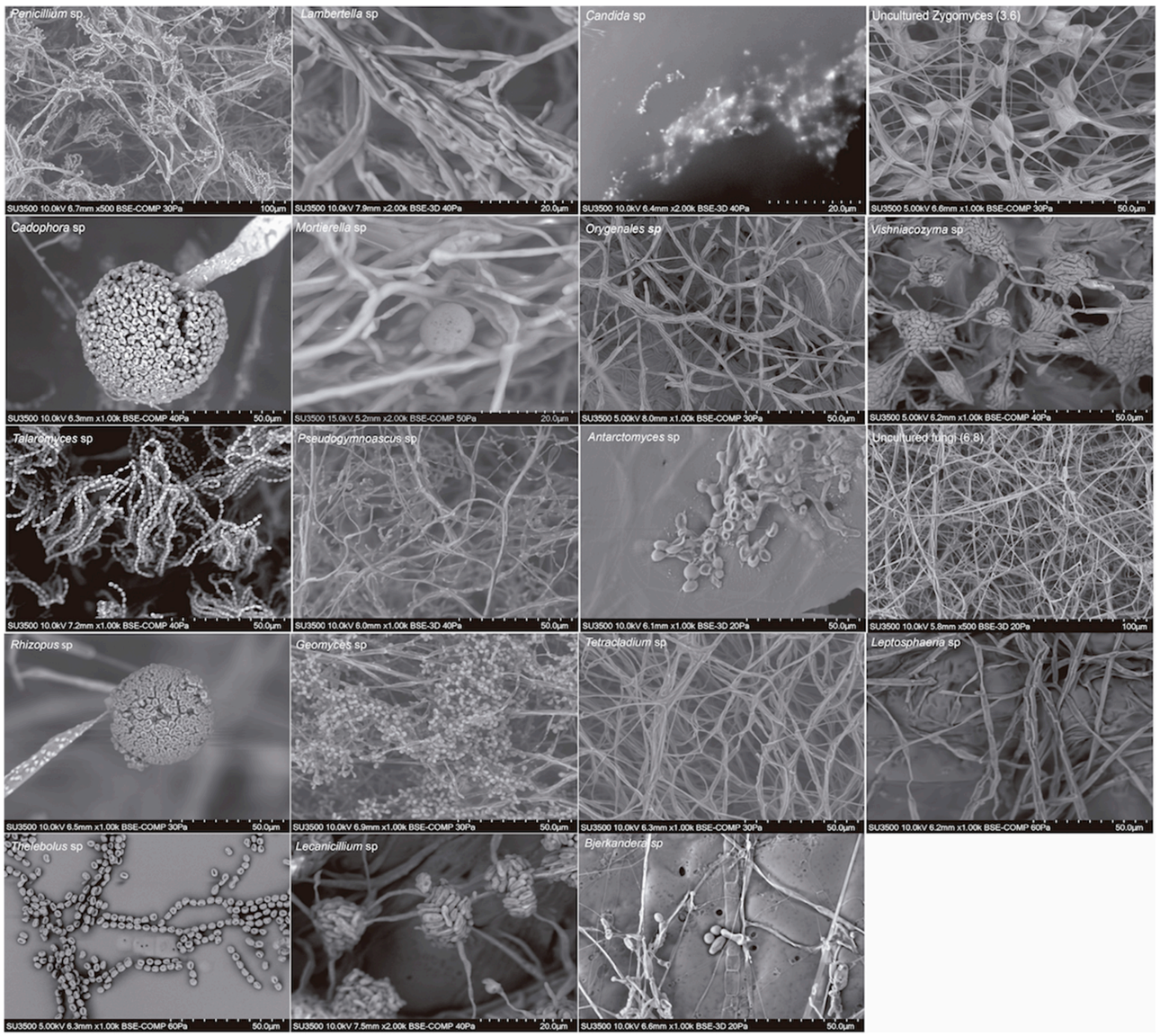


**FIGURE 3 |** Scanning electron micrographs of genera of cultivable fungi isolated from South Shetland Islands.

1) and total N values from 0.01 (soils 4 and 10) to 0.36 (soil 1). Because of the low N content, soil 4 showed the highest C/N ratio (42.10) in comparison with the rest of the samples (from 5.53 to 15.80). The pH ranged from 5.46 (soils 7) to 7.23 (soil 4).

Principal component analysis showed that the soils were not grouped based on their location, where samples varied significantly (**Figure 2**). Soil 4 and soil 1 were grouped independently because of the high C/N ratio and high altitude of soil 4, and the high C and N content of soil 1. In soils 7 and 9, the C and N concentrations were also high, and along with their similar altitudes, they were grouped in the same cluster at a distance of 2.5. The other soil samples (soils 2, 3, 5, 6, 8, 10, 11, and 12) were similar to each other.

## Presence of Culturable Fungi

Our results revealed that in the pristine Antarctic environment, multiple culturable fungal taxa naturally occur. Thus, we isolated 54 fungal strains that, according to identification and phylogenetic affiliation based on the sequencing of the ribosomal internal transcribed spacer 2 (ITS2) region, belonged to 19 genera: *Penicillium*, *Pseudogymnoascus*, *Lambertella*, *Cadophora*, *Candida*, *Mortierella*, *Oxygenales*, *Geomyces*, *Vishniacozyma*, *Talaromyces*, *Rhizopus*, *Antarctomyces*, *Cosmospora*, *Tetracladium*, *Leptosphaeria*, *Lecanicillium*, *Thelebolus*, *Bjerkandera*, and an uncultured Zygomycete. Among these, 70% belonged to the Ascomycota, 10% to the Zygomycota, 10% to the Basidiomycota, 5% to the Deuteromycota and 5% to the Mucoromycota.

**TABLE 3 |** Presence of culturable fungal strains in each soil samples.

| Strain | Soil Samples | | | | | | | | | | | | Total |
|---|---|---|---|---|---|---|---|---|---|---|---|---|---|
| | 1 | 2 | 3 | 4 | 5 | 6 | 7 | 8 | 9 | 10 | 11 | 12 | |
| *Penicillium* sp. | 1 | 1 | – | – | – | – | – | – | – | – | – | – | 2 |
| *Pseudogymnoascus* sp. | 1 | – | – | – | 1 | – | 1 | – | 2 | – | 2 | – | 7 |
| *Lambertella* sp. | – | – | 1 | – | – | – | – | – | – | – | – | – | 1 |
| *Cadophora* sp. | – | – | 3 | – | – | – | – | – | – | – | – | – | 3 |
| *Candida* sp. | – | – | 1 | – | – | – | – | – | – | – | – | – | 1 |
| Uncultured Zygomycete | – | – | 1 | – | – | – | – | – | – | – | – | – | 1 |
| *Mortierella* sp. | – | – | 1 | 1 | 4 | 1 | 1 | 2 | 1 | 1 | – | – | 12 |
| *Onygenales* sp. | – | – | – | 1 | – | – | – | 1 | – | – | – | – | 2 |
| *Geomyces* sp. | – | – | – | 1 | – | – | – | – | 1 | – | – | 1 | 3 |
| *Vishniacozyma* sp. | – | – | – | 1 | – | – | – | – | – | – | – | – | 1 |
| *Talaromyces* sp. | – | – | – | 1 | – | – | – | – | – | – | – | – | 1 |
| *Rhizopus* sp. | – | – | – | – | 2 | 2 | – | 2 | 3 | – | 1 | – | 10 |
| *Ascomycota* sp. | – | – | – | – | 1 | – | – | – | – | – | – | – | 1 |
| *Antarctomyces* sp. | – | – | – | – | – | 1 | – | – | – | – | – | – | 1 |
| Uncultured fungus | – | – | – | – | – | 1 | – | – | – | – | – | – | 1 |
| *Cosmospora* sp. | – | – | – | – | – | – | – | 2 | – | – | – | – | 2 |
| *Tetracladium* sp. | – | – | – | – | – | – | – | – | – | 1 | – | – | 1 |
| *Leptosphaeria* sp. | – | – | – | – | – | – | – | – | – | 1 | – | – | 1 |
| *Lecanicillium* sp. | – | – | – | – | – | – | – | – | – | 1 | – | – | 1 |
| *Thelebolus* sp. | – | – | – | – | – | – | – | – | – | 1 | – | – | 1 |
| *Bjerkandera* sp. | – | – | – | – | – | – | – | – | – | – | – | 1 | 1 |
| Total | 2 | 1 | 7 | 5 | 8 | 5 | 2 | 7 | 7 | 5 | 3 | 2 | 54 |

**TABLE 4 |** Fungal growth at different temperatures.

| Strain | Temperature of growth | | | Psychrophile/ psychrotroph |
|---|---|---|---|---|
| | 4°C | 15°C | 25°C | |
| *Penicilium* sp. | ++ | +++ | ++ | Psychrotroph |
| *Pseudogymnoascus* sp. | + | +++ | – | Psychrophile |
| *Lambertella* sp. | + | ++ | ++ | Psychrotroph |
| *Cadophora* sp. | + | +++ | ++ | Psychrotroph |
| Unculture zygomycete | + | + | – | Psychrophile |
| *Mortierella* sp. | + | ++ | ++ | Psychrotroph |
| *Onygenales* sp. | + | ++ | – | Psychrophile |
| *Geomyces* sp. | + | ++ | – | Psychrophile |
| *Vishniacozyma* sp. | + | +++ | – | Psychrophile |
| *Talaromyces* sp. | + | +++ | – | Psychrophile |
| *Rhizopus* sp. | + | + | – | Psychrophile |
| *Ascomycota* sp. | + | + | – | Psychrophile |
| *Antarctomyces* sp. | +++ | + | + | Psychrotroph |
| Uncultures fungus | + | ++ | + | Psychrotroph |
| *Cosmospora* sp. | + | +++ | ++ | Psychrotroph |
| *Tetracladium* sp. | + | +++ | ++ | Psychrotroph |
| *Leptosphaeria* sp. | + | +++ | – | Psychrophile |
| *Lecanicidium* sp. | + | +++ | ++ | Psychrotroph |
| *Thelebolus* sp. | + | ++ | ++ | Psychrotroph |
| *Bejerkendera* sp. | + | +++ | +++ | Psychrotroph |

*Growth rate capacity was measured as follows: + + +, very high capacity; ++, high capacity; +, normal capacity; and –, no capacity.*

We also found a wide variety of phenotypes, as was observed in scanning electron micrographs (SEM) of each genus (**Figure 3**). The SEM images from spores revealed the presence of teleomorph forms of the following genera from the Ascomycota: *Cadophora*, *Talaromyces*, *Antarctomyces*, *Thelebolus*, *Lecanicillium*; from the Basidiomycota: *Vishniacozyma* and *Bjerkandera* and from the Zygomycota: *Mortierella* and *Rhizopus*. The most frequently represented genus was *Mortierella,* and the soil samples with the highest richness of culturable fungi were soils 3, 5, 8, and 9 (**Table 3**).

Among culturable fungi, ∼70% were associated with similar genera grown in cold environments according to GenBank database (**Table 2**, light blue rows). This was confirmed by the phylogenetic tree with representative 18S rRNA gene sequences (**Supplementary Figure 1**). Our isolates (blue letter) showed no similarity with other reported fungal strains belonging to the same genera growing in tropical or temperate areas (red letter).

## Optimal Fungal Growth Temperatures

Of the total culturable fungi, 55% were psychrotrophs and 45% were psychrophiles (**Table 4**). All strains were able to grow at 4°C, but psychrotrophs were able to grow above 20°C, whereas psychrophiles showed a maximum of growth at 15°C but were not able to grow at 25°C (**Supplementary Figure 2**).

## Fungal Community Composition in Antarctic Pristine Environment

The dominance and diversity of fungal community composition was not related to soil location as revealed by dbRDA, with which microbiological and soil chemical/environmental properties were analyzed (**Figure 4**). The fungal community structure of sample 1 (Collins Glacier) was grouped independently and was influenced by high N content at 60% similarity. The fungal community of sample 10 was also grouped independently, probably due to the lower altitude and N content compared with the rest of the samples. At 60% similarity, the communities of soils 2, 3, and 4 were grouped independently, but at 30% similarity, they were grouped with the rest of the samples (soils 5, 6, 7, 8, 9, 11, and 12) without significant differences among their communities.

## Fungal Richness and Diversity and Relation to Chemical Parameters

Regarding the microbial diversity in the pristine Antarctic environment, in general, samples 1 (Collins Glacier), 2 (Fildes Bay), 11 and 12 (Arctowski Station) showed less richness expressed in species number (S), which ranged from 15 to 33. A similar tendency was observed for N (individual number), ranging from 1,500 to 3,500. The most richness was observed in samples 4 (Fildes Bay), 7 (Coppermine Peninsula) and 10 (Arctowski Station). The Shannon index (H′) that represents richness and dominance ranged from 2.5 to 3.3. Likewise,

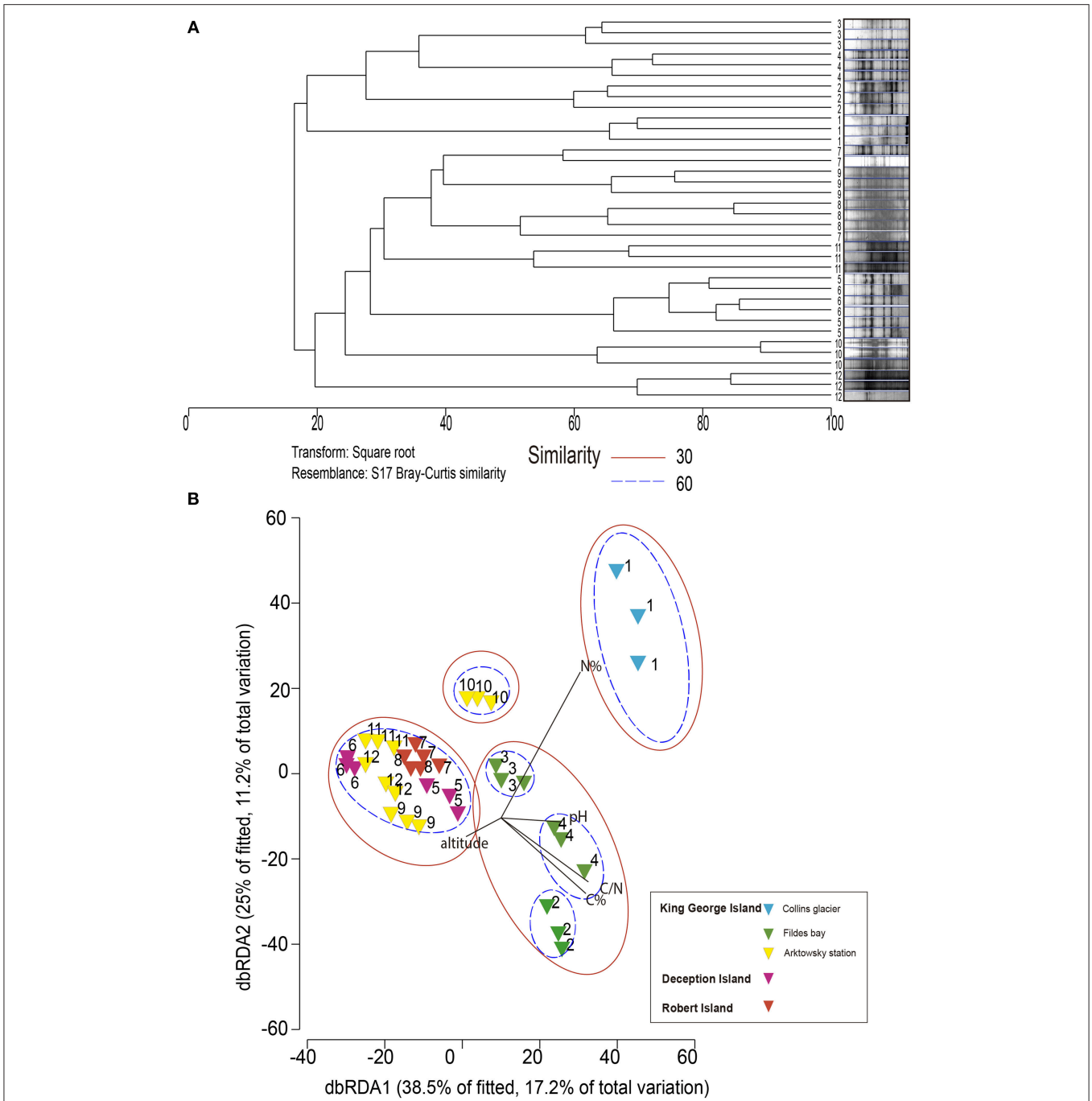


**FIGURE 4 |** Dendrogram **(A)** and nonmetric multidimensional scaling **(B)** analysis of DGGE profiles (18S rRNA gene) from soil communities of the Antarctic pristine environment.

samples 1, 2, 11, and 12 showed major dominance expressed as Simpsons (D) index represented by 1-$\lambda$ (**Figure 5**).

We noted that a positive correlation exists between C/N and index of richness expressed as S (species number) and N (individual number) ($p < 0.05^{*}$ and $p < 0.01^{**}$, respectively, **Figure 6**). The index related to richness and dominance such as the Shannon Wiener index (H') and the index related to dominance only, such as the Simpsons (D) index, represented by 1-$\lambda$ was inversely related to C and N. Thus, we noted high dominance (low diversity) when soil samples showed higher C and N contents (**Figure 6**).

## DISCUSSION

During the Antarctic campaign ECA-53, 12 bulk soils (0–20 cm) were collected from South Shetland Island (62°00′S,

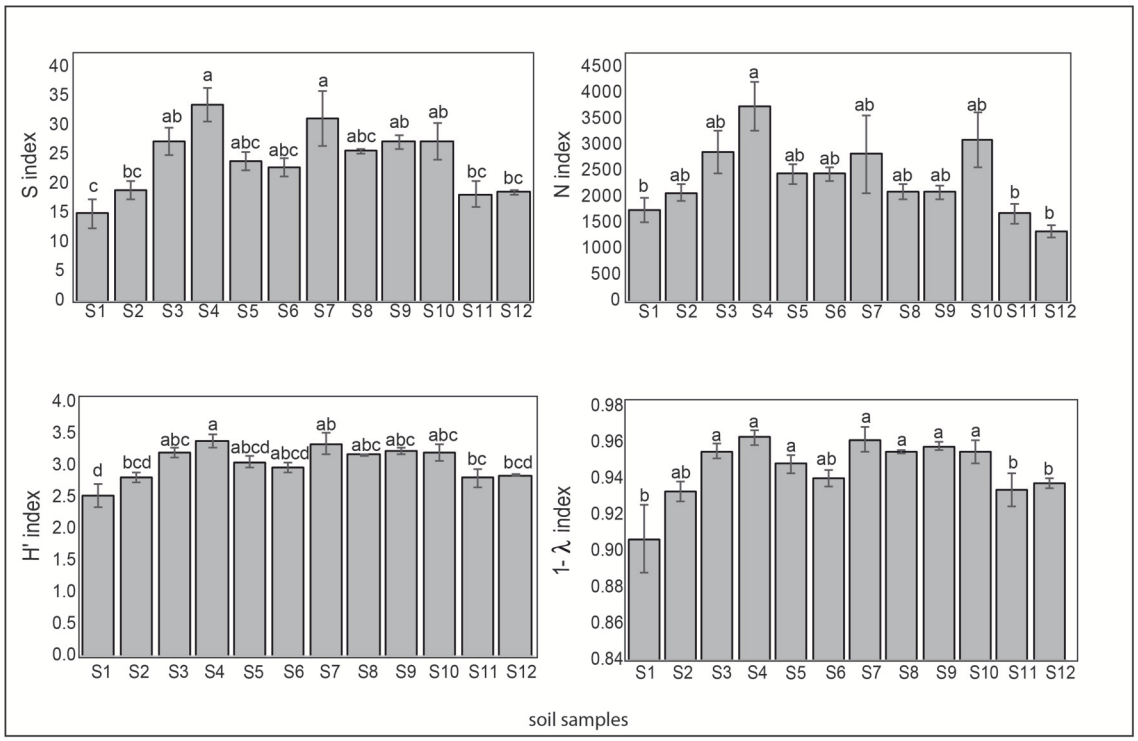


**FIGURE 5 |** Biodiversity indices S (species number), N (individual number), Shannon-Wiener (H) and Simpson (represented by 1- λ) of the soil samples. Tukey's test was used to compare treatment means, and values followed by the same letter do not differ at $P < 0.05$ ($n = 5$).

59°30′W), eight from King George Island (including Collins Glacier), two from Deception Island and two from Robert Island. According to the chemical parameter measurements, pH values were near neutral, from 5.46 to 7.23, with C ranging from 0.10 to 2.65% and N ranging from 0.01 to 0.36%, and Collins Glacier showed the greatest values. Moorhead et al. (2003) showed that wetlands in Taylor Valley (Antarctica) showed an accumulation of soil organic C and total N concentrations of 0.12% and 0.013%, respectively. However, pH values were more alkaline than in our study (∼8.5). Bölter et al. (1997) reported values of pH more acidic, from 3.7 to 7.2 for Arctowski Station and values of 0.09 to 2.60% C and 0.16 to 0.48% N. This variation could be attributed to the high influence of sea birds (penguins) and other birds (Lee et al., 2009).

Fifty-four fungal strains belonging to 20 genera were isolated from King George Island (including Collins Glacier), Deception and Robert Island soils. The predominance of filamentous Ascomycetes (70%) in studies of Antarctic soils has been reported, with *Geomyces* and *Cadophora* widely reported (Högberg et al., 2007). We also found the presence of *Zygomycota, Basidiomycota, Deuteromycota,* and *Mucoromycota*. Similar genera isolated from Antarctic and Arctic environments were reported in other studies by Krishnan et al. (2018), and according to our study, 70% of isolates were associated with similar genera grown in cold environments according to the GenBank database (**Supplementary Figure 1**). Ding et al. (2016) reported high dominance of *Pseudogymnoascus* (or *Geomyces*) in Fildes Peninsula and *Antarctomyces* and *Thelebolus*, which are considered cold-environment-specific genera (Ding et al., 2016). Thus, among all culturable isolates from our study, 100% were able to grow at 4°C, 55% were considered psychrotrophic fungi that were able to grow above 20°C, whereas psychrophilic microorganisms (45%) showed maximum growth at 15°C but were not able to grow at 25°C (Robinson, 2001).

Interestingly, we noted less richness and major dominance in samples collected in Collins Glacier compared with the rest of the soils analyzed, despite the large content of C and N. However, the C/N ratio seems to be a more important parameter influencing soil fungal richness because our results showed that a positive correlation exists between C/N and the index of richness expressed as S (species number) and N (individual number). Calandra et al. (2016) showed that the C:N ratio had an important role in spore shelf life of *Trichoderma harzianun*. Similarly, Dumbrell et al. (2010) showed that ß-diversity of arbuscular mycorrhizal fungi was positively correlated with the C/N ratio. However, the indices related to richness and dominance, such as the Shannon Wiener index (H′) and dominance only, such as Simpsons (D) were inversely related to C and N. Therefore, high fungal dominance (low diversity) was found when soil samples showed a larger C and N content. In this context, Siciliano et al. (2014) reported that soil fertility (i.e., organic matter, nitrogen and chloride content) was consistently the most important driver influencing bacterial and fungal species richness, speculating that

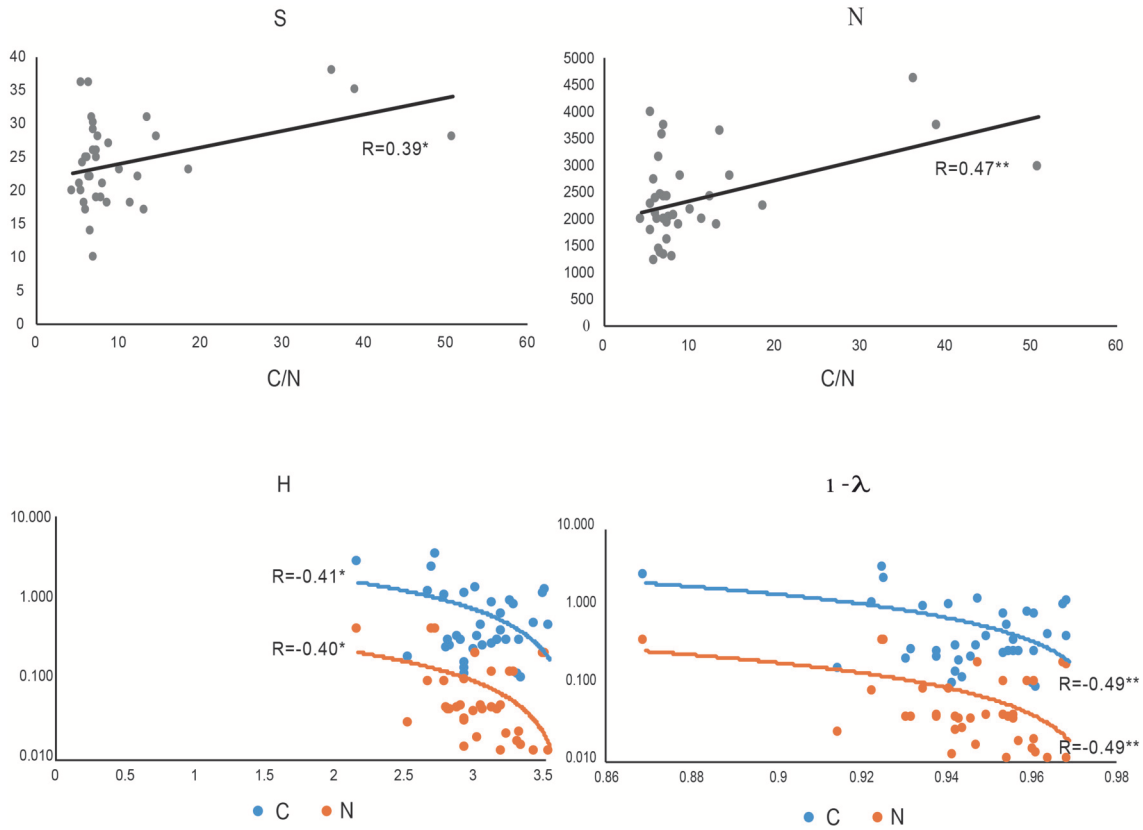


**FIGURE 6 |** The most important correlation between biodiversity index: S (species number), N (individual number, Shannon-Wiener (H) and Simpson (represented by 1- λ) and C/N ratio (gray), C (blue) and N (orange).

soil fertility provides nutritive properties that allow the more adapted species within a community to grow rapidly and to dominate and exclude other members of the community. Thus, it has been reported that the Antarctic microbial community seems to be structured solely by abiotic processes (Cary et al., 2010). Altitude was not a determinate parameter influencing the fungal community, as was the case in a study recently reported by Coleine et al. (2018).

In relation to soil fungal community compositions, our results showed that soil location was not a parameter that defined the microbial community structure, as revealed by dbRDA, as soil parameters were the most prominent influencing factor. For example, soil collected from Collins Glacier (sample 1) was strongly influenced by N and sample 10 by low N and low altitude. Siciliano et al. (2014) noted that soil pH was a major factor determining the bacterial community composition in polar soil because fungi can adapt to different pH ranges. In the case of fungal community compositions, we found that C content was the most important factor.

Because PCR-DGGE is a simple and relatively inexpensive method, it is considered a valuable tool to detect gross shifts in the entire microbial community (Hume et al., 2011; Rychlik et al., 2016). However, further studies considering omics technology (such as genomics, transcriptomics, proteomics, etc.) are needed to identify functional roles of fungal adaptations to extreme environments in order to better understand the endemic nature of these communities for further biotechnological applications.

## CONCLUSIONS

Our results reveal fungi occurrence in twelve soils from South Shetland Island, Antarctica. The most representative group were the Ascomycetes (70%), with *Geomyces* and *Cadophora* widely reported in Antarctic lands. Seventy percentage of isolates were associated with similar genera grown in cold environments, and among the total culturable fungal strains, 55% were considered psychrotrophic (able to grow above 20°C), and 45% were considered psychrophilic with a maximum growth at 15°C and no growth at 25°C. Remarkably, the occurrence of fungi in soils was not correlated with soil locations but was correlated with soil chemical properties. Thus, richness was associated with the C/N ratio, and dominance was inversely correlated with C and N. Most fungal strains were observed in the teleomorph phase, with clear survival structures to allow resistance to extreme environments. Future omic analyses are required to identify the ecological role and fungal adaptation mechanisms at low temperature as well as the to examine potential applications of these fungal strains in biotechnology.

## AUTHOR CONTRIBUTIONS

PD wrote the main manuscript text. MJ, SV, and PB designed the research. CP, MM, MJ, and RB supervised the study and improve the revision, and RB, CF, CP, and PD analyzed the data. All authors critically revised the manuscript and approved the final version.

## FUNDING

This study was supported by Instituto Antártico Chileno (INACH), Regular projects RT_02-16 and RT_06-17 from the Chilean government. We thank the Scientific and Technological Bioresources Nucleus (BIOREN) for technical support and the La Frontera University for logistical support, and INACH for assistance with sampling.

## SUPPLEMENTARY MATERIAL

The Supplementary Material for this article can be found online at: https://www.frontiersin.org/articles/10.3389/fbioe.2019.00028/full#supplementary-material

## REFERENCES

Bölter, M., Blume, H. P., Schneider, D., and Beyer, L. (1997). Soil properties and distributions of invertebrates and bacteria from King George Island (Arctowski Station), maritime Antarctic. *Polar Biol.* 18, 295–304. doi: 10.1007/s003000050191

Calandra, D. M., Mauro, D., Di Cutugno, F., and Di Martino, S. (2016). Navigating wall-sized displays with the gaze: a proposal for cultural heritage. *CEUR Workshop Proc.* 1621, 36–43.

Cary, S. C., Mcdonald, I. R., Barrett, J. E., and Cowan, D. A. (2010). On the rocks: the microbiology of antarctic dry valley soils. *Nat. Rev. Microbiol.* 8, 129–138. doi: 10.1038/nrmicro2281

Cid, F. P., Inostroza, N. G., Graether, S. P., Bravo, L. A., and Jorquera, M. A. (2016). Bacterial community structures and ice recrystallization inhibition activity of bacteria isolated from the phyllosphere of the Antarctic vascular plant *Deschampsia antarctica*. *Polar Biol.* 40, 1319–1331. doi: 10.1007/s00300-016-2036-5

Clarke, K. R. (1993). Non-parametric multivariate analyses of changes in community structure. *Aust. J. Ecol.* 18, 117–143. doi: 10.1111/j.1442-9993.1993.tb00438.x

Coleine, C., Zucconi, L., Onofri, S., Pombubpa, N., Stajich, J., and Selbmann, L. (2018). Sun exposure shapes functional grouping of fungi in cryptoendolithic Antarctic communities. *Life* 8:19. doi: 10.3390/life8020019

Cowan, D. A., Makhalanyane, T. P., Dennis, P. G., and Hopkins, D. W. (2014). Microbial ecology and biogeochemistry of continental antarctic soils. *Front. Microbiol.* 5:154. doi: 10.3389/fmicb.2014.00154

Ding, Z., Li, L., Che, Q., Li, D., Gu, Q., and Zhu, T. (2016). Richness and bioactivity of culturable soil fungi from the Fildes Peninsula, Antarctica. *Extremophiles* 20, 425–435. doi: 10.1007/s00792-016-0833-y

Dumbrell, A. J., Nelson, M., Helgason, T., Dytham, C., and Fitter, A. H. (2010). Relative roles of niche and neutral processes in structuring a soil microbial community. *ISME J.* 4, 337–345. doi: 10.1038/ismej.2009.122

Godinho, M., Furbino, L. E., Santiago, I. F., Pellizzari, F. M., Zani, C. L., Cantrell, C. L., et al. (2013). Diversity and bioprospecting of fungal communities associated with endemic and cold-adapted macroalgae in Antarctica. *ISME J.* 7, 1434–1451. doi: 10.1038/ismej.2013.77

Godinho, V., Gonçalves, V., Santiago, I., Figueredo, H., Vitoreli, GislaineSchaefer, C. E. G. R., Barbosa, E. C., et al. (2015). Diversity and bioprospection of fungal community present in oligotrophic soil of continental Antarctica. *Extremophiles* 19, 585–596. doi: 10.1007/s00792-015-0741-6

Gonc, V. N., Susana, R. C., and Graziele, J. (2015). Antibacterial, antifungal and antiprotozoal activities of fungal communities present in different substrates from Antarctica. *Polar Biol.* 38, 1143–1152. doi: 10.1007/s00300-015-1672-5

Högberg, M. N., Chen, Y., and Högberg, P. (2007). Gross nitrogen mineralisation and fungi-to-bacteria ratios are negatively correlated in boreal forests. *Biol. Fertil. Soils* 44, 363–366. doi: 10.1007/s00374-007-0215-9

Hume, M. E., Barbosa, N. A., Dowd, S. E., Sakomura, N. K., Nalian, A. G., Kley, A. M. V., et al. (2011). Use of Pyrosequencing and denaturing gradient gel electrophoresis to examine the effects of probiotics and essential oil blends on digestive microflora in broilers under mixed eimeria infection. *Foodborne Pathog. Dis.* 8, 1159–1167. doi: 10.1089/fpd.2011.0863

Ihrmark, K., It, B., Schenck, J., Durling, M. B., Cruz-martinez, K., Friberg, H., et al. (2016). Friberg H, Kubartova A, Schenck J et al. New primers to amplify the fungal ITS2 region- evaluation by 454-sequencing of artificial and natura. *FEMS Microbiol. Ecol.* 82, 666–677. doi: 10.1111/j.1574-6941.2012.01437.x

Iwamoto, T., Tani, K., Nakamura, K., Suzuki, Y., Kitagawa, M., Eguchi, M., et al. (2000). Monitoring impact of in situ biostimulation treatment on groundwater bacterial community by DGGE. *FEMS Microbiol. Ecol.* 32, 129–141. doi: 10.1111/j.1574-6941.2000.tb00707.x

Krishnan, A., Alias, S. A., Wong, C. M. V. L., Pang, K.-L., and Convey, P. (2011). Extracellular hydrolase enzyme production by soil fungi from King George Island, Antarctica. *Polar Biol.* 34, 1535–1542. doi: 10.1007/s00300-011-1012-3

Krishnan, A., Convey, P., Gonzalez, M., Smykla, J., and Alias, S. A. (2018). Effects of temperature on extracellular hydrolase enzymes from soil microfungi. *Polar Biol.* 41, 537–551. doi: 10.1007/s00300-017-2215-z

Lee, Y., Il Lim, H. S., and Il Yoon, H., (2009). Carbon and nitrogen isotope composition of vegetation on King George Island, maritime Antarctic. *Polar Biol.* 32, 1607–1615. doi: 10.1007/s00300-009-0659-5

Maida, I., Bosi, E., Fondi, M., Perrin, E., and Orlandini, V. (2015). Antimicrobial activity of Pseudoalteromonas strains isolated from the Ross Sea (Antarctica) versus *Cystic fibrosis* opportunistic pathogens. *Hydrobiologia* 761, 443–457. doi: 10.1007/s10750-015-2190-8

Moorhead, D. L., Barrett, J. E., Virginia, R. A., Wall, D. H., and Porazinska, D. (2003). Organic matter and soil biota of upland wetlands in Taylor Valley, Antarctica. *Polar Biol.* 26, 567–576. doi: 10.1007/s00300-003-0524-x

Pacelli, C., Selbmann, L., Moeller, R., Zucconi, L., Fujimori, A., and Onofri, S. (2017). Cryptoendolithic Antarctic black fungus *Cryomyces antarcticus* irradiated with accelerated helium ions: survival and metabolic activity, DNA and ultrastructural damages. *Front. Microbiol.* 8:2002. doi: 10.3389/fmicb.2017.02002

Purves, K., Macintyre, L., Brennan, D., Hreggvið*sson, G. Ó., and Kuttner, E., Ásgeirsdóttir, M. E., et al. (2016). Using molecular networking for microbial secondary metabolite bioprospecting. *Metabolites* 6, 1–18. doi: 10.3390/metabo6010002

Robinson, C. H. (2001). Cold adaptation in Arctic and Antarctiv fungi. *New Phytol.* 151, 341–353. doi: 10.1046/j.1469-8137.2001.00177.x

Rychlik, T., Szwengiel, A., Bednarek, M., Arcuri, E., Montet, D., Mayo, B., et al. (2016). Application of the PCR-DGGE technique to the fungal community of traditional Wielkopolska fried ripened curd cheese to determine its PGI authenticity. *Food Control.* 73, 1074–1081. doi: 10.1016/j.foodcont.2016.10.024

Sagar, R., and Sharma, G. (2012). Measurement of alpha divers ity using Simpson index (1/λ): the jeopardy. *Environ. Skept. Critics* 1, 23–24.

Sannino, F., Giuliani, M., Salvatore, U., Apuzzo, G. A., Pascale, D., De, and Fani, R. (2017). A novel synthetic medium and expression system for subzero growth and recombinant protein production in *Pseudoalteromonas haloplanktis* TAC125. *Appl. Microbiol. Biotechnol.* 101, 725–734. doi: 10.1007/s00253-016-7942-5

Selbmann, L., Zucconi, L., and Onofri, S. (2007). Fungi in Antarctica. *Rev. Environ. Sci. BioTechnol.* 6, 127–141. doi: 10.1007/s11157-006-9107-y

Siciliano, S. D., Palmer, A. S., Winsley, T., Lamb, E., Bissett, A., Brown, M. V., et al. (2014). Soil fertility is associated with fungal and bacterial richness, whereas pH is associated with community composition in polar soil microbial communities. *Soil Biol. Biochem.* 78, 10–20. doi: 10.1016/j.soilbio.2014.07.005

Tedesco, P., Maida, I., Esposito, F. P., Tortorella, E., Subko, K., Ezeofor, C. C., et al. (2016). Antimicrobial activity of monoramnholipids produced by bacterial strains isolated from the Ross. *Mar. Drugs* 14, 1–14. doi: 10.3390/md14050083

Teixeira, L. C. R. S., Yeargeau, E., Balieiro, F. C., Piccolo, M. C., Peixoto, R. S., Greer, C. W., et al. (2013). Plant and bird presence strongly influences the microbial communities in soils of admiralty bay, Maritime Antarctica. *PLoS ONE* 8:e66109. doi: 10.1371/journal.pone.0066109

**Conflict of Interest Statement:** The authors declare that the research was conducted in the absence of any commercial or financial relationships that could be construed as a potential conflict of interest.

# Advantages of publishing in Frontiers

**OPEN ACCESS**
Articles are free to read for greatest visibility and readership

**FAST PUBLICATION**
Around 90 days from submission to decision

**HIGH QUALITY PEER-REVIEW**
Rigorous, collaborative, and constructive peer-review

**TRANSPARENT PEER-REVIEW**
Editors and reviewers acknowledged by name on published articles

**Frontiers**
Avenue du Tribunal-Fédéral 34
1005 Lausanne | Switzerland

**Visit us:** www.frontiersin.org
**Contact us:** info@frontiersin.org | +41 21 510 17 00

**REPRODUCIBILITY OF RESEARCH**
Support open data and methods to enhance research reproducibility

**DIGITAL PUBLISHING**
Articles designed for optimal readership across devices

**FOLLOW US**
@frontiersin

**IMPACT METRICS**
Advanced article metrics track visibility across digital media

**EXTENSIVE PROMOTION**
Marketing and promotion of impactful research

**LOOP RESEARCH NETWORK**
Our network increases your article's readership